Functional characterization of 4EBP1 in primary brain tumors

Inaugural-Dissertation

zur Erlangung des Doktorgrades
der Mathematisch-Naturwissenschaftlichen Fakultät
der Heinrich-Heine-Universität Düsseldorf

vorgelegt von

Laura Hauffe
aus Nürnberg

Düsseldorf, April 2022

Aus dem Institut für Neuropathologie
der Heinrich-Heine-Universität Düsseldorf

Gedruckt mit der Genehmigung der
Mathematisch-Naturwissenschaftlichen Fakultät der
Heinrich-Heine-Universität Düsseldorf

Berichterstatter:

1. Prof. Dr. Guido Reifenberger

2. Prof. Dr. Sebastian Wesselborg

Tag der mündlichen Prüfung: 28.06.2022

Eidesstattliche Erklärung

Ich versichere an Eides Statt, dass die Dissertation „Functional characterization of 4EBP1 in primary brain tumors“ von mir selbstständig und ohne unzulässige fremde Hilfe unter Beachtung der „Grundsätze zur Sicherung guter wissenschaftlicher Praxis an der Heinrich-Heine-Universität Düsseldorf“ erstellt worden ist.

Die Dissertation wurde in dieser oder ähnlicher Weise noch an keiner anderen Fakultät vorgelegt und es wurde kein vorheriger Promotionsversuch unternommen.

_____

Laura Hauffe

Düsseldorf, April 2022

INDEX

I. LIST OF ABBREVIATIONS IV

II. SUMMARY VI

III. ZUSAMMENFASSUNG VI

1. INTRODUCTION 9

1.1. Tumor cells adapt to extracellular and intracellular stress factors during tumor development 9

1.2. The control of mRNA translation drives metabolic stress response during tumor development 11

1.3. 4EBP1 - a mTORC1 substrate 13

1.3.1. Regulation of 4EBP1 activity and expression 13

1.3.2. Molecular function of 4EBP1 15

1.3.3. Cellular functions of 4EBP1 18

1.3.4. Function of 4EBP1 in cancer 20

1.4. Glioblastoma 23

1.4.1. Metabolic heterogeneity of glioblastoma 23

1.4.2. Glioblastoma classification 24

1.4.3. Genetic evolution of IDH-WT glioblastoma 25

1.4.4. Treatment of glioblastoma 27

2. AIMS OF THE THESIS 29

3. RESULTS 30

3.1. How is *EIF4EBP1* overexpression mediated in glioblastoma? 30

3.1.1. MANUSCRIPT I 31

3.1.2. MYC is an additional transcription factor candidate regulating *EIF4EBP1* promoter activity 42

3.1.3. MYBL2 does not induce *EIF4EBP1* promoter activity through a MYBL2 consensus binding motif 44

3.1.4. *EIF4EBP1* transcription is not regulated by E2F6, JUN or FOXM1 in glioblastoma cell lines 46

3.1.5. Functional impact of 4EBP1 on migration and invasion of glioblastoma cells 49

3.2. Functional impact of 4EBP1 on oncogenic transformation and tumorigenesis 51

3.2.1. MANUSCRIPT II 53

3.2.2. Impact of p53 on the tumorigenic potential of 4EBP1 105

3.2.3. *TP53* mutation status modulates the prognostic role of *EIF4EBP1* levels on overall survival ... 109

3.3. Targeting 4EBP1 - a novel approach 109

3.3.1. Strategy for targeting 4EBP1 activity 109

3.3.2. 4EBP1 protective effect under glucose starvation is mediated by the NC-loop 110

3.3.3. Identification of hot spot residues within the 4EBP1 NC loop-eIF4E binding interface and *in silico* screening for potential binding inhibitors 111

3.3.4. Tryptophan fluorescent quenching assay 112

3.3.4.1. 4EBP1 or eIF4G interaction with eIF4E results in a quenched tryptophan fluorescent signal 113

3.3.4.2. Tryptophan fluorescent quenching identified binding of compounds to eIF4E 114

4. DISCUSSION 118

4.1. Deregulation of *EIF4EBP1* expression in cancer and role of 4EBP1 in cancer cell migration 119

4.2. Tumorigenic potential of 4EBP1 involves control of the redox balance and depends on p53 status 120

4.3. 4EBP1 represents a potential therapeutic target candidate for glioma 123

5. MATERIAL AND METHODS 126

5.1. Data availability and bioinformatic analysis 126

5.2. Cell culture 126

5.3. Transfection of cells with shRNA or siRNA 126

5.4. Migration and invasion assays 127

5.4.1. Oris™ Cell Migration Assay 127

5.4.2. Oris™ 3D Cell Invasion Assay 128

5.4.3. Staining and imaging of the migration and invasion assays 128

5.5. Protein binding assays 128

5.5.1. Peptide synthesis 128

5.5.2. Spectroscopic measurements 129

5.5.3. Candidate 4EBP1 inhibitor compounds, additional PCR primers and antibodies 130

6. APPENDIX 131

6.1. Supplementary figures corresponding to manuscript I 131

6.2. Supplementary tables corresponding to manuscript I 134

6.3. Kaplan-Meier analysis of medulloblastoma patients according to *EIF4EBP1* levels 142

6.4. Manuscript III 142

A. LIST OF FIGURES 173

B. LIST OF TABLES 175

C. AUTHOR CONTRIBUTION TO THE MANUSCRIPTS 176

D. REFERENCES 178

E. ACKNOWLEDGEMENT 195

I. LIST OF ABBREVIATIONS

4EBP1	eukaryotic initiation factor 4E binding protein 1
A	alanine
ATP	adenosine triphosphate
BTIC	brain tumor initiating cells
Ca	canonical α-helix
CERT	cytosine-enriched regulator of translation
CHX	cycloheximide
CNA	copy number alteration
DKO	double knock out
eIF4E	eukaryotic translation initiation factor 4E
EL	elbow loop
EMT	epithelial-mesenchymal transition
ER	endoplasmic reticulum
FL	full length
GLUT	glucose transporter
I	isoleucine
IDH	isocitrate dehydrogenase
IRES	internal ribosomal entry site
KD	knock down
KO	knock out
L	leucine
MEFs	mouse embryonic fibroblasts
MGMT	O^6-methylguanine–DNA methyltransferase

mTORC1	mechanistic target of rapamycin complex 1
MUT	mutant
NC	non-canonical loop
NSCLC	non-small cell lung carcinoma
ROS	reactive oxygen species
TKO	triple knock out
TOFA	5-(Tetradecyloxy)-2-furoic acid
TOP	terminal oligopyrimidine
TSC1/TSC2	tuberous sclerosis complex subunit 1 / 2
uORF	upstream open reading frame
UTR	untranslated region
V	valine
VEGF	vascular endothelial growth factor
W	tryptophan
WHO	World Health Organization
WT	wildtype
Y	tyrosine

II. Summary

Cancer cells are subjected to extrinsic and intrinsic stressors due to the inefficient nature of the tumor vasculature and to oncogenic genetic insults. To survive such hostile conditions, cancer cells need to evolve adaptive responses, such as blocking mRNA translation. One major signaling pathway controlling cap-dependent mRNA translation is the mechanistic target of rapamycin (mTOR)/ eukaryotic initiation factor 4E binding protein (4EBP) pathway. In response to stress conditions, such as nutrient deprivation, mTOR is blocked, thus activating 4EBP1 that in turn binds the translation initiation factor eIF4E to inhibit cap-dependent mRNA translation initiation. The role of 4EBP1 in cancer is controversial. In this thesis, the function and regulation of 4EBP1 was characterized in glioblastoma, which is the most common and most malignant tumor of the central nervous system in adults. Functional assays, such as soft agar assays, and relevant cancer cell models elucidated that 4EBP1 contributes to oncogenic transformation and promotes the tumorigenic potential of glioblastoma cells. The underlying mechanisms implicate 4EBP1-mediated repression of fatty acid synthesis, which allows maintaining the redox balance, thus preventing oxidative stress. To gain further insights into the determining factors of the pro-tumorigenic function of 4EBP1 in glioblastoma cells, the contribution of the *TP53* mutation status was explored and revealed that 4EBP1 promotes tumorigenic potential in *TP53*-wildtype but not in *TP53*-mutant cancer cell lines. Investigation of the clinical relevance of 4EBP1 in glioblastoma uncovered that *EIF4EBP1* (gene encoding 4EBP1) is overexpressed in multiple glioblastoma cohorts and that high *EIF4EBP1* expression associates with poor prognosis. Analysis of cancer patient datasets, combined with molecular approaches and tumor cell models, revealed that the two transcription factors MYBL2 and ETS1 regulate *EIF4EBP1* expression in glioblastoma cells, providing a mechanism for *EIF4EBP1* overexpression in this cancer entity. Following up on these findings, a targeting strategy was designed to selectively inhibit 4EBP1 activity. This took advantage of the results of an *in silico* drug screen followed by validation of several drug candidates using a functional *in vitro* binding assay.

Taken together, the work summarized in this thesis revealed the molecular drivers of *EIF4EBP1* overexpression, characterized the tumor-promoting function of 4EBP1 and highlighted its role in stress adaptation in glioblastomas. The results suggest that targeting of 4EBP1 may represent a possible new approach to treat these yet incurable malignant brain tumors.

III. Zusammenfassung

Aufgrund der ineffizienten Struktur des in Tumoren vorhandenen Gefäßsystems und ihrer onkogenen genetischen Veränderungen sind Krebszellen extrinsischen und intrinsischen Belastungen ausgesetzt. Um solche Bedingungen zu überleben, müssen Krebszellen eine adaptive Antwort, beispielsweise durch Inhibierung der mRNA-Translation, entwickeln. Einer der wesentlichen Signalwege, der die Cap-abhängige mRNA-Translation kontrolliert, ist der mTOR/4EBP (*mechanistic target of rapamycin/eukaryotic initiation factor 4E binding protein*)-Signalweg. Als Reaktion auf Stressbedingungen, beispielsweise Glukosemangel, werden mTOR inhibiert und 4EBP1 aktiviert. Letzteres bindet an den Translationsinitiationsfaktor eIF4E, um die Initiation der Cap-abhängigen mRNA-Translation zu blockieren. Die Rolle von 4EBP1 in Krebs ist derzeit noch umstritten, weshalb in dieser Dissertation die Funktion und Regulierung von 4EBP1 in Glioblastomen, den häufigsten und bösartigsten Tumoren des zentralen Nervensystems im Erwachsenenalter, untersucht wurden. Die Anwendung funktioneller Assays, zum Beispiel des Soft Agar Assays, und relevanter Krebszellmodelle verdeutlichten, dass 4EBP1 zur onkogenen Transformation beiträgt und das pro-tumorigene Potential der Glioblastom-Zelllinien fördert. Der zugrundeliegende Mechanismus ermöglicht die 4EBP1-vermittelte Repression der Fettsäure-Synthese, wodurch das Redox-Gleichgewicht aufrechterhalten und so die Entstehung von oxidativem Stress verhindert wird. Um weitere Erkenntnisse zu den Faktoren zu erlangen, die die Tumorwachstum-fördernde Funktion von 4EBP1 in Glioblastom-Zellen unterstützen, wurde die mögliche Beteiligung des *TP53*-Status untersucht. Die eigenen Ergebnisse zeigten, dass 4EBP1 das pro-tumorigene Potential von *TP53*-Wildtyp- aber nicht von *TP53*-mutierten Krebszelllinien fördert.

Untersuchungen zur möglichen klinischen Relevanz von 4EBP1 in Glioblastompatienten ergaben, dass *EIF4EBP1*, d.h. das für 4EBP1 kodierende Gen, in mehreren Glioblastom-Kohorten überexprimiert war und dass eine hohe *EIF4EBP1*-Expression mit einer schlechten Prognose korrelierte. Durch Analyse von öffentlich zugänglichen molekularen Datensätzen von Patienten mit Krebserkrankungen, kombiniert mit molekularen Untersuchungen in Tumorzellmodellen, wurden die Transkriptionsfaktoren MYBL2 und ETS1 als Regulatoren der *EIF4EBP1*-Expression in Glioblastomzellen identifiziert. Dadurch konnte ein Mechanismus der *EIF4EBP1*-Überexpression in dieser Krebsart erklärt werden. Auf diesen Ergebnissen aufbauend wurde eine Strategie entwickelt, um die 4EBP1-Aktivität selektiv zu inhibieren.

Dabei wurden die Ergebnisse eines *in silico*-Wirkstoffscreenings genutzt, um verschiedene Wirkstoffkandidaten zu identifizieren. Diese wurden anschließend mittels funktionaler *in vitro*-Bindungsexperimente validiert.

Zusammenfassend wurden in dieser Dissertation molekulare Regulatoren der *EIF4EBP1*-Überexpression im Glioblastom identifiziert. Weiterhin wurde die Tumorwachstum fördernde Funktion von 4EBP1 mit dem Fokus auf der Adaption auf Stress charakterisiert. Die erzielten Ergebnisse deuten darauf hin, dass 4EBP1 möglicherweise eine neue therapeutische Zielstruktur ist, um zukünftig Glioblastompatienten besser behandeln zu können.

1. Introduction

1.1. Tumor cells adapt to extracellular and intracellular stress factors during tumor development

Malignant tumors are complex tissue structures consisting of multiple distinct cell types, such as cancer cells, stromal and immune cells, which engage in heterotypic interaction (HANAHAN & WEINBERG 2011). Tumor cells derive from a single normal cell that underwent cellular transformation following multiple oncogenic insults, like for instance MYC overexpression, hyperactivation of RAS or PI3K, or loss of tumor suppressors (RUGGERO 2013). When expanding, cancer cells are confronted to extrinsic, metabolic stress conditions of the tumor microenvironment, due to dysfunctional blood supply. These conditions correspond to hypoxia and depletion of essential nutrients, such as glucose, which are pronounced in the core of the tumor (RUGGERO 2013). While tumor angiogenesis is an important process limiting extrinsic stress by providing cancer cells with enough nutrients and oxygen, it is not efficient. Unlike normal blood vessels, the tumor vasculature is defined by enlarged vessels and irregular branching leading to an unevenly distributed and chaotic vasculature with an irregular perfused blood flow (NAGY *et al.* 2009). In addition, blood vessel density is decreasing with tumor expansion, resulting in differential availability of oxygen and nutrients within the tumor microenvironment. Consequently, some areas within a tumor are metabolically challenged, in particular within the tumor core, which can lead to cell cycle arrest and necrosis (NAGY *et al.* 2009, NAGY *et al.* 2010) (Figure 1). In contrast, cancer cells at proximity to blood vessels are experiencing limited metabolic stress, implying that the heterogeneity of the tumor microenvironment creates niches with distinct levels of metabolic stress within a tumor. This has a strong impact on tumor cells properties. Indeed, tumor cells derived from the tumor core show inferior tumorigenic, migrative and invasive capabilities compared to perivascular-derived tumor cells, which is linked to the level of metabolic stress they encounter (KUMAR *et al.* 2019).

Cancer cells have high energy demands to ensure their rapid proliferation rate. Ensuring proliferation does not only require sufficient amounts of ATP, but also enough macromolecules such as proteins, nucleotides, fatty acids and membrane lipids (HSU & SABATINI 2008). To favor the high demand for macromolecule biosynthesis, cancer cells need to

reprogram their metabolism, which includes induction of the Warburg effect (HSU & SABATINI 2008). The Warburg effect is characterized by increased glucose uptake and its metabolization to ATP through glycolysis, even in aerobic conditions, increased lactate production and decreased oxidative phosphorylation (WARBURG 1956, HSU & SABATINI 2008). Such metabolic features are the results of oncogene activation. In fact, oncogenes such as MYC, RAS or AKT, have been shown to promote glucose uptake, glycolysis and to induce the expression of metabolic genes, hence supporting ATP production (FLIER *et al.* 1987, OSTHUS *et al.* 2000, HSU & SABATINI 2008). However, high glucose consumption by cancer cells, together with the limited supply of environmental glucose due to poor vascularization, lead to a reduction of glucose concentrations in tumor tissues compared to healthy surrounding tissues, as measured in patients (SCHROEDER *et al.* 2005, HIRAYAMA *et al.* 2009). This contributes to create metabolic stress conditions. To cope with such stress and ensure their survival, cancer cells will increase glucose uptake (FLAVAHAN *et al.* 2013), preserve energy and mount an adaptive stress response (reviewed in LEPRIVIER *et al.* 2015). In particular, glucose transporter (GLUT) 1 is upregulated in cancer cells through the action of PI3K/AKT signaling (BARTHEL *et al.* 1999, WIEMAN *et al.* 2007) and RAS oncoproteins (MURAKAMI *et al.* 1992).

Besides metabolic stress, cells have to cope with intrinsic, oxidative stress which accompanies oncogenic transformation. Oncogene activation leads to the stimulation of anabolism and redirects the consumption of co-factors, which are required for antioxidant reactions, leading to a potential accumulation of intracellular reactive oxygen species (ROS) (DENICOLA *et al.* 2011, TRUITT *et al.* 2015). Cells expressing active oncoproteins are unable to become transformed unless they manage to control redox balance and intracellular ROS levels, which they do so by enhancing antioxidant capacity. Indeed, it was shown that the KRAS, MYC, ETV6-NTRK3 and eIF4E oncoproteins direct a transcriptional or translational program supporting increased intracellular antioxidant capacities (DENICOLA *et al.* 2011, TRUITT *et al.* 2015, LIM *et al.* 2019). This program is in part mediated by the master regulator of antioxidant response and transcription factor NRF2, which is required for oncogenic KRAS-driven proliferation and tumorigenesis *in vitro* and *in vivo* (DENICOLA *et al.* 2011). This indicates that neoplastic cells need to maintain their intracellular redox balance, since uncontrolled accumulation of ROS would otherwise prevent cellular transformation and cancer growth. Overall, tumor cells are exposed to a heterogenous tumor microenvironment confronting them with different types of intrinsic and extrinsic stressors that they need to adapt to for ensuring their survival.

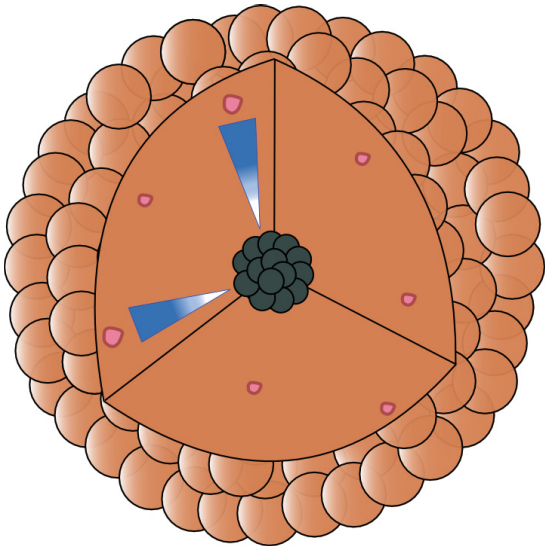

Figure 1: Schematic representation of metabolic heterogeneity within the tumor environment. The unevenly distributed and deficient vasculature (represented by red circles) creates a gradient of nutrient and oxygen availability (blue/white triangle) within a tumor, resulting in a necrotic tumor core (black mass).

1.2. The control of mRNA translation drives metabolic stress response during tumor development

Given that tumor cells are confronted to metabolic stress, tumor progression is highly dependent on the ability of tumor cells to evolve an adaptive response to promote their survival (LEPRIVIER *et al.* 2015). To do so, tumor cells need to preserve their energetic balance. Tumor cells preserve their energy by reprogramming metabolism in a similar manner as normal cells confronted to physiological conditions of ATP depletion. This is achieved, on the one hand, by stimulating catabolic processes like autophagy, which enables cells to break-down proteins and organelles into metabolites that can be recycled and used as an energy source (HANAHAN & WEINBERG 2011). On the other hand, such a metabolic reprogramming relies on the inhibition of anabolic processes, such as protein synthesis (CHOO *et al.* 2010, LIU & QIAN 2014, LEPRIVIER *et al.* 2015), the most highly energy consuming process in a cell (BUTTGEREIT & BRAND 1995). In particular, severe hypoxia quickly reduces rates of protein synthesis by half in normal and cancer cells (KORITZINSKY *et al.* 2007) while nutrient deprivation results in a strong and rapid inhibition of overall mRNA translation rates in both normal and cancer cells (LEPRIVIER & SORENSEN 2014). In accord with the metabolic heterogeneity of the tumor microenvironment, transcriptome and metabolome analysis showed that perivascular cancer cells have a higher rate of protein synthesis and elevated energy production as compared to cancer cells located in hypovascularized tumor regions, where metabolic stress is more

pronounced (KUMAR *et al.* 2019). In response to metabolic stress, restriction of protein synthesis activity is a requirement for cancer cells to avoid cell death (LEPRIVIER *et al.* 2015). The control of protein synthesis is mediated by key signalling pathways, constituted of sensor and regulator proteins, which accommodate rates of protein synthesis to nutrient availability. These pathways, which are evolutionary conserved, coordinate the biological response of normal cells to energy depletion, and are hijacked by tumor cells to adapt to metabolic stress (LEPRIVIER *et al.* 2013, LEPRIVIER *et al.* 2015).

The mTOR pathway

One major signalling pathway that controls protein synthesis and coordinates the response to metabolic stress at the cellular level is the nutrient-sensing mechanistic target of rapamycin (mTOR) pathway, with its central hub mTOR complex 1 (mTORC1) (LAPLANTE & SABATINI 2012). This complex functions as a central metabolic mediator controlling the balance between anabolism and catabolism (SAXTON & SABATINI 2017). In response to energy depletion, the major energy sensor adenosine monophosphate (AMP) activated protein kinase (AMPK) is stimulated, in turn repressing mTORC1. This occurs by activation of the negative regulator of mTORC1 tuberous sclerosis complex proteins 1 and 2 (TSC1/TSC2) by AMPK. This event leads to inhibition of cap-dependent mRNA translation at the initiation step (SENGUPTA *et al.* 2010). Such a negative regulation of mTORC1 in response to metabolic stress may appear paradoxical given that mTORC1 is hyperactive in tumors and stimulates cancer cell proliferation (HAY & SONENBERG 2004, LIU & SABATINI 2020). However, this can be reconciled as mTORC1 activity within a tumor depends on the proximity of blood vessels. Indeed, previous studies clearly indicated that glioblastoma cells exhibit reduced mTORC1 activity, in parallel with higher TSC1 levels, the further they are located from the blood vessels (KUMAR *et al.* 2019). Additionally, *in vivo* experiments showed that glioblastoma (KUMAR *et al.* 2019) and pancreatic cancer cells (PALM *et al.* 2015) are more proliferative in the outer tumor region compared to the inner tumor region, which is hypovascularized and therefore more prone to metabolic stress. The overall consequence is that treatment with mTOR inhibitors, which are being developed for clinical use in cancer patients, has disparate effects depending on the intratumoral levels of metabolic stress. Indeed, application of the mTORC1 inhibitor rapamycin in a mouse model of pancreatic tumors resulted in decreased cell proliferation in outer, well vascularized tumor regions but increased cell proliferation in the inner hypovascularized regions (PALM *et al.*

2015). In this model, the overall effect of such a treatment on tumor development was, unexpectedly, an acceleration of tumor growth (PALM *et al.* 2015). Therefore, while mTORC1 supports proliferation of tumor cells in nutrient rich regions of tumors (areas in proximity of blood vessels), mTORC1 needs to be blocked to promote tumor cell survival in hypovascularized tumor regions characterized by metabolic stress, which on the long term supports tumor development.

1.3. 4EBP1 - a mTORC1 substrate

One of the mTORC1 substrates involved in regulating mRNA translation initiation is the eukaryotic initiation factor 4E binding protein 1 (4EBP1), a member of the 4EBP family which consist of three homologs 4EBP1, 2 and 3 (HAY & SONENBERG 2004). 4EBP1 is responsible of inhibiting mRNA translation initiation in response to various stressors as detailed below.

1.3.1. Regulation of 4EBP1 activity and expression

Post-translational regulation of 4EBP1

The activity of 4EBP1 is regulated by the mTOR kinase through phosphorylation induced in response to different stressors, especially glucose, growth factor and amino acid deprivation as well as hypoxia (LEPRIVIER *et al.* 2015). 4EBP1 contains two motifs, the C-terminally located TOR signaling motif (TOS), which is conserved and found in other mTORC1 substrates, and the N-terminally located RAIP binding motif, which is conserved within the 4EBP family but otherwise much less defined than the TOR signaling motif (TEE & PROUD 2002, NOJIMA *et al.* 2003) (Figure 2). Via those two motifs 4EBP1 interacts with the substrate binding unit of the mTORC1, namely Raptor, in a bidentate fashion (BÖHM *et al.* 2021). This interaction is important for the mTORC1 to regulate 4EBP1 activity by phosphorylation of multiple residues in absence of stress factors. First, 4EBP1 Thr^{37} and Thr^{46} and subsequently Ser^{65}, Thr^{70} and Ser^{83} get phosphorylated by the catalytic subunit of mTOR, rendering 4EBP1 inactive (GINGRAS *et al.* 1999, GINGRAS *et al.* 2001). The more residues are phosphorylated, the stronger is 4EBP1 inactivation. Phosphorylation of 4EBP1 prevents binding to its protein interactor eukaryotic translation initiation factor 4E (eIF4E) (BÖHM *et al.* 2021) and allows mRNA translation to initiate, as detailed below (Figure 3). In contrast, in cells experiencing metabolic stress, because mTORC1 is blocked, this results in unphosphorylated and active 4EBP1 (GINGRAS *et al.* 1999, DING *et al.* 2018).

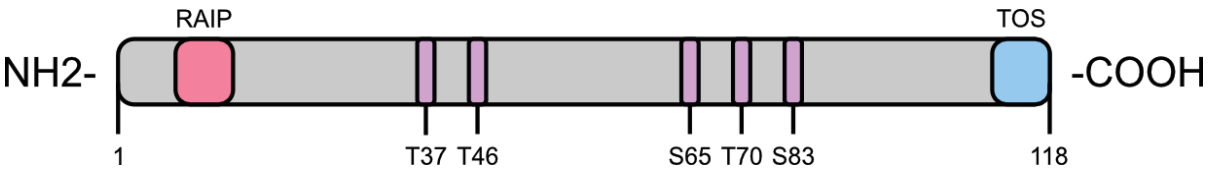

Figure 2: Schematic representation of the 4EBP1 structure including Raptor binding motifs and mTORC1 phosphorylation sites. This scheme was adapted from Musa *et al.* 2016 (MUSA *et al.* 2016). TOS: C-terminally located TOR signaling motif

Transcriptional regulation of *EIF4EBP1*

Besides post-translational regulation, expression of 4EBP1 is also regulated at the transcriptional level. Few transcription factors have been characterized to bind the 4EBP1 encoding gene *EIF4EBP1* promoter and stimulate *EIF4EBP1* transcription in normal and cancer cells. In particular, *EIF4EBP1* expression is induced in response to amino acid starvation and endoplasmic reticulum (ER) stress in various cellular models as a result of ATF4 (YAMAGUCHI *et al.* 2008, KANG *et al.* 2017, TAMEIRE *et al.* 2019) and ATF5 binding to the promoter and transcriptional regulatory region of *EIF4EBP1* (JULIANA *et al.* 2017). In support to that, co-expression of *EIF4EBP1* with ATF4 target genes was observed in various cell lines including human Burkitt's lymphoma cell lines, breast cancer cell lines and colon cancer cell lines. Additionally, ATF4 has been shown to co-regulate *EIF4EBP1* transcription together with MYC. Chromatin immunoprecipitation (ChIP) - sequencing (seq) data revealed common overlapping binding sites of ATF4 and MYC within the *EIF4EBP1* transcriptional regulatory region in a colon adenocarcinoma cell line (TAMEIRE *et al.* 2019). Another report states that MYC alone can induce the *EIF4EBP1* promoter by binding to three E-boxes (MYC binding motifs) (BALAKUMARAN *et al.* 2009). Similarly, MYCN, a member of the MYC oncogene family, induces *EIF4EBP1* promoter activity through three E-boxes (K. Völtzke, personal communication; see Appendix: 6.4. Manuscript III). Expression of *MYC* and *MYCN* each correlated with significantly increased *EIF4EBP1* levels in patients with prostate cancer (BALAKUMARAN *et al.* 2009) or neuroblastoma (K. Völtzke, personal communication; see Appendix: 6.4. Manuscript III), respectively, highlighting the clinical relevance of such transcriptional regulation of *EIF4EBP1*. Another transcription factor that binds and transcriptionally regulates the *EIF4EBP1* promoter in prostate cancer cells is the androgen receptor (LIU *et al.* 2019). It binds to a semi-palindromic response element, located within the *EIF4EBP1* transcriptional regulatory region, which is also known to be recognized by other nuclear receptors (ADLER *et al.* 1993, HSIEH *et al.* 2007). In prostate cancer patients, the expression of the androgen receptor was found to be correlated

with *EIF4EBP1* expression (LIU *et al.* 2019). The *EIF4EBP1* promoter is also regulated by the transcriptional repressor EGR-1, which binds upstream of the transcription start site (ROLLI-DERKINDEREN *et al.* 2003). Interestingly, EGR-1 dissociated from the *EIF4EBP1* promoter upon increases of cell density, in pancreatic cancer cells, allowing HIF-1A to associate with the promoter (AZAR *et al.* 2013). In response to hypoxia, HIF-1A controls *EIF4EBP1* expression by forming a complex with Smad4 in pancreatic cancer cells (AZAR *et al.* 2013). Smad 3/4 interact with the Smad-binding element in the *EIF4EBP1* transcriptional regulatory region and are able to transcriptionally activate it without HIF-1A (AZAR *et al.* 2009). However, in cell lines with homozygous *SMAD4* deletion *EIF4EBP1* levels increased only slightly in response to hypoxia (AZAR *et al.* 2013), suggesting that HIF-1A needs SMAD4 to transcriptionally activate the *EIF4EBP1* promoter. Taken together these data suggest that *EIF4EBP1* expression and not only 4EBP1 activity is regulated by intracellular or extracellular stressors. It remains to be determined whether other transcription factors are involved in the regulation of *EIF4EBP1*.

1.3.2. Molecular function of 4EBP1

The main molecular function of 4EBP1 is to block cap-dependent mRNA translation by interacting with its binding partner eIF4E (HAY & SONENBERG 2004). EIF4E is a translation initiation factor and the key regulator of cap-dependent mRNA translation, which recognizes the m^7G cap-structure located on the 5' end of mRNAs (HAY & SONENBERG 2004). EIF4E associates with other translation initiation factors, amongst them the scaffolding protein eIF4G and the RNA helicase eIF4A, to form the mRNA translation pre-initiation complex eIF4F. This complex facilitates ribosome recruitment near the start codon, resulting in mRNA translation initiation (Figure 3A). In response to stress, when 4EBP1 is unphosphorylated and therefore active, it binds eIF4E thus preventing the assembly of the eIF4F complex and precluding mRNA translation to initiate (Figure 3B). 4EBP1 has three main structural/binding motifs that allow interaction with eIF4E. On the N-terminal end, 4EBP1 possesses a canonical (Ca) α-helix, which binds to the dorsal surface of eIF4E. This motif is followed by an elbow loop (EL), which bends the peptide backbone by 90° and enables the interaction of another motif, the non-canonical loop (NC-loop) with the lateral surface of eIF4E (PETER *et al.* 2015) (Figure 4). However, 4EBP1 is not the only factor binding eIF4E; eIF4G also binds to the dorsal surface of eIF4E as it possesses a highly similar Ca α-helix motif. This creates a binding competition between 4EBP1 and eIF4G (HAGHIGHAT *et al.* 1995, MADER *et al.* 1995) (Figure 4). Although

eIF4G is lacking the NC-loop motif, it has a similar binding affinity as 4EBP1 to eIF4E *in vitro* due to the canonical loop (IGREJA *et al.* 2014). In cells, the NC-loop gives 4EBP1 an advantage in the binding competition, thus, 4EBP1 will preferentially bind eIF4E upon stress and prevent eIF4G binding (GROSS *et al.* 2003, IGREJA *et al.* 2014).

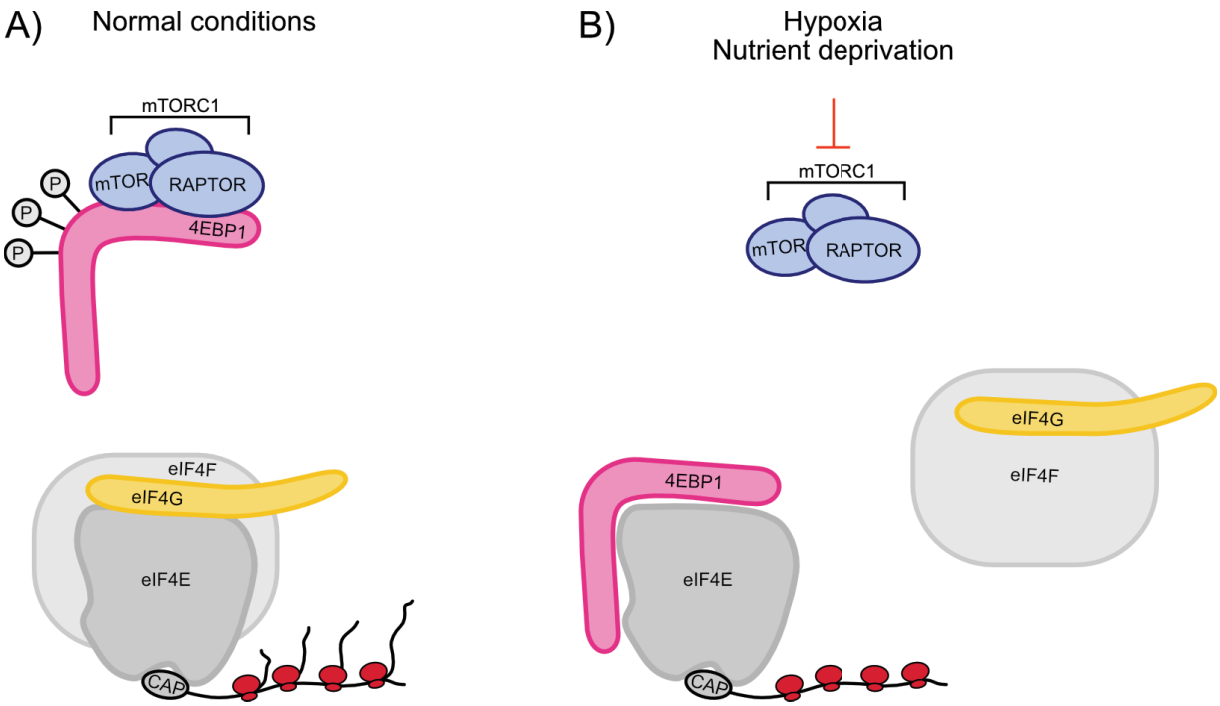

Figure 3: Regulation of mRNA translation initiation by the mTORC1-4EBP1 axis under normal and stress conditions. A) 4EBP1 is phosphorylated and inactive under normal conditions, due to the action of mTORC1, which allows the assembly of the pre-initiation complex resulting in cap-dependent mRNA translation initiation. B) Under extrinsic stress conditions, mTORC1 is blocked, which renders 4EBP1 active. 4EBP1 thus binds to eIF4E, preventing pre-initiation complex formation and cap-dependent translation initiation.

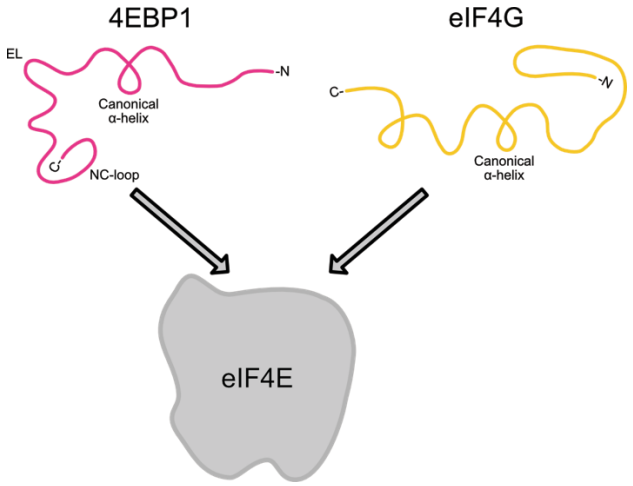

Figure 4: Schematic representation of the eIF4E binding motifs of 4EBP1 and eIF4G. Elements of this figure are adapted from Peter *et al.* 2015 (PETER *et al.* 2015).

As mRNA translation is the most energy consuming process (BUTTGEREIT & BRAND 1995), it is tightly regulated in response to metabolic stress, in particular at the initiation step which is the rate limiting step of mRNA translation (DE BENEDETTI & GRAFF 2004). When active, 4EBP1 inhibits the formation of the eIF4F complex, which results in the inhibition of overall mRNA translation (HAY & SONENBERG 2004). However, recent work indicates that 4EBP1 exerts a more selective action on mRNA translation as it can inhibit or promote the translation of specific transcripts. 4EBP1 can selectively inhibit mRNA translation in different ways. For instance, 4EBP1 selectively blocks the translation of mRNAs containing a 5' terminal oligopyrimidine (TOP) motif, recognized and bound by eIF4E (THOREEN *et al.* 2012), which is mainly found in ribosomal proteins and elongation factors encoding transcripts. By selectively reducing the translation of such mRNAs involved in protein synthesis, 4EBP1 activity consequently leads to reduction of rates of global protein synthesis. The existence of a TOP motif within the 5'UTRs of many mTOR sensitive transcripts has been validated in another study, which also identified another pyrimidine-rich translational element mediating 4EBP1 selectivity (HSIEH *et al.* 2012). The 5'UTRs can contain those two motifs either individually or together. Analysis revealed that most mRNAs containing those motifs are involved in promoting cancer cells migration and invasion (HSIEH *et al.* 2012). A third cytosine-rich motif, named cytosine-enriched regulator of translation (CERT), was deciphered within 4EBP1/eIF4E-sensitive mRNAs, while the length or GC content of 5'UTRs was ruled out as determinants of selective mRNA translation. Oncogenic transformation induced by eIF4E leads to preferential translation of eIF4E target mRNAs containing the CERT motif, such as oxidative stress response encoded transcripts (TRUITT *et al.* 2015). Together those reports characterized a multifaceted system of 5'UTR structural motifs, which serve to mediate selective translational inhibition by 4EBP1 through its interaction with eIF4E.

In contrast, 4EBP1 has been reported to selectively promote translation of specific transcripts. In *Drosophila*, the 4EBP1 ortholog d4EBP supports selective translation of mRNAs under dietary restricted conditions, while overall mRNA translation rate is decreased (ZID *et al.* 2009). Such subset of mRNAs encodes proteins necessary for mitochondrial ATP generation and oxidative phosphorylation, which are critical for the response to dietary restriction. The mechanism underlying 4EBP1-mediated selective mRNA translation relies on structural properties of the 5'UTRs (ZID *et al.* 2009). It was proposed that translation of mRNAs containing short 5' UTRs with a weak secondary structure was preferentially upregulated by

4EBP1 under dietary restricted conditions (ZID *et al.* 2009). In mammals, 4EBP1 was reported to mediate a translational switch by inhibiting cap-dependent mRNA translation while promoting cap-independent translation of specific transcripts under hypoxic conditions. Cap-independent translation represents an alternative mechanism of mRNA translation initiation that allows specific transcripts to escape global translational repression, particularly in response to stress. By mediating a translational switch in response to hypoxia, 4EBP1 induces the selective translation of internal ribosome entry site (IRES) containing mRNAs, such as *vascular endothelial growth factor* (*VEGF*) and *HIF-1A* (BRAUNSTEIN *et al.* 2007). Taken together, these reports indicate that active 4EBP1 controls selective translation of a certain subset of mRNA transcripts either by preventing the interaction of the mRNAs with eIF4E or by supporting selective translation, especially under stress conditions.

1.3.3. Cellular functions of 4EBP1

The main cellular functions of 4EBP1 are to control cellular proliferation and mitochondrial activity in response to intracellular and extracellular stress factors.

4EBP1 blocks proliferation under metabolic stress

Cell growth (increase in cell mass) and cell cycle progression are two tightly coupled processes allowing cells to proliferate while maintaining their size. This coupling is crucial since rapidly proliferating cells would undergo cell death if they are unable to keep up their size (FINGAR & BLENIS 2004). Rates of proliferation are modulated upon nutritional stimuli, which is orchestrated by the mTOR pathway and 4EBP1 through the control of mRNA translation (FINGAR *et al.* 2004, DOWLING *et al.* 2010). The control of proliferation and cell growth by mTOR is conserved in various species such as yeast, *Drosophila* and mammals (reviewed in SCHMELZLE & HALL 2000, JACINTO & HALL 2003, OLDHAM & HAFEN 2003). Various experiments point to mTORC1 and 4EBP1 as important regulators of cell cycle progression, proliferation and cell size. The impact of 4EBP1 on cell size is seemingly contradictory, as opposing results have been reported. Initially, it has been reported that the overexpression of constitutively active 4EBP1 leads to reduced cell size in a human osteosarcoma cell line (FINGAR *et al.* 2002). A more recent and more substantiated study demonstrated that while mTORC1 inhibition results in decreased cell size of mouse embryonic fibroblasts (MEFs), this also occurred in absence of 4EBP1/2 (DOWLING *et al.* 2010). The results of Dowling *et al.* (2010) convincingly support that

4EBP1/2 are not involved in regulating cell size. The function of 4EBP1/2 in cell cycle progression and proliferation is well established. Treatment of rat fibroblasts with the mTOR inhibitor rapamycin resulted in blocking of cell cycle progression in all cell cycle phases (FINGAR *et al.* 2002), while eIF4E overexpression resulted in accelerated S-phase entry (FINGAR *et al.* 2002, FINGAR *et al.* 2004). These earlier reports strongly suggested that 4EBP1, as an eIF4E inhibitor, might play a role in halting cell cycle progression. In particular, studies showed that active 4EBP1 impaired cell cycle progression from G1 to S-phase (FINGAR *et al.* 2004). A more recent study demonstrated that 4EBP1/2 are critical regulators of proliferation downstream of mTORC1. Dowling *et al.* (2010) revealed that genetic or pharmacological inactivation of mTORC1 decreased proliferation rate of 4EBP1/2 wild type cells, but not of 4EBP1/2 double knock out (DKO) or knock down cells which keep proliferating (DOWLING *et al.* 2010). Furthermore, 4EBP1/2 have been shown to control proliferation rates in response to metabolic stress. Serum or amino acid starvation, while impairing mTORC1 activity and activating 4EBP1, leads to a decreased proliferation rate only in 4EBP1/2 wild type MEFs, but not in 4EBP1/2 DKO MEFs. The function of 4EBP1/2 in restraining proliferation is due to 4EBP1/2-mediated selective inhibition of translation of three important pro-proliferative factors encoding mRNAs, namely *ornithine decarboxylase*, *cyclin D3* and *VEGF* (DOWLING *et al.* 2010). Taken together, metabolic stressors, such as serum starvation and amino acids starvation, activate 4EBP1/2, which thus restrain cell proliferation by selectively inhibiting mRNA translation.

4EBP1 regulates mitochondrial activity through selective translation

Mitochondria are the main ATP producers and their activity is important to meet the high energy demand of specific anabolic processes, such as mRNA translation. At the same time, a balance between energy production and consumption has to be met, especially under stress conditions (BUTTGEREIT & BRAND 1995). Such a balance is orchestrated by the mTOR pathway, which adjusts both protein synthesis and mitochondrial activities according to energy levels. Indeed, mTORC1 inhibition decreases mitochondrial respiration, resulting in decreased ATP turnover and reduced ATP levels (MORITA *et al.* 2013). These effects on mitochondrial respiration and energy metabolism were shown to be mediated by 4EBP1/2 *in vitro* and *in vivo* (MORITA *et al.* 2013). MTORC1 inhibition also resulted in decreased levels of mitochondrial DNA, indicating restriction of mitochondrial biogenesis, which was demonstrated to be due to

the action of 4EBP1/2 (MORITA *et al.* 2013). The proposed mechanism is that 4EBP1/2 selectively repress synthesis of a subset of mitochondrial-related proteins, ATP synthase (such as ATP50) or transcription factors regulating mitochondrial genes, like TFAM (MORITA *et al.* 2013). Together, these data show that 4EBP1 blocks mitochondrial activity and biogenesis by selectively repressing translation of a subset of mitochondrial-related transcripts.

The impact of 4EBP1/2 on regulating mitochondrial activity under stress was also investigated in a *Drosophila* model (ZID *et al.* 2009). Upon dietary restriction, rates of overall mRNA translation decreases, while the translation of mitochondrial proteins increases in d4EBP-wildtype flies but not in 4EBP1-KO flies. This indicates that d4EBP selectively mediates translation of mitochondrial proteins under dietary restriction, which was shown to support mitochondrial activity (ZID *et al.* 2009). This was linked to increased survival span of flies with d4EBP compared to d4EBP null flies under dietary restricted conditions (ZID *et al.* 2009). Together, these studies (ZID *et al.* 2009, MORITA *et al.* 2013) do not allow to ascertain the role of 4EBP1 in regulating mitochondrial activity, as reported results appear contradictory. An explanation might be the different study design. Zid *et al.* (2009) used a physiological approach with *Drosophila*, which were subjected to nutrient deprivation, whereas Morita *et al.* (2013) treated MEFs with an mTORC1 inhibitor. Overall, 4EBP1 regulates mitochondrial activity by selective regulation of mRNA translation which leads to repression or promotion of mitochondrial activity, depending on the type of model and the environmental stimuli.

1.3.4. Function of 4EBP1 in cancer

The precise role of 4EBP1 in cancer is still under investigation since reports in the literature point either to pro- or anti-oncogenic functions.

Tumor suppressive role of 4EBP1

4EBP1 is considered a tumor suppressor due to its ability to bind to and repress the oncoprotein eIF4E, which was shown to transform mouse and rat fibroblasts *in vitro* and *in vivo* when overexpressed (LAZARIS-KARATZAS *et al.* 1990). Active 4EBP1 results in selective translational inhibition of pro-proliferative mRNAs, thus hampering cell proliferation in various cancer cell lines (DOWLING *et al.* 2010, LIU *et al.* 2019) and prostate tumor growth *in vivo* (LIU *et al.* 2019). In addition, using wild type and 4EBP1/2 DKO mice it was reported that

4EBP1/2 reduce susceptibility to chemical induction of head and neck squamous cell carcinoma *in vivo* (WANG *et al.* 2019) and that 4EBP1/2 restrict growth of prostate cancer in a genetically engineered mouse model of prostate cancer driven by loss of the tumor suppressor PTEN (DING *et al.* 2018). In particular, triple KO (TKO) of 4EBP1/2 and PTEN reduced mouse survival when compared to PTEN KO mice (DING *et al.* 2018). A similar finding was also observed with p53 and 4EBP1/2 TKO mice, as these animals exhibited a significantly lower tumor-free survival compared to p53 KO mice (PETROULAKIS *et al.* 2009). Consistently, overexpression of a constitutively active 4EBP1 mutant reduced growth of head and neck squamous cell carcinomas in mice, which was linked to decreased proliferation rates and enhanced apoptosis in the tumors (WANG *et al.* 2019). However, the reported function of 4EBP1 on apoptosis in other models is contradictory, and thus it cannot be concluded that the regulation of apoptosis by 4EBP1 contributes to its tumor suppressive role (LI *et al.* 2002, YELLEN *et al.* 2011, BI *et al.* 2017). In addition, 4EBP1/2 contribute to decrease vascular density in prostate tumors of the PTEN-deficient mouse model of prostate cancer (DING *et al.* 2018), which may represent another mechanism of 4EBP1/2-mediated tumor suppression. While these findings together are supporting that 4EBP1 behaves as a tumor suppressor, it is noteworthy to mention that 4EBP1 KO or 4EBP1/2 DKO mice do not develop tumors spontaneously (TSUKIYAMA-KOHARA *et al.* 2001, DING *et al.* 2018, WANG *et al.* 2019), excluding 4EBP1 as a genuine tumor suppressor.

Pro-tumorigenic role of 4EBP1

A number of studies highlight a potential pro-tumorigenic function of 4EBP1 in response to specific stress. In particular, 4EBP1 was demonstrated to play a role in the response of cancer cells to hypoxia. Indeed, 4EBP1 was shown to protect prostate carcinoma, colon carcinoma and glioblastoma cells from hypoxia-induced cell death (DUBOIS *et al.* 2009, DING *et al.* 2018). In addition, in response to hypoxia 4EBP1 reprograms breast cancer cells to induce angiogenesis, eventually supporting tumor growth (BRAUNSTEIN *et al.* 2007). 4EBP1 holds an important role in promoting angiogenesis by stimulating expression of VEGF, as it was demonstrated in ovarian and breast cancer models *in vitro* and *in vivo* (BRAUNSTEIN *et al.* 2007, LEE *et al.* 2016). Another common intrinsic stress cancer cells are subjected to is ER stress, which can be caused by abnormal protein synthesis activity leading to accumulation of misfolded proteins (HARDING *et al.* 2000). MYC overexpression is known to enhance protein

synthesis and induce ER stress, as observed in colorectal carcinoma (BEN-DAVID *et al.* 2014), which if unresolved can lead to apoptosis (TAMEIRE *et al.* 2019). It was proposed that 4EBP1, by inhibiting protein synthesis activity, reduces MYC-induced ER stress, thus preventing cell death of MYC-driven colon carcinoma cell lines (TAMEIRE *et al.* 2019). The pro-tumorigenic function of 4EBP1 is further supported by another study demonstrating that 4EBP1 is required for RAS oncogenic transformation of MEFs *in vivo* and *in vitro* (PETROULAKIS et al. 2009). Indeed, 4EBP1/2 KO was shown to reduce colony formation ability of RAS expressing MEFs, as monitored by focus forming and soft agar assays, and to prevent tumor formation *in vivo*, compared to RAS expressing 4EBP1/2 WT cells (PETROULAKIS *et al.* 2009). However, this effect was only observed in p53 WT or $p53^{-/+}$ MEFs, but not in $p53^{-/-}$ MEFs, indicating that 4EBP1 pro-tumorigenic function requires an intact p53 protein. It was reported that p53 KO restored colony forming potential of RAS expressing 4EBP1/2 DKO cells. These results were linked to the regulation of senescence by p53, downstream of 4EBP1/2. Petroulakis *et al.* (2009) observed that 4EBP1/2 prevent the stabilization of p53, which normally induces senescence, leading to abrogated senescence thus allowing transformation of primary MEFs expressing RAS. Based on the literature, the function of 4EBP1 in cancer cannot be clearly defined. It can be proposed that the role of 4EBP1 in cancer depends on the tumor type, with a pro-tumorigenic function possibly in the tumor types harboring severe metabolic stress, as well as on the expression status of the tumor suppressor gene *TP53*.

Clinical relevance of *EIF4EBP1* in cancer

In accordance with the cancer type-specific function of 4EBP1, the clinical relevance of 4EBP1 expression is strongly dependent on the tumor entity. Loss and low levels of *EIF4EBP1* have been linked to poor survival of patients with prostate cancer (DING *et al.* 2018) or head and neck squamous cell carcinoma (WANG *et al.* 2019). On the contrary, a recent study reported elevated levels of *EIF4EBP1* in a number of adult tumor entities based on The Cancer Genome Atlas (TCGA) data sets, and that high *EIF4EBP1* levels are associated with poor survival in all TCGA cancer entities combined (WU & WAGNER 2021). More specifically, *EIF4EBP1*, as part of the 8p11-12 amplicon, is frequently amplified in breast cancer and high *EIF4EBP1* expression is correlated with poor prognosis in this tumor type (KARLSSON *et al.* 2011, KARLSSON *et al.* 2013, RUTKOVSKY *et al.* 2019). Furthermore, patients with high *EIF4EBP1* expression have decreased relapse-free survival (KARLSSON *et al.* 2011, RUTKOVSKY *et al.* 2019) and do not respond to chemotherapy or endocrine treatment as well as patients expressing low *EIF4EBP1* levels

(KARLSSON *et al.* 2013, RUTKOVSKY *et al.* 2019). In neuroblastoma, *EIF4EBP1* expression is increased according to disease aggressiveness (K. Völtzke, personal communication; see Appendix: 6.4. Manuscript III). Furthermore, high *EIF4EBP1* expression has also been linked to poor survival in patients with colorectal cancer (CHAO *et al.* 2015), hepatocellular carcinoma (CHA *et al.* 2015), neuroblastoma (K. Völtzke, personal communication; see Appendix: 6.4. Manuscript III) or diffuse large B-cell lymphoma (TAMEIRE *et al.* 2019). While the prognostic relevance of *EIF4EBP1* expression has been investigated in few tumor entities, it has not been explored in a large number of other cancer types which warrants further investigation.

1.4. Glioblastoma

1.4.1. Metabolic heterogeneity of glioblastoma

Glioblastomas belong to the group of diffuse gliomas and are the most common and most malignant primary glial tumor type of the central nervous system in adults that correspond to the World Health Organization (WHO) grade 4 (LOUIS *et al.* 2007, LOUIS *et al.* 2016, OSTROM *et al.* 2017, LOUIS *et al.* 2021). Glioblastomas grow invasively in the brain parenchyma, are highly proliferative and angiogenic (DECORDOVA *et al.* 2020). This tumor entity is highly heterogenous in terms of cell types (DECORDOVA *et al.* 2020), as it might be constituted of up to 30% macrophages (BADIE & SCHARTNER 2001). Compared to lower grade gliomas, glioblastomas are characterized by development of a necrotic core (LOUIS *et al.* 2007), creating intra-tumoral metabolic heterogeneity (TEICHER *et al.* 1981, OKUNIEFF *et al.* 1993, TEICHER 1994, HUANG *et al.* 2016, KUMAR *et al.* 2019, DECORDOVA *et al.* 2020). The necrotic core is surrounded by dense packing of neoplastic cells, which migrated away from the acidic necrotic area. The arrangements of stacked rows of elongated nuclei of the neoplastic cells leads to a pseudo-palisade like appearance commonly seen in glioblastoma tissue sections (BRAT & MAPSTONE 2003, BRAT *et al.* 2004, WIPPOLD *et al.* 2006, KUMAR *et al.* 2019). Necrosis forms due to hypoxia (TEICHER *et al.* 1981, OKUNIEFF *et al.* 1993, TEICHER 1994, HUANG *et al.* 2016, KUMAR *et al.* 2019) and likely to glucose-deprived conditions (TANAKA *et al.* 2021), which may be more pronounced in this type of cancer given that glucose concentrations in the brain are low compared to plasma glycemia (GRUETTER *et al.* 1992, FELLOWS & BOUTELLE 1993). This indicates that glioblastoma cells are exposed to metabolic stress. While such challenging metabolic conditions are inducing massive cell death of glioblastoma cells, with estimated rates of 69% to 92% cell death (KÖRBER *et al.* 2019), some glioblastoma cell clones are adapting. The

heterogenous cancer cell population, which is composed of differentiated and undifferentiated tumor cells exhibiting different morphologies and capacities for self-renewal and proliferation (BONAVIA *et al.* 2011, SOEDA *et al.* 2015), allows for the selection of tumor clones with more aggressive traits by stress conditions (FLAVAHAN *et al.* 2013, DECORDOVA *et al.* 2020). In particular, hypoxia was shown to select for glioblastoma cancer clones with more aggressive features, as it promotes the expansion of cancer stem cells and induces upregulation of stem cell markers in non-stem cancer cells, resulting in a stem-cell like phenotype (HEDDLESTON *et al.* 2009). Similarly, glucose deprived conditions favour enrichment of a more tumorigenic glioblastoma cell population referred to as brain tumor initiating cells (BITC) (FLAVAHAN *et al.* 2013). These cells, which express stem cell markers, are able to differentiate toward multiple lineages, and exhibit resistance to radio- and chemotherapy (FLAVAHAN *et al.* 2013), have been observed in necrotic areas of glioblastoma tissues (LI *et al.* 2009). Exposure of glioblastoma cells derived from dissociated tumors to glucose restriction enhanced the frequency of BITC (FLAVAHAN *et al.* 2013), and increased tumorigenic potential *in vivo* as evidenced by decreased survival of orthotopically transplanted mice (FLAVAHAN *et al.* 2013). Glioblastoma intra-tumoral clonal and metabolic heterogeneity is connected to treatment failure as well as disease recurrence (YAES 1989, MURAT *et al.* 2008, BEDARD *et al.* 2013). Therefore, even with the standard of care treatment the median survival time is only around 15 months after diagnosis (LOUIS *et al.* 2016) while without treatment the median survival time is as short as three months after diagnosis (MALMSTROM *et al.* 2012).

1.4.2. Glioblastoma classification

Until recently glioblastomas were classified by the WHO classification of CNS tumors as either isocitrate dehydrogenase (IDH)-WT or IDH-mutant glioblastoma (LOUIS *et al.* 2016). The IDH status is one of the molecular key factors for glioma classification and the most important prognostic factor, as IDH-mutant gliomas associate with a better survival in comparison to IDH-WT gliomas (KAMINSKA *et al.* 2019). In 2021 the WHO revised the classification for glioblastomas (LOUIS *et al.* 2021). While the term glioblastoma, CNS WHO grade 4 now comprises only IDH-WT tumors (LOUIS *et al.* 2021), the former IDH-mutant glioblastomas are now referred to as IDH-mutant astrocytoma, CNS WHO grade 4 (LOUIS *et al.* 2021). In this thesis, the term malignant glioma or glioblastoma refers to the old classification and includes

IDH-WT and the former IDH-mutant glioblastomas. If information or data are specifically referring to IDH-WT glioblastoma, it will be indicated as such.

1.4.3. Genetic evolution of IDH-WT glioblastoma

The initiation and progression of IDH-WT glioblastomas is driven by genetic alterations that inactivate tumor suppressor genes like *PTEN*, *CDKN2A, RB1, NF1* and *TP53*, or activate cellular oncogenes like *EGFR, PDGFRA, CDK4, MDM2* and *PIK3CA* (AGNIHOTRI *et al.* 2013, BRENNAN *et al.* 2013, SOTTORIVA *et al.* 2013, BRAT *et al.* 2018, KÖRBER *et al.* 2019). In addition, chromosome 7 gain and chromosome 10 loss are common alterations detected in the majority of IDH-WT glioblastoma patient samples (SOTTORIVA *et al.* 2013, KÖRBER *et al.* 2019). Glioblastomas consist of heterogeneous subclones that gain genetic alterations over time during their evolutionary development as depicted in Figure 5.

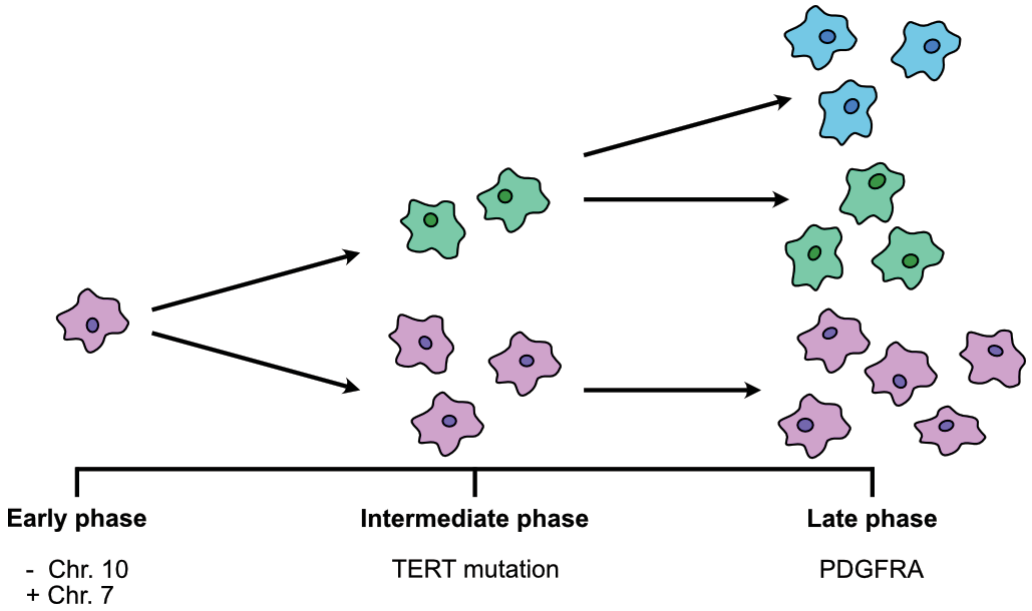

Figure 5: Evolutionary timeline of genetic alterations contributing to subclonal heterogeneity in IDH-WT glioblastoma. Scheme was adapted from Körber *et al.* 2019 (KÖRBER *et al.* 2019).

Genes involved in IDH-WT glioblastoma progression such as *EGFR* or *PTEN* are, amongst others, located on altered chromosomes 7 and 10, leading to early-onset copy number alterations (CNA) of these genes (SOTTORIVA *et al.* 2013, ABOU-EL-ARDAT *et al.* 2017, KÖRBER *et al.* 2019) (Figure 5). Indeed, *EGFR* amplification is present in more than 50% and *PTEN* loss/mutation is present in approximately 40% of patients (BRENNAN *et al.* 2013). Another alteration suspected to occur either as an early (ABOU-EL-ARDAT *et al.* 2017) or a subsequently acquired (KÖRBER *et al.* 2019) event during glioblastoma evolution is mutation of the

telomerase reverse transcriptase (*TERT*) promoter (Figure 5). The *TERT* promoter is mutated in approximately 80-90% of IDH-WT glioblastoma patient samples (DRAAISMA *et al.* 2020, ULGEN *et al.* 2020) and correlates with poor prognosis (GAO *et al.* 2013, KILLELA *et al.* 2013). Mutations of the *TERT* promoter create binding sites for the GABP transcription factor, which leads to upregulation of *TERT* mRNA expression (BELL *et al.* 2015). By reactivating the telomerase, this is expected to promote telomere maintenance (BRENNAN *et al.* 2013). However, recent analysis of IDH-WT glioma did not find any association between *TERT* promoter mutations and telomere length (CECCARELLI *et al.* 2016). Still, *TERT* promoter mutations are, together with chromosome 7 gain, chromosome 10 loss and *EGFR* amplification, considered diagnostic markers for IDH-WT glioblastoma (LOUIS *et al.* 2021, WELLER *et al.* 2021). It is noteworthy to mention that *EGFR* amplification as well as *TERT* promoter mutations are not exclusively present in IDH-WT glioblastomas, but also in other tumor entities (KILLELA *et al.* 2013, LOUIS *et al.* 2021, WELLER *et al.* 2021). In addition to those three main genetic alterations, multiple other alterations are present within IDH-WT glioblastomas (as mentioned above). While at early phase of glioblastoma tumor growth CNA largely target chromosomes 7 and 10, CNA are broader and more scattered across the genome at later phases, reflecting a multiclonal evolution (SOTTORIVA *et al.* 2013). Not only does the genetic profile vary between patients, but it has been shown to also vary within the same tumor. CNA analysis of different regions within the same tumor showed aberrations of different IDH-WT glioblastoma drivers, including amplification of *PDGFRA* or *PTEN* deletion, pointing to spatial intratumoral heterogeneity (SOTTORIVA *et al.* 2013). In addition, alteration of transcription factor-driven gene expression and epigenetic changes contribute to glioblastoma pathogenesis (BAI *et al.* 2016). In particular, MYC, E2F and FOXM1 transcription factor gene networks, including cell cycle genes, are commonly aberrant in glioblastoma (BAI *et al.* 2016) and altered expression of *FOXM1*, *MYBL2* (ZHANG *et al.* 2017), *E2F1* (ALONSO *et al.* 2005, YU *et al.* 2020) and *E2F6* oncogenes (YU *et al.* 2020) has been reported and linked to poor prognosis in glioblastoma. The most common and relevant epigenetic change in glioblastoma is the methylation of the promoter of O^6-methylguanine–DNA methyltransferase (*MGMT*), which codes for a DNA repair protein (HEGI *et al.* 2005, WELLER *et al.* 2021). The methylation status of the *MGMT* promoter is not a diagnostic factor but the most important biomarker guiding treatment decisions and a powerful prognostic parameter in patients treated with temozolomide (WELLER *et al.* 2021).

To improve glioblastoma patient stratification, Verhaak *et al.* (2010) identified four different subtypes, namely classical, mesenchymal, proneural and neural, based on gene expression profiles present in glioblastoma (VERHAAK *et al.* 2010). Although those subtypes were validated in different data sets, their clinical relevance can be questioned as they are not associated with different prognosis (VERHAAK *et al.* 2010) and tumor regions corresponding to different subtypes coexist within the same tumor, underlining the heterogeneity within a tumor mass (SOTTORIVA *et al.* 2013, PATEL *et al.* 2014).

1.4.4. Treatment of glioblastoma

This intratumoral genetic and subclonal heterogeneity makes it difficult to successfully treat IDH-WT glioblastoma. Currently, standard treatment of patients younger than 70 years at diagnosis consist of surgical resection of the tumor mass. Macroscopically complete surgical resection of gliomas significantly increases overall survival compared to a biopsy only (VUORINEN *et al.* 2003). Post-surgical standard of care treatment consists of concomitant radiotherapy and chemotherapy with temozolomide treatment plus six cycles of maintenance temozolomide (STUPP *et al.* 2005, WELLER *et al.* 2021). The benefit of temozolomide treatment, however, is mostly rather limited to patients with *MGMT* promoter-methylated glioblastomas. Methylation of the *MGMT* promoter occurs in approximately 45% of glioblastoma cases (HEGI *et al.* 2005, PERRY *et al.* 2017) and is correlated with increased overall survival in patients treated with alkylating agent chemotherapy (HEGI *et al.* 2005). Patients with *MGMT* promoter methylation exhibit a significantly lower two-year overall survival rate when receiving only radiotherapy treatment compared to concomitant radiotherapy and temozolomide treatment (HEGI *et al.* 2005, PERRY *et al.* 2017). Patients whose tumors have no *MGMT* promoter methylation did not experience a better outcome under the same treatment conditions (HEGI *et al.* 2005). Temozolomide treatment causes formation of O^6-methylguanine by addition of alkyl groups to the O^6 position of the guanine. Such a DNA alteration creates mutations, triggering cell cytotoxicity and apoptosis when not repaired (LIU *et al.* 1996, OCHS & KAINA 2000). The alkyl groups are normally removed from the DNA by MGMT. In case of *MGMT* promoter methylation, MGMT is not expressed, thus preventing DNA repair. Despite these treatment options, glioblastomas recur rapidly in almost all patients (SEYSTAHL *et al.* 2016). Resection of the whole tumor is difficult to achieve since glioblastomas are soft aggressive tissue masses that infiltrate the rigid surrounding brain matter diffusively

(STREITBERGER *et al.* 2020). Such a difference in the biophysical properties of glioblastomas and normal brain tissues explains that tumor invasion results in so-called fingering with undetectable boundaries (STREITBERGER *et al.* 2020). Additionally, recurrence could be supported by escape of tumor cells from radiotherapy and/or temozolomide treatment, which in fact might contribute to the selection for more resistant subclones left from the initial tumor (KÖRBER *et al.* 2019).

Ultimately, the current treatment options for IDH-WT glioblastoma can prolong survival only for a limited amount of time, which advocates for further delineating the pathways of glioblastoma tumorigenesis in order to develop novel, molecularly guided treatment strategies.

2. Aims of the thesis

As displayed in the introduction, the role of 4EBP1 in cancer is still under debate as both an anti-tumorigenic function as well as a pro-tumorigenic function have been reported. Additionally, the function of 4EBP1 in glioblastoma is rarely addressed in the literature. Therefore, the major aim of this dissertation was to characterize the function and relevance of 4EBP1 in this clinically important type of brain cancer.

EIF4EBP1 has been reported to be overexpressed in various different tumor entities, amongst them glioblastoma, but the regulation of *EIF4EBP1* expression is not well understood. Therefore, a first goal was to examine *EIF4EBP1* expression in glioblastoma, to characterize the underlying pathological mechanism of *EIF4EBP1* overexpression, as well as to investigate potential roles of 4EBP1 in glioblastoma cells migration and invasion.

Secondly, the pathophysiological roles of 4EBP1 in cancer remain contradictory. Here, the contribution of 4EBP1 to oncogenic transformation, as well as to tumorigenesis in glioblastoma was addressed. Additionally, the underlying mechanism supporting 4EBP1 function in this tumor entity was characterized. Specifically, the role of 4EBP1 in regulating the fatty acid synthesis pathway and the concomitant maintenance of the redox balance was investigated.

Finally, as a pro-oncogenic role of 4EBP1 in glioblastoma was suggested by the own data, the thesis aimed to develop a targeting approach to inhibit 4EBP1 activity. This approach aimed to disrupt the interaction between 4EBP1 with eIF4E. An *in silico* screen was performed to identify potential targeting compounds and first *in vitro* binding experiments testing these compounds were performed.

3. Results

3.1. How is *EIF4EBP1* overexpression mediated in glioblastoma?

The role of 4EBP1 in cancer is still under debate since pro- and anti-tumorigenic effects have been described in the literature. In patient samples, *EIF4EBP1* was reported to be overexpressed in various cancer types, among them glioblastoma (WU & WAGNER 2021), suggesting that *EIF4EBP1*/4EBP1 may contribute to tumor development in these tumor entities. In this chapter, we investigated how *EIF4EBP1* expression is regulated in glioblastoma patients. To this aim, we extended analyses of *EIF4EBP1* expression in additional glioblastoma patient datasets and determined the mechanisms underlying *EIF4EBP1* overexpression, with a particular focus on transcription factors. Finally, we assessed the functional role of 4EBP1 in glioblastoma cell migration and invasion. Overall, we combined large-scale data, molecular approaches and tumor cell models to uncover factors involved in deregulating *EIF4EBP1* gene expression in such a pathological context.

3.1.1. MANUSCRIPT I

Supplementary Figures and Tables corresponding to the publication are displayed in the Appendix (see 6.1. and 6.2.).

CDDpress

www.nature.com/cddiscovery

ARTICLE OPEN

Check for updates

Eukaryotic translation initiation factor 4E binding protein 1 (*EIF4EBP1*) expression in glioblastoma is driven by ETS1- and MYBL2-dependent transcriptional activation

Laura Hauffe[1], Daniel Picard[1,2,3], Julian Musa[4,5,6,7], Marc Remke[1,2,3], Thomas G. P. Grünewald[4,5,6,8], Barak Rotblat[9,10], Guido Reifenberger[1,3] and Gabriel Leprivier[1]✉

Eukaryotic translation initiation factor 4E binding protein 1 (*EIF4EBP1*) encodes the 4EBP1 protein, a negative regulator of mRNA translation and a substrate of the mechanistic target of rapamycin (mTOR), whose function and relevance in cancer is still under debate. Here, we analyzed *EIF4EBP1* expression in different glioma patient cohorts and investigated its mode of transcriptional regulation in glioblastoma cells. We verified that *EIF4EBP1* mRNA is overexpressed in malignant gliomas, including isocitrate dehydrogenase (IDH)-wildtype glioblastomas, relative to non-neoplastic brain tissue in multiple publically available datasets. Our analyses revealed that *EIF4EBP1* overexpression in malignant gliomas is neither due to gene amplification nor to altered DNA methylation, but rather results from aberrant transcriptional activation by distinct transcription factors. We found seven transcription factor candidates co-expressed with *EIF4EBP1* in gliomas and bound to the *EIF4EBP1* promoter, as revealed by chromatin immunoprecipitation (ChIP)-sequencing data. We investigated the ability of these candidates to activate the *EIF4EBP1* promoter using luciferase reporter assays, which supported four transcription factors as candidate *EIF4EBP1* regulators, namely MYBL2, ETS1, HIF-1A, and E2F6. Finally, by employing transient knock-down experiments to repress either of these transcription factors, we identified MYBL2 and ETS1 as the relevant transcriptional drivers of enhanced *EIF4EBP1* expression in malignant glioma cells. Taken together, our findings confirm enhanced expression of *EIF4EBP1* in malignant gliomas relative to non-neoplastic brain tissue and characterize the underlying molecular pathomechanisms.

Cell Death Discovery (2022)8:91 ; https://doi.org/10.1038/s41420-022-00883-z

INTRODUCTION

Eukaryotic initiation factor 4E binding protein 1 (*EIF4EBP1*) encodes 4EBP1, a substrate of the nutrient-responsive hub mechanistic target of rapamycin complex 1 (mTORC1). Upon nutrient deprivation, 4EBP1 gets activated [1] and in turn inhibits mRNA translation initiation by binding the mRNA cap-binding protein eIF4E [2]. The role of 4EBP1 in cancer is still being debated, as 4EBP1 exhibits both tumor-suppressive [3–6] and pro-tumorigenic functions [7, 8], depending on the tumor types. Accordingly, the clinical relevance of *EIF4EBP1* expression is strongly dependent on the tumor entity. On the one hand, loss of *EIF4EBP1* and low 4EBP1 levels have been linked to poor survival of patients with head and neck squamous cell carcinoma [3] or prostate cancer [9]. On the other hand, *EIF4EBP1*, as part of the 8p11-12 amplicon, is frequently amplified in breast cancer [10, 11]. Furthermore, high *EIF4EBP1* levels are associated with poor survival in all The Cancer Genome Atlas (TCGA) cancer entities combined [12], as well as in breast cancer [10, 11], colorectal cancer [13], hepatocellular carcinoma [14] or diffuse large B-cell lymphoma [15]. However, the prognostic relevance of *EIF4EBP1* expression in other individual tumor entities is poorly established, and the mechanisms regulating *EIF4EBP1* expression in distinct types of cancer warrant further investigations.

To date, only a few transcription factors have been characterized to bind the *EIF4EBP1* promoter and stimulate *EIF4EBP1* transcription in normal and cancer cells. These include the MYC oncoprotein [15], the androgen receptor [16], the stress response regulators ATF4 [15] and ATF5 [17], as well as HIF-1A [18]. In particular, MYC and ATF4 have been shown to co-regulate *EIF4EBP1* transcription in cancer cells [15], providing one potential mechanism underlying *EIF4EBP1* overexpression in cancer. The possible involvement of yet other transcription factors in regulating *EIF4EBP1* expression in human cancers remains to be investigated.

[1]Institute of Neuropathology, Medical Faculty, University Hospital Düsseldorf, Heinrich Heine University, Düsseldorf, Germany. [2]Department of Pediatric Oncology, Hematology, and Clinical Immunology, Medical Faculty, University Hospital Düsseldorf, Heinrich Heine University, Düsseldorf, Germany. [3]German Cancer Consortium (DKTK), partner site Essen/Düsseldorf, Düsseldorf, Germany. [4]Max-Eder Research Group for Pediatric Sarcoma Biology, Institute of Pathology, Faculty of Medicine, LMU Munich, Munich, Germany. [5]Division of Translational Pediatric Sarcoma Research, German Cancer Research Center (DKFZ), Heidelberg, Germany. [6]Hopp Children's Cancer Center (KiTZ), Heidelberg, Germany. [7]Department of General Visceral and Transplantation Surgery, Heidelberg University Hospital, Heidelberg, Germany. [8]Institute of Pathology, Heidelberg University Hospital, Heidelberg, Germany. [9]Department of Life Sciences, Ben-Gurion University of the Negev, Beer Sheva, Israel. [10]The National Institute for Biotechnology in the Negev, Beer Sheva, Israel. ✉email: gabriel.leprivier@med.uni-duesseldorf.de

Received: 30 November 2021 Revised: 4 February 2022 Accepted: 10 February 2022
Published online: 28 February 2022

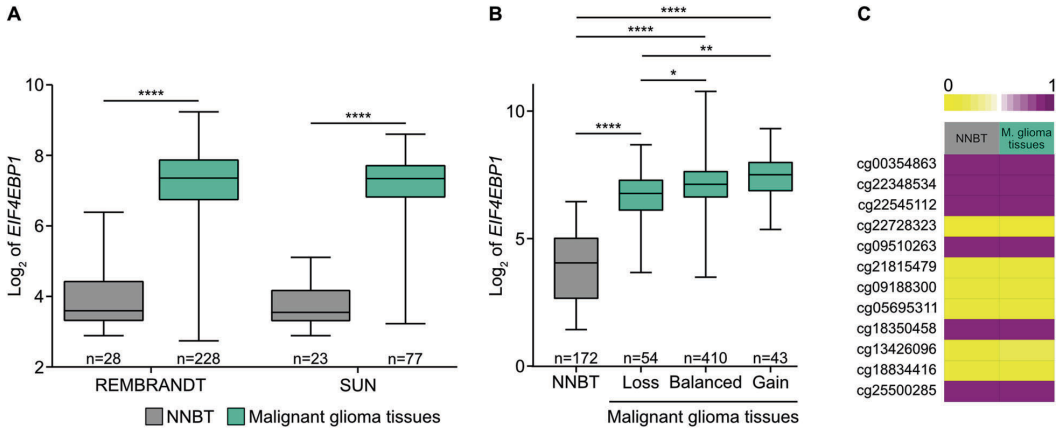

Fig. 1 Increased expression of *EIF4EBP1* mRNA in malignant gliomas relative to non-neoplastic brain tissue. A Expression levels of *EIF4EBP1* in non-neoplastic brain tissue (NNBT) and glioblastoma tissues from the REMBRANDT [26] and SUN [27] cohorts. **B** Expression levels of *EIF4EBP1* in 172 NNBT samples (BERCHTOLD [67]) and according to *EIF4EBP1* copy number variation in 507 malignant gliomas of CNS WHO grade 4 of TCGA cohort [32] categorized as *EIF4EBP1* copy number loss (hemizygous deletion [loss]), *EIF4EBP1* balanced copy number (balanced), or *EIF4EBP1* low-level copy number gain (gain). **C** DNA methylation levels of 12 CpG sites located within the *EIF4EBP1* promoter region (hg19; Chr8: 37,886,520–37,889,020) using the datasets GSE112179 and GSE156374 for NNBT ($n = 13$) and GSE119774 for malignant glioma (M. glioma) tissues ($n = 40$) with 0 representing unmethylated and 1 representing fully methylated CpG sites. Note identical methylation patterns in normal brain tissue and the glioblastoma samples. Significance in **A**, **B** was calculated using an unpaired and two-tailed parametric *t* test (*$p < 0.05$, **$p < 0.01$, ****$p < 0.0001$).

Glioblastoma is the most common and most malignant primary glial tumor type of the central nervous system (CNS) that according to the World Health Organization (WHO) classification of CNS tumors corresponds to CNS WHO grade 4 [19, 20]. This tumor entity nowadays comprises only isocitrate dehydrogenase (IDH)-wildtype tumors [20], as opposed to the previous WHO classification of CNS tumors which also included IDH-mutant tumors [19]. IDH-wildtype glioblastomas are diffuse astrocytic gliomas that grow invasively in the brain parenchyma, are highly proliferative and angiogenic, and are characterized by the presence of hypoxic and necrotic regions [21]. Median survival time is only around 15 months after diagnosis [19], despite standard of care treatment [22, 23]. The initiation and progression of IDH-wildtype glioblastomas are driven by genetic alterations that inactivate tumor suppressor genes like *PTEN*, *CDKN2A*, *RB1*, *NF1*, and *TP53*, or activate cellular oncogenes like *EGFR*, *PDGFRA*, *CDK4*, *MDM2*, and *PIK3CA* [24]. In addition, epigenetic changes and alteration of transcription factor-driven gene expression contribute to glioblastoma pathogenesis [25].

Using different publically available malignant glioma datasets and chromatin immunoprecipitation (ChIP)-sequencing data, we confirmed that *EIF4EBP1* mRNA expression is elevated in malignant glioma tissues, relative to non-neoplastic brain tissue, and identified seven transcription factor candidates supporting *EIF4EBP1* overexpression. We showed with promoter-reporter assays and genetic knockdown experiments that among these factors, ETS1 and MYBL2 regulate *EIF4EBP1* transcription in IDH-wildtype glioblastoma cells.

RESULTS

EIF4EBP1 mRNA levels in malignant gliomas are elevated independently of gene amplification or promoter methylation

Based on a glioma dataset from TCGA database, a recent study reported on overexpression of *EIF4EBP1* in glioblastoma tissue samples compared to non-neoplastic brain tissues [12]. To further delineate the expression of *EIF4EBP1* in malignant gliomas including IDH-wildtype and IDH-mutant tumors, we determined the levels of *EIF4EBP1* in additional publically available glioma datasets and investigated its association with common genetic alterations as well as *EIF4EBP1* gene copy number alteration and promoter methylation. We confirmed and extended the reported finding [12] in six independent and non-overlapping patient datasets, namely REMBRANDT [26], SUN [27], FRENCH [28], HEGI [29], TUYSUZ [30], and DONSON [31] (a pediatric glioblastoma dataset). Thereby, we confirmed that malignant glioma tissues showed higher levels of *EIF4EBP1* mRNA expression compared to non-neoplastic brain tissues in each of the analyzed cohorts (Fig. 1A and Fig. S1A, B). We then asked whether *EIF4EBP1* mRNA expression is associated with common genetic and epigenetic alterations found in malignant gliomas. Specifically, we analyzed *EIF4EBP1* mRNA expression levels in *EGFR*-amplified and *EGFR*-non-amplified as well as in O6-methylguanine DNA methyltransferase (*MGMT*) promoter-methylated and promoter-unmethylated IDH-wildtype glioblastoma patient samples using publically available datasets [32]. We found that *EIF4EBP1* mRNA level is not impacted by either of these alterations (Fig. S1C, D). We also investigated the potential association of *EIF4EBP1* expression with the IDH mutation status in primary glioma samples and found that *EIF4EBP1* mRNA expression is not dependent on the IDH mutation status in three independent datasets (Fig. S1E–G). Among IDH-mutant gliomas, there was no difference in *EIF4EBP1* expression levels in 1p/19q-codeleted oligodendrogliomas versus 1p/19q-intact astrocytomas included in the FRENCH cohort dataset [28] (Fig. S1H) or TCGA dataset [32] (Fig. S1I).

Next, we asked whether *EIF4EBP1* overexpression in malignant gliomas might be caused by *EIF4EBP1* gene amplification. Analyzing the copy number status of *EIF4EBP1* in 507 malignant glioma samples did not reveal any amplification of *EIF4EBP1* (Fig. 1B). This observation stands in contrast to a previous report stating that *EIF4EBP1* is amplified in approximately 13% of breast cancers [11]. While approximately 8.5% of TCGA malignant glioma cases analyzed here exhibited a low-level gain of *EIF4EBP1* [33, 34], there was no association with higher *EIF4EBP1* mRNA expression as compared to tumors without *EIF4EBP1* copy number gain (Fig. 1B and Table S1). We then assessed whether *EIF4EBP1* mRNA overexpression is due to differential promoter methylation in non-neoplastic brain versus malignant glioma tissues. We analyzed the

DNA methylation level of 12 CpG sites within the *EIF4EBP1* promoter region (hg19; Chr8: 37,886,520–37,889,020), which showed that non-neoplastic brain tissues and malignant glioma tissues exhibited a very similar methylation profile (Fig. 1C). This goes along with a previous study reporting no difference of *EIF4EBP1* promoter methylation in glioma compared to control samples [35]. Based on these analyses, we can exclude *EIF4EBP1* gene amplification or altered *EIF4EBP1* promoter methylation as possible mechanisms driving *EIF4EBP1* overexpression in malignant gliomas.

Identification of potential transcription factors driving enhanced transcription of *EIF4EBP1* in malignant gliomas

We next reasoned that the increased *EIF4EBP1* mRNA expression in malignant gliomas might be driven by specific transcription factors. To identify potential transcription factor candidates, we searched for transcription factors that are positively co-expressed with *EIF4EBP1* in malignant gliomas, overexpressed in these tumors as compared to non-neoplastic brain tissues, and known to bind the endogenous *EIF4EBP1* promoter by ChIP. This allowed us to uncover seven transcription factors that fulfilled these criteria. We searched for transcription factors that are positively co-expressed with *EIF4EBP1* in gliomas and found *EIF4EBP1* mRNA expression to be significantly and positively associated with the mRNA expression levels of *MYBL2*, *FOXM1*, *ETS1*, *HIF-1A*, *JUN*, *E2F1*, and *E2F6* in the REMBRANDT dataset [26] (Fig. 2A–G). These associations were validated for each of these transcription factors, excluding *E2F1*, in at least three additional glioma cohorts, including the SUN [27] (Fig. S2A–G), KAWAGUCHI [36], FRENCH [28], or FREIJE [37] datasets (Table S2). In support of the co-expression data, we analyzed the expression of these transcription factors in malignant glioma tissues using TCGA [32, 38] and the REMBRANDT [26] datasets, as well as non-neoplastic brain tissues [39]. This demonstrated a significant overexpression of *MYBL2*, *FOXM1*, *ETS1*, *HIF-1A*, and *JUN* in both glioma cohorts compared to non-neoplastic brain tissues (Fig. S3A, B). Expression of *E2F1* and *E2F6* was previously reported to be higher in glioblastomas (using TCGA dataset) compared to non-neoplastic brain tissues [40], which we validated in the REMBRANDT dataset [26] (Fig. S3B). Of note, the expression of these transcription factors was independent of the IDH mutation status in malignant gliomas, except for *ETS1* (Fig S3C). Finally, we analyzed existing ChIP-sequencing (seq) data from the Encode consortium [41, 42], which demonstrated direct binding of FOXM1, ETS1, E2F1, and E2F6 to the *EIF4EBP1* promoter region, exon 1 and intron 1 (−1500 to +1000) in various normal and cancer cells, however not including glioblastoma cells (Fig. 2H). The transcriptional regulatory region for *EIF4EBP1* is not restricted to its promoter but also encompasses exon 1 and the 5′ region of intron 1, as indicated by histone H3K27 acetylation and H3K4 trimethylation signals (Fig. 2H). In addition, by using other ChIP-seq datasets [43, 44] we found signals for MYBL2 and HIF-1A binding to the *EIF4EBP1* promoter (Fig. 2H). In accordance, ChIP analyses demonstrating HIF-1A binding to its putative responsive element within the *EIF4EBP1* promoter segment −278 to +64 have been published [18]. Taken together, these data indicate that seven transcription factors could contribute to driving increased expression of *EIF4EBP1* in malignant gliomas.

E2F6, ETS1, HIF-1A, and MYBL2 induce *EIF4EBP1* promoter activity

We next investigated the ability of the seven transcription factor candidates to induce *EIF4EBP1* promoter activity, which was only reported for HIF-1A [18]. To assess promoter activity, we used a luciferase reporter containing the −661 to +705 *EIF4EBP1* promoter region, exon 1, and part of intron 1 (Fig. 3A), as this region is predicted to be bound by the seven transcription factor candidates based on the ChIP-seq data (Fig. 2H). Overexpression of FOXM1 (Fig. 3B) or JUN (Fig. 3C) did not unequivocally induce *EIF4EBP1* promoter activity. While we noticed a significant increase of luciferase activity with low (100 ng) and medium (200 ng) amounts of FOXM1, this was below 1.5-fold and therefore was not considered as biologically relevant. Unexpectedly, overexpression of E2F1, a well-characterized transcriptional activator, led to a decrease of *EIF4EBP1* promoter activity in a dose-dependent manner (Fig. 3D). On the contrary, forced expression of E2F6, a known transcriptional repressor, caused induction of *EIF4EBP1* promoter activity even with low E2F6 expression level (Fig. 3E). Additionally, we showed that ectopic expression of either ETS1 (Fig. 3F), HIF-1A (Fig. 3G), or MYBL2 (Fig. 3H) was able to increase *EIF4EBP1* promoter activity in a dose-dependent manner. The overexpression of each transcription factor was validated by immunoblot analyses (Fig. 3B–H). These experiments proved that among the seven transcription factor candidates, E2F6, ETS1, HIF-1A, and MYBL2 were able to induce *EIF4EBP1* promoter activity. Given that HIF-1A has been previously reported to stimulate *EIF4EBP1* promoter activity [18], we focused on the three other transcription factor candidates for further investigation.

ETS1 and MYBL2 regulate 4EBP1 mRNA and protein expression

To determine whether ETS1, E2F6, and MYBL2 activate the transcription of endogenous *EIF4EBP1* in glioblastoma cells, each transcription factor was transiently knocked down in U-87 MG and U-118 MG glioblastoma cell lines. At the mRNA level, we achieved at least 50% knock-down for *MYBL2*, *ETS1*, and *E2F6* in both cell lines (Fig. 4A–F). This was confirmed at the protein level, as we observed a decrease of ETS1 and E2F6 in U-118 MG and U-87 MG, and of MYBL2 in U-118 MG upon knock-down. However, while the knock-down of MYBL2 in U-87 MG was strong at the mRNA level, we could not detect it at the protein level due to low endogenous MYBL2 levels in this cell line (Fig. 4E, F). We then assessed the effect of the respective transcription factor knock-downs on 4EBP1 transcript and protein levels. With the half-life of 4EBP1 being longer than 48 h [18], we transfected cells twice with siRNA over a period of 192 h to ensure that 4EBP1 protein is degraded and thus allow for observing potential changes of 4EBP1 protein levels. We observed that E2F6 knock-down in U-87 MG (Fig. 4A) and U-118 MG (Fig. 4B) had no impact on 4EBP1 mRNA and protein levels, eliminating E2F6 as a transcriptional regulator of *EIF4EBP1* in these glioblastoma cell lines. In contrast, transient knock-down of either ETS1 or MYBL2 resulted in a significant decrease of 4EBP1 mRNA and protein levels in both glioblastoma cell lines (Fig. 4C–F). These results were confirmed at the protein levels, i.e., MYBL2 or ETS1 knock-down each resulted in lower 4EBP1 protein levels in both cell lines (Fig. 4C–F). Based on these results, we identified two transcription factors, ETS1 and MYBL2, that regulate *EIF4EBP1* expression in glioblastoma cells.

***EIF4EBP1* is co-expressed with *MYBL2*, but not with *ETS1*, in other non-CNS cancer types**

We further analyzed the potential co-expression of *EIF4EBP1* and either *ETS1* or *MYBL2* at the mRNA level in multiple different cancer types using datasets available in R^2 AMC (Table S3). These studies indicated that *EIF4EBP1* expression correlates positively with *MYBL2* expression in each of the analyzed tumor entities, whereas co-expression of *EIF4EBP1* with *ETS1* was restricted to CNS tumors (adult-type gliomas and certain pediatric brain cancers) (Fig. 5A). In particular, while we observed that both *MYBL2* and *ETS1* are co-expressed with *EIF4EBP1* in adult-type glioma, as exemplified by the KAWAGUCHI cohort [36] (Fig. 5B, C), only *MYBL2* mRNA levels, but not *ETS1* mRNA levels, showed a positive correlation with *EIF4EBP1* mRNA levels in non-CNS tumor entities, such as breast and lung cancers, as exemplified by the BLACK and CHUANG cohorts [45, 46], respectively (Fig. 5D–G). These analyses indicate that the co-expression between *MYBL2* and *EIF4EBP1* is not restricted to glioblastomas, suggesting that MYBL2 might

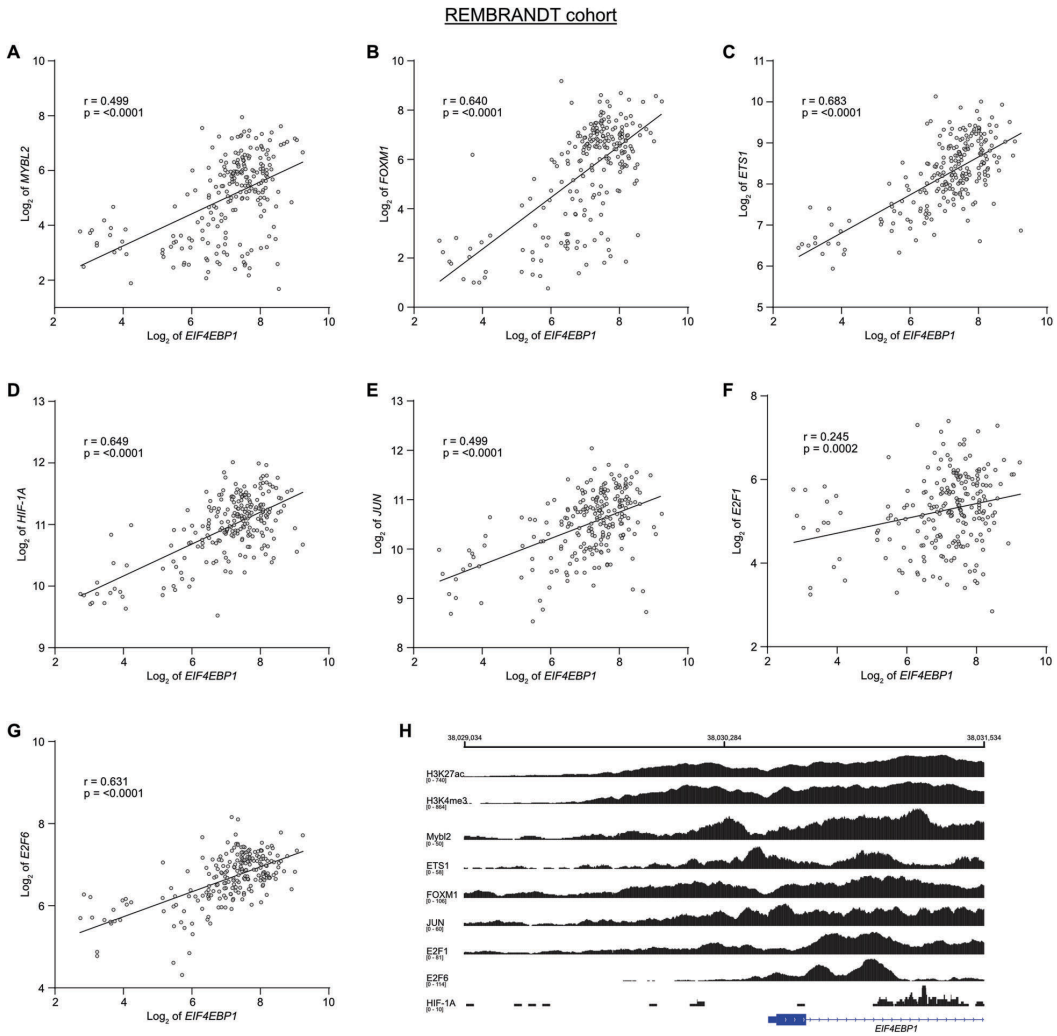

Fig. 2 Co-expression of *EIF4EBP1* and *EIF4EBP1* promoter binding transcription factor genes in glioblastoma tissue samples. A–G Expression levels of *EIF4EBP1* mRNA in glioblastoma patient samples plotted against the mRNA expression levels of (**A**) *MYBL2*, (**B**) *FOXM1*, (**C**) *ETS1*, (**D**) *HIF-1A*, (**E**) *JUN*, (**F**) *E2F1* or (**G**) *E2F6* in the REMBRANDT cohort ($n = 228$ patients) [26]. Co-expression levels were quantified by calculating the Pearson correlation coefficient. **H** ChIP peak locations within the human *EIF4EBP1* promoter, exon 1 and part of intron 1 (−1500 to +1000; hg38; Chr8: 38,029,034–38,031,534) from ChIP-sequencing data for histone H3K27 acetylation (H3K27ac) and H3K4 trimethylation (H3K4me3), ETS1, FOXM1, JUN, E2F1, and E2F6 (Encode consortium, Encyclopedia of DNA Elements at UCSC; [41, 42]), HIF-1A (accession code GSE39089; name GSM955978; run SRR518265 [43]) and MYBL2 (accession code GSE119972; name GSM3389599 [44]).

represent a more general regulatory mechanism driving *EIF4EBP1* expression in different cancer entities.

DISCUSSION

EIF4EBP1 gene expression and its clinical relevance in cancer are highly tumor-type specific [47]. We found that *EIF4EBP1* is overexpressed in glioblastoma tissue samples in different patient cohorts as compared to non-neoplastic brain tissues, thus extending previous observations made in the TCGA cohort [12]. Elevated mRNA expression may lead to increased active 4EBP1 protein levels in glioblastoma, as it was reported that mTOR activity is reduced regionally in this tumor entity, thus leading to 4EBP1 activation in poorly vascularized areas [48]. We searched for the underlying causes of increased *EIF4EBP1* mRNA expression in malignant gliomas and observed that the *EIF4EBP1* gene is not amplified in glioblastomas although amplification of 8p11.23, which encompasses *EIF4EBP1*, has been reported in other cancer entities, such as lung squamous cell carcinoma, bladder cancer, and breast cancer, and correlated with higher *EIF4EBP1* expression [49]. By bioinformatic analysis, we identified seven transcription factors that may potentially drive overexpression of *EIF4EBP1* in gliomas. Each of these transcription factors harbors oncogenic or tumor-promoting functions and some of them were reported to be overexpressed in cancer, including overexpression of *E2F1*, *E2F6* [40], *FOXM1*, and *MYBL2* [50] in glioblastomas. Among the

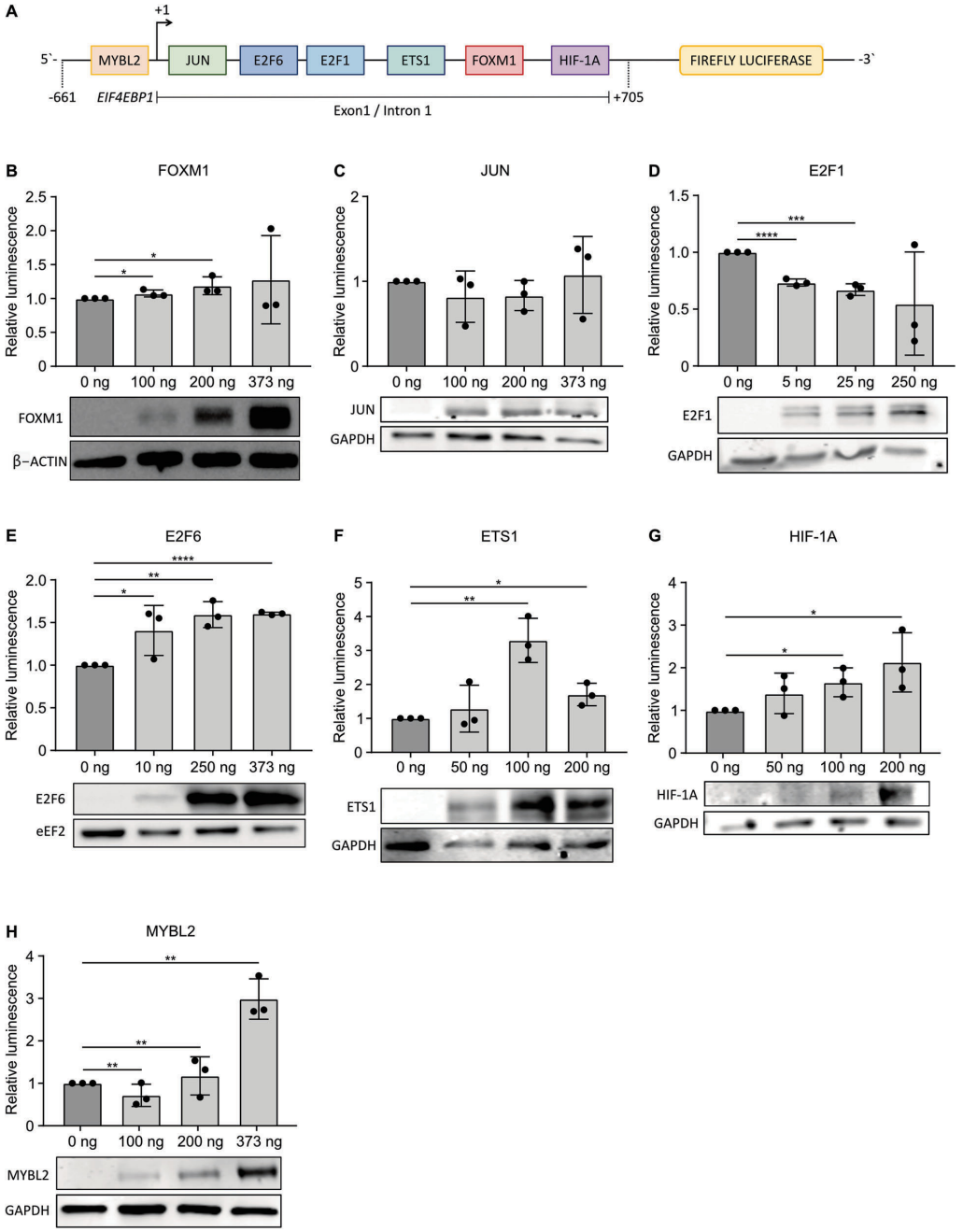

Fig. 3 Induction of *EIF4EBP1* promoter activity by E2F6, ETS1, HIF-1A, and MYBL2. A Scheme of the luciferase reporter construct containing the *EIF4EBP1* promoter, exon 1, and part of intron 1 (−661; +705), coupled to Firefly luciferase, with the indicated binding sites of transcription factor candidates. **B**–**H** HEK293-T cells were transfected with the −661; +705 *EIF4EBP1* promoter reporter construct, together with increasing amounts of plasmids expressing either one of the indicated transcription factors and a vector expressing *Renilla* luciferase. Luciferase activities were detected using the Dual-Luciferase Reporter Assay. Firefly luciferase activity was normalized to *Renilla* luciferase activity and the ratio was normalized to the corresponding 0 ng condition. Data represent the mean of three independent replicates ± standard deviation (SD). Significance was calculated using an unpaired and one-tailed parametric *t*-test (*$p < 0.05$, **$p < 0.01$, ***$p < 0.001$ ****$p < 0.0001$). Below each diagram, a representative immunoblot analyzing overexpression of each of the indicated transcription factors is presented.

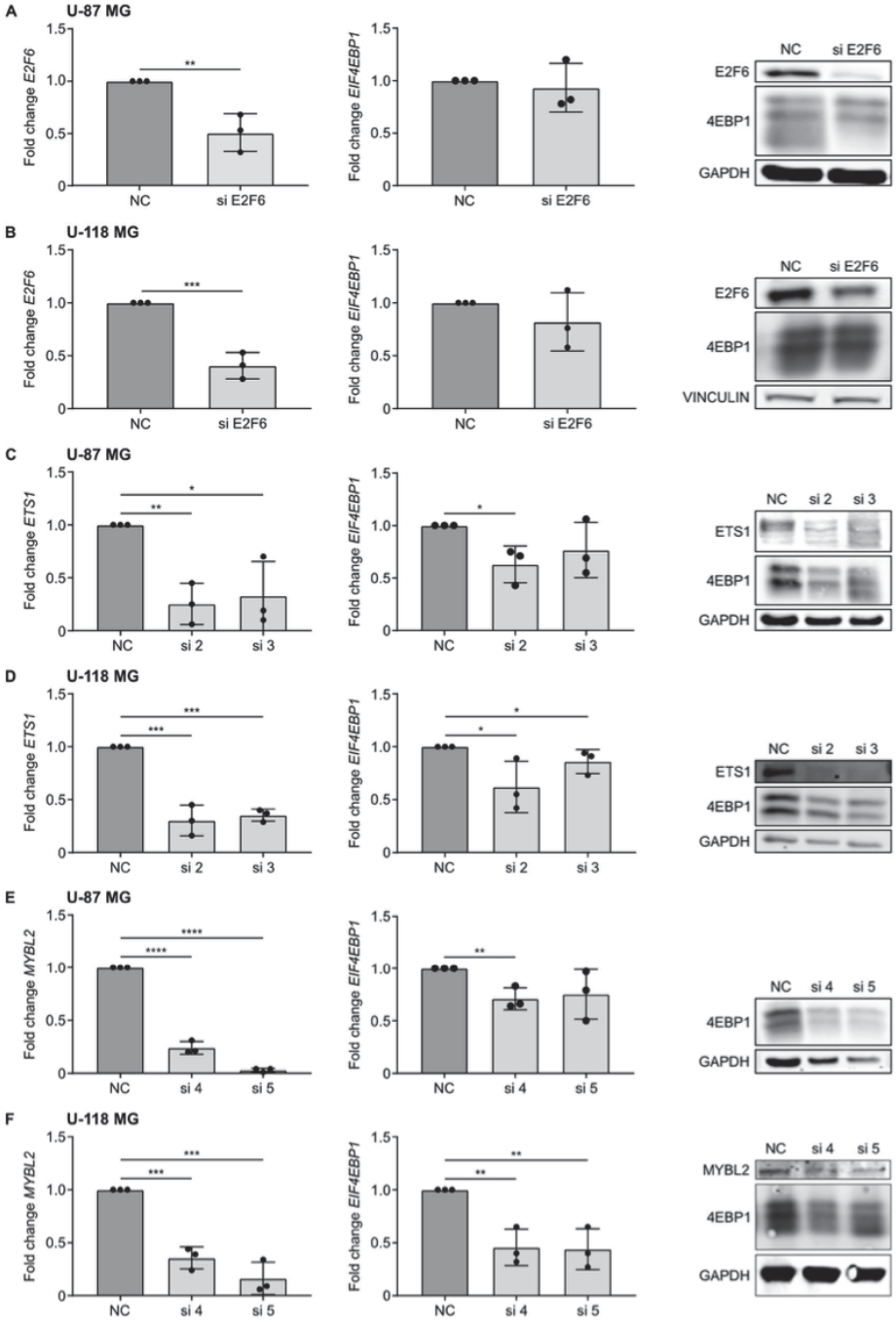

Fig. 4 Regulation of *EIF4EBP1* mRNA and protein expression by MYBL2 and ETS1 in glioblastoma cells. A–**F** U-118 MG and U-87 MG glioblastoma cells were transiently transfected with negative control siRNAs (NC), and an siRNA pool targeting (**A**, **B**) *E2F6* (si E2F6) or two different siRNAs each targeting either (**C**, **D**) *ETS1* (si 2 and si 3) or (**E**, **F**) *MYBL2* (si 4 and si 5). Cells were re-transfected after 96 h with their corresponding siRNA and incubated for a total of 192 h. MRNA and protein were harvested to determine the expression levels of *EIF4EBP1*/4EBP1 and (**A**, **B**) E2F6, (**C**, **D**) ETS1 or (**E**, **F**) MYBL2 by qRT-PCR and immunoblots. Data obtained by qRT-PCR represent the mean of three independent replicates ±SD and the fold change in expression was normalized to the negative control. Results of representative immunoblot are depicted on the right-hand side of the diagrams representing the qRT-PCR results. Significance was calculated using an unpaired and one-tailed parametric *t*-test (*$p < 0.05$, **$p < 0.01$, ***$p < 0.001$, ****$p < 0.0001$).

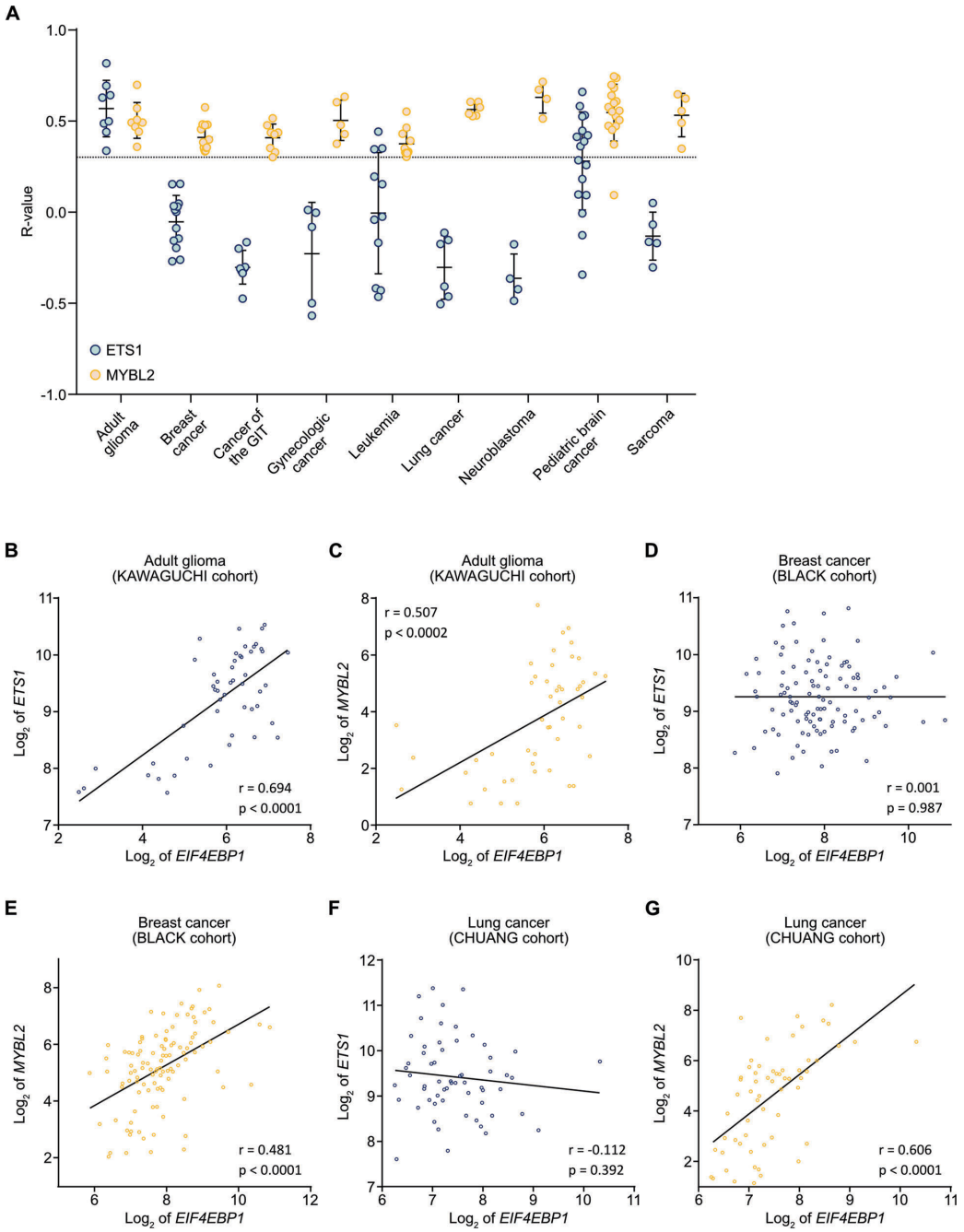

Fig. 5 Co-expression of *EIF4EBP1* and *MYBL2* or *ETS1* in different cancer entities. A Correlation between the mRNA expression levels of *EIF4EBP1* and *ETS1* (light blue dots) or *MYBL2* (yellow dots) in the indicated human cancer types (Table S3). Co-expression levels were quantified by calculating the Pearson correlation coefficient. Each dot represents the *R*-value for one cohort. The dotted line corresponds to an *R*-value of 0.3, chosen as the cut-off for positive correlation. **B**–**H** Representative co-expression analysis between *EIF4EBP1* mRNA and **B**, **D**, **F** *ETS1* (light blue dots) or **C**, **E**, **G** *MYBL2* (yellow dots) mRNA levels in the indicated tumor type and cohort. The represented cohorts are (**B**, **C**) glioma (KAWAGUCHI cohort; $n = 50$) [36], **D**, **E** breast cancer (BLACK cohort; $n = 107$) [45], and **F**, **G** lung cancer (CHUANG cohort; $n = 60$) cohort [46]. Co-expression levels were quantified by calculating the Pearson correlation coefficient. GIT, gastrointestinal tract.

seven transcription factor candidates, we found that HIF-1A, E2F6, ETS1, and MYBL2 activated the *EIF4EBP1* promoter in vitro while E2F1, JUN, and FOXM1 did not. Surprisingly, E2F1 a transcriptional activator repressed *EIF4EBP1* promoter activity while E2F6, which is a transcriptional repressor, induced *EIF4EBP1* promoter activity. Of note, E2F1 has been shown to repress transcription of *YAP1* by binding to the transcription factor TEAD [51], so we cannot exclude that E2F1 may repress the endogenous *EIF4EBP1* promoter. While JUN was not validated as a transcriptional regulator of *EIF4EBP1* promoter with our assays, this may be explained by the absence of a consensus binding motif (5′-TGAC/GTCA-3′) [52] within the −661; +705 *EIF4EBP1* promoter construct we used. Of note, the endogenous *EIF4EBP1* promoter contains two JUN consensus binding motifs, which are located further upstream and downstream of the −661; +705 promoter region, suggesting that JUN is still a possible candidate that might regulate the *EIF4EBP1* promoter.

By functional knockdown experiments, we uncovered that ETS1 and MYBL2 regulate the transcription of endogenous *EIF4EBP1* in glioblastoma cells, highlighting novel regulators of *EIF4EBP1* transcription that complement the transcription factors previously reported, including MYC [15], the androgen receptor [16], ATF4 [15], ATF5 [17], and HIF-1A [18]. Since *ETS1* and *MYBL2* as well as *EIF4EBP1* are overexpressed in other cancer entities, for instance in colorectal cancer [12, 13, 53, 54] or breast cancer [12, 53, 55], these transcription factors might also regulate *EIF4EBP1* expression in cancers outside the CNS. In support of this assumption, we found that *MYBL2*, but not *ETS1*, is co-expressed with *EIF4EBP1* at the mRNA level in a variety of non-CNS cancer entities, suggesting that MYBL2 might represent a general transcriptional driver of *EIF4EBP1* overexpression in human cancers while ETS1-dependent regulation of *EIF4EBP1* may be more restricted to CNS tumors. The molecular mechanisms underlying *MYBL2* and *ETS1* overexpression in malignant gliomas are to date unknown. In the case of *MYBL2*, this may be due to EGFR signaling, which is frequently amplified and overexpressed in IDH-wildtype glioblastomas [56] and was reported to activate the *MYBL2* promoter in association with E2F1 [57]. ETS1 activity is directly induced by the RAS/RAF/MEK/ERK pathway [53], which is overactive in a large number of IDH-wildtype glioblastomas [58] and leads to *ETS1* promoter activation [53].

Given that we found *EIF4EBP1* to be a target gene of the ETS1 and MYBL2 oncoproteins in malignant gliomas, 4EBP1 may possibly contribute to ETS1 and MYBL2 tumorigenic functions in these tumors. Functions of both transcription factors as well as 4EBP1 have been linked to support angiogenesis. Indeed, ETS1 is known to regulate the *VEGF* promoter and its transcription [59], and ETS1 expression is associated with a higher density of microvessels in tumors [60]. MYBL2 expression was reported to be induced under ischemic conditions in rat brains [61], stabilized by HIF-2α [62], and to protect cells toward hypoxia-induced apoptosis [63]. Additionally, 4EBP1 has been shown to promote the selective translation of *VEGF* or *HIF-1A* mRNAs in response to hypoxia [7]. Taken together, this raises the possibility that the induction of *EIF4EBP1* expression by ETS1 and MYBL2 in glioblastoma cells may be a previously unrecognized mechanism mediating angiogenesis in this tumor type. Independently of ETS1 or MYBL2, 4EBP1 may exhibit other functions in glioblastomas. It has been reported that 4EBP1 is required for oncogenic RAS transformation of mouse embryonic fibroblasts in vitro and in vivo [64], pointing to a tumor-supporting role of 4EBP1. Thus, it is possible that 4EBP1 may also contribute to glioma tumorigenesis by supporting oncogenicity.

In summary, we elucidated molecular mechanisms of enhanced *EIF4EBP1* levels in glioblastoma cells, revealing the oncogenic transcription factors ETS1 and MYBL2 as responsible transcriptional regulators.

MATERIALS AND METHODS

Data availability and bioinformatics analysis

We used publically available cancer datasets (Table S3) as well as glioma and non-neoplastic brain tissue datasets derived from various cohorts for correlative analyses of RNA expression data. Table S4 provides an overview of the glioma datasets that were used including accession numbers, patient numbers, original diagnoses, and information on IDH mutation status, if available. As these datasets were generated before the current WHO classification, the provided diagnoses are mostly based on histological classification only. RNA expression data were analyzed with the Gepia website [38] using the publicly available GTEx non-neoplastic brain tissue and TCGA [32] (tumor tissues) datasets or obtained from the R^2 Genomic Analysis Visualization Platform (R^2 AMC; http://r2.amc.nl) using the REMBRANDT [26] datasets to analyze the expression levels of *EIF4EBP1*, *MYBL2*, *FOXM1*, *ETS1*, *HIF-1A*, *JUN*, *E2F1*, and *E2F6* in non-neoplastic brain tissue versus malignant glioma patient samples. Additionally, the expression levels of *EIF4EBP1* were analyzed with R^2 AMC using the SUN [27], FRENCH [28], HEGI [29], DONSON [31] (microarray platforms u133p2) and TUYSUZ [30] (microarray platform hugene21t) datasets. For co-expression analyses, the above-mentioned cohorts as well as the KAWAGUCHI [36], FREIJE [37], and PAUGH [65] cohorts were used. Expression data of IDH-wildtype glioblastoma patient samples according to the *MGMT* promoter methylation status were retrieved from cBioportal [33, 34] (TCGA [32]) and data related to the *EGFR* amplification status in IDH-wildtype glioblastomas were retrieved with R^2 AMC using the FRENCH [28] cohort. Expression data according to 1p/19q codeletion were obtained for IDH-mutant CNS WHO grade 2, 3, and 4 gliomas from R^2 AMC using the FRENCH [28] cohort or from https://portal.gdc.cancer.gov using TCGA datasets for lower-grade glioma and glioblastoma [32]. MRNA expression data according to IDH mutation status were analyzed using the CGGA [66], FRENCH [28], and TCGA [32] datasets for *EIF4EBP1* expression and TCGA dataset [32] for the expression of the transcription factors. TCGA data were accessed using cBioportal [33, 34]. Copy number variations for *EIF4EBP1* and corresponding *EIF4EBP1* expression in glioma patient samples were acquired from cBioportal and R^2 AMC, respectively [33, 34] (TCGA [32]) and compared to expression data of *EIF4EBP1* in non-neoplastic brain tissue [67] from R^2 AMC. DNA methylation data were downloaded from R^2 AMC (GSE112179 [68] and GSE156374 [69] for non-neoplastic brain tissue and GSE119774 [70] for tumor tissues). CpG sites included within the −1500 to +1000 of *EIF4EBP1* (human genome GRCh 38/hg38; Chr8: 38,029,034–38,031,534) were selected for analysis and the mean was determined for each group and CpG site. ChIP-seq data for H3K27ac (UCSC Accession: wgEncodeEH000030, wgEncodeEH000997, wgEncodeEH000111, wgEncodeEH000055, wgEncodeEH000043, wgEncodeEH000064, wgEncodeEH000097), H3K4me3 (wgEncodeEH000913, wgEncodeEH000909, wgEncodeEH002876, wgEncodeEH001882), ETS1 (wgEncodeEH002290; wgEncodeEH001580), FOXM1 (wgEncodeEH002529), JUN (wgEncodeEH000746, wgEncodeEH000719, wgEncodeEH002805, wgEncodeEH000620), E2F1 (wgEncodeEH000699, wgEncodeEH000688, wgEncodeEH000693) and E2F6 (wgEncodeEH000692 wgEncodeEH000676; wgEncodeEH001598) were downloaded from ENCODE (Encyclopedia of DNA Elements at UCSC; [41, 42]) using the human genome GRCh 38/hg 38, whereas NCBI Geo datasets were used to access ChIP-seq data for HIF-1A (human genome GRCh 38/hg 38; accession code GSE39089; name GSM955978; run SRR518265; [43]) and MYBL2 (human genome GRCh 37/hg 19; accession code GSE119972; name GSM3389599; [44]). Fastq files for HIF-1A were aligned to human reference genome hg38 using STAR v2.4.1d, whereas MYBL2 data were re-aligned from hg19 to hg38. ChIP seq data from ENCODE [41, 42] included data from seven cell lines. These files were combined into a single BAM file. BAM files were then visualized using IGV version 2.9.1 (https://igv.org; [71]).

Statistical analyses

Unpaired *t*-tests were performed when comparing gene expression in gliomas versus non-neoplastic brain tissues samples, as well as between IDH-mutant glioma groups stratified according to 1p/19q co-deletion, or IDH-wildtype glioblastoma groups stratified according to *EGFR* amplification and *MGMT* promoter methylation status. ANOVA analysis was used to determine the significance of copy number status between glioma and non-neoplastic brain tissue samples. Correlation analyses were performed by calculating Pearson correlation. GraphPad Prism version 7.04 (GraphPad Software, San Diego, CA, USA) was used for the statistical analysis.

Cell culture

HEK293-T embryonic kidney cells as well as the human glioblastoma cell lines U-118 MG and U-87 MG were originally obtained from American Type Culture Collections (ATCC). Cells were maintained in Dulbecco's modified Eagle Medium (10569010, Thermo Fisher Scientific, Waltham, MA, USA) supplemented with 10% fetal bovine serum (FBS) (10270-106, Thermo Fisher Scientific) and 1% penicillin/streptomycin (10270-106, Sigma Aldrich, St Louis, USA) and cultured in a humidified incubator at 37 °C with 5% CO_2. The cell lines were confirmed to be mycoplasma-free by Venor GeM Classic (11-1050, Minerva Biolabs, Berlin, Germany) kit and validated by STR-profiling (Genomics & Transcriptomics Labor (GTL), Heinrich Heine University, Düsseldorf, Germany).

siRNA transfection

Cells were transfected in 6-well plates at 70% confluency with 25 nM control siRNA (D-001206-14-50, Dharmacon, Cambridge, UK) or negative control siPool (siTools Biotech, Planegg, Germany) or siRNAs targeting *ETS1* (D-003887-02-0010 & D-003887-03-0010, Dharmacon), *MYBL2* (D-010444-04-0005 and D-010444-05-0005, Dharmacon) or *E2F6* (siTools Biotech) using siLentFect transfection reagent (1703362, Biorad, Hercules, CA, USA) (see Table S5 for siRNA sequences). Briefly, a master mix containing 125 µl Opti-MEM (31985-070, Thermo Fisher Scientific) and 3 µl siLentFect was prepared and incubated for 5 min at room temperature (RT). Meanwhile, 125 µl Opti-MEM were mixed with 25 nM of siRNA for each well. The siRNA mix was mixed 1:1 with the master mix, incubated for 20 min at RT, and added dropwise onto the cells. The medium was changed the day after transfection. Cells were re-transfected after 96 h. At 192 h following the first transfection, RNA and protein were harvested for further analysis.

Plasmid construction

The promoter region of the human *EIF4EBP1* gene, spanning from nucleotide −661 to +705 (human genome GRCh 38/hg38; Chr8: 38,029,873–38,031,239), was inserted into the SacI and BglII restriction sites of the Firefly Luciferase expressing pGL4.22 plasmid (E6771, Promega, Madison, WI, USA). Cloning was performed by GENEWIZ Germany GmbH (Leipzig, Germany).

Luciferase reporter assays

HEK 293-T cells were seeded in 12-well plates to reach 50% confluency on the day of transfection. Cells were transfected with 125 ng of the *EIF4EBP1* promoter Firefly luciferase plasmid, 2 ng of *Renilla* luciferase-expressing pRL SV40 plasmid (E2231, Promega), as internal control, and 5–373 ng of either of the transcription factor expressing plasmids, completed to 500 ng total DNA with pCMV-Neo-Bam (16440, Addgene) or pcDNA3.1 (V79020, Thermo Fisher Scientific) plasmids using CalFectin™ Cell Transfection Reagent (SL100478, SignaGen Laboratories; Frederick, MD; USA) according to the manufacturer's guidelines. The used transcription factor expressing plasmids were pcDNA3 E2F1 (kind gift from Dr. Tony Kouzarides, University of Cambridge, UK), pSG3.1 ETS1 (kindly provided by Dr. Lawrence McIntosh, University of British Columbia, Vancouver, Canada), pcDNA3 FoxM1 (kindly provided by Dr. Pradip Raychaudhuri, University of Illinois Cancer Center, Chicago, IL, USA), pcDNA3 HA-HIF-1A (gift from Dr. William Kaelin [Addgene plasmid # 18949; http://n2t.net/addgene:18949; RRID: Addgene_18949; [72]]), pcDNA3 MYBL2 (gift from Dr. Rob Lewis [Addgene plasmid # 25965; http://n2t.net/addgene:25965; RRID:Addgene_25965; [73]]), pCMV6 JUN (kind gift of Dr. Marguerite Buzza, University of Maryland, College Park, MD, USA). Cells were harvested 48 h post-transfection and the activity of Firefly and *Renilla* luciferases were sequentially determined using the Dual-Luciferase Reporter Assay System (E1980, Promega) and analyzed with Beckman Coulter microtiter plate reader (Beckman Coulter, Krefeld, Germany). All samples were performed in triplicate and the final luciferase quantification was formulated as the ratio of Firefly luciferase to *Renilla* luciferase luminescence.

RNA extraction, cDNA synthesis, and qRT-PCR

RNA was extracted using the RNeasy Plus Mini Kit (74136, QIAgen, Hilden, Germany). The extraction was performed according to the protocol provided by the manufacturer. Isolated RNA was retro-transcribed to cDNA using 1 µg of RNA per reaction with either the QuantiTect Reverse Transcription Kit (205311, QIAgen) or the High-Capacity cDNA Reverse Transcription Kit (4368813, Applied Biosystems, Waltham, MA, USA) according to the manufacturer's protocol. Real-time PCR was performed in triplicates using 1 µl cDNA and 9 µl master mix consisting of 5 µl SYBR Green PCR Mix (4309155, Applied Biosystems), 3 µl H_2O and 1 µl of forward and reverse primers (0.5 µM final concentration). PPIA, GusB, and β-actin were used as housekeepers. For primer sequences, see Table S6.

Protein extraction and immunoblot analysis

Cells were lysed in RIPA buffer (150 mM NaCl, 50 mM Tris-HCl, pH 8, 1% Triton X100, 0.5% Sodium deoxycholate, and 0.1% SDS) supplemented with proteinase inhibitor cocktail (11873580001, Roche, Basel, Switzerland) and phosphatase inhibitor (04906837001, Roche). Cell lysates were centrifuged at 14,000 × *g* for 15 min at 4 °C and supernatants were collected. Protein concentration was quantified using the Pierce™ BCA Protein Assay Kit (23225, Thermo Fisher Scientific) according to the manufacturer's protocol. Twenty micrograms of total protein were loaded either on a 12% polyacrylamide-SDS gel or on a NativePAGE™ 4–12%, Bis-Tris Gels (NP0336BOX, Thermo Fisher Scientific) and transferred to a 0.2 µm nitrocellulose membrane (No10600001, GE Healthcare; Chicago, IL, USA). Membranes were blocked with 5% bovine serum albumin (BSA) (8076.3, Carl Roth, Karlsruhe, Germany) TBS-Tween (20 mM Tris-HCl, pH 7.4, 150 mM NaCl, 0.1% Tween 20) and probed with primary antibodies (as detailed in table S7) diluted 1:1000 in 5% BSA TBS overnight at 4 °C if not stated otherwise. Membranes were then incubated with a corresponding anti-mouse (926-32210, Li-Cor, Bad Homburg, Germany) or anti-rabbit (926-32211, Li-Cor) fluorescent secondary antibody diluted 1:10,000. The fluorescent signal was visualized with the LI-COR Odyssey® CLx system (Li-Cor).

Statistical analysis of experimental data

All experiments were carried out in three biological replicates. Data are represented as mean +/− standard deviation (SD). A one- or two-sided Student's *t*-test was used to compare differences between control and experimental groups. Results were considered as being statistically significant at $p < 0.05$. Statistical tests were calculated with GraphPad Prism version 7.04.

DATA AVAILABILITY

The data that support the findings of this study are available from the corresponding author upon reasonable request.

REFERENCES

1. Saxton RA, Sabatini DM. mTOR signaling in growth, metabolism, and disease. Cell. 2017;168:960–76.
2. Haghighat A, Mader S, Pause A, Sonenberg N. Repression of cap-dependent translation by 4E-binding protein 1: competition with p220 for binding to eukaryotic initiation factor-4E. EMBO J. 1995;14:5701–9.
3. Wang Z, Feng X, Molinolo AA, Martin D, Vitale-Cross L, Nohata N, et al. 4E-BP1 is a tumor suppressor protein reactivated by mTOR inhibition in head and neck cancer. Cancer Res. 2019;79:1438–50.
4. Ding M, Van der Kwast TH, Vellanki RN, Foltz WD, McKee TD, Sonenberg N, et al. The mTOR targets 4E-BP1/2 restrain tumor growth and promote hypoxia tolerance in PTEN-driven prostate cancer. Mol Cancer Res. 2018;16:682–95.
5. Dowling RJ, Topisirovic I, Alain T, Bidinosti M, Fonseca BD, Petroulakis E, et al. mTORC1-mediated cell proliferation, but not cell growth, controlled by the 4E-BPs. Science. 2010;328:1172–6.
6. Morita M, Gravel SP, Chenard V, Sikstrom K, Zheng L, Alain T, et al. mTORC1 controls mitochondrial activity and biogenesis through 4E-BP-dependent translational regulation. Cell Metab. 2013;18:698–711.
7. Braunstein S, Karpisheva K, Pola C, Goldberg J, Hochman T, Yee H, et al. A hypoxia-controlled cap-dependent to cap-independent translation switch in breast cancer. Mol Cell. 2007;28:501–12.
8. Dubois L, Magagnin MG, Cleven AH, Weppler SA, Grenacher B, Landuyt W, et al. Inhibition of 4E-BP1 sensitizes U87 glioblastoma xenograft tumors to irradiation by decreasing hypoxia tolerance. Int J Radiat Oncol Biol Phys. 2009;73:1219–27.
9. Graff JR, Konicek BW, Lynch RL, Dumstorf CA, Dowless MS, McNulty AM, et al. eIF4E activation is commonly elevated in advanced human prostate cancers and significantly related to reduced patient survival. Cancer Res. 2009;69:3866–73.
10. Karlsson E, Waltersson MA, Bostner J, Perez-Tenorio G, Olsson B, Hallbeck AL, et al. High-resolution genomic analysis of the 11q13 amplicon in breast cancers identifies synergy with 8p12 amplification, involving the mTOR targets S6K2 and 4EBP1. Genes Chromosomes Cancer. 2011;50:775–87.
11. Rutkovsky AC, Yeh ES, Guest ST, Findlay VJ, Muise-Helmericks RC, Armeson K, et al. Eukaryotic initiation factor 4E-binding protein as an oncogene in breast cancer. BMC Cancer. 2019;19:491.

12. Wu S, Wagner G. Deep computational analysis details dysregulation of eukaryotic translation initiation complex eIF4F in human cancers. Cell Syst. 2021;12:907. e6–23.e6.
13. Chao MW, Wang LT, Lai CY, Yang XM, Cheng YW, Lee KH, et al. eIF4E binding protein 1 expression is associated with clinical survival outcomes in colorectal cancer. Oncotarget. 2015;6:24092–104.
14. Cha YL, Li PD, Yuan LJ, Zhang MY, Zhang YJ, Rao HL, et al. EIF4EBP1 overexpression is associated with poor survival and disease progression in patients with hepatocellular carcinoma. PLoS ONE 2015;10:e0117493.
15. Tameire F, Verginadis II, Leli NM, Polte C, Conn CS, Ojha R, et al. ATF4 couples MYC-dependent translational activity to bioenergetic demands during tumour progression. Nat Cell Biol. 2019;21:889–99.
16. Liu Y, Horn JL, Banda K, Goodman AZ, Lim Y, Jana S, et al. The androgen receptor regulates a druggable translational regulon in advanced prostate cancer. Sci Transl Med. 2019;11:eaaw4993.
17. Juliana CA, Yang J, Rozo AV, Good A, Groff DN, Wang SZ, et al. ATF5 regulates beta-cell survival during stress. Proc Natl Acad Sci USA. 2017;114:1341–6.
18. Azar R, Lasfargues C, Bousquet C, Pyronnet S. Contribution of HIF-1alpha in 4E-BP1 gene expression. Mol Cancer Res. 2013;11:54–61.
19. Louis DN, Perry A, Reifenberger G, von Deimling A, Figarella-Branger D, Cavenee WK, et al. The 2016 World Health Organization Classification of Tumors of the Central Nervous System: a summary. Acta Neuropathol. 2016;131:803–20.
20. Louis DN, Perry A, Wesseling P, Brat DJ, Cree IA, Figarella-Branger D, et al. The 2021 WHO Classification of Tumors of the Central Nervous System: a summary. Neuro Oncol. 2021;23:1231–51.
21. Furnari FB, Fenton T, Bachoo RM, Mukasa A, Stommel JM, Stegh A, et al. Malignant astrocytic glioma: genetics, biology, and paths to treatment. Genes Dev. 2007;21:2683–710.
22. Stupp R, Mason WP, van den Bent MJ, Weller M, Fisher B, Taphoorn MJ, et al. Radiotherapy plus concomitant and adjuvant temozolomide for glioblastoma. N Engl J Med. 2005;352:987–96.
23. Weller M, van den Bent M, Preusser M, Le Rhun E, Tonn JC, Minniti G, et al. EANO guidelines on the diagnosis and treatment of diffuse gliomas of adulthood. Nat Rev Clin Oncol. 2021;18:170–86.
24. Agnihotri S, Burrell KE, Wolf A, Jalali S, Hawkins C, Rutka JT, et al. Glioblastoma, a brief review of history, molecular genetics, animal models and novel therapeutic strategies. Arch Immunol Ther Exp. 2013;61:25–41.
25. Bai H, Harmanci AS, Erson-Omay EZ, Li J, Coskun S, Simon M, et al. Integrated genomic characterization of IDH1-mutant glioma malignant progression. Nat Genet. 2016;48:59–66.
26. Gusev Y, Bhuvaneshwar K, Song L, Zenklusen JC, Fine H, Madhavan S. The REMBRANDT study, a large collection of genomic data from brain cancer patients. Sci Data. 2018;5:180158.
27. Sun L, Hui AM, Su Q, Vortmeyer A, Kotliarov Y, Pastorino S, et al. Neuronal and glioma-derived stem cell factor induces angiogenesis within the brain. Cancer Cell. 2006;9:287–300.
28. Gravendeel LA, Kouwenhoven MC, Gevaert O, de Rooi JJ, Stubbs AP, Duijm JE, et al. Intrinsic gene expression profiles of gliomas are a better predictor of survival than histology. Cancer Res. 2009;69:9065–72.
29. Murat A, Migliavacca E, Gorlia T, Lambiv WL, Shay T, Hamou MF, et al. Stem cell-related "self-renewal" signature and high epidermal growth factor receptor expression associated with resistance to concomitant chemoradiotherapy in glioblastoma. J Clin Oncol. 2008;26:3015–24.
30. Gulluoglu S, Tuysuz EC, Sahin M, Kuskucu A, Kaan Yaltirik C, Ture U, et al. Simultaneous miRNA and mRNA transcriptome profiling of glioblastoma samples reveals a novel set of OncomiR candidates and their target genes. Brain Res. 2018;1700:199–210.
31. Griesinger AM, Birks DK, Donson AM, Amani V, Hoffman LM, Waziri A, et al. Characterization of distinct immunophenotypes across pediatric brain tumor types. J Immunol. 2013;191:4880–8.
32. Cancer Genome Atlas Research N, Weinstein JN, Collisson EA, Mills GB, Shaw KR, Ozenberger BA, et al. The Cancer Genome Atlas Pan-Cancer analysis project. Nat Genet. 2013;45:1113–20.
33. Cerami E, Gao J, Dogrusoz U, Gross BE, Sumer SO, Aksoy BA, et al. The cBio cancer genomics portal: an open platform for exploring multidimensional cancer genomics data. Cancer Discov. 2012;2:401–4.
34. Gao J, Aksoy BA, Dogrusoz U, Dresdner G, Gross B, Sumer SO, et al. Integrative analysis of complex cancer genomics and clinical profiles using the cBioPortal. Sci Signal. 2013;6:1.
35. Court F, Le Boiteux E, Fogli A, Muller-Barthelemy M, Vaurs-Barriere C, Chautard E, et al. Transcriptional alterations in glioma result primarily from DNA methylation-independent mechanisms. Genome Res. 2019;29:1605–21.
36. Kawaguchi A, Yajima N, Tsuchiya N, Homma J, Sano M, Natsumeda M, et al. Gene expression signature-based prognostic risk score in patients with glioblastoma. Cancer Sci. 2013;104:1205–10.
37. Freije WA, Castro-Vargas FE, Fang Z, Horvath S, Cloughesy T, Liau LM, et al. Gene expression profiling of gliomas strongly predicts survival. Cancer Res. 2004;64:6503–10.
38. Tang Z, Li C, Kang B, Gao G, Li C, Zhang Z. GEPIA: a web server for cancer and normal gene expression profiling and interactive analyses. Nucleic Acids Res. 2017;45:W98–W102.
39. GT Consortium. The Genotype-Tissue Expression (GTEx) project. Nat Genet. 2013;45:580–5.
40. Liao P, Han S, Qu H. Expression, prognosis, and immune infiltrates analyses of E2Fs in human brain and CNS cancer. Biomed Res Int. 2020;2020:6281635.
41. Davis CA, Hitz BC, Sloan CA, Chan ET, Davidson JM, Gabdank I, et al. The Encyclopedia of DNA elements (ENCODE): data portal update. Nucleic Acids Res. 2018;46:D794–801.
42. Consortium EP. An integrated encyclopedia of DNA elements in the human genome. Nature. 2012;489:57–74.
43. Mimura I, Nangaku M, Kanki Y, Tsutsumi S, Inoue T, Kohro T, et al. Dynamic change of chromatin conformation in response to hypoxia enhances the expression of GLUT3 (SLC2A3) by cooperative interaction of hypoxia-inducible factor 1 and KDM3A. Mol Cell Biol. 2012;32:3018–32.
44. Musa J, Cidre-Aranaz F, Aynaud MM, Orth MF, Knott MML, Mirabeau O, et al. Cooperation of cancer drivers with regulatory germline variants shapes clinical outcomes. Nat Commun. 2019;10:4128.
45. Caldon CE, Sergio CM, Kang J, Muthukaruppan A, Boersma MN, Stone A, et al. Cyclin E2 overexpression is associated with endocrine resistance but not insensitivity to CDK2 inhibition in human breast cancer cells. Mol Cancer Ther. 2012;11:1488–99.
46. Lu TP, Tsai MH, Lee JM, Hsu CP, Chen PC, Lin CW, et al. Identification of a novel biomarker, SEMA5A, for non-small cell lung carcinoma in nonsmoking women. Cancer Epidemiol Biomark Prev. 2010;19:2590–7.
47. Musa J, Orth MF, Dallmayer M, Baldauf M, Pardo C, Rotblat B, et al. Eukaryotic initiation factor 4E-binding protein 1 (4E-BP1): a master regulator of mRNA translation involved in tumorigenesis. Oncogene. 2016;35:4675–88.
48. Kumar S, Sharife H, Kreisel T, Mogilevsky M, Bar-Lev L, Grunewald M, et al. Intratumoral metabolic zonation and resultant phenotypic diversification are dictated by blood vessel proximity. Cell Metab. 2019;30:201.e6–11.e6.
49. Voutsadakis IA. 8p11.23 Amplification in breast cancer: molecular characteristics, prognosis and targeted therapy. J Clin Med. 2020;9:3079.
50. Zhang X, Lv QL, Huang YT, Zhang LH, Zhou HH. Akt/FoxM1 signaling pathway-mediated upregulation of MYBL2 promotes progression of human glioma. J Exp Clin Cancer Res. 2017;36:105.
51. Zhang P, Pei C, Wang X, Xiang J, Sun BF, Cheng Y, et al. A balance of Yki/Sd activator and E2F1/Sd repressor complexes controls cell survival and affects organ size. Dev Cell. 2017;43:603–17. e5.
52. Li M, Ge Q, Wang W, Wang J, Lu Z. c-Jun binding site identification in K562 cells. J Genet Genomics. 2011;38:235–42.
53. Dittmer J. The role of the transcription factor Ets1 in carcinoma. Semin Cancer Biol. 2015;35:20–38.
54. Ren F, Wang L, Shen X, Xiao X, Liu Z, Wei P, et al. MYBL2 is an independent prognostic marker that has tumor-promoting functions in colorectal cancer. Am J Cancer Res. 2015;5:1542–52.
55. Thorner AR, Hoadley KA, Parker JS, Winkel S, Millikan RC, Perou CM. In vitro and in vivo analysis of B-Myb in basal-like breast cancer. Oncogene. 2009;28:742–51.
56. Brennan CW, Verhaak RG, McKenna A, Campos B, Noushmehr H, Salama SR, et al. The somatic genomic landscape of glioblastoma. Cell. 2013;155:462–77.
57. Hanada N, Lo HW, Day CP, Pan Y, Nakajima Y, Hung MC. Co-regulation of B-Myb expression by E2F1 and EGF receptor. Mol Carcinog. 2006;45:10–7.
58. Ceccarelli M, Barthel FP, Malta TM, Sabedot TS, Salama SR, Murray BA, et al. Molecular profiling reveals biologically discrete subsets and pathways of progression in diffuse glioma. Cell. 2016;164:550–63.
59. Hashiya N, Jo N, Aoki M, Matsumoto K, Nakamura T, Sato Y, et al. In vivo evidence of angiogenesis induced by transcription factor Ets-1: Ets-1 is located upstream of angiogenesis cascade. Circulation. 2004;109:3035–41.
60. Arderiu G, Pena E, Aledo R, Espinosa S, Badimon L. Ets-1 transcription is required in tissue factor driven microvessel formation and stabilization. Angiogenesis. 2012;15:657–69.
61. Iyirhiaro GO, Zhang Y, Estey C, O'Hare MJ, Safarpour F, Parsanejad M, et al. Regulation of ischemic neuronal death by E2F4-p130 protein complexes. J Biol Chem. 2014;289:18202–13.
62. Okumura F, Joo-Okumura A, Nakatsukasa K, Kamura T. Hypoxia-inducible factor-2alpha stabilizes the von Hippel-Lindau (VHL) disease suppressor, Myb-related protein 2. PLoS ONE. 2017;12:e0175593.
63. Shao M, Ren Z, Zhang R. MYBL2 protects against H9c2 injury induced by hypoxia via AKT and NFkappaB pathways. Mol Med Rep. 2018;17:4832–8.
64. Petroulakis E, Parsyan A, Dowling RJ, LeBacquer O, Martineau Y, Bidinosti M, et al. p53-dependent translational control of senescence and transformation via 4E-BPs. Cancer Cell. 2009;16:439–46.

65. Paugh BS, Broniscer A, Qu C, Miller CP, Zhang J, Tatevossian RG, et al. Genome-wide analyses identify recurrent amplifications of receptor tyrosine kinases and cell-cycle regulatory genes in diffuse intrinsic pontine glioma. J Clin Oncol. 2011;29:3999–4006.
66. Zhao Z, Zhang KN, Wang Q, Li G, Zeng F, Zhang Y, et al. Chinese Glioma Genome Atlas (CGGA): a comprehensive resource with functional genomic data from Chinese glioma patients. Genomics Proteomics Bioinformatics. 2021;19:1–12.
67. Berchtold NC, Cribbs DH, Coleman PD, Rogers J, Head E, Kim R, et al. Gene expression changes in the course of normal brain aging are sexually dimorphic. Proc Natl Acad Sci USA. 2008;105:15605–10.
68. Pai S, Li P, Killinger B, Marshall L, Jia P, Liao J, et al. Differential methylation of enhancer at IGF2 is associated with abnormal dopamine synthesis in major psychosis. Nat Commun. 2019;10:2046.
69. Kobow K, Jabari S, Pieper T, Kudernatsch M, Polster T, Woermann FG, et al. Mosaic trisomy of chromosome 1q in human brain tissue associates with unilateral polymicrogyria, very early-onset focal epilepsy, and severe developmental delay. Acta Neuropathol. 2020;140:881–91.
70. Mack SC, Singh I, Wang X, Hirsch R, Wu Q, Villagomez R, et al. Chromatin landscapes reveal developmentally encoded transcriptional states that define human glioblastoma. J Exp Med. 2019;216:1071–90.
71. Robinson JT, Thorvaldsdottir H, Winckler W, Guttman M, Lander ES, Getz G, et al. Integrative genomics viewer. Nat Biotechnol. 2011;29:24–6.
72. Kondo K, Klco J, Nakamura E, Lechpammer M, Kaelin WG Jr. Inhibition of HIF is necessary for tumor suppression by the von Hippel-Lindau protein. Cancer Cell. 2002;1:237–46.
73. Johnson TK, Schweppe RE, Septer J, Lewis RE. Phosphorylation of B-Myb regulates its transactivation potential and DNA binding. J Biol Chem. 1999;274:36741–9.

ACKNOWLEDGEMENTS

The results published here are in part based on data generated by TCGA Research Network (https://www.cancer.gov/tcga). We would like to acknowledge the ENCODE Consortium and the Bernstein, Farnham, Myers, and Snyder laboratories for generating the respective datasets.

AUTHOR CONTRIBUTIONS

Conception and design: LH, GL. Experimental procedures: LH. Data analysis and interpretation: LH, DP, JM, GL. Critical review and discussion: BR, MR, TG, GR. Manuscript writing: LH, GR, GL. All authors read and approved the final manuscript.

FUNDING

GL was supported by grants from the Elterninitiative Düsseldorf e.V. (grant no. 701910003), the Research Commission of the Medical Faculty, Heinrich Heine University Düsseldorf (grant no. 2016-056), the Deutsche Forschungsgemeinschaft (grant no. LE 3751/2-1), the German Cancer Aid (grant no. 70112624), and the Dr. Rolf M. Schwiete Stiftung (grant no. 2020-018). LH was funded by the Dr. Rolf M. Schwiete Stiftung (grant no. 2020-018). GR and MR were supported by a joint grant from the Deutsche Forschungsgemeinschaft (grant nos. RE 938 4-1 and RE 2857/2-1). The laboratory of TGPG was supported by the German Cancer Aid (Max-Eder program, 70112257), the Matthias-Lackas foundation, the Dr. Leopold and Carmen Ellinger foundation, and the Barbara and Wilfried Mohr foundation. JM was supported by a scholarship of the Kind-Philipp foundation and the Rudolf und Brigitte Zenner foundation. BR was supported by the Israel Science Foundation (grant no. 1436/19). Open Access funding enabled and organized by Projekt DEAL.

COMPETING INTERESTS

The authors declare no competing interests.

ADDITIONAL INFORMATION

Supplementary information The online version contains supplementary material available at https://doi.org/10.1038/s41420-022-00883-z.

Correspondence and requests for materials should be addressed to Gabriel Leprivier.

Reprints and permission information is available at http://www.nature.com/reprints

Publisher's note Springer Nature remains neutral with regard to jurisdictional claims in published maps and institutional affiliations.

3.1.2. MYC is an additional transcription factor candidate regulating *EIF4EBP1* promoter activity

In addition to the data presented in manuscript I, MYC was investigated as an additional transcription factor candidate. Recent literature described MYC as a direct regulator of *EIF4EBP1* transcription either alone (BALAKUMARAN *et al.* 2009) or by interacting with ATF4 (TAMEIRE *et al.* 2019). Therefore, it was not surprising that MYC fulfilled the three defined criteria (as explained in the manuscript) for a transcription factor potentially regulating *EIF4EBP1*. *MYC* has been reported to be overexpressed in glioblastoma and lower grade glioma (TANG *et al.* 2021). Functionally, MYC was shown to protect glioma cells of DNA damage and to support their invasion (TANG *et al.* 2021). The own analyses revealed that *MYC* is co-expressed with *EIF4EBP1* in 8 glioma and glioblastoma cohorts (Figure 6A-B; Table 1), overexpressed in 6 glioblastoma cohorts (Figure 6C-D), and ChIP-seq indicates binding of MYC to the *EIF4EBP1* promoter from analysing ENCODE datasets (Figure 6E), in accordance with a previous study (TAMEIRE *et al.* 2019). Whether *MYC* overexpression is dependent of IDH mutation status in glioma is inconclusive, since analyses in three different cohorts showed three different results (Figure 6F-H). Next, a luciferase reporter containing the -661; +705 *EIF4EBP1* promoter was used to assess whether MYC is able to induce *EIF4EBP1* promoter activity in HEK293-T cells. This showed that MYC dose-dependently activated the *EIF4EBP1* promoter when overexpressed in these cells (Figure 6I), thereby confirming previous reports that *EIF4EBP1* is a target gene of MYC (BALAKUMARAN *et al.* 2009, TAMEIRE *et al.* 2019).

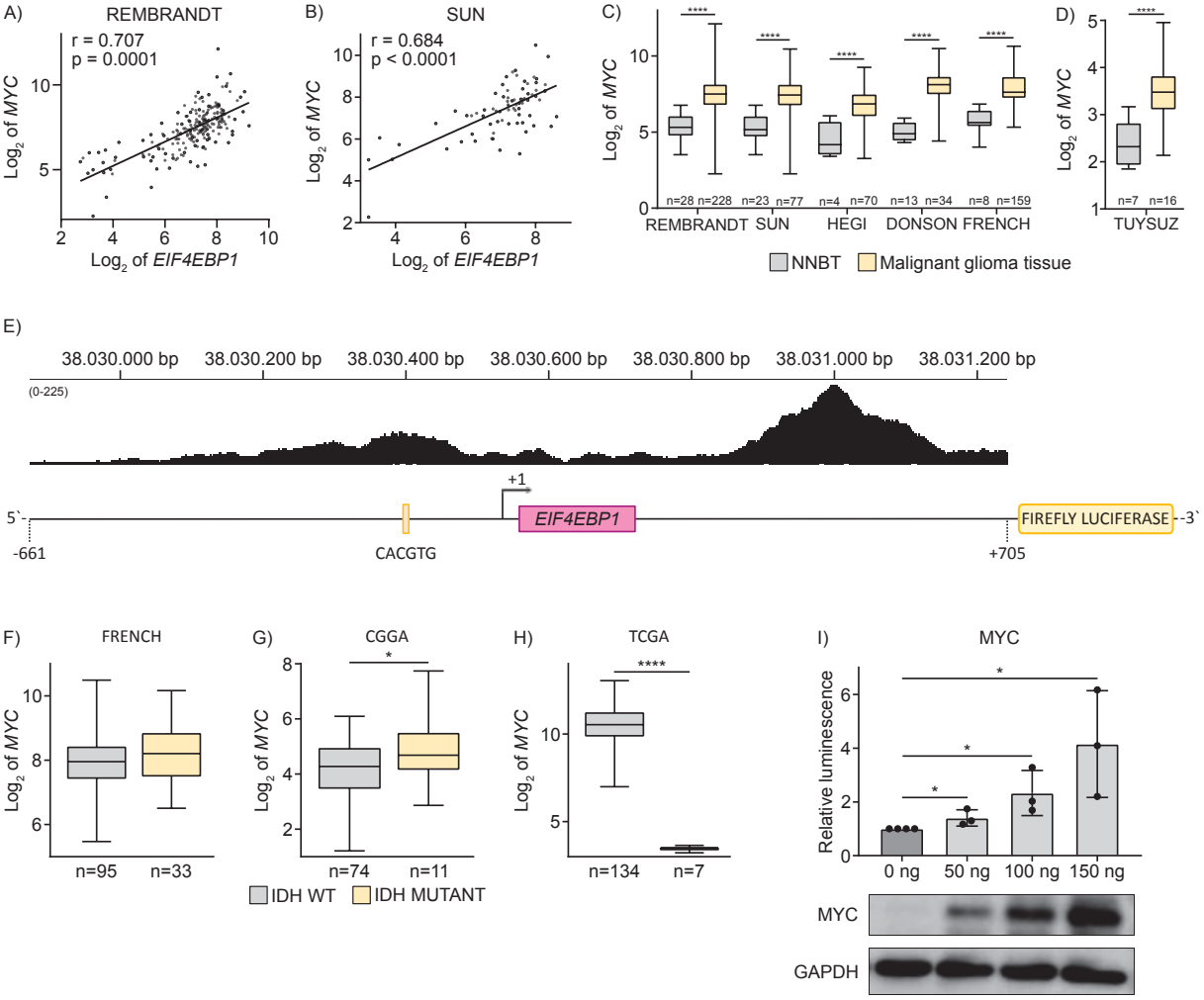

Figure 6: MYC is a promising transcription factor candidate for regulating *EIF4EBP1* expression in glioblastoma. A and B) Expression levels of *EIF4EBP1* mRNA in glioblastoma patient samples plotted against the mRNA expression levels of *MYC* in the (A) REMBRANDT (n=228) (Gusev et al. 2018) and (B) SUN cohort (n=77) (Sun et al. 2006). Co-expression levels were quantified by calculating the Pearson correlation coefficient. C and D) Expression levels of *MYC* in non-neoplastic brain tissue (NNBT) and in malignant glioma tissue samples from the indicated patient cohorts (C) REMBRANDT (Gusev et al. 2018), SUN (Sun et al. 2006), HEGI (Murat et al. 2008), DONSON (Griesinger et al. 2013), FRENCH (Gravendeel et al. 2009) (microarray platforms u133p2) and (D) TUYSUZ (Gulluoglu et al. 2018) (microarray platforms hugene21t). E) ChIP peak locations for MYC and the MYC consensus binding motif (yellow rectangle) within the human *EIF4EBP1* promoter, exon 1 and part of intron 1 (hg38; Chr8: 38,029,873 - 38,031,239), from ChIP-sequencing data (Encode consortium, Encyclopedia of DNA Elements at UCSC; (Consortium 2012, Davis et al. 2018). F)-H) Expression levels of *MYC* according to the IDH mutation status in malignant glioma tissues were analyzed using the (F) FRENCH (Gravendeel et al. 2009), (G) CGGA (Zhao et al. 2021) and (H) TCGA cohorts (Cancer Genome Atlas Research et al. 2013). I) HEK293-T cells were transfected with the -661; +705 *EIF4EBP1* promoter reporter construct, together with increasing amounts of a plasmid expressing MYC and a vector expressing *Renilla* luciferase. Luciferase activities were detected using the dual luciferase reporter assay. Firefly luciferase activity was normalized to *Renilla* luciferase activity and the ratio was normalized to the corresponding 0 ng condition. Data represent the mean of three independent replicates ± standard deviation (SD).

Significance was calculated using an unpaired and two-tailed parametric t-test (*p<0.05, ****p<0.0001). A representative immunoblot analyzing overexpression of MYC indicates the presence of the transcription factors.

Table 1: Overview of the co-expression analysis between *EIF4EBP1* and *MYC* in various glioma cohorts analyzed.

Transcription factor	Cohort	r-value	p-value
MYC	SUN (SUN *et al.* 2006)	0.684	6.91e-12
	REMBRANDT (MADHAVAN *et al.* 2009, GUSEV *et al.* 2018)	0.708	5.96e-36
	HEGI (MURAT *et al.* 2008)	0.462	5.75e-05
	TCGA (CANCER GENOME ATLAS RESEARCH *et al.* 2013)	0.378	4.77e-18
	FREIJE (FREIJE *et al.* 2004)	0.560	3.82e-07
	FRENCH (GRAVENDEEL *et al.* 2009)	0.445	4.10e-09
	KAWAGUCHI (KAWAGUCHI *et al.* 2013)	0.628	1.20e-04
	CGGA (ZHAO *et al.* 2021)	0.507	8.74e−07

3.1.3. MYBL2 does not induce *EIF4EBP1* promoter activity through a MYBL2 consensus binding motif

Manuscript I reported that MYBL2 induced *EIF4EBP1* promoter activity in a dose-dependent manner when using a -661; +705 *EIF4EBP1* promoter construct (Manuscript I Figure 3H). As a complement to that, the MYBL2 binding motif(s) mediating the action of MYBL2 on

EIF4EBP1 promoter were characterized. While ChIP peaks indicated binding of MYBL2 within the -661; +705 *EIF4EBP1* promoter region (Manuscript I Figure 2H), *in silico* analysis of the sequence did not reveal any MYBL2 consensus binding site within this region. However, this analysis revealed a MYBL2 consensus binding motif containing the core motif GTTA/TAAC, as reported by JASPAR, at -1428 upstream of the *EIF4EBP1* transcription start site (Figure 7A and B). Therefore, the contribution of this MYBL2 binding site was investigated using a -1532; -31 *EIF4EBP1* promoter construct. As expected, overexpression of MYBL2 significantly increased -1532; -31 *EIF4EBP1* promoter activity when transfected in HEK293-T cells (Figure 7C). Surprisingly, mutation of the MYBL2 consensus binding motif (MUT1) did not reduce *EIF4EBP1* promoter activity in response to MYBL2 but resulted in an increase of promoter activity (Figure 7D). A search for other potential MYBL2 binding sequences within the -1532; -31 promoter region revealed the GTTA core motif twice and its reverse complementary sequence TAAC once. Although this is only half the MYBL2 consensus motif reported by JASPAR, those bases are of high importance for MYBL2 binding (Figure 7B). To determine which potential MYBL2 binding sites supports MYBL2-mediated activation of the *EIF4EBP1* promoter, all four potential MYBL2 binding sites were mutated, individually or all together, in the -1532; -31 *EIF4EBP1* promoter luciferase construct (Figure 7A). Neither single mutations nor mutation of the 4 binding sites reduced or abrogated the activation of *EIF4EBP1* promoter by MYBL2 (Figure 7D). It was determined in the literature that MYBL2 can bind to the consensus motif (T/C)(G/A)(G/A/T)C(A/C)GTT of the MYB family member c-MYB with a similar affinity (HOWE & WATSON 1991). Based on this information, screening for the c-MYB consensus motifs within the promoter region indeed revealed two c-MYB binding motifs that are contained within the promoter construct (Figure 7A). This might explain why induction of the *EIF4EBP1* promoter by MYBL2 was not suppressed by mutations of all potential MYBL2 binding sites. Collectively, these data indicate that MYBL2 can activate the *EIF4EBP1* promoter independently of the detected MYBL2 consensus motif and MYBL2 core motifs. Instead, MYBL2 might bind to the consensus motif of c-MYB within the promoter or interact with a binding partner, which is directly binding to the *EIF4EBP1* promoter.

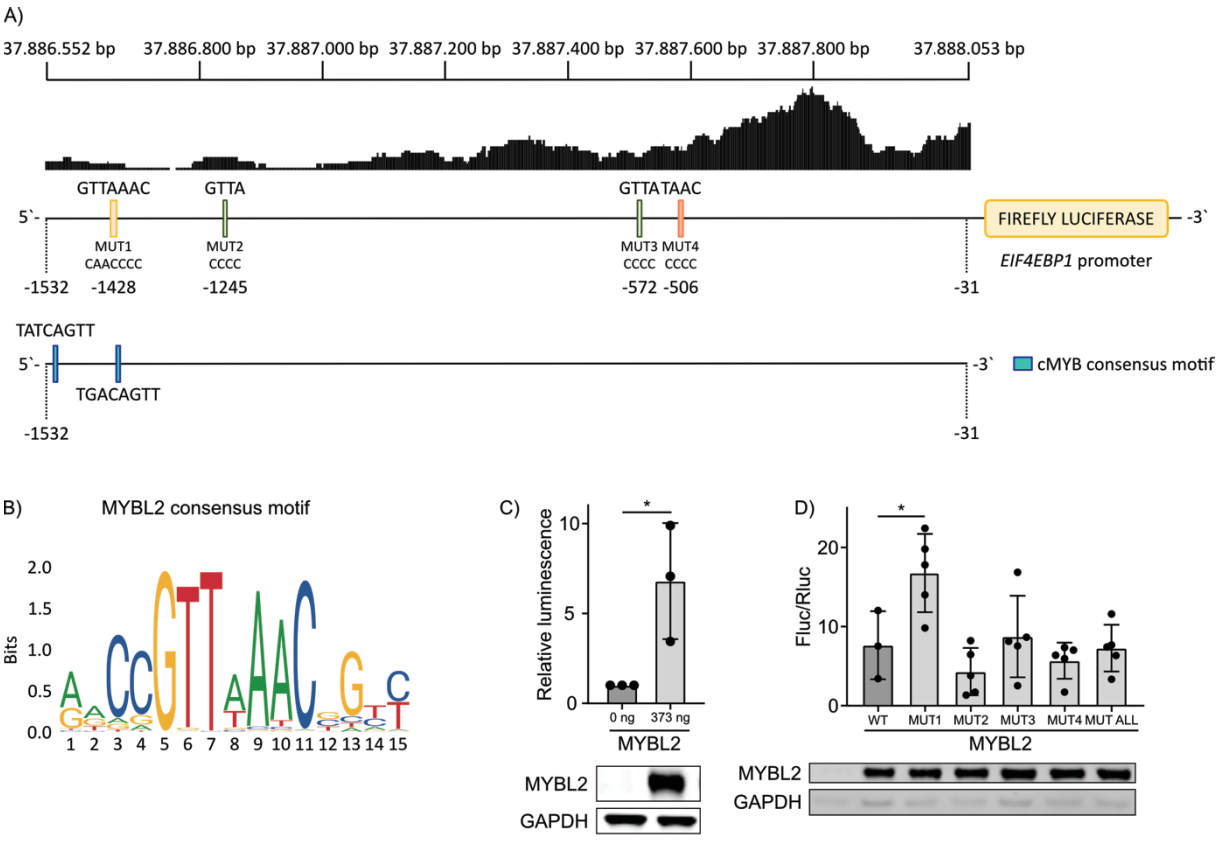

Figure 7: MYBL2 does not mediate *EIF4EBP1* transcription through its consensus binding site. A) ChIP peak locations for MYBL2 and the MYBL2 consensus binding motif (yellow rectangle) within the human *EIF4EBP1* promoter, upstream of the transcription start site (hg19; Chr8: 37,886,552 - 37,888,053) from ChIP-sequencing data (NCBI Geo data: accession code GSE119972; (MUSA et al. 2019)). Potential binding motifs and the mutated sequences are marked as rectangles. Blue rectangles represent the consensus motifs of c-MYB. B) MYBL2 consensus binding motif from JASPAR (SANDELIN et al. 2004). C) and D) HEK293-T cells were transfected with the -1532; -31 *EIF4EBP1* promoter reporter construct (C) without or (D) with mutations of the potential MYBL2 binding motifs as indicated in A, together with 373 ng of plasmids expressing MYBL2 and a vector expressing *Renilla* luciferase. Luciferase activities were detected using the dual luciferase reporter assay. Firefly luciferase activity was normalized to *Renilla* luciferase activity and the ratio was normalized to the corresponding 0 ng condition. Data represent the mean of three independent replicates ± standard deviation (SD). Significance was calculated using an unpaired and two-tailed parametric t-test (*p<0.05, ****p<0.0001). Below each diagram, a representative immunoblot analysing overexpression of each of the indicated transcription factors is presented. Bp: base pairs

3.1.4. *EIF4EBP1* transcription is not regulated by E2F6, JUN or FOXM1 in glioblastoma cell lines

Next, it was investigated whether the selected transcription factor candidates are regulating *EIF4EBP1* gene expression by transiently knocking down the transcription factors and investigating 4EBP1 mRNA and protein levels. To estimate the half-life of the 4EBP1 protein,

U-118 MG were treated with cycloheximide (CHX), which blocks protein synthesis, for 0 h, 72 h, 96 h and 120 h and an immunoblot was performed. 4EBP1 protein levels did not decrease drastically after 120 h of CHX treatment indicating that the protein is quite stable (Figure 8A). One transcription factor that was investigated more closely in the manuscript as a potential regulator of *EIF4EBP1* transcription was E2F6. E2F6, although reported to be a transcriptional repressor, induced *EIF4EBP1* promoter activity in our experiment (Manuscript I Figure 3E). Upon transient KD of *E2F6* in two glioblastoma cell lines, U-87 MG and U-118 MG, no change of 4EBP1 mRNA or protein levels was detected (Manuscript I Figure 4A-B). In addition, the same experiment was performed in two additional glioblastoma cell lines, namely LN-229 and U-251 MG. In both cell lines, *E2F6* transcript levels were significantly decreased following transfection of a siRNA pool targeting *E2F6*, which was confirmed at the protein level (Figure 8A-B). Upon *E2F6* KD, *EIF4EBP1* transcript levels were significantly decreased in LN-229 cells, whereas *EIF4EBP1* mRNA levels were not altered in U-251 MG cells (Figure 8A-B). Levels of 4EBP1 protein were not reduced in both cell lines upon *E2F6* KD (Figure 8A-B), indicating that E2F6 is not a regulator of *EIF4EBP1* expression in glioblastoma cells. Furthermore, we investigated whether FOXM1 regulates *EIF4EBP1* transcription since the luciferase reporter assay showed a small but significant induction of the *EIF4EBP1* promoter following FOXM1 overexpression (Manuscript I Figure 3B). Transient KD of *FOXM1* in U-118 MG, using two different siRNAs targeting *FOXM1*, resulted in a strong decrease of *FOXM1* mRNA levels and protein levels (for si3). However, 4EBP1 mRNA and protein levels were not altered by *FOXM1* KD in this cell line (Figure 8C). This indicates that FOXM1 exhibits no regulatory function on *EIF4EBP1* transcription in glioblastoma cells.

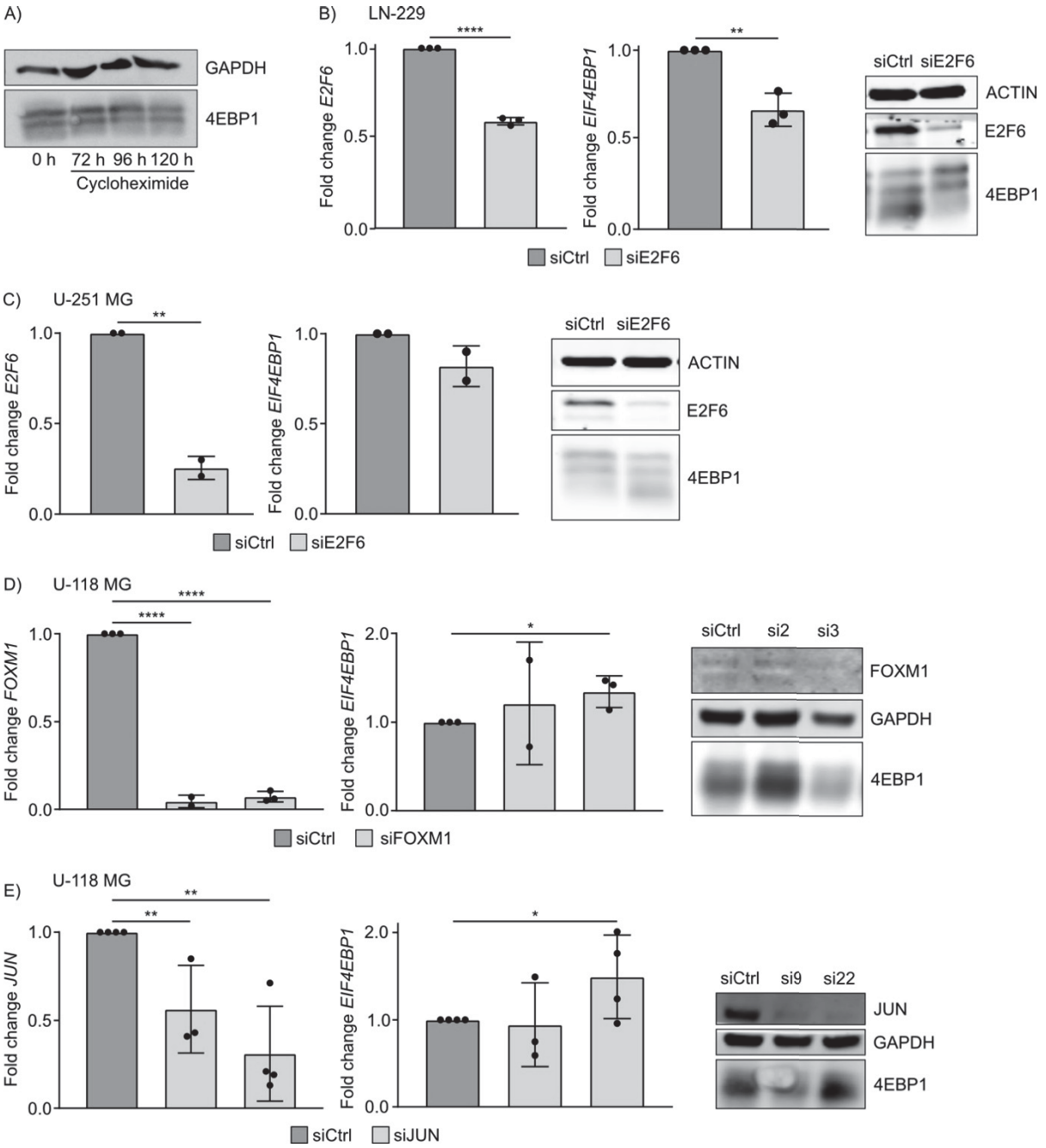

Figure 8: *EIF4EBP1* mRNA and protein expression is not regulated by E2F6, FOXM1 or JUN. A) U-118 MG were treated with 50 µg/ml cycloheximide and samples were harvested at the indicated time points. 4EBP1 levels were determined by immunoblot. Glioblastoma cells were transiently transfected with negative control siRNAs or control siPool (siCtrl), and a siRNA pool targeting (B and C) E2F6 (si E2F6) in LN-229 and U-251 MG or two different siRNAs each targeting either (D) FOXM1 (si 2 and si 3) or (E) JUN (si 9 and si 22) in U-118 MG. Cells were re-transfected after 96 h with their corresponding siRNA and incubated for a total of 192 h. MRNA and protein were harvested to determine the expression levels of *EIF4EBP1*/4EBP1 and (B and C) E2F6, (D) FOXM1 or (E) JUN by qRT-PCR and immunoblots. Data obtained by qRT-PCR represent the mean of two or three independent replicates ± SD, as indicated by the number of dots in the bar graph, and the fold change in expression was normalized to the negative control. Results of representative immunoblot are depicted on the right-hand side of the diagrams representing the qRT-PCR results. Significance was calculated using an unpaired and one-tailed parametric t-test (*p<0.05, **p<0.01, ****p<0.0001).

In manuscript I, it was not possible to conclude whether JUN regulates the *EIF4EBP1* promoter. While JUN overexpression had no effect on the activity of the -661, +705 *EIF4EBP1* promoter (Manuscript I Figure 3C), no JUN consensus binding motif was detected in this promoter region. Based on the ChIP data for JUN binding to *EIF4EBP1* promoter, this suggested that JUN may bind outside the studied -661, +705 promoter region and thus may regulate *EIF4EBP1* transcription. *In silico* analysis highlighted multiple JUN consensus binding motifs, TGAC/GTCA (LI *et al.* 2011), with the closest ones to the *EIF4EBP1* transcription start site being located at -3644, +1910 and +2815. It thus was explored whether JUN is a regulator of the *EIF4EBP1* promoter in glioblastoma cells. Transient *JUN* KD in U-118 MG cells decreased *JUN* mRNA and protein levels but did not lead to decreases of 4EBP1 mRNA and protein levels, confirming that JUN does not regulate endogenous *EIF4EBP1* transcription in glioblastoma cell lines (Figure 8D). Taken all data together, MYBL2 and ETS1 remain the most promising transcription factors regulating the *EIF4EBP1* promoter and transcription in glioblastoma cells.

3.1.5. Functional impact of 4EBP1 on migration and invasion of glioblastoma cells

Both MYBL2 and ETS1 have been shown to promote invasion and migration of tumor cells (REN *et al.* 2015, ZHANG *et al.* 2017). Therefore, experiments were performed to explore whether 4EBP1, as a downstream factor of both transcription factors, impacts migration and/or invasion of cancer cells, and thus could mediate the functions of MYBL2 and ETS1. To assess this, the ORIS™ cell migration and invasion assay was used, which contains a cell stopper in the middle of each well of a 96 wells plate. Stable Ctrl and 4EBP1 KD U-87 MG and U-118 MG cells (Figure 9D) were plated around the cell stoppers; for the invasion assay cells were prepared in a collagen suspension. Following overnight incubation, cell stoppers were removed. Cells were incubated for another 48 h before they were stained with HOECHST 33342 and pictures were taken capturing the fluorescent signal of each cell which migrated or invaded. When analyzing the number of cells migrating or invading through the space left after removing the stopper, there was no difference of migration or invasion between Ctrl and 4EBP1 KD lines for both U-87 MG and U-118 MG cells (Figure 9A and B). To ascertain that Ctrl and 4EBP1 KD cells grew at a similar pace, these cells were plated in a 96 well plate and cell viability was measured using CellTiter-Glo at 0 h and after 48 h. No difference of cell viability was detected between Ctrl and 4EBP1 KD U-87 MG and U-118 MG

cells (Figure 9C), which goes along with observations from the literature that 4EBP1 does not impact cellular proliferation of glioblastoma cells in basal conditions (DUBOIS *et al.* 2009). Taken together, these data suggests that 4EBP1 does not impact migration or invasion of glioblastoma cells and thus may mediate another cellular function of its upstream regulators ETS1 and MYBL2.

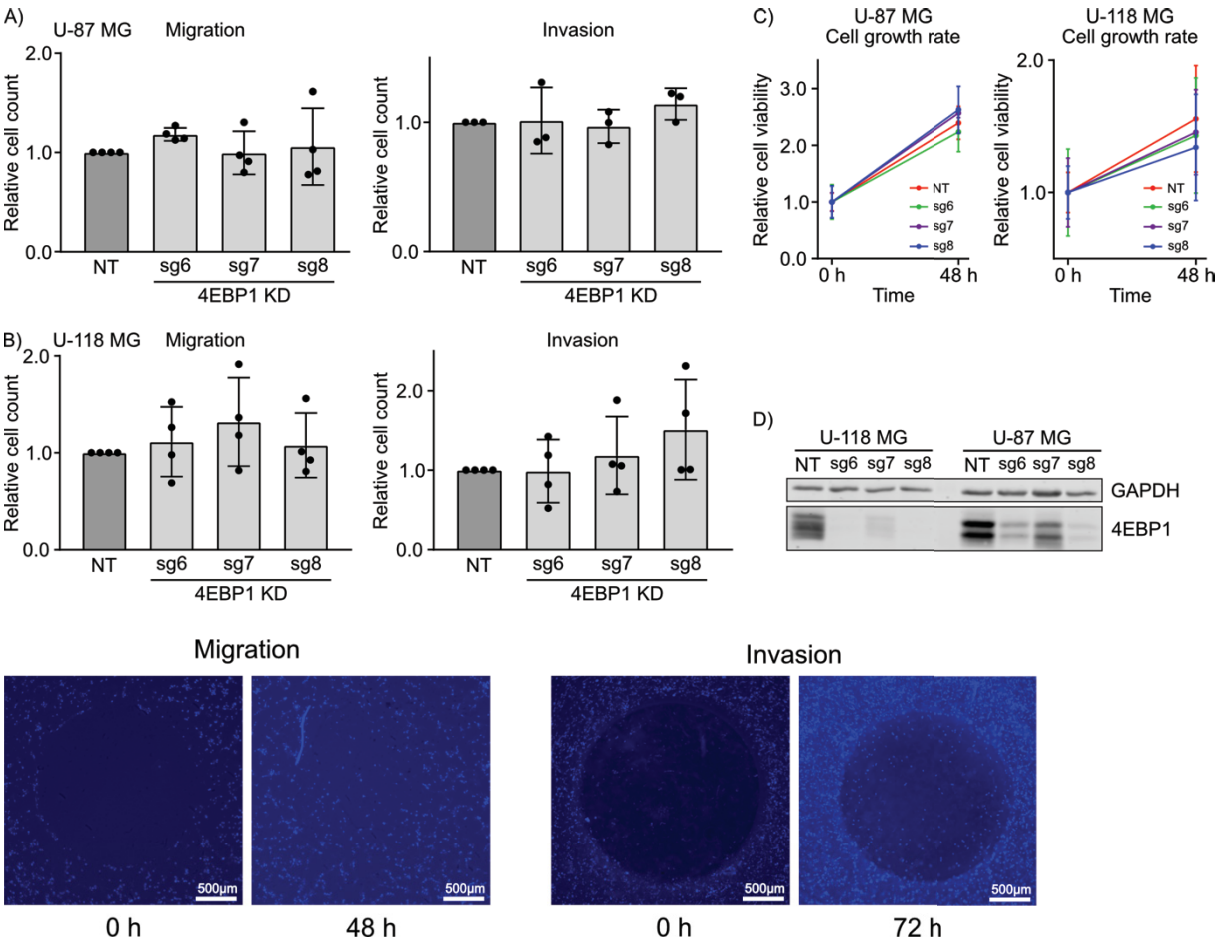

Figure 9: 4EBP1 does not impact migration or invasion in glioblastoma cell lines. A) and B) U-87 MG and U-118 MG 4EBP1 Non-target (NT) or 4EBP1 KD cells were plated (25.000 cells/wells) in a 96 wells plate, using the ORIS^{TM} cell migration and invasion assays, containing a cell stopper in the middle of each well, and covered with medium (migration) or embedded in collagen (invasion). After cell stopper removal, cells were incubated for 48 h (migration) or 72 h (invasion), stained with Hoechst 33342 and pictures of migrated/invaded area were taken. The cell number within this area were counted with Image J. Data represent the mean of four independent replicates ± standard deviation (SD). Representative pictures for 0 h and 48 h/72 h time points of migration and invasion assays are represented on the bottom of the figure. C) U-87 MG and U-118 MG NT or 4EBP1 KD cells were plated in 96 wells and cell viability was measured at 0 h and 48 h using CellTiter-Glo assay. Data represent the mean of three independent replicates ± SD. D) Representative immunoblot indicates 4EBP1 KD in U-118 MG and U-87 MG cell lines.

3.2. Functional impact of 4EBP1 on oncogenic transformation and tumorigenesis

Cancer cells, as well as normal cells, are subjected to metabolic stress conditions like glucose starvation, which they need to adapt to ensure their survival. The biological adaptation of normal cells is an evolutionary conserved response, which is hijacked by cancer cells when confronted to metabolic stress of the tumor microenvironment. The players and regulators of such adaptative processes are poorly characterized, so far.

In manuscript II, 4EBP1 was unraveled as a protective factor under glucose deprivation, a function conserved in yeast, mouse and human, which is exploited by cancer cells for stress adaptation. Functionally, 4EBP1 blocks fatty acid synthesis by translationally inhibiting Acetyl-CoA Carboxylase (ACC) 1 expression, in turn preventing dysregulation of the intracellular redox balance under glucose starvation (Figure 10). Metabolic stress is highly relevant for cancer, not only because cancer cells are often confronted with nutrient poor conditions, but because it resembles the stress occurring during oncogenic transformation and the first steps of tumor initiation (SCHAFER *et al.* 2009, JEON *et al.* 2012). Oncogenes rely on adaptive mechanisms to overcome the stress associated with transformation. Since 4EBP1/2 was reported to be required for oncogenic Ras transformation (PETROULAKIS *et al.* 2009), we asked how 4EBP1/2 contributes to oncogenic transformation and whether 4EBP1/2 supports transformation by other oncogenes.

In manuscript II, I specifically contributed by investigating: i) the role of 4EBP1/2 in oncogenic transformation by HER2, ii) the role of 4EBP1 in tumorigenesis of various cancer types, iii) the underlying mechanism of 4EBP1 function in transformation and tumorigenicity. Furthermore, I used publically available data sets to investigate the clinical relevance of *EIF4EBP1* in various cancer entities, in particular glioblastoma. Summarizing the contributing data, I could show that 4EBP1/2 deficiency, induced 4EBP1/2 DKO or 4EBP1 KD, prevented oncogenic HER2 transformation and reduced the tumorigenic potential of tumor cells of different origin (Manuscript II Figure 6A, Figure 7E and F). Additionally, I uncovered that 4EBP1 promotes transformation and tumorigenicity by maintaining the redox balance, through blocking fatty acid synthesis (Figure 10A and B; Manuscript II Figure 6B and C, Figure 7G and H, Supplementary Figure 6A and B). As *EIF4EBP1* has been reported previously to be overexpressed in many different cancer entities (WU & WAGNER 2021), I determined the

expression of *EIF4EBP1* according to grade in glioma (Manuscript II Figure 7B), which indicates that *EIF4EBP1* expression positively correlates with disease progression. In contrast, *EIF4EBP2* expression was found not to be overexpressed in most cancer types, indicating little clinical relevance (Manuscript II Supplementary Figure 5B). High levels of *EIF4EBP1* correlated with poor prognosis in various cancer types, including glioblastoma and glioma (Manuscript II Figure 7C and D, Supplementary Figure 5C-E). Taken together, this data supports a pro-tumorigenic function for 4EBP1 in gliomas including glioblastoma.

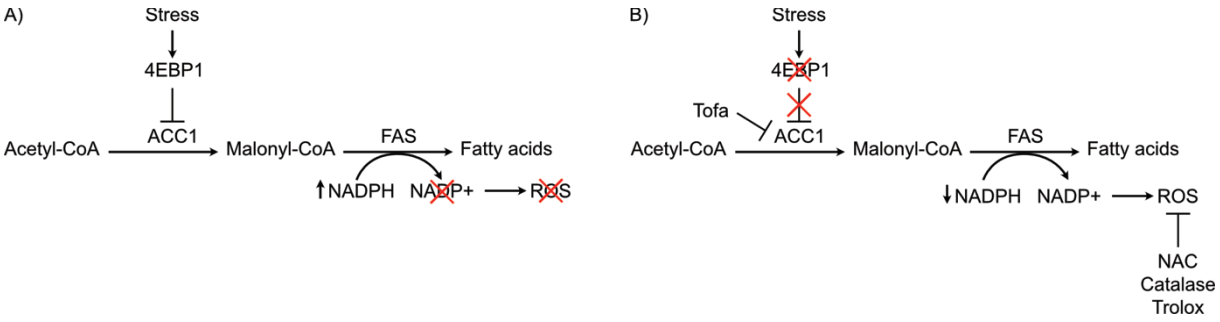

Figure 10: Illustration of the mechanism underlying the protective role of 4EBP1 under stress conditions. A) Upon activation, 4EBP1 selectively blocks translation of *ACACA* transcripts, coding for ACC1, the rate limiting enzyme of the fatty acid synthesis pathway. In consequence, fatty acid synthesis is inhibited and NADPH consumption is reduced, which allows maintaining the redox balance and supporting cell survival. B) Cells lacking 4EBP1 cannot block fatty acid synthesis under stress conditions, resulting in NADPH consumption and ROS accumulation leading to an unbalanced redox state. Treatment of cells with either antioxidants or the ACC1 inhibitor 5-(Tetradecyloxy)-2-furoic acid (Tofa) would, theoretically, maintain the redox balance by neutralizing ROS or by blocking fatty acid synthesis.

3.2.1. MANUSCRIPT II

4EBP1/2 support cell survival under metabolic stress by translationally regulating fatty acid synthesis

Tal Levy[1,2*], Kai Voeltzke[3*], Laura Hauffe[3*], Khawla Alasad[1,2*], Marteinn Snaebjörnsson[4], Ran Marciano[1,2], Katerina Scharov[3,5], Melanie Planque[6], Kim Vriens[6], Stefan Christen[6], Christina Hassiepen[3], Alisa Kahler[3], Beate Heider[3], Daniel Picard[3,5,7], Katja Bendrin[8], Andres Vargas-Toscano[9], Ulf Kahlert[9], Christiane Knobbe-Thomsen[3], Marc Remke[3,5,7], Moshe Elkabets[10,11], Thomas GP Grünewald[12,13,14,15], Andreas Reichert[8], Sarah-Maria Fendt[6], Almut Schulze[4], Guido Reifenberger[3], Barak Rotblat[1,2#], Gabriel Leprivier[3#]

[1]The National Institute for Biotechnology in the Negev, Ben-Gurion University of the Negev, Beer Sheva 84105, Israel.

[2]Department of Life Sciences, Faculty of Life Science, Ben-Gurion University of the Negev, Beer-Sheva 84105, Israel.

[3]Institute of Neuropathology, Heinrich Heine University, Medical Faculty, Düsseldorf, Germany.

[4]Biochemistry and Molecular Biology, Theodor-Boveri-Institute, Biocenter, Am Hubland, 97074 Würzburg, Germany; Division of Tumor Metabolism and Microenvironment, German Cancer Research Center, Im Neuenheimer Feld 581, 69120 Heidelberg, Germany.

[5]Department of Pediatric Oncology, Hematology, and Clinical Immunology, Medical Faculty, Heinrich Heine University, Düsseldorf, Germany.

[6]Laboratory of Cellular Metabolism and Metabolic Regulation, VIB-KU Leuven Center for Cancer Biology, VIB, Leuven, Belgium; Laboratory of Cellular Metabolism and Metabolic Regulation, Department of Oncology, KU Leuven and Leuven Cancer Institute (LKI), Leuven, Belgium.

[7]German cancer consortium (DKTK) partner site Essen/Düsseldorf, Munich, Germany.

[8]Institute for Biochemistry and Molecular Biology I, Medical Faculty, Heinrich-Heine University Düsseldorf, Germany

[9]Clinic for Neurosurgery, Medical Faculty Heinrich-Heine University, Moorenstrasse 5, 40225, Duesseldorf, Germany.

[10]The Shraga Segal Department of Microbiology, Immunology and Genetics, Faculty of Health Science, Ben-Gurion University of the Negev, Beer-Sheva 84105, Israel.

[11]Faculty of Health Sciences, Ben-Gurion University of the Negev, Beer-Sheva 84105, Israel.

[12]Max-Eder Research Group for Pediatric Sarcoma Biology, Institute of Pathology, Faculty of Medicine, LMU Munich, Munich, Germany.

[13]Division of Translational Pediatric Sarcoma Research, German Cancer Research Center (DKFZ), Heidelberg, Germany.

[14]Hopp Children's Cancer Center (KiTZ), Heidelberg, Germany.

[15]Institute of Pathology, Heidelberg University Hospital, Heidelberg, Germany.

*These authors contributed equally

Key words: nutrient stress response, 4EBP1, mRNA translation, tumorigenesis

[#]Corresponding authors:

Dr. Barak Rotblat, Department of Life Sciences, Faculty of Life Science and The National Institute for Biotechnology in the Negev, Ben-Gurion University of the Negev, Beer Sheva 84105, Israel; E-mail: rotblat@bgu.ac.il.

Dr. Gabriel Leprivier, Institute of Neuropathology, Heinrich Heine University Düsseldorf, Moorenstrasse 5, D-40225 Düsseldorf, Germany; E-mail: gabriel.leprivier@med.uni-duesseldorf.de.

SUMMARY

Metabolic stress compels cells to evolve adaptive mechanisms to maintain homeostasis. The regulation of such cellular response is not well understood. Here, we found that eukaryotic initiation factor 4E binding proteins 1/2 (4EBP1/2) are essential to promote the survival of mammalian cells and budding yeast under glucose starvation. 4EBP1/2 block fatty acid synthesis, sparing NADPH and in turn preserving intracellular redox balance upon energy stress via 4EBP1/2-mediated inhibition of *Acetyl-CoA Carboxylase Alpha* (*ACACA*) mRNA translation. This has important relevance in cancers, as we uncovered that oncogenically transformed cells and glioma cells exploit 4EBP1/2 regulation of *ACACA* and redox balance to combat metabolic stress, thereby supporting transformation and tumorigenicity. Clinically, high *eIF4EBP1* expression (4EBP1 gene) is associated with poor outcome in several cancers, including glioma. Our data reveal that 4EBP1/2 are conserved mediators of the survival response to metabolic stress by translationally controlling fatty acid synthesis.

INTRODUCTION

Glucose is one of the most important nutrients for living organisms. Lack of glucose has a profound biological impact on cell fate. Therefore, in order to adapt to glucose deprivation, cells have evolved highly coordinated and conserved metabolic responses. When glucose levels drop, anabolic processes, such as protein synthesis and fatty acid synthesis, are inhibited while catabolic processes, such as autophagy and fatty acid oxidation, are activated. Together, these responses preserve energetic and redox balances, thus maintaining cellular homeostasis (Caro-Maldonado, 2011). A well-characterized pathological condition of glucose deprivation occurs in cancer (Warburg, 1956). Cancer cells growing within solid tumors are experiencing glucose deprivation due high glucose consumption combined with defects in tumor vasculature (Nagy et al., 2009; Warburg, 1956). While such stress condition initially restricts cell division and induces cell death in some instances, it may on the long-term drive adaptation and emergence of more highly tumorigenic and chemo-resistant cancer clones (Flavahan et al., 2013; Jones and Thompson, 2009). Furthermore, similarly to glucose deprivation, matrix detachment triggers energy stress characterized by ATP depletion and elevated reactive oxygen species (Schafer et al., 2009). Mechanisms promoting cell survival under matrix detachment, a hallmark of transformation and tumorigenicity, are also supporting cancer cell adaptation to glucose deprivation (Jeon et al., 2012). It is therefore

important to delineate the mechanisms underlying metabolic adaptation to glucose deprivation.

Protein synthesis, as the most highly energy consuming cellular process (Buttgereit and Brand, 1995), is tuned to cellular energetics. While this process is inhibited under energy stress, failure to do so leads to cell death in both normal and tumor cells, in part due to ATP depletion (Choo et al., 2010; Leprivier et al., 2013; Ng et al., 2012). Protein synthesis is regulated at both the initiation and elongation steps by key evolutionary conserved signaling pathways that sense cellular metabolic state (Leibovitch and Topisirovic, 2018; Leprivier et al., 2015). One major cellular energetics sensor is AMP-activated protein kinase (AMPK), which is allosterically activated when intracellular AMP:ATP or ADP:ATP ratios raise (Trefts and Shaw, 2021). In response to glucose deprivation, AMPK inhibits mRNA translation elongation by activating eukaryotic translation elongation factor 2 kinase (eEF2K) (Horman et al., 2002), which in turn phosphorylates and inactivates the translation elongation factor eEF2 (Ryazanov et al., 1988). EEF2K-mediated inhibition of mRNA translation elongation is essential for survival of normal and tumor cells during nutrient starvation, a function that is conserved in *C. elegans* (Leprivier et al., 2013). Importantly, the expression and activity of eEF2K was found to be increased in numerous cancers (Leprivier et al., 2013), altogether supporting the notion that negative regulators of mRNA translation have evolved to promote cell survival during energetic stress and are hijacked by cancer cells to mediate metabolic adaptation.

Another key regulator of protein synthesis is the nutrient sensing kinase complex mechanistic target of rapamycin complex 1 (mTORC1), which couples the rate of mRNA translation initiation to glucose availability (Leprivier and Rotblat, 2020; Orozco et al., 2020). In keeping with the notion raised above, mTORC1 inhibition is required to preserve viability of normal and cancer cells under glucose starvation (Choo et al., 2010; Inoki et al., 2003). When glucose is abundant, mTORC1 is active and promotes mRNA translation initiation by phosphorylating and activating 70-kDa ribosomal protein S6 kinase (p70S6K) and inhibiting the eukaryotic initiation factor 4E binding protein 1-3 (4EBP-1/-2/-3). During glucose deprivation mTORC1 is inhibited, in turn releasing 4EBP-1/-2/-3 from inhibition, which leads to inhibition of mRNA translation initiation (Liu and Sabatini, 2020; Valvezan and Manning, 2019).

4EBP-1/-2/-3 (4EBPs) are major repressors of protein synthesis regulated by glucose levels (Pause et al., 1994; Poulin et al., 1998), and thus may represent underappreciated regulators of the cellular and metabolic response to glucose starvation. In response to various stresses,

4EBPs inhibit mRNA translation initiation by binding eukaryotic initiation factor 4E (eIF4E) to prevent the formation of the eIF4E-containg pre-initiation complex required for cap-dependent mRNA translation (Silvera et al., 2010; Truitt and Ruggero, 2016). Initially, 4EBPs was thought to exert a general inhibitory effect on the rate of protein synthesis (Sonenberg and Hinnebusch, 2009). However, recent findings highlight that 4EBPs exert a selective regulatory function on mRNA translation, by preferentially blocking the translation of a subset of transcripts (Dowling et al., 2010; Hsieh et al., 2012; Morita et al., 2013; Thoreen et al., 2012). This allows 4EBPs to inhibit the activity of specific cellular processes, such as cellular proliferation, mitochondrial activity and tumor cell invasion (Dowling et al., 2010; Hsieh et al., 2012; Morita et al., 2013; Thoreen et al., 2012). Whether these processes are controlled by 4EBPs in response to glucose starvation is unknown. 4EBP was shown to promote survival of Drosophila larva under nutrient starvation (Teleman et al., 2005; Tettweiler et al., 2005; Zid et al., 2009), nevertheless, the cellular functions of 4EBPs in eukaryotic cells challenged by energetic stress are not known. In addition, the functions of 4EBPs in cancer are still under debate (Musa et al., 2016). On one hand, numerous reports support a tumor suppressive function of 4EBPs, as 4EBP1/2 double knock out leads to reduced tumor-free survival of p53-/- mice (Petroulakis et al., 2009) and accelerates tumor development in genetically engineered mouse models of head and neck squamous cell carcinoma and prostate cancer (Ding et al., 2018; Wang et al., 2019). On the other hand, 4EBPs were shown to exert a pro-tumorigenic function by mediating oncogenic RAS transformation (Petroulakis et al., 2009) and supporting breast cancer progression *in vivo* through promoting angiogenesis (Braunstein et al., 2007).

Here, we found that 4EBP1/2 are fundamental regulators of the cellular and metabolic response to glucose starvation, conserved in yeast, mouse and human. Mechanistically, 4EBP1/2 curb fatty acid synthesis in response to glucose starvation by selectively repressing the translation of acetyl-CoA carboxylase 1 (ACC1) mRNA. This allows preserving NADPH levels, which are normally consumed by fatty acid synthesis, and thus prevents oxidative stress and cell death during glucose starvation. Furthermore, we report that 4EBP1/2 regulation of ACC1 is exploited by cancer and transformed cells to survive in anchorage-independent conditions and grow tumors *in vivo*. Finally, we reveal that 4EBP1 expression has clinical relevance in multiple cancers and is functional in glioma to promote tumor growth and aggressiveness, altogether highlighting a pro-tumorigenic function for the mRNA translation inhibitor 4EBP1.

RESULTS

4EBP1/2 promote cell survival under glucose deprivation by controlling mRNA translation

We investigated the functions of 4EBPs in the cellular response to glucose starvation. To do so, we used cells deficient for 4EBP activity, such as 4ebp11/2 double knock out (DKO) mouse embryonic fibroblasts (MEFs) or stable 4EBP1/2 knock down (KD) (sh4EBP1/2) HEK293 cells (Dowling et al., 2010). We assessed the impact of 4EBP1/2 depletion on cell survival during glucose starvation. Glucose starvation led to massive cell death of 4ebp1/2 DKO MEFs or sh4EBP1/2 HEK293 cells compared to the respective control counterparts (WT and shSCR, respectively), which was not the case in basal conditions (Fig. 1A&B). This was confirmed in other cell lines of different origins, including induced pluripotent stem cells (iPSC), glioblastoma U-87 MG cells, breast cancer MCF7 cells, and neuroblastoma cells. In these cells, stable KD of both 4EBP1 and 4EBP2, or of 4EBP1 alone, severely restricted survival under glucose deprivation (Fig. S1A-E). Conversely, overexpression of a constitutively active 4EBP1 mutant, 4EBP1 (T37A/T46A) (4EBP1^{AA}), was sufficient to protect glucose withdrawal-sensitive HeLa cells against induction of cell death under glucose-deprived conditions (Fig. 1C). In sharp contrast, manipulating 4EBP1/2 expression levels had no impact on the rates of cell death triggered by amino acid starvation (Fig. 1A-C), pointing towards a specific role of 4EBP1/2 in the response to glucose starvation.

We next determined the cellular processes involved in mediating 4EBP1/2 protective function under glucose starvation. We first tested whether this was due to 4EBP1/2 control of cell proliferation, as reported upon serum starvation (Dowling et al., 2010). Unexpectedly, while the rate of proliferation was severely reduced following 24 hrs glucose deprivation, there was no difference between WT and 4ebp1/2 DKO MEFs, nor between shSCR and sh4EBP1/2 HEK293 cells under these conditions (Fig. 1D&E). In addition, we found no evidence that autophagy was responsible for the observed function of 4EBP1/2, as rates of autophagy were similar in control and 4EBP1/2 deficient MEFs and HEK293 cells under glucose starvation (Fig. S1F&G).

Since 4EBP1/2 are major repressors of mRNA translation initiation, we examined the contribution of mRNA translation activity to 4EBP1/2 protective function under glucose starvation. Pharmacological inhibition of protein synthesis, using cycloheximide (CHX), fully rescued 4EBP1/2 deficient MEFs and HEK293 cells from glucose starvation-induced cell death

(Fig. 1F&G) and significantly reduced cell death in sh4EBP1 MCF7 cells (Fig. S1C). This suggests that uncontrolled protein synthesis contributes to glucose starvation-induced cell death observed in cells lacking 4EBP1/2. Unexpectedly, we measured similar rates of overall protein synthesis under glucose starvation in control and 4EBP1/2 deficient MEFs and HEK293 cells using AHA labeling and Click Chemistry (Marciano et al., 2018) (Fig. 1H&I). In contrast, 4EBP1/2 deficient HEK293 cells showed high rates of global protein synthesis vs. control cells upon pharmacological inhibition of mTORC1 (using KU-0063794) (Fig. S1H), suggesting that 4EBPs protective function under glucose starvation is independent from inhibiting total protein synthesis. Putting our data together suggests that selective, rather than global, regulation of mRNA translation by 4EBP1/2 promotes cell viability under glucose deprivation.

Given that 4EBP1/2 function by binding to eIF4E to selectively repress the translation of a subset of transcripts (Dowling et al., 2010; Hsieh et al., 2012; Morita et al., 2013; Thoreen et al., 2012), we tested the involvement of eIF4E in the protective function of 4EBP1/2. Knock down of eIF4E in both 4ebp1/2 DKO MEFs and sh4EBP1/2 HEK293 cells led to a significant reduction of cell death under glucose starvation (Fig. 1J&K). In addition, forced expression of an eIF4E- non-binding mutant of 4EBP1^{AA}, 4EBP1 (Y54A/L59A) (4EBP1$^{AA, YL}$) failed to prevent cell death of HeLa cells upon glucose depletion, in contrast to 4EBP1^{AA} (Fig. 1L), indicating that binding of 4EBP1/2 to eIF4E is required for 4EBP1/2-mediated cellular protection under glucose-deprived conditions. Together, these data highlight that 4EBP1/2 exert a pro-survival function under glucose deprivation by binding eIF4E to regulate mRNA translation.

4EBP1/2 maintain redox balance to preserve cell viability under glucose deprivation

To dissect how 4EBP1/2 protect cells under glucose-deprived conditions, we assessed the impact of 4EBP1/2 on the energetic and redox balances, which are major cellular parameters influenced by glucose availability. While ATP levels were reduced following glucose starvation as anticipated, 4EBP1/2 deficient MEFs and HEK293 cells showed the same amount of ATP as compared with the corresponding control cells under these conditions (Suppl. Fig. S2A&B). Given that protein synthesis is the most ATP-consuming process within a cell (Buttgereit and Brand, 1995), this result is consistent with the lack of impact of 4EBP1/2 on rates of overall protein synthesis under these conditions (Fig. 1H&I). In contrast, levels of endogenous H_2O_2 were higher under glucose deprivation in 4ebp1/2 DKO MEFs and sh4EBP1/2 HEK293 cells compared to their respective controls (WT and shSCR, respectively) (Fig. 2A&B). In addition, overexpression of 4EBP1^{AA} prevented increases of H_2O_2 levels in HeLa cells during glucose

depletion (Fig. 2C). These findings suggest a role for 4EBP1/2 in controlling redox balance upon glucose starvation. Glutathione is a major cellular antioxidant and cells recycle the oxidized form, GSSG, to the reduced form, GSH. The GSH to GSSG ratio is an indication for oxidative stress (Flohe, 2013). 4ebp1/2 DKO MEFs and sh4EBP1/2 HEK293 cells exhibited a lower GSH/GSSG ratio as compared with the respective control cells under glucose starvation, indicative of lower antioxidant capacity in 4EBP1/2 deficient cells (Fig. 2D&E). Conversely, $4EBP1^{AA}$ overexpression precluded severe depletion of GSH/GSSH ratio in HeLa cells during glucose removal (Fig. 2F). Since we did not observe changes in the level of total glutathione in 4EBP1/2 deficient MEFs and HEK293 nor $4EBP1^{AA}$ overexpressing cells during glucose deprivation, in comparison to the respective control cells (Fig. S2C-E), we reasoned that in glucose starved cells, 4EBP1/2 may contribute to glutathione recycling rather than its biosynthesis.

The conversion of GSSG to GSH requires the oxidation of NADPH to $NADP^+$, whose levels are determinant for cellular survival during glucose deprivation (Jeon et al., 2012). In comparison to the respective control cells, 4ebp1/2 DKO MEFs and sh4EBP1/2 HEK293 cells were characterized by severe reduction of NADPH/$NADP^+$ ratio under glucose withdrawal (Fig. 2G&H). Furthermore, $4EBP1^{AA}$ overexpression led to a significant increase of NADPH/$NADP^+$ ratio in HeLa cells during glucose starvation (Fig. 2I). These results are consistent with a role of 4EBP1/2 in promoting NADPH levels under glucose depletion. We next asked whether increased oxidative stress, observed in glucose starved 4EBP depleted cells, is linked to increased sensitivity to glucose starvation. We thus supplemented glucose starved 4ebp1/2 DKO MEFs and sh4EBP1/2 HEK293 cells with antioxidants, N-acetyl cysteine (NAC) or Catalase (CAT), and found these antioxidants significantly reduce cell death compared to vehicle (Fig. 2J&K). Therefore, 4EBP1/2 protective function under glucose deprivation relies on curbing oxidative stress by promoting NADPH levels.

4EBP1/2 controls fatty acid synthesis under glucose deprivation to preserve NADPH levels

We next asked how 4EBP1/2 support NADPH levels under glucose deprivation. We reasoned that to do so, 4EBP1/2 either promote NADPH production or restrict NADPH consumption. Noteworthy, the most NADPH-consuming process within a cell, namely fatty acid synthesis (Fan et al., 2014), is inhibited in response to glucose starvation to preserve NADPH levels and promote cell survival (Jeon et al., 2012). Therefore, we asked whether 4EBP1/2 contribute to the inhibition of fatty acid synthesis during glucose starvation. Using ^{14}C acetate labeling, we

measured the impact of 4EBP1/2 on fatty acid synthesis activity by quantifying ^{14}C incorporation in the cellular lipid fraction under basal conditions and after 16 hrs of glucose starvation. We found that under glucose deprivation 4ebp1/2 DKO MEFs as well as sh4EBP1/2 HEK293 cells accumulated higher amounts of ^{14}C-labelled lipids as compared to corresponding control cells (Fig. 3A&B). Noteworthy, in control cells levels of ^{14}C-labelled lipid was reduced upon glucose withdrawal, which is consistent with expected inhibition of fatty acid synthesis activity in response to glucose deprivation. We therefore concluded that 4EBP1/2 restrict fatty acid synthesis activity in response to glucose removal.

We next wondered whether increased fatty acid synthesis is responsible for reduced NADPH levels and increased ROS observed in glucose starved 4EBP depleted cells. Pharmacological inhibition of fatty acid synthesis, using the acetyl-CoA carboxylase (ACC) inhibitor TOFA, in 4ebp1/2 DKO MEFs and sh4EBP1/2 HEK293 cells led to significant elevation of NADPH/$NADP^+$ ratio (Fig. 3C&D) and reduced ROS levels during glucose withdrawal (Fig. 3E&F). Thus, 4EBP1/2 control redox balance under glucose-limited conditions by curbing fatty acid synthesis. Given that fatty acid synthesis activity is determinant for cell viability under glucose starvation, we next assessed whether increased fatty acid synthesis contributes to glucose starvation sensitivity of 4EBP1/2 depleted cells. Treatment of 4EBP1/2 deficient MEFs and HEK293 cells with TOFA efficiently protected cells under glucose deprivation (Fig. 3G&H). This was confirmed by selectively targeting the NADPH consuming enzyme fatty acid synthase (FASN). Si-RNA mediated knockdown of fasn/*FASN* in 4ebp1/2 DKO MEFs and sh4EBP1/2 HEK293 cells significantly reduced the levels of glucose withdrawal-induced cell death, as compared to control siRNA (SCR) (Fig. 3I&J). Altogether, our findings suggest that during glucose starvation, 4EBP1/2 promote cell viability by inhibiting fatty acid synthesis to preserve NADPH levels and reduce ROS accumulation.

4EBP1/2 selectively regulate the translation of ACC1 to preserve cell viability under glucose deprivation

We next wondered by which mechanisms 4EBP1/2 regulate fatty acid synthesis in response to glucose starvation. Since 4EBP1/2 were reported to selectively block the translation of specific transcripts, we asked whether 4EBP1/2 restrict the synthesis of one of the fatty acid synthesis enzymes. Immunoblots analysis showed that levels of ATP citrate lyase (ACLY), ACC2 and FASN were similar in control and 4ebp1/2 DKO MEFs and sh4EBP1/2 HEK293 cells under glucose starvation (Fig. 4A&B). In contrast, ACC1 expression was severely decreased in control

MEFs and HEK293 cells by 16 hrs glucose depletion, which was not the case in the corresponding 4EBP1/2 deficient cells, thus revealing that ACC1 is highly expressed in 4EBP1/2 deficient cells under glucose starvation (Fig. 4A&B). In agreement, $4EBP1^{AA}$ overexpression led to reduction of ACC1 levels in HeLa cells under glucose deprivation (Fig. S3A). The difference of ACC1 expression between control and 4EBP1/2 deficient HEK293 cells under glucose deprivation was not due to changes in *ACACA* (gene encoding ACC1) mRNA level (Fig. 4C), suggesting a potential regulation at the translational level. To discern whether 4EBP1/2 preferentially control *ACACA* translation under glucose starvation, we quantified levels of *ACACA* transcripts in polysomal and total mRNA and calculated the translation efficiency (TE) as the ratio of polysomal to total mRNA levels. We found that TE of *ACACA* transcript was significantly higher in sh4EBP1/2 HEK293 cells compared to control cells under glucose deprivation (Fig. 4D).

Given that 4EBPs/eIF4E-mediated selective translational control is mediated by the target's 5'UTR, we investigated the potential regulation of *ACACA* 5'UTR by 4EBP1/2 in response to glucose starvation. Since *ACACA* encodes several isoforms harboring different 5'UTR (Damiano et al., 2018), we focused on the 5'UTR most highly expressed in our cell models (data not shown). This 5'UTR, present in human *ACACA* transcript variant 3 (Damiano et al., 2018), is highly conserved in mouse. We observed that *ACACA* 5'UTR activity, as monitored with a luciferase reporter, was significantly decreased upon glucose starvation in control MEFs and HEK293 cells (Fig. 4E&F). In addition, *ACACA* 5'UTR activity was higher in 4ebp1/2 DKO MEFs and sh4EBP1/2 HEK293 cells under glucose starvation compared to respective control cells (Fig. 4E&F). To determine the contribution of the 5'UTR to 4EBP1/2 regulation of ACC1 expression in the context of the *ACACA* transcript, we ectopically expressed HA tagged *ACACA* in HEK293 cells, flanked or not by the 5'UTR, and monitored the impact of 4EBP1/2 on exogenous ACC1 protein levels during glucose starvation. While the expression of ACC1 with no 5'UTR did not differ between sh4EBP1/2 and control cells under glucose starvation, the level of 5'UTR containing ACC1 was higher in sh4EBP1/2 cells as compared with controls during glucose starvation (Fig. 4G). Altogether, these data support that *ACACA* 5' UTR is essential for 4EBP1/2 inhibition of *ACACA* translation under glucose-deprived conditions.

To determine the contribution of increased ACC1 expression to the sensitivity of 4ebp1/2 DKOs and sh4EBP1/2 HEK293 cells to glucose starvation, we knocked down ACC1 and assessed the impact on cell viability during glucose starvation (Fig. 4H&I). We found that *ACACA*

knockdown rescued 4EBP1/2 deficient cells from glucose starvation-induced cell death (Fig. 4H&I). These data are in line with our findings using an ACC inhibitor (Fig. 3G&H). The simplest interpretation of these results is that 4EBP1/2 protect cells from glucose starvation by inhibiting the translation of *ACACA* in a 5'UTR dependent manner thus reducing fatty acid synthesis, preserving NADPH and limiting oxidative stress.

The 4EBP1/2 orthologue Eap1 preserves viability of yeast under glucose deprivation

Since living organisms need to cope with glucose-starved conditions, we asked whether 4EBP1/2 protective function under glucose starvation represents an evolutionary conserved biological response to such a stress. In support to that, it was previously reported that 4EBP facilitates survival of Drosophila under nutrient deprivation. We aimed to delineate the function of 4EBP under glucose deprivation in the evolutionary distant model organism *Saccharomyces cerevisiae*, by studying the two functional 4EBP orthologues in yeast, namely Eap1p and Caf20p (Cosentino et al., 2000; Lanker et al., 1992). In rich glucose-containing YPD media, disruption of *EAP1* (*EAP1Δ*) or *CAF20* (*CAF20Δ*) had no impact on the growth rate of serially diluted yeast cultures on agar in comparison to WT strain (Fig. 5A), which is in agreement with previous reports stating that *EAP1* and *CAF20* are not essential genes (Cosentino et al., 2000; Lanker et al., 1992). In sharp contrast, the growth of *EAP1Δ* strain, but not of *CAF20Δ* strain, was severely compromised in solid rich glucose-free YP media, as compared to WT strain (Fig. 5A). Deletion of both *EAP1* and *CAF20* (*EAP1Δ*/*CAF20Δ*) had no further impact on growth in glucose-free media when compared to *EAP1Δ* strain (Fig. 5A). Our data indicate that the 4EBP orthologue Eap1p, but not Caf20p, supports growth of *Saccharomyces cerevisiae* in glucose-deprived conditions. Such functional difference between Eap1p and Caf20p is in line with differential requirements of these proteins for growth under other types of nutrient depleted conditions, and can be due to differences in the set of transcripts translationally regulated by Eap1p and Caf20p, as reported (Cridge et al., 2010). We confirmed that in liquid media *EAP1* disruption had a pronounced negative effect on growth in glucose-free YP media compared to WT strain (Fig. 5B). We next assessed whether such phenotype was due to a reduction in survival under glucose-deprived conditions. Clonogenic assays of WT and *EAP1*Δ strains grown in liquid conditions in absence of glucose indicated that disruption of *EAP1* prevented survival of yeast upon glucose withdrawal (Fig. 5C). Our data points to a role of Eap1p in protecting yeast under glucose starvation, supporting

the premise that 4EBP1/2 protective function, under such stress conditions, is conserved in the evolution.

Next, we determined whether *EAP1* and its orthologue *EIF4EBP1* respond to glucose deprivation, as part of a transcriptional program, as is expected from genes evolved to function during such stress. We observed that levels of *EAP1* were induced following 24 hrs of glucose removal in yeast cultures (Fig. 5D). Similarly, *EIF4EBP1* expression was increased upon glucose starvation in a three mammalian cell lines (Fig. 5E). Together, these data suggest that 4EBPs are conserved components of the biological response to glucose starvation.

4EBP1/2 promote oncogenic transformation by mitigating oxidative stress and controlling ACC1 level

Cellular response to glucose starvation is closely linked to oncogenic transformation and tumorigenicity, as similar mechanisms controlling redox balance and fatty acid synthesis are involved in these biological processes (Jeon et al., 2012; Schafer et al., 2009; Truitt et al., 2015). While 4EBP1/2 are required for oncogenic RAS transformation of primary fibroblasts (Petroulakis et al., 2009), it is not known whether 4EBP1/2 support transformation by other oncogenes or contribute to the maintenance of the oncogenic transformation state, as is expected if indeed 4EBP1/2 promote survival during energetic stress (Jeon et al., 2012). Using soft agar assays, we uncovered that 4EBP1/2 is necessary for HER2 transformation of mouse mammary epithelial cells (NT2197) *in vitro* (Fig. 6A). In addition, we found that 4EBP1/2 KD restricted the ability of immortalized NIH3T3 $KRAS^{V12}$ transformed fibroblasts to form colonies in soft agar (Suppl. Fig. 4A). These data show that 4EBP1/2 pro-tumorigenic functions are not restricted to RAS oncogene nor to initiation of cellular transformation. To determine how 4EBP1/2 deficiency leads to restricted oncogenic transformation, we assessed the possible involvement of oxidative stress and uncontrolled fatty acid synthesis. Treatment of 4ebp1/2 DKO NT2197 cells with antioxidants - CAT, NAC or Trolox - or with an ACC inhibitor - TOFA - largely rescued colony formation in soft agar (Fig. 6B), while it had no effects on 4EBP1/2 WT NT2197 cells (Suppl. Fig. 4B). Similarly, antioxidants treatment restored colony formation of NIH3T3 $KRAS^{V12}$ 4EBP1/2 KD cells in soft agar (Suppl. Fig. 4C). Importantly, we found that genetic inhibition of ACC1 expression, by CRISPRi-mediated knockdown, was sufficient to restore colony formation of 4EBP1/2 deficient NT2197 cells (Fig. 6C). Thus, 4EBP1/2 support oncogenic transformation by negatively regulating ACC1 and oxidative stress.

We next tested our model *in vivo* and found that 4ebp1/2 DKO NT2197 cells were unable to form any detectable tumors when injected in the flank of immunocompromised mice, in sharp contrast to WT NT2197 cells (Fig. 6D&E). To ascertain the contribution of ACC1 to the observed phenotype in NT2197 tumors *in vivo*, we assessed the impact of targeting ACC1 expression on the growth of 4ebp1/2 DKO NT2197 tumors. Remarkably, Acc1 knockdown (shAcaca) led to a major increase of tumor mass as compared to control (shScr) 4ebp1/2 DKO NT2197 tumors (Fig. 6F&G).

Next, we characterized the impact of ectopic expression of 4EBP1 on tumorigenicity. In support to our data obtained with 4EBP1/2 deficient cells, we found that overexpression of $4EBP1^{AA}$ in HeLa cells led to a significant increase in colony formation in soft agar as compared to control cells (EV) (Fig. 6H). This was recapitulated *in vivo* as $4EBP1^{AA}$ HeLa cells developed larger tumors than control HeLa cells when injected in the flank of immunocompromised mice (Fig. 6I&J). Collectively, these data support a model whereby 4EBP1/2 promote oncogenic transformation, tumorigenicity and survival during glucose starvation through a common mechanism entailing reduced ACC1 expression to restrain fatty acid synthesis and, thus, oxidative stress.

4EBP1 is clinically relevant and functional in brain tumors

Having found that 4EBP1/2 promote survival upon glucose starvation, a condition encountered in solid tumors, and that 4EBP1/2 support oncogenic transformation, we investigated the clinical relevance of 4EBP1/2 in cancer. By analyzing levels of *EIF4EBP1* and *EIF4EBP2* in patient samples (using TCGA and GTEx datasets), we uncovered that *EIF4EBP1* is overexpressed in 16 different tumor types as compared to corresponding normal tissues (Fig. S5A). In contrast, *EIF4EBP2* was only found to be overexpressed in 3 out of the 17 tumor types (Fig. S5B), therefore we focused our analyses on *EIF4EBP1*. Furthermore, high *EIF4EBP1* expression correlated with significantly decreased overall survival in 3 different tumor types (Fig. S5C-E), including glioma (Fig. S5E), highlighting *EIF4EBP1* expression as a potential prognostic biomarker in these tumor entities.

Glucose levels are low in the interstitial compartment of the brain as compared with blood (Fellows and Boutelle, 1993; Gruetter et al., 1992), because, for the most part, glucose is up taken and metabolized by astroglial cells (Pellerin, 2008). To survive in the low glucose microenvironment existing in the brain, cancer cells metastasizing to the brain or glioma

tumors acquire resistance to glucose starvation (Chen et al., 2015; Flavahan et al., 2013). To further investigate the relevance of *EIF4EBP1* in cancer, we turned out attention to the most common form of brain tumor in which low glucose levels have been detected, glioma (Tanaka et al., 2021). *EIF4EBP1* expression is higher in malignant glioma versus non-neoplastic brain tissues (NNBT) (Fig. 7A) and is increased according to tumor grade, with highest expression in the most aggressive grade IV glioblastoma (GB) compared to low grade malignant glioma (grades 2 and 3) (Fig. 7B). Proteomics data analyses further indicated that 4EBP1 protein is overexpressed in GB tissues compared to non-tumorigenic brain (Fig. S5F). Furthermore, high *EIF4EBP1* expression was associated with reduced overall survival in one additional independent and non-overlapping glioma cohort (Fig. 7C). This trend is observed in GB patients but to a lower extent (Fig. 7D), illustrating the clinical relevance of *EIF4EBP1* in such a highly malignant form of adult brain tumor.

To functionally dissect the role of 4EBP1 in malignant glioma, we analyzed the impact of 4EBP1 KD on tumorigenic potential of human and mouse glioma cells, U-87 MG (Fig. S1B) and GL-261 respectively. We first confirmed that 4EBP1 KD sensitizes glioma cells to glucose starvation-induced cell death (Fig. S5G), as with other cell lines, and secondly we showed that treatment with CHX and NAC rescued cell survival under glucose starvation (Fig. S5G). In addition, 4EBP1 KD severely restricted the ability of glioma cells to form colonies in soft agar (Fig. 7E&F). Importantly, inhibiting ACC with TOFA or supplementing cells with antioxidants rescued colony formation of the different 4EBP1 deficient cells (Fig. 7G&H, and Fig. S6A&B). In contrast, such treatments had no impact on 4EBP1 proficient U-87 MG and GL-261 (Fig. S6C&D). These data indicate that in glioma cells, 4EBP1 promotes tumorigenicity *in vitro* by means of controlling redox balance and fatty acid synthesis.

We next evaluated *in vivo* 4EBP1 pro-tumorigenic functions in glioma cells by first injecting control (shSCR) and 4EBP1 KD U-87 MG cells to the flanks of NOD-SCID gamma mice. 4EBP1 depleted cells grew significantly smaller tumors as compared with controls (Fig. 7I). To decipher whether 4EBP1 is also important for tumor maintenance, we used a doxycycline inducible shRNA system to target 4EBP1 expression in established tumors. 4EBP1 KD was induced once tumors formed by injection of engineered U-87 MG models had reached 100 mm^3 in size. We observed an inhibition of tumor growth in doxycycline treated mice harboring the sh4EBP1 U-87 MG tumors but not in shSCR-U-87 MG tumors or tumors in mice unexposed to doxycycline (Fig. 7J). These data suggest that 4EBP1 promotes growth of

established glioma tumors *in vivo*. To determine whether 4EBP1 supports tumor growth in brain, we performed orthotopic injection of control and sh4EBP1-U-87 MG cells. While both control and 4EBP1 deficient cells generated tumors, mice bearing sh4EBP1-U-87 MG tumors survived longer as compared with controls (Fig. 7K). To assess 4EBP1 function in an immunocompetent mouse model, we injected control and sh4EBP1 GL-261 to brains of C57 mice. Mice carrying sh4ebp1 GL-261 tumors showed a significant extension of survival compared to mice with control (shScr) tumors (Fig. 7L), suggesting that 4EBP1 promotes glioma aggressiveness also in presence of a functional immune system. Acc1 KD in sh4ebp1 GL-261 cells enhanced tumor aggressiveness (Fig. 7M), supporting the model where 4EBP1 is exploited by tumor cells to reduced ACC1 expression to promote tumor aggressiveness. Collectively, our data highlight that *EIF4EBP1* has clinical relevance in various human tumor types, including glioma, and that 4EBP1 exerts a pro-tumorigenic function in malignant glioma by reducing ACC1 expression.

DISCUSSION

4EBP1/2 are evolutionary conserved factors promoting cell survival under glucose deprivation

Glucose starvation represents a physiological stress, which requires/triggers a proper cellular response to prevent cell death. Here we report that 4EBPs promote cell survival during glucose starvation, a biological function conserved in human, mouse and yeast cells. The yeast orthologue of 4EBPs, Eap1p, shows little sequence homology with mammalian 4EBPs, although, similarly to mammalian 4EBPs, it binds yeast eIF4E to inhibit cap-dependent translation (Cosentino et al., 2000) and promotes survival under glucose starvation. Unlike its mammalian orthologue, Eap1 protects against other forms of metabolic stress, such as ammonium sulfate, serine or glutamate depletion (Cridge et al., 2010) suggesting that promoting viability specifically during glucose starvation, is an evolutionary conserved 4EBPs function.

In addition, we found that EIF4EBP1 has evolved as a glucose starvation-responsive gene. Both yeast *EAP1* and mammalian *EIF4EBP1* expression are induced by glucose starvation, in line with observations made in adipocytes (Agudelo et al., 2021) and in muscle tissues of food-deprived mice (Jagoe et al., 2002). Given that glucose starvation induced expression of another pro-survival factor and negative regulator of mRNA translation, namely eEF2K

(Leprivier et al., 2013), this raises the notion that negative regulators of mRNA translation, and 4EBPs in particular, have evolved to protect cells against glucose starvation.

4EBP1/2 act as metabolic switches by translationally restricting fatty acid synthesis

Cellular response to glucose starvation proceeds through profound metabolic reprogramming, during which anabolic processes are blocked and catabolic processes are activated (Caro-Maldonado, 2011). These mechanisms are hijacked by cancer cells to adapt to the glucose deprived conditions of the tumor microenvironment (Flavahan et al., 2013; Jones and Thompson, 2009). We uncovered that 4EBPs are key mediators of the metabolic switch induced by glucose withdrawal, and that they do so by binding eIF4E to restrict fatty acid synthesis and promote NADPH levels, thus linking mRNA translation to energy levels and regulation of fatty acid synthesis, and cellular redox balance. The regulation of cell metabolism by 4EBPs, through inhibition of fatty acid synthesis, proliferation (Dowling et al., 2010) and mitochondrial activity (Morita et al., 2013), is compatible with 4EBPs acting as metabolic switches responding to stress which steer cells to a more quiescent or low energy state.

4EBPs control metabolic processes rely on their ability to selectively restrict the translation of specific transcripts, including pro-proliferative *cyclin D3* and *ornithine decarboxylase* (Dowling et al., 2010) as well as mitochondrial coding *ATP5O* and *TFAM* (Morita et al., 2013). Here we uncovered that 4EBPs restrain fatty acid synthesis by selectively inhibiting the synthesis of the fatty acid synthesis rate limiting enzyme ACC1. Previously it was reported that eIF4E selectively promotes *ACACA* translation in T-cells (Ricciardi et al., 2018) and in liver tissue of mice fed with a high fat diet (Conn et al., 2021). In particular, the transition of CD4+ T cell from quiescence to activation, which metabolically mirror changes in glucose availability, is driven by eIF4E-promoted of *ACACA* translation which is dependent upon the 5'UTR of *ACACA* (Ricciardi et al., 2018). Similarly, we report that another 5'UTR of *ACACA* supports 4EBPs-mediated control of *ACACA* translation, highlighting that this *ACACA* 5'UTR represents a genetic element linking fatty acid synthesis activity to the energetic state of the cell. Altogether, our data support the model whereby in addition to AMPK-mediated phosphorylation of ACC1, cells evolved a parallel mechanism to inhibit ACC1 in response to energetic stress, through 4EBPs-mediated translational repression of ACACA mRNA. These may represent two complementary mechanisms, as phosphorylation is fast but easily reversible, especially due to the action of phosphatases, while mRNA translation repression is slower but may be more efficient at blocking ACC1 on the long-term. Noteworthy, in bacteria

ACC is also regulated both at the translational and post-translational levels in response to glucose availability (Broussard et al., 2013), in agreement with the possibility that the modes of ACC1 regulation are evolutionary conserved.

4EBP1 exerts a pro-tumorigenic function in glioma

The role of 4EBP1 in cancer is still unclear (Musa et al., 2016). While 4EBP1 exhibits tumor suppressive function in mouse models of lymphoma, head and neck squamous cell carcinoma and prostate cancer (Ding et al., 2018; Wang et al., 2019), 4EBP1 knockout mice per se do not develop tumor excluding that 4EBP1 is a tumor suppressor (Tsukiyama-Kohara et al., 2001). More than that, 4EBP1 has been shown to exert pro-tumorigenic functions, as it is required for oncogenic RAS transformation (Petroulakis et al., 2009) and it promotes breast cancer development *in vivo* (Braunstein et al., 2007). Our data support a pro-tumorigenic function of 4EBP1, as we uncovered that 4EBP1 mediates HER2 transformation and tumorigenicity of glioma cells *in vitro* and *in vivo*.

It is possible that the role of 4EBP1 in cancer is determined by the levels of metabolic stress present in tumors and that 4EBP1 pro-tumorigenic function predominates in metabolically challenged tumor environment, as was previously proposed for AMPK (Chhipa et al., 2018; Eichner et al., 2019; Faubert et al., 2014). In particular, glucose concentrations in the brain are low compared to plasma glycemia (Fellows and Boutelle, 1993; Gruetter et al., 1992), and aggressive glioma are characterized by the presence of large necrotic areas (Homma et al., 2006), indicative of oxygen and nutrient deprivation. To survive the low glucose microenvironment of the brain, glioma tumors or breast cancer cells metastazing to the brain, acquire resistance to glucose starvation (Chen et al., 2015; Flavahan et al., 2013), which adversely select for more highly tumorigenic cancer cell clones (Flavahan et al., 2013). We propose that 4EBP1 confers glioma cells the ability to adapt to metabolic stress by preserving the redox balance and restricting ACC1 expression, similarly to the mechanisms of 4EBP1 function in response to glucose deprivation. This is in line with the proposed function of AMPK in mediating cell survival under glucose starvation and tumorigenesis through inhibition of ACC1 and prevention of oxidative stress (Jeon et al., 2012). 4EBP1 is, therefore, a metabolic regulator exploited by cancer cells to adapt adverse conditions of the tumor microenvironment.

Since 4EBP1 is post-translationally inhibited by mTORC1, which is overactive in numerous cancers, it is assumed that 4EBP1 is inactive in tumors as evidenced by increased levels of phosphorylated 4EBP1 reported in various tumor tissues (Musa et al., 2016). However, the amount of total 4EBP1 protein is rarely monitored. Importantly, the activity of 4EBP1 in glioblastoma was shown to be directly dependent on the proximity to blood vessels, with highest 4EBP1 activity detected in areas furthest from blood vessels, corresponding to oxygen and glucose deprived areas (Kumar et al., 2019). This raises the possibility that upregulation of *EIF4EBP1*, as observed in numerous cancer types (Wu and Wagner, 2021), leads to increased 4EBP1 activity in metabolically challenged tumor areas. It is noteworthy that oncogenic transcription factors, such as MYC, MYCN, ETS1 and MYBL2 (Tameire et al., 2019) promote *EIF4EBP1* overexpression, further supporting the clinical relevance of *EIF4EBP1* as a pro-tumorigenic gene.

Our findings together with our previous work (Leprivier et al., 2013) support a model whereby translational repressors promote cell survival under glucose starvation and are hijacked by tumor cells to cope with energy stress.

EXPERIMENTAL PROCEDURES

Resource Availability

Lead Contact

Further information and requests for reagents may be directed to, and will be fulfilled by the corresponding authors (rotblat@bgu.ac.il and gabriel.leprivier@med.uni-duesseldorf.de).

Material Availability

The unique reagents generated in this study are available from the Lead Contacts:

Experimental Model and Subject Details

Cell culture

Cells were maintained using standard tissue culture procedures in a humidified incubator at 37°C with 5% CO_2 and atmospheric oxygen. Stable HEK293 (human, female) control (shScr) and knock down for 4EBP1/4EBP2 (sh4EBP1/2) cell lines, WT ($p53^{-/-}$) and 4EBP1/4EBP2 double

knockout (DKO) ($p53^{-/-}$) MEFs (mouse, sex unspecified) were kind gifts from Prof. Nahum Sonenberg (McGill University, Canada). NMuMG-NT2197 (mouse, female) (NT2197) control and 4ebp1/2 DKO cell lines were kind gifts from Dr. Ivan Topisirovic (McGill University, Canada). GL-261 (mouse) glioma cell line was a kind gift from Prof. Reuven Stein (Tel Aviv University, Israel). NIH 3T3 cells (mouse, male) stably expressing K-Ras^{V12} have been previously described (Leprivier et al., 2013). Wild type HEK293, HEK293-T (human, female), HeLa (human, female), U-87 MG (human, male), MCF7 (human, female), Kelly (human, female) and IMR-32 (human, male). cell lines were originally obtained from American Type Culture Collections (ATCC).

NT2197 were cultured in Dulbecco's modified Eagle medium (DMEM) supplemented with 10% fetal bovine serum (FBS), 1% penicillin/streptomycin (pen/strep), 10 µg/ml insulin, and 20 mM HEPES, pH 7.5. NIH 3T3 K-Ras^{V12} were cultured in DMEM supplemented with 10% bovine calf serum. All other cell lines were maintained in DMEM supplemented with 10% FBS, 1% penicillin/streptomycin (pen/strep).

All cell lines were routinely confirmed to be mycoplasma-free using Venor®GeM Classic kit (Minerva Biolabs, Berlin, Germany). All human cell lines were authenticated by STR-profiling (Genomics and Transcriptomics Laboratory, Heinrich-Heine University, Germany).

Yeast culture

Yeast strains (all isogenic to BY4742, see table below) were grown in complex medium containing 1% (w/v) yeast extract and 2% (w/v) peptone without (YP) or with (YPD) 2% glucose. To pour solid agar plates, 2% agar was added to medium. For dot spot assays, yeast strains were grown to an OD600 of approximately 1, washed and diluted in a series of fivefold dilutions before eventually being stamped on the corresponding agar plate before incubation at 30°C or 37°C for 3-5 days. For incubation in liquid complete YPD or glucose-free YP medium, suspensions were adjusted to an OD600 of 0.1 prior to incubation at 200 rpm at 30°C. The OD600 was measured throughout the experiment with a spectrophotometer. For survival analysis, BY4742 control or Eap1Δ yeast strains were incubated in liquid YP medium at an OD600 of 0.1 for 2 weeks at 30°C shaking at 300 rpm prior to streaking serial dilutions onto complete YPD agar plates.

Name	Genotype
BY4742	MATα his3Δ1 leu2Δ0 lys2Δ0 ura3Δ0
Eap1Δ	MATα his3Δ1 leu2Δ0 lys2Δ0 ura3Δ0 eap1Δ::NatMX4
Caf20Δ	MATα his3Δ1 leu2Δ0 lys2Δ0 ura3Δ0 caf20Δ::KanMX4
Eap1Δ/Caf20Δ	MATα his3Δ1 leu2Δ0 lys2Δ0 ura3Δ0 eap1Δ::NatMX4 caf20Δ::KanMX4

Animal models

All mouse work was performed in accordance with the institutional animal care use committee and relevant guidelines at the Ben-Gurion University, with protocols 34-06-2016, 35-06-2016 and 59-08-2019E. C57WT, NOD-SCID and NOD-SCID gamma mice. Both male and female mice from 5-8 weeks of age were used for all experiments in this study. In specific experiment all mice were from the same sex and same age. All mice were housed under specific-pathogen-free (SPF) condition at the Ben-Gurion University facility.

Xenograft tumor models

For sub-cutaneous injection, cancer cells ($5X10^6$-$1X10^7$) were injected into the flank of mice. Tumors size were monitor-using caliper. When tumors reach the wanted size, mice were sacrificed, tumor were excised and weighed. Each tumor were cut in half and either fixed in formaldehyde 4% or snap-frozen in liquid nitrogen. When inducible system were used, mice received 10 mg/kg/day, such that 0.05 mg/mL of doxycycline was added to the drinking water twice a week.

For orthotropic/ intracranial injection, cancer cells were engrafted into a mouse brain using stereotactic device. For MRI imaging, mice were anesthetized by isoflurane inhalation anesthesia (1.5 l O_2/min and 2.5% isoflurane), placed in the MRI T2 cranial images were acquired. Mice survival/mortality rate were monitored. At the end of the experiment, mice were sacrificed; their brains were excised and processed for IHC.

Method details

Reagents

Cycloheximide (CHX), N-acetylcysteine (NAC), Catalase (CAT), 5-(Tetradecyloxy)-2-furoic acid (TOFA), and 6-hydroxy-2,5,7,8-tetramethylchroman-2-carboxylic acid (Trolox) were from Sigma-Aldrich.

Glucose and amino acids starvation of cell culture

Glucose or amino acids starvation was performed with subconfluent cultures (~50% confluency). For glucose starvation, full media was replaced with DMEM (RPMI for the IMR-32 and Kelly) containing no glucose and no sodium pyruvate supplemented with 10% dialyzed FBS and 1 mM glucose. For amino acid starvation, full media was replaced with Earle's Balanced Salt Solution (EBSS) supplemented with 10% dialyzed FBS and 25 mM glucose. When indicated, cells were treated with either CHX (2 μg/ml), NAC (3 mM), Catalase (400 U/ml), TOFA (5 μM) at the time of media replacement.

Vectors for genetically manipulating cell lines

shRNA expression plasmids

To make the shRNA expression vectors which were not commercially available, complementary oligonucleotides corresponding to shRNAs targeting mouse *eif4ebp1 or* mouse *acaca* were custom cloned (Genewiz) into AgeI and EcoRI restriction sites of the pLKO.1-neo cloning vector (Addgene 13425), or of the pLKO.1-puro (Addgene 10878), or of the Tet-pLKO-puro (Addgene 21915), or into EcoRI and PacI restriction sites of the pLKO.3G (Addgene). All other pLKO.1 lentiviral shRNA vectors were pLKO.1-puro based and were retrieved from the arrayed Mission TRC genome-wide shRNA collections purchased from Sigma-Aldrich Corporation.

CRISPRi/Cas9 plasmids

To construct CRISPRi/Cas9 targeting vectors, single guide RNAs (sgRNAs) targeting human *EIF4EBP1* or mouse *acaca* were synthesized and custom cloned (Genewiz) into BsmBI restriction site of gRNA-dCas9-KRAB GFP (Addgene 71237).

cDNA expression plasmids

The cDNA sequences of human 4EBP1 (T37A/T46A) [4EBP1^{AA}] and 4EBP1^{AA} (Y54A/L59A) (4EBP1$^{AA, YL}$) were synthesized and custom cloned (Genewiz) into the EcoRI restriction site of the pLJM1 expression vector (Addgene 91980).

siRNA transfections

Cells were transfected at ~25% confluency in 6-well plates with 25 nM control ON TARGET plus non-targeting siRNA (Dharmacon) or with 25 nM of single siRNAs targeting human or mouse *EIF4E*, human or mouse *FASN*, human or mouse *ACACA*, mouse *EIF4EBP1* and *EIF4EBP2* using siLentFect transfection reagent (Bio-Rad) according to the manufacturer's instructions. When indicated, cells were glucose starved 48 hours post-transfection.

Virus production and viral transduction of cell lines

HEK293T cells were transfected with expression vectors and lentiviral packaging plasmids psPAX2 (Addgene 12260) and pMD2.G (Addgene 12259) in a ratio of 4:3:1 using CalFectin transfection reagent (Signagen) according to the manufacturer's guidelines. Media was harvested 72 hours post-transfection, passed through a 0.45 µm nitrocellulose filter and frozen at -80°C. Recipient cells were seeded in 6-well plates and were infected the next day when reaching ~50% confluency. For infection, 0.3 ml of virus-containing media was added to each well in a final volume of 2 mL media containing 8 µg/ml polybrene. Stable cell lines were either selected with 2 µg/ml puromycin or 1 mg/ml G418, or FACS sorted for cells expressing GFP.

Immunoblot analyses of protein expression

Cells were lysed in RIPA buffer (150 mM NaCl, 50 mM Tris-HCl, pH 8, 1% Triton X-100, 0.5% sodium deoxycholate, and 0.1% SDS) supplemented with cOmplete™, EDTA-free Protease Inhibitor Cocktail (Sigma) and phosphatase inhibitors (PhosphoSTOP, Roche). Cell lysates were centrifuged at 14,000 x g for 15 min at 4°C and supernatants were collected. Protein concentration was measured using the BCA kit (Pierce) according to manufacturer's protocol. Protein lysates were resolved by SDS-PAGE and transferred to nitrocellulose membranes (GE Healthcare). Membranes were blocked with 5% BSA TBS-Tween (20 mM Tris-HCl, pH 7.4, 150 mM NaCl, 0.1% Tween 20) and probed with the primary antibodies indicated in supplementary

table. Secondary anti-mouse (926-32210, Li-Cor) or anti-rabbit (926-32211, Li-Cor) antibodies were used and fluorescent signal was detected with the LI-COR Odyssey CLx system.

RNA analysis

RNA was extracted using the RNeasy mini kit (QIAgen) according to manufacturer's instruction. cDNAs were synthesized from total RNAs using either QuantiTect Reverse Transcription Kit (Quiagen) or High-Capacity cDNA Reverse Transcription Kit (Applied Biosystems) according to manufacturer's instruction. The cDNAs were quantified by real-time PCR analysis using SYBR Green Master Mix (Bio-Rad, CA). The primer sequences are listed in the Table below. As internal controls, PPIA, GusB and β-actin were amplified.

Gene	Primer Sequence
EIF4EBP1	FW: AGCCCTTCCAGTGATGAGC RV: TGTCCATCTCAAACTGTGACTCTT
PPIA	F: CCAGACTGAGATGCACAAGTG R: GTGGCGGATTTGATCATTTGG
GusB	F: GTTTTTGATCCAGACCCAGATG R: GCCCATTATTCAGAGCGAGTA
ACTB	F: TCCCCCAACTTGAGATGTATG R: ACTGGTCTCAAGTCAGTGTACAGG
Act1 (yeast)	F: CCAGAAGCTTTGTTCCATCC R:CGGACATAACGATGTTACCG
Eap1 (yeast)	F: CAGCCGCTACTCACAAATC R: GCTTTCTTTATTGTTACCGCTC

ROS measurements

Cells were incubated with 5 µM chloromethyl-2',7'-dichlorodihydrofluorescein diacetate (CM-H2DCFDA) at 37°C for 20 minutes. Cells were harvested and resuspended in PBS. Green fluorescence intensity was measured with a CytoFLEX flow cytometer (Beckmann Coulter). Data analysis was performed with FlowJo 10 software (FlowJo).

Reduced and oxidized glutathione measurements

Cells were seeded into 12-well plates and allowed to attach overnight. Cells were collected and cellular concentrations of reduced and total GSH were quantified using the GSH-Glo assay

kit, according to the manufacturer's protocol (Promega). Luminescence was measured using the Spark® plate reader (Tecan).

$NADP^+$/NADPH measurements

Cells were lysed in a base solution (100 mM sodium carbonate, 20 mM sodium bicarbonate, 10 mM nicotinamide, 0.05% Triton X-100) containing 1% of Dodecyltrimethylammoniumbromid (DTAB). Cell lysates were split in two equal fractions. The pH of one of the fraction was adjusted by adding 0.4 N HCl according to the manufacturer's protocol. Both fractions were then heated for 15 minutes at 60°C and subsequently incubated at RT for 10 minutes. According to the manufacturer's protocol, before adding the detection reagent, Trizma base or HCl/Trizma solution were used to adjust pH each fraction. Finally, luminescence of each fraction was analyzed with Spark® plate reader (Tecan) to measure NADP+ and NADPH levels, and the $NADP^+$/NADPH ratio was calculated.

Protein synthesis rate

To quantify levels of newly synthesized proteins, 50 µM of azidohomoalanine (AHA) (C10102, Thermo Fisher Scientific, Massachusetts) was added to the cell culture medium and cells were incubated for 4 hours. Cells were then washed with ice-cold PBS, collected and lysed with EDTA-free RIPA lysis buffer (150 mM NaCl, 50 mM Tris pH 8, 1% Triton X-100, 0.5% sodium deoxycholate, 0.1% SDS). The concentration of proteins was measured by bicinchoninic acid assay using Pierce™ BCA Protein Assay Kit (PIR-23227, Thermo Fisher Scientific), and a Click reaction was performed with Click-iT® Protein Reaction Buffer Kit (C10276, Thermo Fisher Scientific) according to manufacturer's instructions.

Cell proliferation

To assess cell proliferation, cells plated in 6-wells were incubated in fresh media containing 10 µM 5-ethynyl-2'-deoxyuridine (EdU) (Invitrogen) for 60 min at 37°C. EdU staining was conducted using Click-iT™ EdU Alexa Fluor™ 488 Flow Cytometry Assay Kit (Invitrogen, Carlsbad, CA) according to the manufacturer's protocol. Briefly, cells were harvested, fixed with 4% paraformaldehyde in phosphate buffer saline (PBS) for 15 min, and permeabilized with 1X Click-iT™ saponin-based permeabilization reagent. Cells were incubated with a Click-iT™ reaction cocktail containing Click-iT™ reaction buffer, $CuSO_4$, Alexa Fluor® 488 Azide, and reaction buffer additive for 30 min while protected from light. Green fluorescence intensity

was measured with a CytoFLEX flow cytometer (Beckmann Coulter). Data analysis was performed with FlowJo 10 software (FlowJo).

Cell death assays

Cell death was measured by flow cytometry using Propidium iodide (PI) staining. Briefly, attached and detached cells were harvested, centrifuged and resuspended in PBS containing 1 µg/ml PI (Sigma). Cell death quantification was performed using a CytoFLEX flow cytometer (Beckmann Coulter). A minimum of 50.000 events were recorded for each replicate. Data analysis was performed with FlowJo 10 software (FlowJo).

Soft agar colony assays

Cells were plated in 6-well plates with 8,000 cells per well in DMEM 10% FBS or DMEM 10% bovine calf serum in a top layer of 0.25% agar added over a base layer of 0.4% agar in DMEM 10% FBS or DMEM 10% bovine calf serum. Cells were fed once a week with 1ml of corresponding medium onto the top layer. Where indicated, NAC (5 mM), Catalase (200 U/ml), Trolox (100 µM), or TOFA (10 µM) were added to the top agar layer, as well as every 2-3 days in the feeder medium. After 2-4 weeks at 37°C, colonies were stained with 0.01% crystal violet and 10 random fields were counted manually for each well. The percentage of colony forming cells was calculated.

^{14}C labeling and fatty acid synthesis activity

Cells were labeled with 10 µCi of [1-^{14}C]-acetate (Perkin Elmer) in basal media or in glucose starved media for 16 h. Cells were snapped frozen and lipids were extracted by methanol-water-chloroform extraction. Phase separation was achieved by centrifugation at 4°C and the methanol-water phase containing polar metabolites was used as negative control. Radioactivity in the chloroform phase containing fatty acids was quantified by liquid scintillation counting and values were normalized to protein concentration determined in the dried protein interphase.

5'UTR Luciferase assays

The 5'UTR Firefly Luciferase reporter plasmids were custom cloned (Genewiz) by inserting the 5'UTR of human *ACACA* isoform 3 into the SacI and BglII restriction sites of pGL3 control vector (Promega).

For transfection, HEK293 cells were seeded in 12-well plates and transfected with 250 ng of each 5'UTR Firefly Luciferase reporter and 3 ng Renilla Luciferase expressing pRL null plasmid (Promega), completed to 500 ng DNA with pcDNA3.1 plasmid, using CalFectin transfection reagent (Signagen) according to the manufacturer's guidelines. Cells were harvested 48 hours post-transfection and activity of Firefly and Renilla Luciferase were sequentially determined using the Dual-Luciferase Reporter Assay System (Promega) and analyzed with the Spark® plate reader (Tecan). All samples were performed in triplicate and the final luciferase quantification was formulated as the ratio of Firefly luciferase to Renilla luciferase luminescence.

Polysome analysis

Cells were treated with 10 µg/ml of cycloheximide for 10 min, washed twice with PBS containing 100 µg/ml cycloheximide, then cells were scrapped and collected. Cells were pelleted by centrifugation (300 x g, 5 min, 4°C), lysed with 434 µl of lysis buffer (50 mM Tris-base pH 8, 2.5 mM $MgCl_2$, 1.5 mM KCl, 115 µg/ml cycloheximide, 2.3 mM DTT and 0.27 U/µl RNaseOUT [10777019, Thermo Fisher Scientific]), and vortexed. 25 µl of 100% Triton X-100 and 25 µl of 10% sodium deoxycholate were added to the cell lysates, which were vortexed and centrifuged (17,800 x g, 2 min, 4°C). 50 µl of the lysates were saved as the total fraction and the remaining were loaded on top of a three layers sucrose gradient (5%, 34% and 55% sucrose) that were prepared by dissolving sucrose in gradient buffer (4 mM HEPES pH 7.6, 20 mM KCl, 1 mM $MgCl_2$). The lysates loaded on top of the sucrose gradient were subjected to ultracentrifugation (229,884 x g, 2.5 hours, 4°C). The polysome profile was read using a piston gradient collector (Biocomp) fitted with a UV detector (Tirax). Three polysomal fractions were collected and placed in Trizol (Sigma-Aldrich Company, location). RNA was extracted from frozen fractions using manufacturer's instructions.

Bioinformatics analyses of gene expression patterns in human tissue samples

For expression analysis, RNA-seq data from TCGA and the GTEx projects were analyzed with Gepia (PMID: 28407145). For survival analysis, RNA-seq and microarrays data were analyzed with Kaplan-Meier Plotter (PMID: 34527184) or Chinese Glioma Genome Atlas (CGGA; PMID: 33662628).

Quantification and Statistical Analysis

All experiments were, if not otherwise stated, independently carried out three times. Statistical significance was calculated using Student's t-test in GraphPad Prism 8. The data is represented as means +/- standard deviation. A p-value of less than 0,05 was considered to be significant.

FIGURE LEGENDS

Figure 1. 4EBP1/2 prevent cell death in response to glucose starvation through control of eIF4E and mRNA translation.

(A) WT or 4ebp1/2 DKO MEF were grown in complete media, depleted for amino acids (AA) or for glucose (Glc) starved for 48 hrs. Cell death was measured by propidium iodide (PI) staining, and analyzed by flow cytometry.

(B) Control (shSCR) or stable 4EBP1/4EBP2 knocked down (sh4EBP1/2) HEK293 cells were grown in complete media, depleted for AA or Glc starved for 48 hrs. Cell death was measured by PI staining, and analyzed by flow cytometry.

(C) Control (MSCV) or stable $4EBP1^{AA}$ overexpressing HeLa cells were grown in complete media, depleted for AA or Glc starved for 48 hrs. Cell death was measured by PI staining, and analyzed by flow cytometry.

(D) WT or 4ebp1/2 DKO MEF were grown in complete media or Glc starved for the indicated times and labeled with 5-Ethynyl-2'-deoxyuridine (EdU). EdU incorporation was analyzed by flow cytometry.

(E) ShSCR or sh4EBP1/2 HEK293 cells were grown in complete media or Glc starved for the indicated times and labeled with EdU. EdU incorporation was analyzed by flow cytometry.

(F) 4ebp1/2 DKO MEF were grown in Glc starved media and treated or not treated with cycloheximide (CHX) for 48 hrs. Cell death was measured by PI staining, and analyzed by flow cytometry.

(G) Sh4EBP1/2 HEK293 cells were grown in glucose starved media and treated or not with CHX for 48 hrs. Cell death was measured by PI staining, and analyzed by flow cytometry.

(H) WT or 4ebp1/2 DKO MEF were grown in complete media or Glc starved for the indicated times and labeled with azidohomoalanine (AHA). Levels of AHA-labelled proteins was detected by immunoblotting with a streptavidin conjugate.

(I) ShSCR or sh4EBP1/2 HEK293 cells were grown in complete media or Glc starved for the indicated times and labeled with AHA. Levels of AHA-labelled proteins was detected by immunoblotting with a streptavidin conjugate.

(J) 4ebp1/2 DKO MEF were transfected with control siRNA (scr) or siRNAs targeting *eif4e* and were grown in Glc starved media for 48 hrs. Cell death was measured by PI staining, and analyzed by flow cytometry.

(K) Sh4EBP1/2 HEK293 cells were transfected with control siRNA (SCR) or siRNAs targeting *EIF4E* and were grown in Glc starved media for 48 hrs. Cell death was measured by propidium iodide (PI) staining, and analyzed by flow cytometry.

(L) HeLa cells stably expressing empty vector (EV), $4EBP1^{AA}$ or $4EBP1^{AA,YL}$ were grown in Glc starved media for 48 hrs. Cell death was measured by PI staining, and analyzed by flow cytometry.

(A-L) Data represent the mean of three independent replicates ± standard deviation (SD). Significance was calculated using an unpaired and two-tailed parametric t-test (*p<0.05, **p<0.01, ***p<0.001).

Figure 2. 4EBP1/2 preserve the redox balance under glucose starvation by maintaining antioxidant power.

(A) WT or 4ebp1/2 DKO MEF grown in complete media or glucose (Glc) starved for 24 hrs were assayed for H_2O_2 levels by flow cytometry using 2',7'-Dichlorofluorescein diacetate (DCFDA).

(B) ShSCR or sh4EBP1/2 HEK293 cells grown in complete media or Glc starved for 24 hrs were assayed for H_2O_2 levels by flow cytometry using DCFDA.

(C) Control (MSCV) or $4EBP1^{AA}$ overexpressing HeLa cells grown in complete media or Glc starved for 24 hrs were assayed for H_2O_2 levels by flow cytometry using DCFDA.

(D) WT or 4ebp1/2 DKO MEF were grown in complete media or Glc starved for 24 hrs, and reduced and total glutathione were measured and expressed as the ratio of reduced (GSH) to oxidized (GSSG) glutathione.

(E) ShSCR or sh4EBP1/2 HEK293 cells were grown in complete media or Glc starved for 24 hrs, and reduced and total glutathione were measured and expressed as the ratio of reduced GSH to oxidized GSSG.

(F) MSCV or 4EBP1^{AA} overexpressing HeLa cells were grown in complete media or Glc starved for 24 hrs, and reduced and total glutathione were measured and expressed as the ratio of reduced GSH to oxidized GSSG.

(G) WT or 4ebp1/2 DKO MEF were grown in complete media or Glc starved for 24 hrs, and $NADP^+$ and NADPH were measured.

(H) ShSCR or sh4EBP1/2 HEK293 cells were grown in complete media or Glc starved for 24 hrs, and $NADP^+$ and NADPH were measured.

(I) MSCV or 4EBP1^{AA} overexpressing HeLa cells were grown in complete media or Glc starved for 24 hrs, and $NADP^+$ and NADPH were measured.

(J) 4ebp1/2 DKO MEF were grown in Glc starved media and treated with vehicle (V), N-acetyl cysteine (NAC) or Catalase (CAT) for 48 hrs. Cell death was measured by propidium iodide (PI) staining, and analyzed by flow cytometry.

(K) Sh4EBP1/2 HEK293 cells were grown in Glc starved media and treated with V, NAC or CAT for 48 hrs. Cell death was measured by PI staining, and analyzed by flow cytometry.

(A-K) Data represent the mean of three independent replicates ± standard deviation (SD). Significance was calculated using an unpaired and two-tailed parametric t-test (*$p<0.05$, **$p<0.01$).

Figure 3. 4EBP1/2 controls fatty acid synthesis activity in response to glucose starvation to preserve redox balance and protects cells.

(A) WT or 4ebp1/2 DKO MEF were grown in complete media or glucose (Glc) starved media and labelled with [^{14}C] acetate for 16 hrs. Lipids were extracted and amounts of labelled lipids were quantified with a scintillation counter and normalized to protein content.

(B) ShSCR or sh4EBP1/2 HEK293 cells were grown in complete media or Glc starved media and labelled with [^{14}C] acetate for 16 hrs. Lipids were extracted and amounts of labelled lipids were quantified with a scintillation counter and normalized to protein content.

(C) 4ebp1/2 DKO MEF were grown in Glc starved media for 24 hrs, treated or not with 5-(Tetradecyloxy)-2-furoic acid (TOFA), and $NADP^+$ and NADPH were measured.

(D) Sh4EBP1/2 HEK293 cells were grown in Glc starved media for 24 hrs, treated or not with TOFA, and $NADP^+$ and NADPH were measured.

(E) 4ebp1/2 DKO MEF grown in Glc starved media for 24 hrs and treated or not with TOFA were assayed for H_2O_2 levels by flow cytometry using 2',7'-Dichlorofluorescein diacetate (DCFDA).

(F) Sh4EBP1/2 HEK293 cells grown in Glc starved media for 24 hrs and treated or not with TOFA were assayed for H_2O_2 levels by flow cytometry using DCFDA.

(G) 4ebp1/2 DKO MEF grown in Glc starved media were treated or not with TOFA for 48 hrs. Cell death was measured by propidium iodide (PI) staining, and analyzed by flow cytometry.

(H) Sh4EBP1/2 HEK293 cells grown in Glc starved media were treated or not with TOFA for 48 hrs. Cell death was measured by PI staining, and analyzed by flow cytometry.

(I) 4ebp1/2 DKO MEF were transfected with control siRNA (scr) or siRNAs targeting *fasn* and were grown in Glc starved media for 48 hrs. Cell death was measured by PI staining, and analyzed by flow cytometry.

(J) Sh4EBP1/2 HEK293 cells were transfected with control siRNA (SCR) or siRNAs targeting *FASN* and were grown in Glc starved media for 48 hrs. Cell death was measured by PI staining, and analyzed by flow cytometry.

(A-J) Data represent the mean of at least three independent replicates ± standard deviation (SD). Significance was calculated using an unpaired and two-tailed parametric t-test (*$p<0.05$, **$p<0.01$, ***$p<0.001$).

Figure 4. 4EBP1/2 represses *ACACA* translation under glucose starvation.

(A) WT or 4ebp1/2 DKO MEF were grown in complete media or glucose (Glc) starved for the indicated times, and analyzed by immunoblotting using the indicated antibodies.

(B) ShSCR or sh4EBP1/2 HEK293 cells were grown in complete media or Glc starved for the indicated times, and analyzed by immunoblotting using the indicated antibodies.

(C) ShSCR or sh4EBP1/2 HEK293 cells were grown in complete media or Glc starved for 16 hrs, and *ACACA* mRNA expression was analyzed by qRT-PCR.

(D) ShSCR or sh4EBP1/2 HEK293 cells were grown in complete media or Glc starved for 6 hrs, and translation efficiency (TE) of *ACACA* mRNA was calculated by measuring the levels of polysomal and total *ACACA* mRNA by qRT-PCR.

(E) WT or 4ebp1/2 DKO MEF were transfected with an *ACACA* 5'UTR-containing Firefly Luciferase construct and a control *Renilla* Luciferase vector. Cells grown in complete or Glc starved media for 6 hrs, and luminescence was measured.

(F) ShSCR or sh4EBP1/2 HEK293 cells were transfected with an *ACACA* 5'UTR-containing Firefly Luciferase construct and a control *Renilla* Luciferase vector. Cells grown in complete or Glc starved media for 6 hrs, and luminescence was measured.

(G) HEK293 cells were transfected with HA tagged ACC1 expressing vector containing or not *ACACA* 5'UTR. Cells were grown in complete or Glc starved media for the indicated times, and analyzed by immunoblotting using the indicated antibodies.

(H) 4ebp1/2 DKO MEF were transfected with control siRNA (scr) or siRNAs targeting *acaca* and were grown in Glc starved media for 48 hrs. Cell death was measured by propidium iodide (PI) staining, and analyzed by flow cytometry.

(I) Sh4EBP1/2 HEK293 cells were transfected with control siRNA (SCR) or siRNAs targeting *ACACA* and were grown in Glc starved media for 48 hrs. Cell death was measured by PI staining, and analyzed by flow cytometry.

(C-F,H&I) Data represent the mean of at least three independent replicates ± standard deviation (SD). Significance was calculated using an unpaired and two-tailed parametric t-test (*p<0.05, **p<0.01, ***p<0.001).

Figure 5. Yeast 4EBPs orthologue promotes survival under glucose deprivation.

(A) WT, *EAP1Δ, CAF20Δ or EAP1Δ, CAF20Δ* strains were plated by serial dilution on solid complex medium with (YPD) or without (YP) 2% glucose.

(B) WT or *EAP1Δ* were grown in liquid YPD or YP medium for the indicated times at which OD was measured.

(C) WT or *EAP1Δ* were grown in liquid YPD or YP medium for 2 weeks at 30°C and then were plated by serial dilutions onto complete YPD agar plates.

(D) WT strains were grown in liquid YPD or YP medium, and *EAP1* mRNA expression was analyzed by qRT-PCR.

(E) HEK293, MEF and HeLa cells were grown in complete media or glucose (Glc) starved for 24 hrs indicated times, and *EIF4EBP1* mRNA expression was analyzed by qRT-PCR.

(D&E) Data represent the mean of three independent replicates ± standard deviation (SD). Significance was calculated using an unpaired and two-tailed parametric t-test (*p<0.05, **p<0.01, ***p<0.001).

Figure 6. 4EBP1 supports oncogenic transformation *in vitro* and *in vivo*.

(A) WT or 4ebp1/2 DKO NT2197 cells were grown in soft agar for 21 days. Colonies and single cells were counted, and colony formation efficiency was calculated.

(B) 4ebp1/2 DKO NT2197 cells were grown in soft agar for 21 days and treated with Dimethyl sulfoxide (DMSO), N-acetyl cysteine (NAC), Catalase (CAT), 6-hydroxy-2,5,7,8-tetramethylchroman-2-carboxylic acid (TROLOX) or 5-(Tetradecyloxy)-2-furoic acid (TOFA). Colonies and single cells were counted, and colony formation efficiency was calculated.

(C) Control or *Acaca1* targeting CRISPRi (sgAcaca) 4ebp1/2 DKO NT2197 cells were grown in soft agar for 21 days. Colonies and single cells were counted, and colony formation efficiency was calculated.

(D, E) WT (n=12) or 4ebp1/2 DKO (n=12) NT2197 cells were injected in the flank of NOD-SCID gamma mice. Tumors were harvested, photographed (D) and weighed (E).

(F, G) Control (n=8) or stable Acaca1 knocked down 4ebp1/2 DKO (n=10) NT2197 cells were injected in the flank of NOD-SCID gamma mice. Tumors were harvested, photographed (F) and weighed (G).

(H) HeLa cells stably expressing empty vector (EV) or $4EBP1^{AA}$ were grown in soft agar for 21 days. Colonies and single cells were counted, and colony formation efficiency was calculated.

(I, J) HeLa cells stably expressing empty vector (EV) (n=7) or $4EBP1^{AA}$ (n=6) were injected in the flank of NOD-SCID gamma mice. Tumors were harvested, photographed (I) and weighed (J).

(A-C & H) Data represent the mean of three independent replicates ± standard deviation (SD). Significance was calculated using an unpaired and two-tailed parametric t-test (*p<0.05, ***p<0.001, ****p<0.0001).

(E, G, J) Significance was calculated using an unpaired and two-tailed parametric t-test (*p<0.05).

Figure 7. 4EBP1 has clinical relevance in glioma and promotes glioma tumorigenesis.

(A) Expression levels of *EIF4EBP1* expression in non-tumorigenic brain tissue (NNBT) and malignant glioma tissues in the FRENCH cohort.

(B) Expression levels of *EIF4EBP1* per glioma stage in the CCGA cohort.

(C, D) Kaplan-Meier survival estimates of overall survival of malignant glioma (C) or glioblastoma (D) patients stratified by their *EIF4EBP1* mRNA (cut-off first quartile) in the CCGA cohort.

(E) Control or *EIF4EBP1* targeting CRISPRi (sg4EBP1#1 and #2) U-87 MG cells were grown in soft agar for 21 days. Colonies and single cells were counted, and colony formation efficiency was calculated.

(F) Control (Scr) or stable 4EBP1 knocked down (sh4ebp1#1 and #2) GL-261 cells were grown in soft agar for 21 days. Colonies and single cells were counted, and colony formation efficiency was calculated.

(G) *EIF4EBP1* targeted CRISPRi (sg4EBP1#1) U-87 MG cells were grown in soft agar for 21 days and treated with Dimethyl sulfoxide (DMSO), N-acetyl cysteine (NAC), Catalase (CAT), 6-hydroxy-2,5,7,8-tetramethylchroman-2-carboxylic acid (TROLOX) or 5-(Tetradecyloxy)-2-furoic acid (TOFA). Colonies and single cells were counted, and colony formation efficiency was calculated.

(H) 4EBP1 knocked down (sh4ebp1 #1) GL-261 cells were grown in soft agar for 21 days and treated with DMSO, NAC, CAT, TROLOX or TOFA. Colonies and single cells were counted, and colony formation efficiency was calculated.

(I) Control (shSCR) (n=12) or stable 4EBP1 knocked down (sh4EBP1#1 (n=12) and #2 (n=12)) U-87 MG cells were injected in the flank of NOD-SCID gamma mice. Tumors were harvested, photographed and weighed.

(J) ShSCR or stable inducible 4EBP1 knocked down (sh4EBP1) U-87 MG cells were injected in the flank of NOD-SCID gamma mice. When tumors reached 100 mm^3, mice were given or not given doxycycline (DOX). Tumor volumes were measured at the indicated times.

Parental+DMSO: n=10; parental+DOX: n=10; shSCR+DOX: n=8; sh4EBP1+DMSO: n=8; sh4EBP1+DOX: n=8.

(K) ShSCR (n=7) or stable 4EBP1 knocked down (sh4EBP1) (n=8) U-87 MG cells were injected intracranially in NOD-SCID gamma mice. Survival of mice was monitored post injection.

(L) ShScr (n=10) or stable 4EBP1 knocked down (sh4ebp1) (n=10) GL-261 cells were injected intracranially in C57 WT mice. Survival of mice was monitored post injection.

(M) Stable 4EBP1 knocked down (sh4ebp1) GL-261 cells with ShScr (n=9) or shAcaca (n=8) were injected intracranially in C57 WT mice. Survival of mice was monitored post injection.

(A & B) Significance was calculated using an unpaired and two-tailed parametric t-test (**p<0.01, ****p<0.0001).

(E-H) Data represent the mean of three independent replicates ± standard deviation (SD). Significance was calculated using an unpaired and two-tailed parametric t-test (**p<0.01, ***p<0.001, ****p<0.0001).

(I & J) Significance was calculated using an unpaired and two-tailed parametric t-test (*p<0.05).

(K-M) Significance was calculated using a Log rank (Mantel Cox) test.

SUPPLEMENTARY FIGURE LEGENDS

Supplementary Figure 1. Related to Figure 1.

(A) Control (shSCR) or stable 4EBP1/2 knocked down (sh4EBP1/2) iPSC were grown in complete media or glucose (Glc) starved for 48 hrs. Cell death was measured by propidium iodide (PI) staining, and analyzed by flow cytometry.

(B) Control (shSCR) or stable 4EBP1 knocked down (sh4EBP1#1 and #2) U-87 MG cells were grown in complete media or Glc starved for 48 hrs. Cell death was measured by PI staining, and analyzed by flow cytometry.

(C) Control (shSCR) or stable 4EBP1 knocked down (sh4EBP1#1 and #2) MCF-7 cells were grown in complete media or Glc starved for 48 hrs. Cell death was measured by PI staining, and analyzed by flow cytometry.

(D) Control (shSCR) or stable 4EBP1 knocked down (sh4EBP1#1 and #2) IMR-32 cells were grown in complete media or Glc starved for 48 hrs. Cell death was measured by PI staining, and analyzed by flow cytometry.

(E) Control (shSCR) or stable 4EBP1 knocked down (sh4EBP1#1 and #2) Kelly cells were grown in complete media or Glc starved for 48 hrs. Cell death was measured by PI staining, and analyzed by flow cytometry.

(F) Control (shSCR) or stable 4EBP1 knocked down (sh4EBP1#1 and #2) Med8a cells were grown in complete media or Glc starved for 48 hrs. Cell death was measured by PI staining, and analyzed by flow cytometry.

(G) Control (shSCR) or stable 4EBP1 knocked down (sh4EBP1#1 and #2) HDMB03 cells were grown in complete media or Glc starved for 48 hrs. Cell death was measured by PI staining, and analyzed by flow cytometry.

(H) ShSCR and sh4EBP1/2 HEK293 cells were grown complete media or Glc starved for the indicated times and treated or not with chloroquine (CHQ). Cell lysates were analyzed by immunoblotting using the indicated antibodies.

(I) WT or 4ebp1/2 DKO MEF were grown complete media or Glc starved for the indicated times and treated or not with CHQ. Cell lysates were analyzed by immunoblotting using the indicated antibodies.

(J) ShSCR and sh4EBP1/2 HEK293 cells were grown in complete media, treated or not with rapamycin (Rapa) or Ku-0063794 (KU), and labeled with azidohomoalanine (AHA). Levels of AHA-labelled proteins was detected by immunoblotting with a streptavidin conjugate.

(A-G) Data represent the mean of three independent replicates ± standard deviation (SD). Significance was calculated using an unpaired and two-tailed parametric t-test (*$p<0.05$, **$p<0.01$, ***$p<0.001$).

Supplementary Figure 2. Related to Figure 2.

(A) WT or 4ebp1/2 DKO MEF were grown in complete media or glucose (Glc) starved for 24 hrs, and ATP levels were measured by Gas chromatography–mass spectrometry (GC-MS).

(B) ShSCR or sh4EBP1/2 HEK293 cells were grown in complete media or Glc starved for 24 hrs, and ATP levels were measured by GC-MS.

(C) WT or 4ebp1/2 DKO MEF were grown in complete media or Glc starved for 24 hrs, and total glutathione was measured.

(D) ShSCR or sh4EBP1/2 HEK293 cells were grown in complete media or Glc starved for 24 hrs, and total glutathione was measured.

(E) MSCV or 4EBP1^{AA} overexpressing HeLa cells were grown in complete media or Glc starved for 24 hrs, and total glutathione was measured.

(A-E) Data represent the mean of three independent replicates ± standard deviation (SD). Significance was calculated using an unpaired and two-tailed parametric t-test (*p<0.05).

Supplementary Figure 3. Related to Figure 4.

(A) MSCV or 4EBP1^{AA} overexpressing HeLa cells were grown in complete media or glucose (Glc) starved for the indicated times, and analyzed by immunoblotting using the indicated antibodies.

Supplementary Figure 4. Related to Figure 6.

(A) NIH 3T3 transfected with control (scr) and *eif4ebp1* and *eif4ebp2* targeting siRNAs were grown in soft agar for 21 days. Colonies and single cells were counted, and colony formation efficiency was calculated.

(B) NT2197 Ctrl cells were grown in soft agar for 21 days and treated with Dimethyl sulfoxide (DMSO), N-acetyl cysteine (NAC), Catalase (CAT), 6-hydroxy-2,5,7,8-tetramethylchroman-2-carboxylic acid (TROLOX) or 5-(Tetradecyloxy)-2-furoic acid (TOFA). Colonies and single cells were counted, and colony formation efficiency was calculated.

(C) NIH 3T3 transfected with *eif4ebp1* and *eif4ebp2* (NIH 3T3 4ebp1/2 DKD) targeting siRNAs were grown in soft agar for 21 days and treated with DMSO, NAC, CAT or TROLOX. Colonies and single cells were counted, and colony formation efficiency was calculated.

(A-C) Data represent the mean of three independent replicates ± standard deviation (SD). Significance was calculated using an unpaired and two-tailed parametric t-test (*p<0.05, **p<0.01).

Supplementary Figure 5. Related to Figure 7.

(A, B) Expression levels of *EIF4EBP1* (A) and *EIF4EBP2* (B) in tumor tissues and corresponding non-tumorigenic tissues (NNBT) from TCGA. Abbreviations: BLCA: bladder urothelial

carcinoma, CESC: cervical squamous cell carcinoma and endocervical adenocarcinoma, CHOL: cholangio carcinoma, COAD: colon adenocarcinoma, DLBC: lymphoid neoplasm diffuse large B-cell lymphoma, GBM: glioblastoma multiforme, KIRC: kidney renal clear cell carcinoma, LGG: brain lower grade glioma, LUSC: lung squamous cell carcinoma, OV: ovarian serous cystadenocarcinoma, READ: rectum adenocarcinoma, SKCM: skin cutaneous melanoma, STAD: stomach adenocarcinoma, TGCT: testicular germ cell tumors, THYM: thymoma, UCEC: uterine corpus endometrial carcinoma, UCS: uterine carcinosarcoma.

(C, D, E) Kaplan-Meier survival estimates of overall survival of bladder urothelial carcinoma (C), kidney renal clear cell carcinoma (D), and malignant glioma (E) patients stratified by their *EIF4EBP1* mRNA (median first quartile) in the indicated cohort.

(F) Expression levels of 4EBP1 in proteomics data in NNBT and malignant glioma tissues. Significance was calculated using a two-tailed Mann Whitney test (**p<0.01).

(G) Control (shScr) or stable 4EBP1 knocked down (sh4EBP1#1 and #2) GL-261 cells were grown in complete media or glucose (Glc) starved for 48 hrs. Cell death was measured by propidium iodide (PI) staining, and analyzed by flow cytometry. Data represent the mean of at least four independent replicates ± standard deviation (SD). Significance was calculated using an unpaired and two-tailed parametric t-test (****p<0.0001).

Supplementary Figure 6. Related to Figure 7.

(A) *EIF4EBP1* targeted CRISPRi (sg4EBP1#2) U-87 MG cells were grown in soft agar for 21 days and treated with Dimethyl sulfoxide (DMSO), N-acetyl cysteine (NAC), Catalase (CAT), 6-hydroxy-2,5,7,8-tetramethylchroman-2-carboxylic acid (TROLOX) or 5-(Tetradecyloxy)-2-furoic acid (TOFA). Colonies and single cells were counted, and colony formation efficiency was calculated.

(B) 4EBP1 knocked down (sh4ebp1 #2) GL-261 cells were grown in soft agar for 21 days and treated with DMSO, NAC, CAT, TROLOX or TOFA. Colonies and single cells were counted, and colony formation efficiency was calculated.

(C) Control U-87 MG cells were grown in soft agar for 21 days and treated with DMSO, NAC, CAT, TROLOX or TOFA. Colonies and single cells were counted, and colony formation efficiency was calculated.

(D) Control GL-261 (shScr) cells were grown in soft agar for 21 days and treated with DMSO, NAC, CAT, TROLOX or TOFA. Colonies and single cells were counted, and colony formation efficiency was calculated.

(A-D) Data represent the mean of three independent replicates ± standard deviation (SD). Significance was calculated using an unpaired and two-tailed parametric t-test (*p<0.05, **p<0.01).

REFERENCES

Agudelo, L.Z., Tuyeras, R., Llinares, C., Morcuende, A., Park, Y., Sun, N., Linna-Kuosmanen, S., Atabaki-Pasdar, N., Ho, L.-L., Galani, K.*, et al.* (2021). Metabolic resilience is encoded in genome plasticity. bioRxiv, 2021.2006.2025.449953.

Braunstein, S., Karpisheva, K., Pola, C., Goldberg, J., Hochman, T., Yee, H., Cangiarella, J., Arju, R., Formenti, S.C., and Schneider, R.J. (2007). A Hypoxia-Controlled Cap-Dependent to Cap-Independent Translation Switch in Breast Cancer. Molecular Cell *28*, 501-512.

Broussard, T.C., Price, A.E., Laborde, S.M., and Waldrop, G.L. (2013). Complex formation and regulation of Escherichia coli acetyl-CoA carboxylase. Biochemistry *52*, 3346-3357.

Buttgereit, F., and Brand, M.D. (1995). A hierarchy of ATP-consuming processes in mammalian cells. The Biochemical journal *312 (Pt 1*, 163-167.

Caro-Maldonado, A. (2011). Dying for Something to Eat: How Cells Respond to Starvation. The Open Cell Signaling Journal *3*, 42-51.

Chen, J., Lee, H.J., Wu, X., Huo, L., Kim, S.J., Xu, L., Wang, Y., He, J., Bollu, L.R., Gao, G.*, et al.* (2015). Gain of glucose-independent growth upon metastasis of breast cancer cells to the brain. Cancer Res *75*, 554-565.

Chhipa, R.R., Fan, Q., Anderson, J., Muraleedharan, R., Huang, Y., Ciraolo, G., Chen, X., Waclaw, R., Chow, L.M., Khuchua, Z.*, et al.* (2018). AMP kinase promotes glioblastoma bioenergetics and tumour growth. Nat Cell Biol *20*, 823-835.

Choo, A.Y., Kim, S.G., Vander Heiden, M.G., Mahoney, S.J., Vu, H., Yoon, S.O., Cantley, L.C., and Blenis, J. (2010). Glucose Addiction of TSC Null Cells Is Caused by Failed mTORC1-Dependent Balancing of Metabolic Demand with Supply. Molecular Cell *38*, 487-499.

Conn, C.S., Yang, H., Tom, H.J., Ikeda, K., Oses-Prieto, J.A., Vu, H., Oguri, Y., Nair, S., Gill, R.M., Kajimura, S.*, et al.* (2021). The major cap-binding protein eIF4E regulates lipid homeostasis and diet-induced obesity. Nat Metab *3*, 244-257.

Cosentino, G.P., Schmelzle, T., Haghighat, A., Helliwell, S.B., Hall, M.N., and Sonenberg, N. (2000). Eap1p, a novel eukaryotic translation initiation factor 4E-associated protein in Saccharomyces cerevisiae. Mol Cell Biol *20*, 4604-4613.

Cridge, A.G., Castelli, L.M., Smirnova, J.B., Selley, J.N., Rowe, W., Hubbard, S.J., McCarthy, J.E., Ashe, M.P., Grant, C.M., and Pavitt, G.D. (2010). Identifying eIF4E-binding protein translationally-controlled transcripts reveals links to mRNAs bound by specific PUF proteins. Nucleic Acids Res *38*, 8039-8050.

Damiano, F., Testini, M., Tocci, R., Gnoni, G.V., and Siculella, L. (2018). Translational control of human acetyl-CoA carboxylase 1 mRNA is mediated by an internal ribosome entry site in response to ER stress, serum deprivation or hypoxia mimetic CoCl2. Biochim Biophys Acta Mol Cell Biol Lipids *1863*, 388-398.

Ding, M., Van der Kwast, T.H., Vellanki, R.N., Foltz, W.D., McKee, T.D., Sonenberg, N., Pandolfi, P.P., Koritzinsky, M., and Wouters, B.G. (2018). The mTOR Targets 4E-BP1/2 Restrain Tumor Growth and Promote Hypoxia Tolerance in PTEN-driven Prostate Cancer. Mol Cancer Res *16*, 682-695.

Dowling, R.J.O., Topisirovic, I., Alain, T., Bidinosti, M., Fonseca, B.D., Petroulakis, E., Wang, X., Larsson, O., Selvaraj, A., Liu, Y.*, et al.* (2010). mTORC1-mediated cell proliferation, but not cell growth, controlled by the 4E-BPs. Science (New York, NY) *328*, 1172-1176.

Eichner, L.J., Brun, S.N., Herzig, S., Young, N.P., Curtis, S.D., Shackelford, D.B., Shokhirev, M.N., Leblanc, M., Vera, L.I., Hutchins, A.*, et al.* (2019). Genetic Analysis Reveals AMPK Is Required to Support Tumor Growth in Murine Kras-Dependent Lung Cancer Models. Cell Metab *29*, 285-302 e287.

Fan, J., Ye, J., Kamphorst, J.J., Shlomi, T., Thompson, C.B., and Rabinowitz, J.D. (2014). Quantitative flux analysis reveals folate-dependent NADPH production. Nature *510*, 298-302.

Faubert, B., Vincent, E.E., Poffenberger, M.C., and Jones, R.G. (2014). The AMP-activated protein kinase (AMPK) and cancer: Many faces of a metabolic regulator. Cancer Letters.

Fellows, L.K., and Boutelle, M.G. (1993). Rapid changes in extracellular glucose levels and blood flow in the striatum of the freely moving rat. Brain Res *604*, 225-231.

Flavahan, W.a., Wu, Q., Hitomi, M., Rahim, N., Kim, Y., Sloan, A.E., Weil, R.J., Nakano, I., Sarkaria, J.N., Stringer, B.W.*, et al.* (2013). Brain tumor initiating cells adapt to restricted nutrition through preferential glucose uptake. Nature neuroscience *16*, 1373-1382.

Flohe, L. (2013). The fairytale of the GSSG/GSH redox potential. Biochim Biophys Acta *1830*, 3139-3142.

Gruetter, R., Novotny, E.J., Boulware, S.D., Rothman, D.L., Mason, G.F., Shulman, G.I., Shulman, R.G., and Tamborlane, W.V. (1992). Direct measurement of brain glucose concentrations in humans by 13C NMR spectroscopy. Proc Natl Acad Sci U S A *89*, 1109-1112.

Homma, T., Fukushima, T., Vaccarella, S., Yonekawa, Y., Di Patre, P.L., Franceschi, S., and Ohgaki, H. (2006). Correlation among pathology, genotype, and patient outcomes in glioblastoma. J Neuropathol Exp Neurol *65*, 846-854.

Horman, S., Browne, G., Krause, U., Patel, J., Vertommen, D., Bertrand, L., Lavoinne, A., Hue, L., Proud, C., and Rider, M. (2002). Activation of AMP-activated protein kinase leads to the phosphorylation of elongation factor 2 and an inhibition of protein synthesis. Current biology : CB *12*, 1419-1423.

Hsieh, A.C., Liu, Y., Edlind, M.P., Ingolia, N.T., Janes, M.R., Sher, A., Shi, E.Y., Stumpf, C.R., Christensen, C., Bonham, M.J*., et al.* (2012). The translational landscape of mTOR signalling steers cancer initiation and metastasis. Nature *485*, 55-61.

Inoki, K., Zhu, T., and Guan, K.-L. (2003). TSC2 mediates cellular energy response to control cell growth and survival. Cell *115*, 577-590.

Jagoe, R.T., Lecker, S.H., Gomes, M., and Goldberg, A.L. (2002). Patterns of gene expression in atrophying skeletal muscles: response to food deprivation. FASEB J *16*, 1697-1712.

Jeon, S.M., Chandel, N.S., and Hay, N. (2012). AMPK regulates NADPH homeostasis to promote tumour cell survival during energy stress. Nature *485*, 661-665.

Jones, R.G., and Thompson, C.B. (2009). Tumor suppressors and cell metabolism: A recipe for cancer growth. Genes and Development *23*, 537-548.

Kumar, S., Sharife, H., Kreisel, T., Mogilevsky, M., Bar-Lev, L., Grunewald, M., Aizenshtein, E., Karni, R., Paldor, I., Shlomi, T*., et al.* (2019). Intra-Tumoral Metabolic Zonation and Resultant Phenotypic Diversification Are Dictated by Blood Vessel Proximity. Cell Metab *30*, 201-211 e206.

Lanker, S., Muller, P.P., Altmann, M., Goyer, C., Sonenberg, N., and Trachsel, H. (1992). Interactions of the eIF-4F subunits in the yeast Saccharomyces cerevisiae. J Biol Chem *267*, 21167-21171.

Leibovitch, M., and Topisirovic, I. (2018). Dysregulation of mRNA translation and energy metabolism in cancer. Adv Biol Regul *67*, 30-39.

Leprivier, G., Remke, M., Rotblat, B., Dubuc, A., Mateo, A.R.F., Kool, M., Agnihotri, S., El-Naggar, A., Yu, B., Prakash Somasekharan, S*., et al.* (2013). The eEF2 kinase confers resistance to nutrient deprivation by blocking translation elongation. Cell *153*.

Leprivier, G., and Rotblat, B. (2020). How does mTOR sense glucose starvation? AMPK is the usual suspect. Cell Death Discov *6*, 27.

Leprivier, G., Rotblat, B., Khan, D., Jan, E., and Sorensen, P.H. (2015). Stress-mediated translational control in cancer cells. Biochimica et Biophysica Acta - Gene Regulatory Mechanisms *1849*, 845-860.

Liu, G.Y., and Sabatini, D.M. (2020). mTOR at the nexus of nutrition, growth, ageing and disease. Nat Rev Mol Cell Biol *21*, 183-203.

Marciano, R., Leprivier, G., and Rotblat, B. (2018). Puromycin labeling does not allow protein synthesis to be measured in energy-starved cells. Cell Death Dis *9*, 39.

Morita, M., Gravel, S.P., Chénard, V., Sikström, K., Zheng, L., Alain, T., Gandin, V., Avizonis, D., Arguello, M., Zakaria, C*., et al.* (2013). MTORC1 controls mitochondrial activity and biogenesis through 4E-BP-dependent translational regulation. Cell Metabolism *18*, 698-711.

Musa, J., Orth, M.F., Dallmayer, M., Baldauf, M., Pardo, C., Rotblat, B., Kirchner, T., Leprivier, G., and Grünewald, T.G.P. (2016). Eukaryotic initiation factor 4E-binding protein 1 (4E-BP1): a master regulator of mRNA translation involved in tumorigenesis. Oncogene.

Nagy, J.a., Chang, S.H., Dvorak, a.M., and Dvorak, H.F. (2009). Why are tumour blood vessels abnormal and why is it important to know? British journal of cancer *100*, 865-869.

Ng, T.L., Leprivier, G., Robertson, M.D., Chow, C., Martin, M.J., Laderoute, K.R., Davicioni, E., Triche, T.J., and Sorensen, P.H. (2012). The AMPK stress response pathway mediates anoikis resistance through inhibition of mTOR and suppression of protein synthesis. Cell Death Differ *19*, 501-510.

Orozco, J.M., Krawczyk, P.A., Scaria, S.M., Cangelosi, A.L., Chan, S.H., Kunchok, T., Lewis, C.A., and Sabatini, D.M. (2020). Dihydroxyacetone phosphate signals glucose availability to mTORC1. Nat Metab *2*, 893-901.

Pause, A., Belsham, G.J., Gingras, A.C., Donze, O., Lin, T.A., Lawrence, J.C., Jr., and Sonenberg, N. (1994). Insulin-dependent stimulation of protein synthesis by phosphorylation of a regulator of 5'-cap function. Nature *371*, 762-767.

Pellerin, L. (2008). Brain energetics (thought needs food). Curr Opin Clin Nutr Metab Care *11*, 701-705.

Petroulakis, E., Parsyan, A., Dowling, R.J.O., LeBacquer, O., Martineau, Y., Bidinosti, M., Larsson, O., Alain, T., Rong, L., Mamane, Y*., et al.* (2009). p53-Dependent Translational Control of Senescence and Transformation via 4E-BPs. Cancer Cell *16*, 439-446.

Poulin, F., Gingras, A.C., Olsen, H., Chevalier, S., and Sonenberg, N. (1998). 4E-BP3, a new member of the eukaryotic initiation factor 4E-binding protein family. J Biol Chem *273*, 14002-14007.

Ricciardi, S., Manfrini, N., Alfieri, R., Calamita, P., Crosti, M.C., Gallo, S., Muller, R., Pagani, M., Abrignani, S., and Biffo, S. (2018). The Translational Machinery of Human CD4(+) T Cells Is Poised for Activation and Controls the Switch from Quiescence to Metabolic Remodeling. Cell Metab *28*, 895-906 e895.

Ryazanov, a.G., Shestakova, E.a., and Natapov, P.G. (1988). Phosphorylation of elongation factor 2 by EF-2 kinase affects rate of translation. Nature *334*, 170-173.

Schafer, Z.T., Grassian, A.R., Song, L., Jiang, Z., Gerhart-Hines, Z., Irie, H.Y., Gao, S., Puigserver, P., and Brugge, J.S. (2009). Antioxidant and oncogene rescue of metabolic defects caused by loss of matrix attachment. Nature *461*, 109-113.

Silvera, D., Formenti, S.C., and Schneider, R.J. (2010). Translational control in cancer. Nat Rev Cancer *10*, 254-266.

Sonenberg, N., and Hinnebusch, A.G. (2009). Regulation of Translation Initiation in Eukaryotes: Mechanisms and Biological Targets. Cell *136*, 731-745.

Tameire, F., Verginadis, II, Leli, N.M., Polte, C., Conn, C.S., Ojha, R., Salas Salinas, C., Chinga, F., Monroy, A.M., Fu, W*., et al.* (2019). ATF4 couples MYC-dependent translational activity to bioenergetic demands during tumour progression. Nat Cell Biol *21*, 889-899.

Tanaka, K., Sasayama, T., Nagashima, H., Irino, Y., Takahashi, M., Izumi, Y., Uno, T., Satoh, N., Kitta, A., Kyotani, K*., et al.* (2021). Glioma cells require one-carbon metabolism to survive glutamine starvation. Acta Neuropathol Commun *9*, 16.

Teleman, A.a., Chen, Y.W., and Cohen, S.M. (2005). 4E-BP functions as a metabolic brake used under stress conditions but not during normal growth. Genes and Development *19*, 1844-1848.

Tettweiler, G., Miron, M., Jenkins, M., Sonenberg, N., and Lasko, P.F. (2005). Starvation and oxidative stress resistance in Drosophila are mediated through the eIF4E-binding protein, d4E-BP. Genes and Development *19*, 1840-1843.

Thoreen, C.C., Chantranupong, L., Keys, H.R., Wang, T., Gray, N.S., and Sabatini, D.M. (2012). A unifying model for mTORC1-mediated regulation of mRNA translation. Nature *485*, 109-113.

Trefts, E., and Shaw, R.J. (2021). AMPK: restoring metabolic homeostasis over space and time. Mol Cell *81*, 3677-3690.

Truitt, Morgan L., Conn, Crystal S., Shi, Z., Pang, X., Tokuyasu, T., Coady, Alison M., Seo, Y., Barna, M., and Ruggero, D. (2015). Differential Requirements for eIF4E Dose in Normal Development and Cancer. Cell, 1-13.

Truitt, M.L., and Ruggero, D. (2016). New frontiers in translational control of the cancer genome. Nat Rev Cancer *16*, 288-304.

Tsukiyama-Kohara, K., Poulin, F., Kohara, M., DeMaria, C.T., Cheng, a., Wu, Z., Gingras, a.C., Katsume, a., Elchebly, M., Spiegelman, B.M*., et al.* (2001). Adipose tissue reduction in mice lacking the translational inhibitor 4E-BP1. Nature medicine *7*, 1128-1132.

Valvezan, A.J., and Manning, B.D. (2019). Molecular logic of mTORC1 signalling as a metabolic rheostat. Nat Metab *1*, 321-333.

Wang, Z., Feng, X., Molinolo, A.A., Martin, D., Vitale-Cross, L., Nohata, N., Ando, M., Wahba, A., Amornphimoltham, P., Wu, X*., et al.* (2019). 4E-BP1 Is a Tumor Suppressor Protein Reactivated by mTOR Inhibition in Head and Neck Cancer. Cancer Res *79*, 1438-1450.

Warburg, O. (1956). On the origin of cancer cells. Science *123*, 309-314.

Wu, S., and Wagner, G. (2021). Deep computational analysis details dysregulation of eukaryotic translation initiation complex eIF4F in human cancers. Cell Syst *12*, 907-923 e906.

Zid, B.M., Rogers, A.N., Katewa, S.D., Vargas, M.a., Kolipinski, M.C., Lu, T.a., Benzer, S., and Kapahi, P. (2009). 4E-BP Extends Lifespan upon Dietary Restriction by Enhancing Mitochondrial Activity in Drosophila. Cell *139*, 149-160.

Figure 1

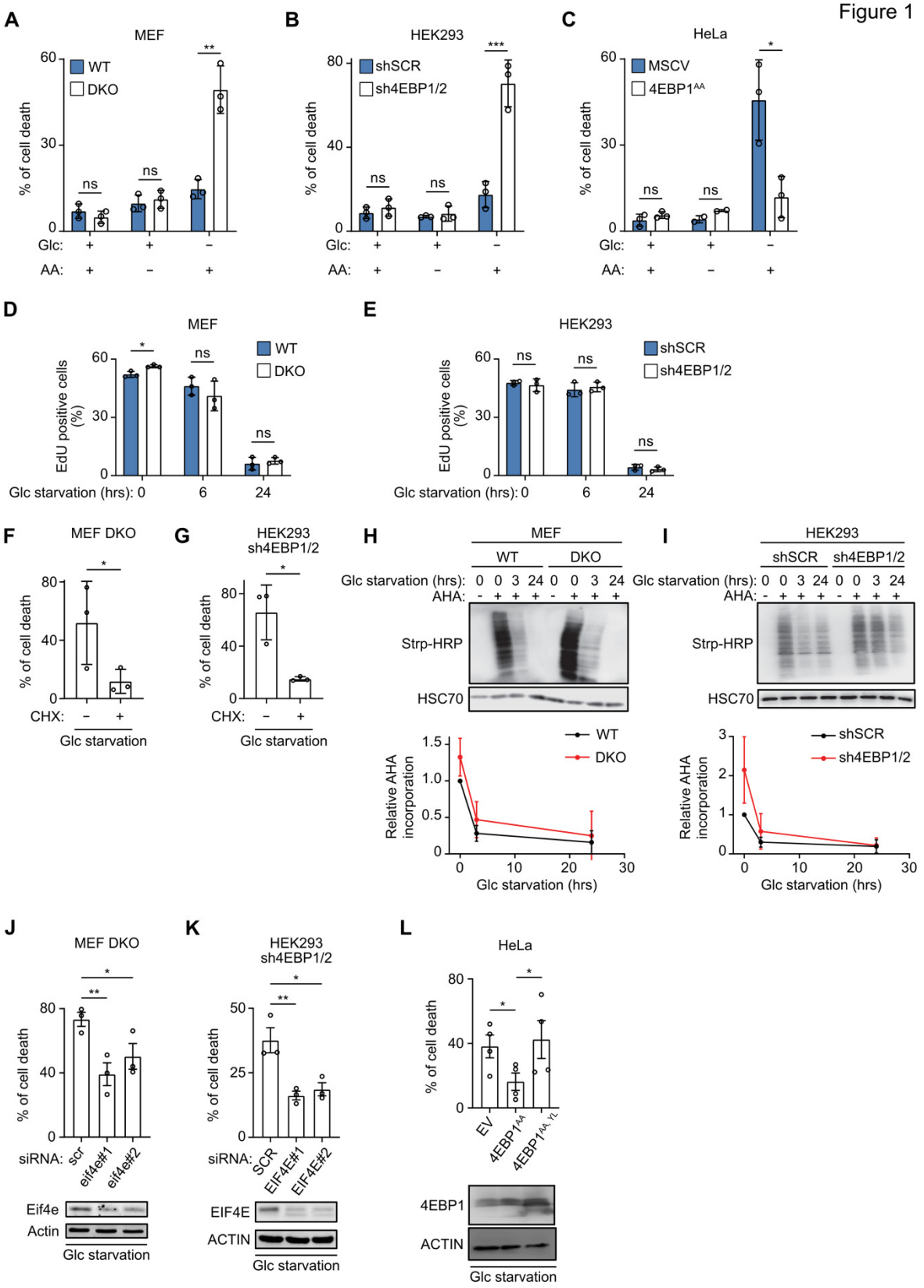
A
MEF
WT
DKO
% of cell death
Glc:
AA:
B
HEK293
shSCR
sh4EBP1/2
C
HeLa
MSCV
4EBP1AA
D
MEF
EdU positive cells (%)
Glc starvation (hrs): 0 6 24
E
HEK293
F
MEF DKO
CHX:
Glc starvation
G
HEK293 sh4EBP1/2
H
MEF
Glc starvation (hrs): 0 0 3 24 0 0 3 24
AHA:
Strp-HRP
HSC70
Relative AHA incorporation
Glc starvation (hrs)
I
HEK293
J
MEF DKO
siRNA: scr eif4e#1 eif4e#2
Eif4e
Actin
K
HEK293 sh4EBP1/2
siRNA: SCR EIF4E#1 EIF4E#2
EIF4E
ACTIN
L
HeLa
EV
4EBP1AA
4EBP1AA, YL
4EBP1
ACTIN

Figure 2

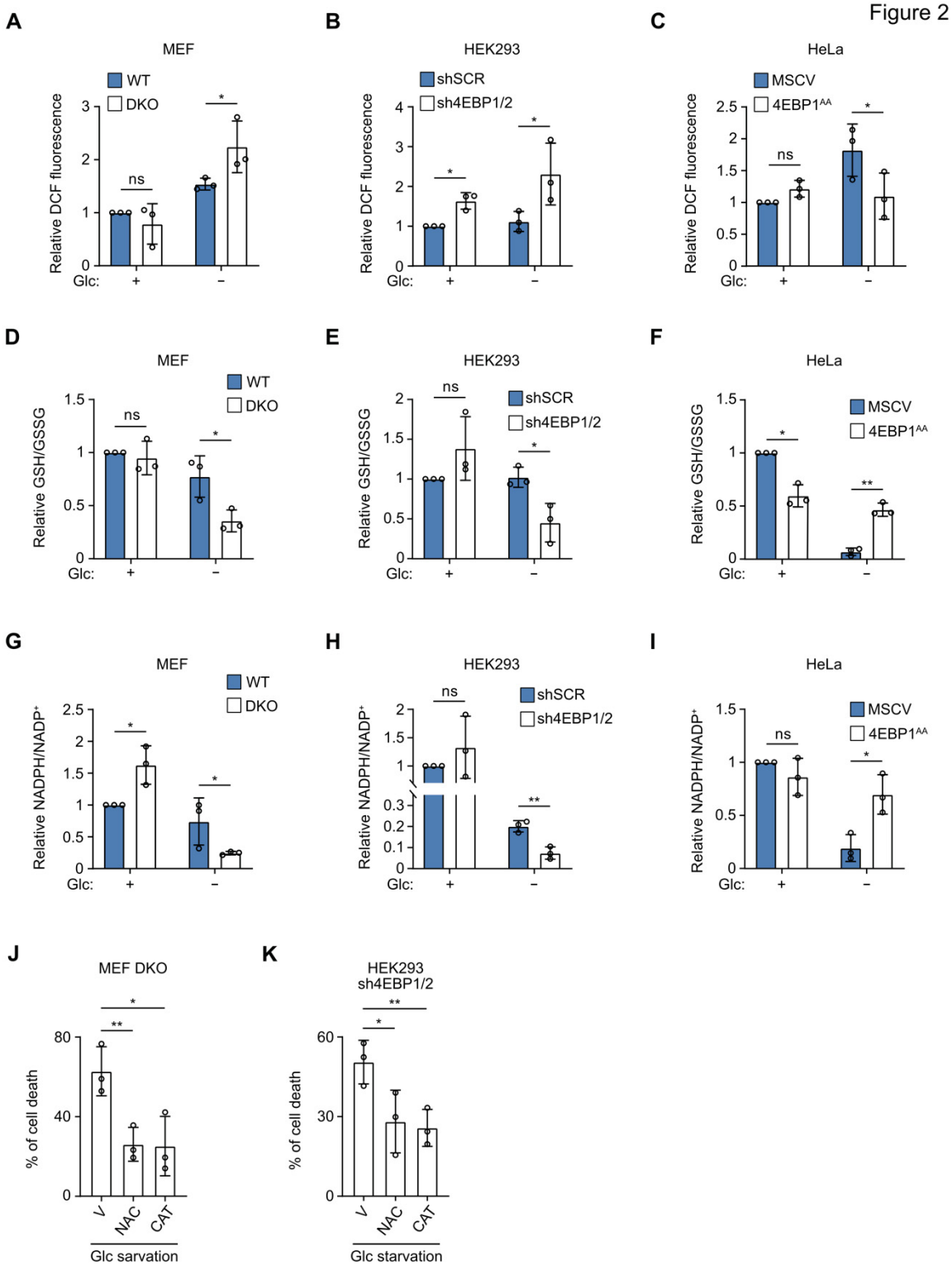
A
MEF
WT
DKO
Relative DCF fluorescence
ns
*
Glc: + −
B
HEK293
shSCR
sh4EBP1/2
Relative DCF fluorescence
*
*
Glc: + −
C
HeLa
MSCV
4EBP1AA
Relative DCF fluorescence
ns
*
Glc: + −
D
MEF
WT
DKO
Relative GSH/GSSG
ns
*
Glc: + −
E
HEK293
shSCR
sh4EBP1/2
Relative GSH/GSSG
ns
*
Glc: + −
F
HeLa
MSCV
4EBP1AA
Relative GSH/GSSG
*
**
Glc: + −
G
MEF
WT
DKO
Relative NADPH/NADP+
*
*
Glc: + −
H
HEK293
shSCR
sh4EBP1/2
Relative NADPH/NADP+
ns
**
Glc: + −
I
HeLa
MSCV
4EBP1AA
Relative NADPH/NADP+
ns
*
Glc: + −
J
MEF DKO
% of cell death
*
**
V
NAC
CAT
Glc sarvation
K
HEK293
sh4EBP1/2
% of cell death
**
*
V
NAC
CAT
Glc starvation

Figure 3

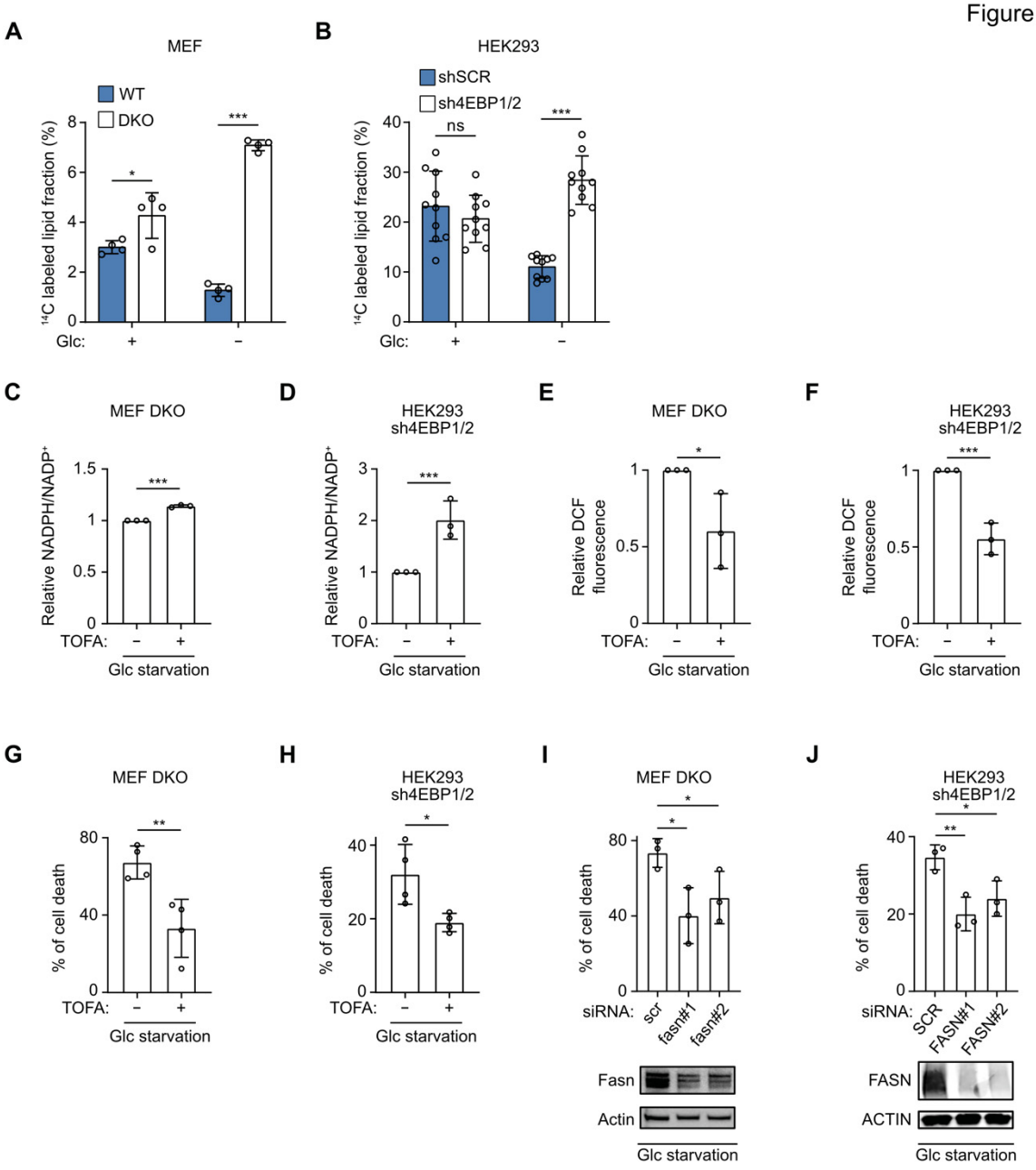
A
MEF
WT
DKO
^{14}C labeled lipid fraction (%)
Glc:
B
HEK293
shSCR
sh4EBP1/2
ns
C
MEF DKO
Relative NADPH/NADP$^+$
TOFA:
Glc starvation
D
HEK293 sh4EBP1/2
E
MEF DKO
Relative DCF fluorescence
F
HEK293 sh4EBP1/2
G
MEF DKO
% of cell death
H
HEK293 sh4EBP1/2
I
MEF DKO
siRNA:
scr
fasn#1
fasn#2
Fasn
Actin
J
HEK293 sh4EBP1/2
SCR
FASN#1
FASN#2
FASN
ACTIN

Figure 4

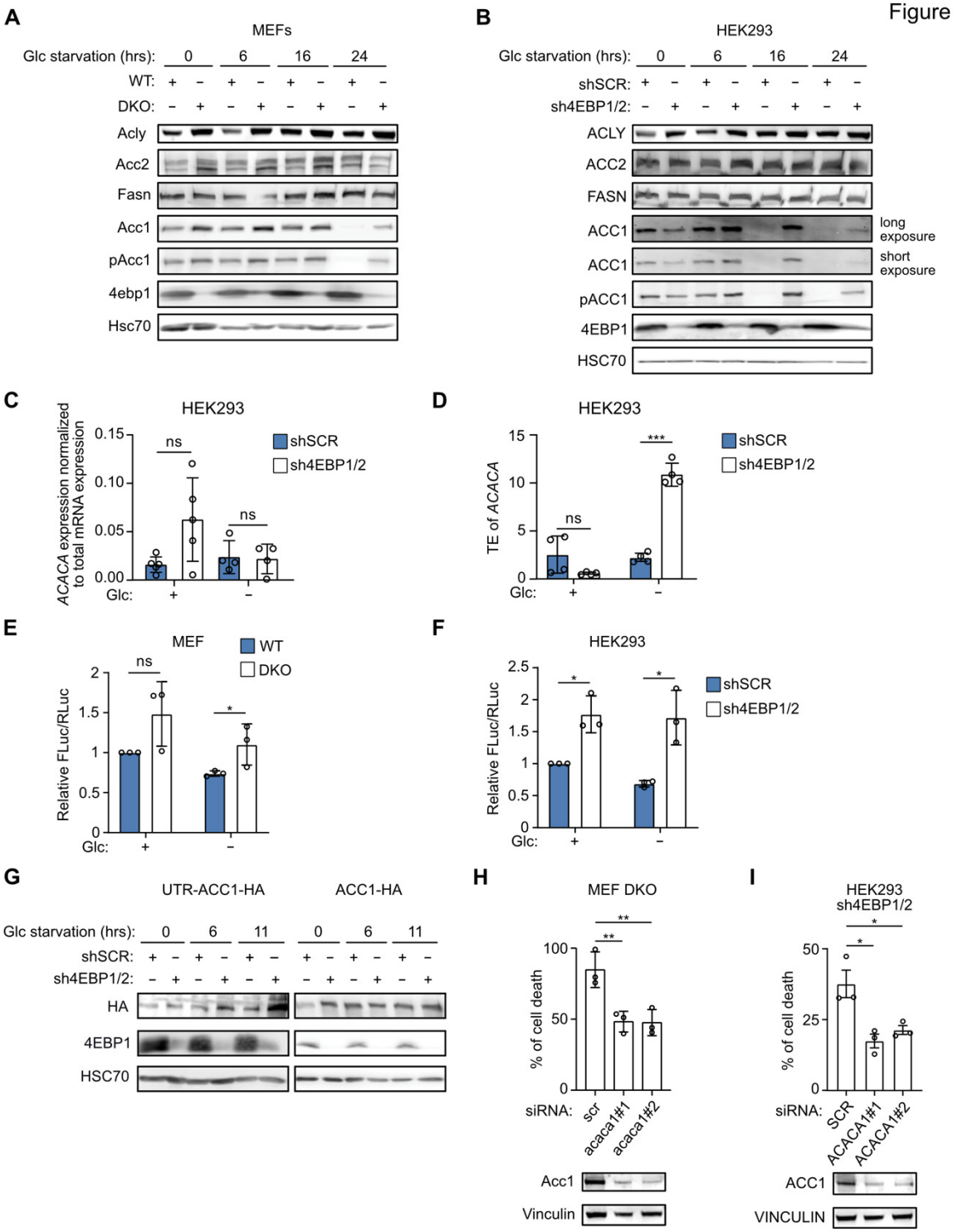
A
MEFs
Glc starvation (hrs): 0 6 16 24
WT:
DKO:
Acly
Acc2
Fasn
Acc1
pAcc1
4ebp1
Hsc70
B
HEK293
Glc starvation (hrs): 0 6 16 24
shSCR:
sh4EBP1/2:
ACLY
ACC2
FASN
ACC1
long exposure
ACC1
short exposure
pACC1
4EBP1
HSC70
C
HEK293
ACACA expression normalized to total mRNA expression
ns
ns
shSCR
sh4EBP1/2
Glc:
D
HEK293
TE of ACACA
ns
***
shSCR
sh4EBP1/2
Glc:
E
MEF
WT
DKO
Relative FLuc/RLuc
ns
*
Glc:
F
HEK293
Relative FLuc/RLuc
*
*
shSCR
sh4EBP1/2
Glc:
G
UTR-ACC1-HA
ACC1-HA
Glc starvation (hrs): 0 6 11 0 6 11
shSCR:
sh4EBP1/2:
HA
4EBP1
HSC70
H
MEF DKO
% of cell death
**
**
siRNA: scr acaca1#1 acaca1#2
Acc1
Vinculin
I
HEK293 sh4EBP1/2
% of cell death
*
*
siRNA: SCR ACACA1#1 ACACA1#2
ACC1
VINCULIN

Figure 5

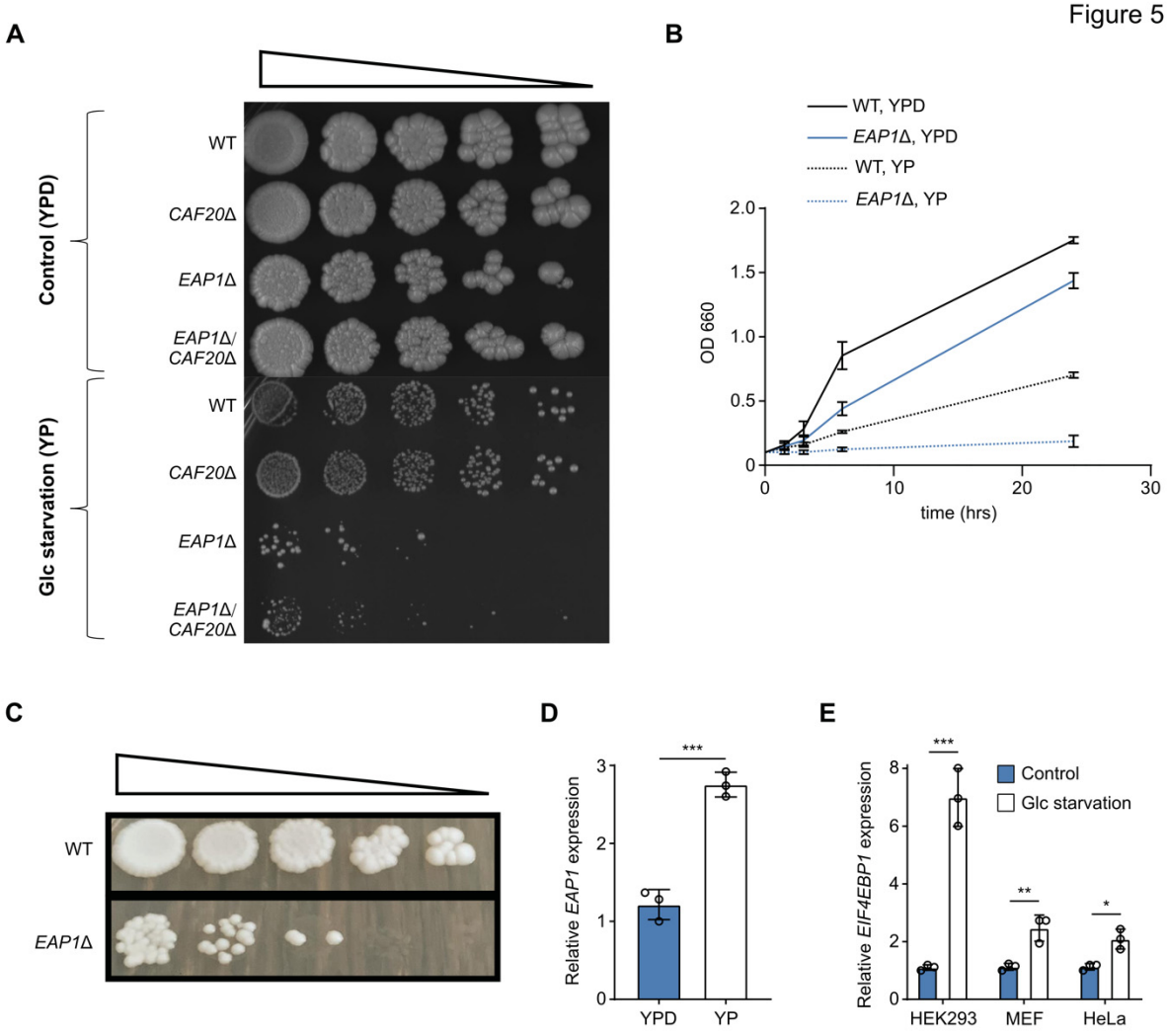
A
Control (YPD)
Glc starvation (YP)
WT
CAF20Δ
EAP1Δ
EAP1Δ/ CAF20Δ
WT
CAF20Δ
EAP1Δ
EAP1Δ/ CAF20Δ
B
WT, YPD
EAP1Δ, YPD
WT, YP
EAP1Δ, YP
OD 660
time (hrs)
C
WT
EAP1Δ
D
Relative EAP1 expression
YPD
YP
E
Relative EIF4EBP1 expression
Control
Glc starvation
HEK293
MEF
HeLa

Figure 6

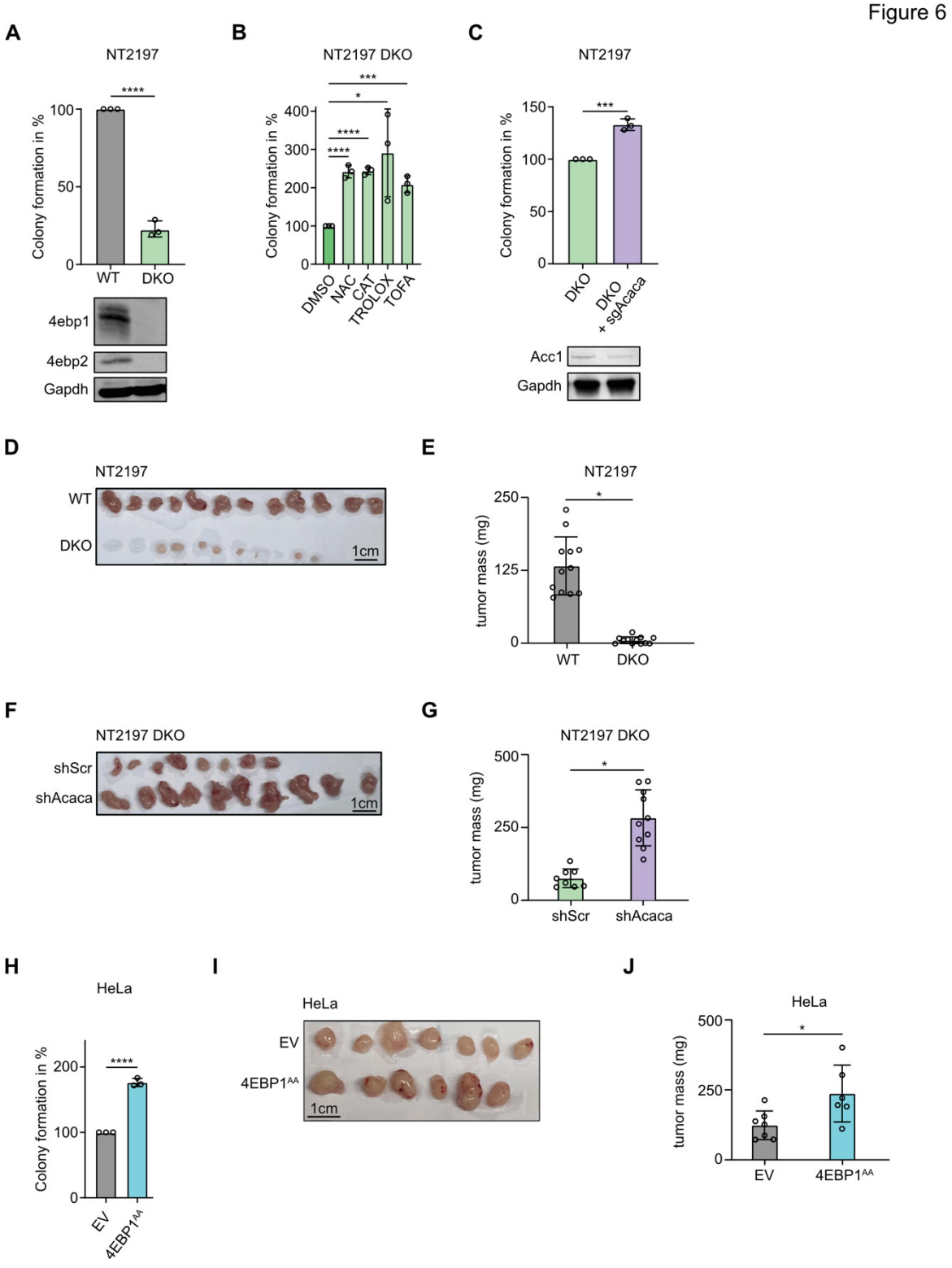
A
NT2197
Colony formation in %
WT
DKO
4ebp1
4ebp2
Gapdh
B
NT2197 DKO
Colony formation in %
DMSO
NAC
CAT
TROLOX
TOFA
C
NT2197
Colony formation in %
DKO
DKO + sgAcaca
Acc1
Gapdh
D
NT2197
WT
DKO
1cm
E
NT2197
tumor mass (mg)
WT
DKO
F
NT2197 DKO
shScr
shAcaca
1cm
G
NT2197 DKO
tumor mass (mg)
shScr
shAcaca
H
HeLa
Colony formation in %
EV
4EBP1AA
I
HeLa
EV
4EBP1AA
1cm
J
HeLa
tumor mass (mg)
EV
4EBP1AA

Figure 7

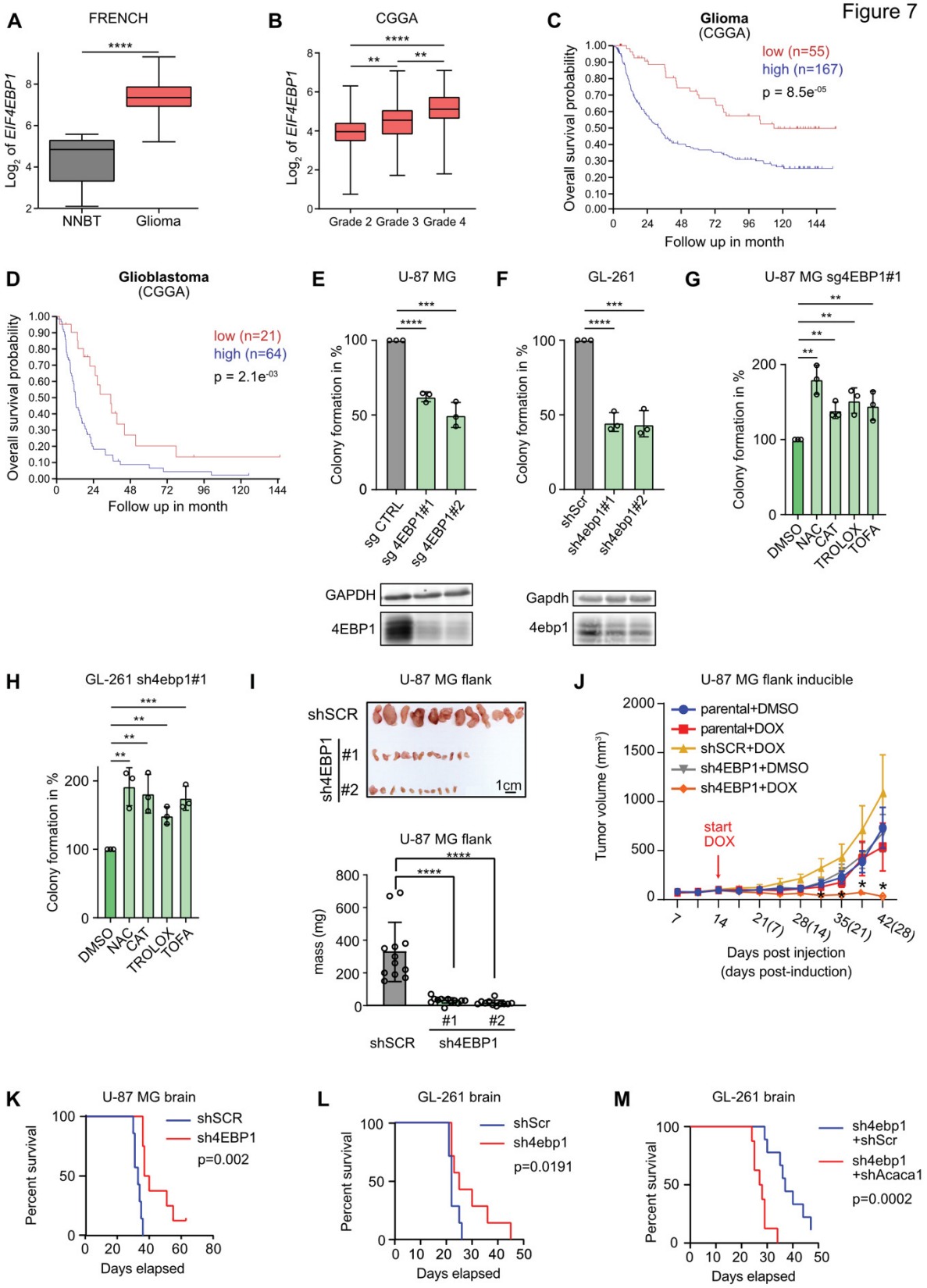
A
FRENCH
Log2 of EIF4EBP1
NNBT
Glioma
B
CGGA
Log2 of EIF4EBP1
Grade 2 Grade 3 Grade 4
C
Glioma
(CGGA)
low (n=55)
high (n=167)
p = 8.5e-05
Overall survival probability
Follow up in month
D
Glioblastoma
(CGGA)
low (n=21)
high (n=64)
p = 2.1e-03
Overall survival probability
Follow up in month
E
U-87 MG
Colony formation in %
sg CTRL
sg 4EBP1#1
sg 4EBP1#2
GAPDH
4EBP1
F
GL-261
Colony formation in %
shScr
sh4ebp1#1
sh4ebp1#2
Gapdh
4ebp1
G
U-87 MG sg4EBP1#1
Colony formation in %
DMSO
NAC
CAT
TROLOX
TOFA
H
GL-261 sh4ebp1#1
Colony formation in %
DMSO
NAC
CAT
TROLOX
TOFA
I
U-87 MG flank
shSCR
sh4EBP1
#1
#2
1cm
U-87 MG flank
mass (mg)
#1
#2
shSCR
sh4EBP1
J
U-87 MG flank inducible
parental+DMSO
parental+DOX
shSCR+DOX
sh4EBP1+DMSO
sh4EBP1+DOX
start
DOX
Tumor volume (mm3)
Days post injection
(days post-induction)
K
U-87 MG brain
shSCR
sh4EBP1
p=0.002
Percent survival
Days elapsed
L
GL-261 brain
shScr
sh4ebp1
p=0.0191
Percent survival
Days elapsed
M
GL-261 brain
sh4ebp1
+shScr
sh4ebp1
+shAcaca1
p=0.0002
Percent survival
Days elapsed

Suppl Figure 1

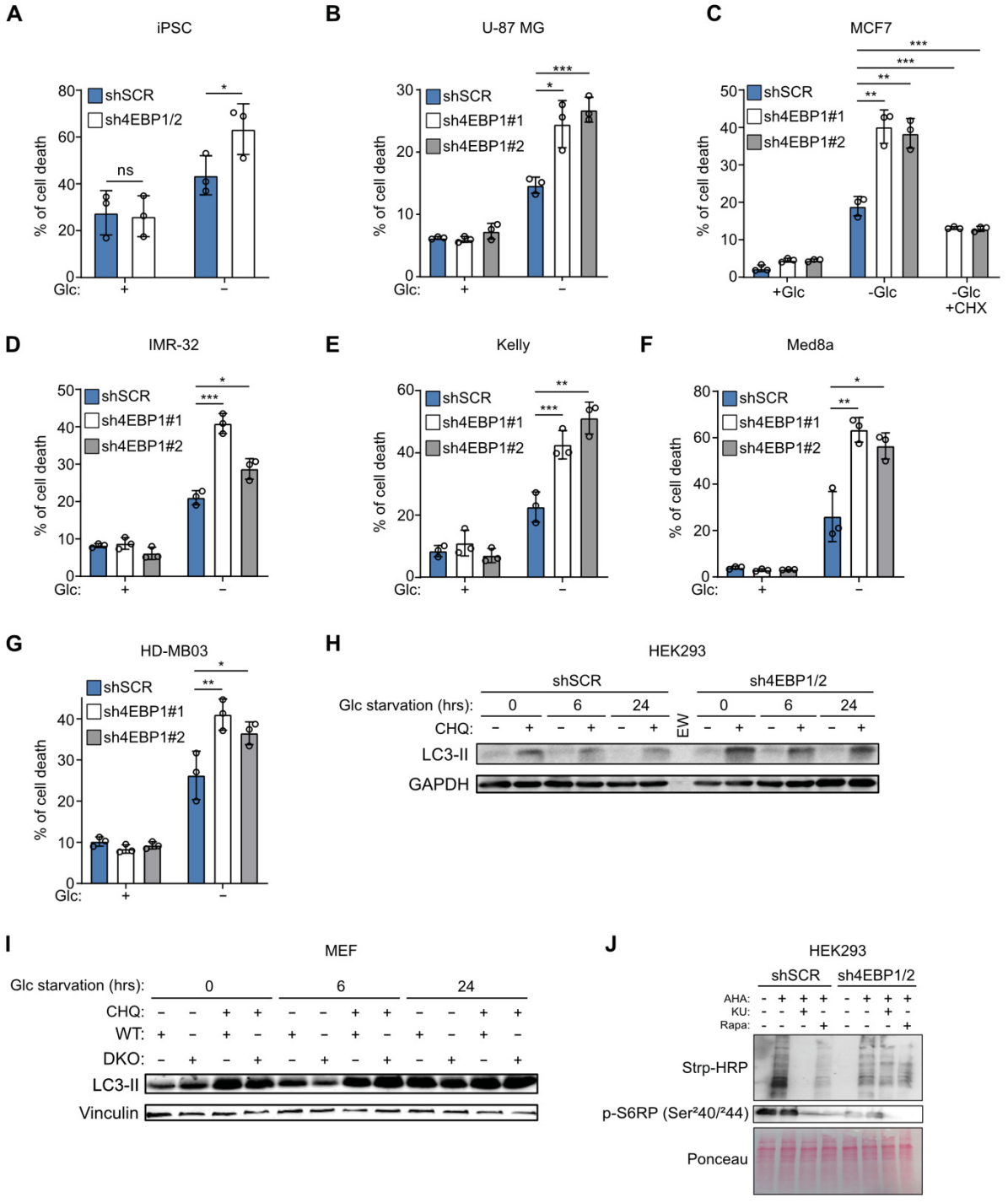

Suppl Figure 2

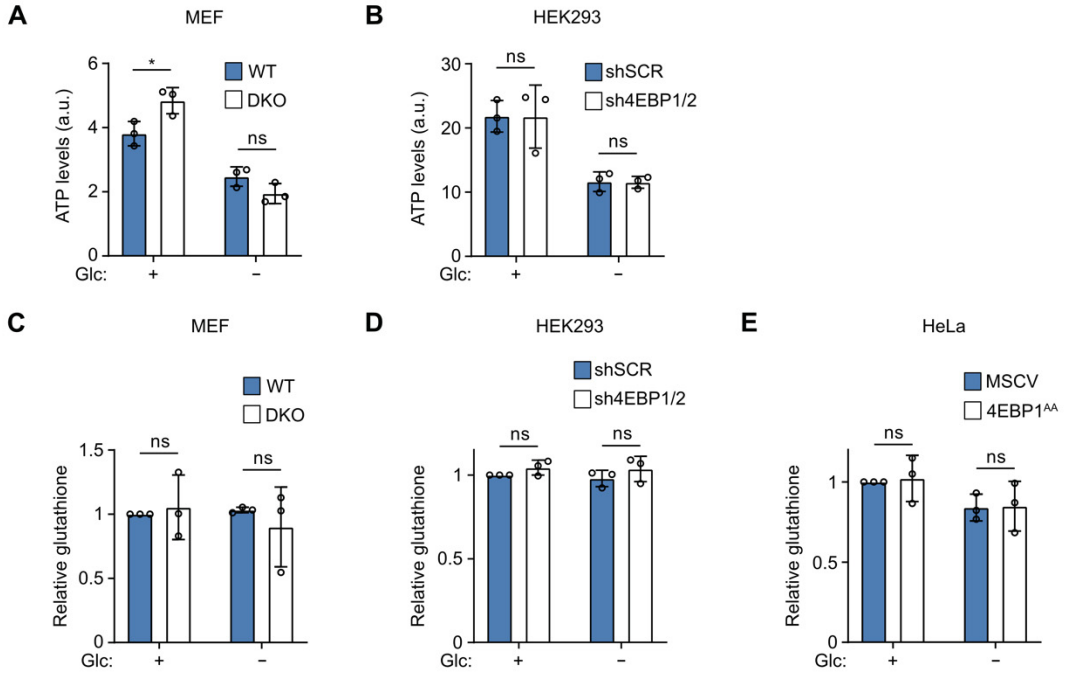

Suppl Figure 3

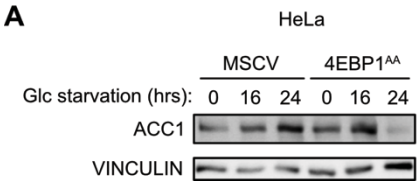

Suppl Figure 4

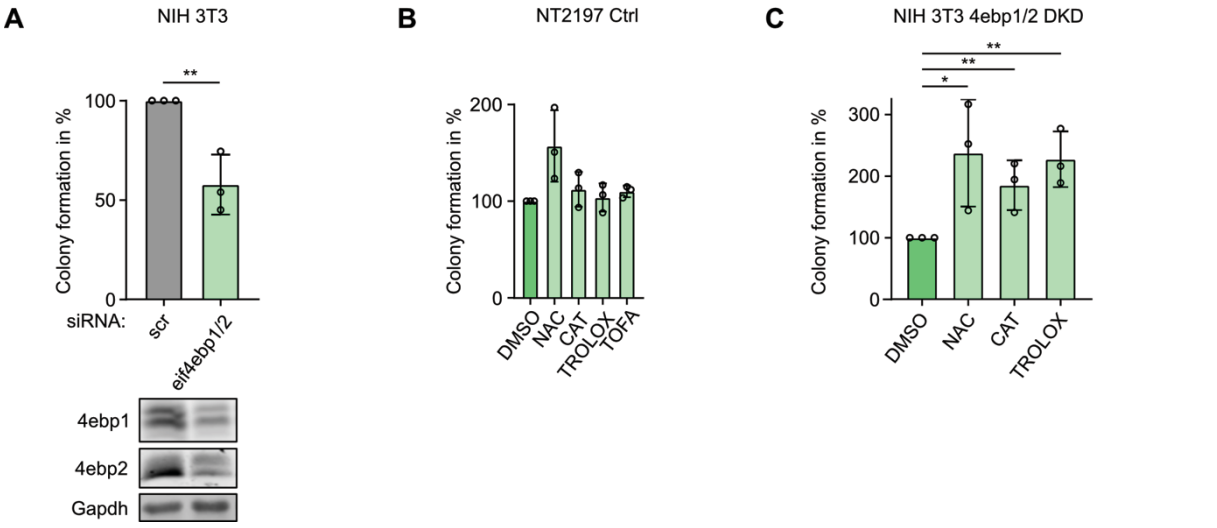

Suppl Figure 5

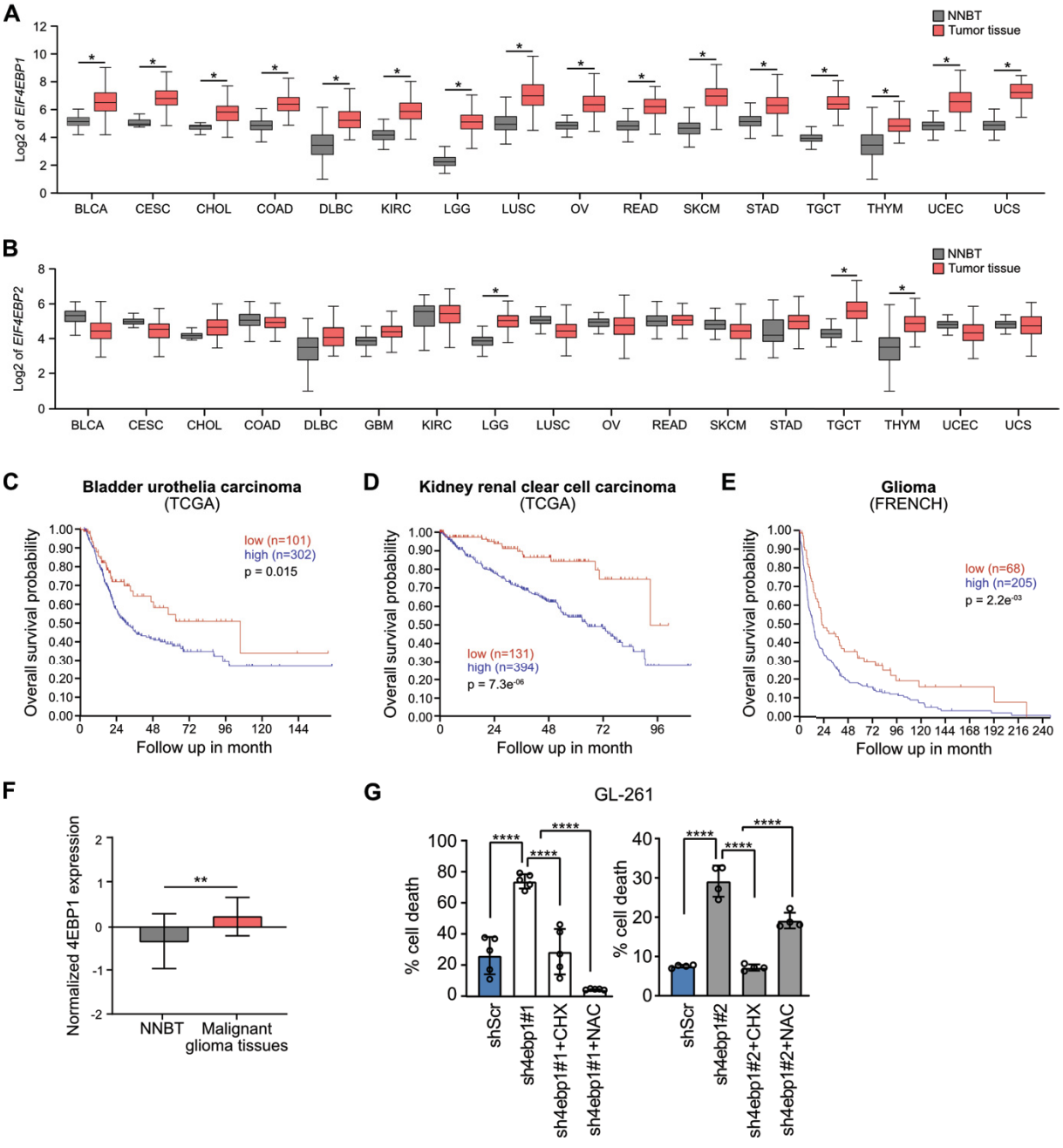

Suppl Figure 6

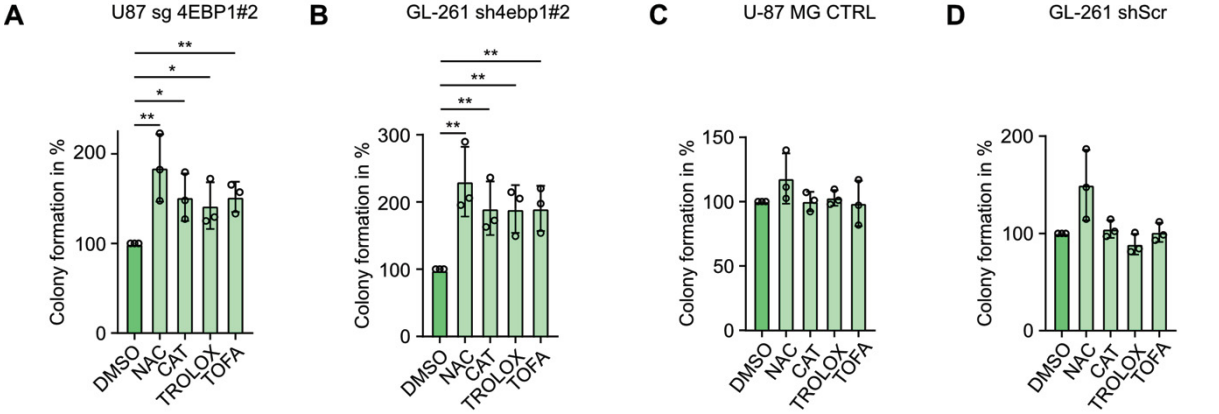

3.2.2. Impact of p53 on the tumorigenic potential of 4EBP1

Manuscript II reported that 4EBP1 supported tumorigenesis of GL-261 glioma and U-87 MG glioblastoma cell lines. As such a pro-tumorigenic function of 4EBP1 might be more general, additional glioblastoma cell lines were investigated. To this aim, cellular models of stable 4EBP1 targeted depletion were engineered in three different glioblastoma cells lines, namely U-118 MG and U-251 MG for which a CRISPRi approach was used, and LN-229 in which 4EBP1 was knocked down with an inducible shRNA system. When these cells were subjected to soft agar assays, no decrease of colony formation was observed in 4EBP1 KD U-118 MG, U-251 MG (experiment for the U-251 MG cell line was performed by the former master student Alisa Kahler who I supervised) and LN-229, as compared to respective Ctrl/Scrl cells, in contrast to what was expected (Figure 11A-C). To expand the original findings in another tumor type in which *EIF4EBP1* is overexpressed, namely non-small cell lung carcinoma (NSCLC) (WU & WAGNER 2021), the contribution of 4EBP1 to the tumorigenic potential of a NSCLC cell line (referred to as ACF 1055.1) isolated from a tumor of a $Kras^{LSLG12D/+:}$ $p53^{fl/fl}$ (KP) mouse model of NSCLC (EICHNER *et al.* 2019) was assessed. In this cell line, which is p53 KO, 4EBP1 was stably knocked down using mouse shRNAs. Genetic targeting of 4EBP1 had no impact on the tumorigenic capabilities of ACF 1055.1, as measured by soft agar colony formation (Figure 11D), pointing to another cancer cell line for which 4EBP1 was dispensable. In order to understand the factors that determine the responsiveness of cancer cells to 4EBP1 pro-tumorigenic function, the possibility that p53 functionality is one such a factor was explored. This is based on a report linking p53 status to the pro-tumorigenic function of 4EBP1 (PETROULAKIS *et al.* 2009), such that expression of functional p53 is absolutely required for 4EBP1 to exert a pro-tumorigenic effect (Figure 11E). This predicted that such a 4EBP1 function may be abrogated in cancer cell lines harboring mutant dysfunctional p53. Thus, the p53 status was determined in all the cancer cell lines used for the soft agar assays. This revealed that all the cell lines in which 4EBP1 supported oncogenic transformation or tumorigenesis, namely NT-2197, GL-261 and U-87 MG, were p53 WT (Table 2). Originally, GL-261 were reported to be p53 WT (BLASZCZYK-THURIN *et al.* 2002), while another study later detected a point mutation within the DNA binding domain of p53 (SZATMARI *et al.* 2006). The latter may have been acquired during cell passaging, as suggested by Szatmari *et al.* (2006) (SZATMARI *et al.* 2006). On the contrary, the cell lines in which 4EBP1 was ineffective in term of tumorigenic potential all harbor genetic alterations in the *TP53* gene encoding p53. Indeed,

the ACF 1055.1 cell line is p53 KO, while LN-229, U-118 MG and U-251 MG carry mutations in *TP53* (Table 2). Because *TP53* mutations have a wide range of effect on p53 function, from inactivation to gain of function, it is crucial to examine the functionality of the different mutants. Thus, the activity of p53 was determined in the different cancer cell lines and particularly in the glioblastoma cell lines. This was achieved by using three different but complementary approaches to measure p53 activity. For all these experiments, cells were treated with hydrogen peroxide (H_2O_2) to induce genotoxic stress and activate p53.

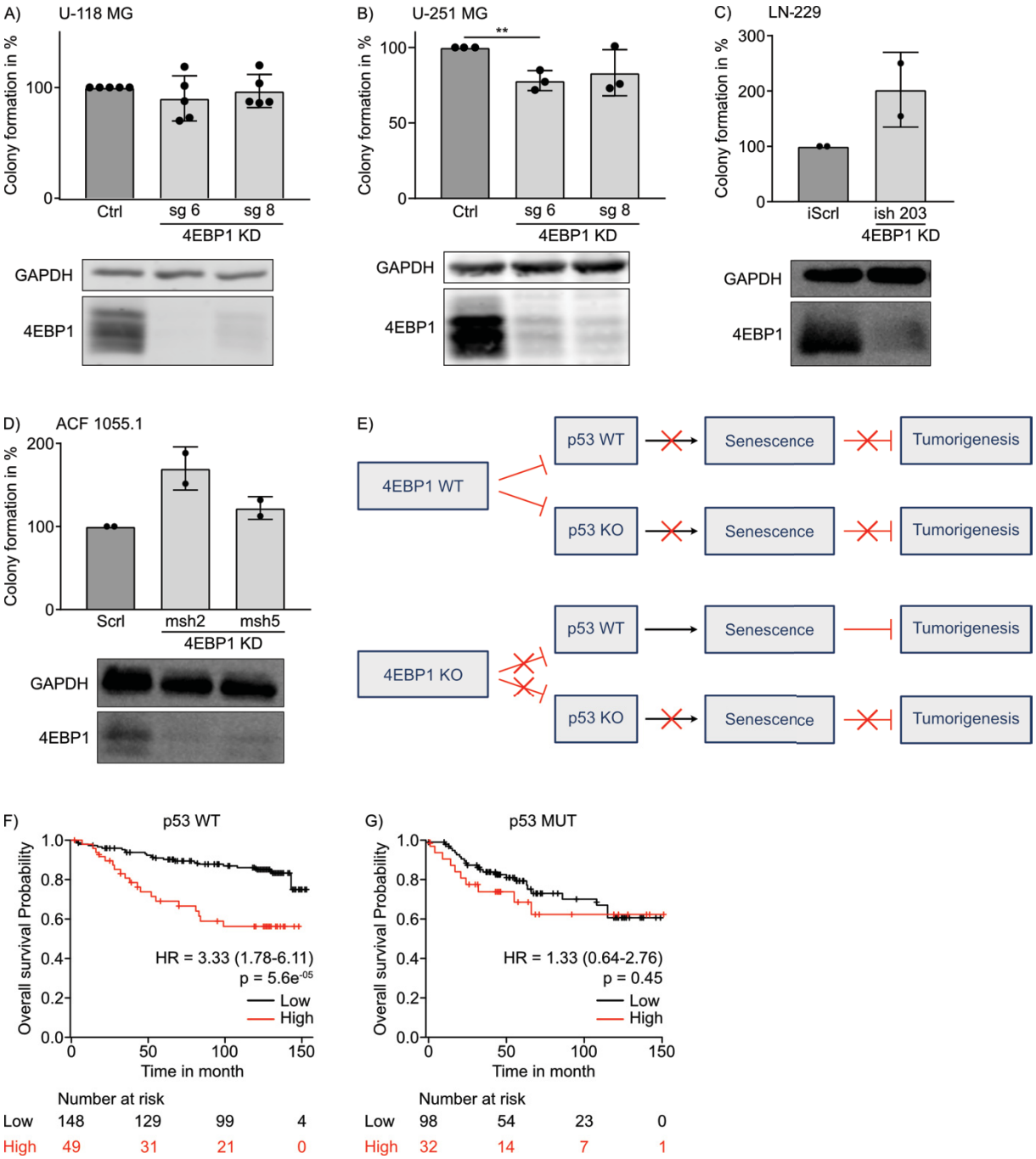

Figure 11: 4EBP1 function in cancer and *EIF4EBP1* prognostic value is dependent on the p53 mutation status. A)-D) Control/Scrl/iScrl or *EIF4EBP1* targeting CRISPRi (sg6, sg8), inducible or mouse shRNA (ish or msh) containing (A) U-118 MG, (B) U-251 MG and (C) LN-229 cells were grown in soft agar for three weeks and stained/fixed with 0.01% crystal violet. The colony forming efficiency was calculated by dividing the total number of cells by the number of formed colonies, which was counted for ten fields of each well. Ability to form colonies was normalized to Ctrl cells (100%) ± SD. Data represent the mean of two, three or five independent replicates ± SD, as indicated in the bar graphs. Significance was calculated using a two-tailed parametric t-test **p<0.01. Representative immunoblots indicate 4EBP1 KD in (A) U-118 MG, (B) U-251 MG, (C) LN-229 and (D) ACF 1055.1 cell lines. E) Scheme illustrating the connection between 4EBP1 function and p53 status and the resulting outcome in term of tumorigenic potential (based on reports of Petroulakis *et al.* (2009)). 4EBP1 prevents stabilization of WT p53, resulting in inhibition of senescence and thus promotion of transformation by oncogenic RAS. In cells with p53 KO, transformation will take place as senescence cannot be induced. 4EBP1 KO cells cannot be transformed by oncogenic RAS cells, as WT p53 is stabilized and senescence induced. 4EBP1 KO in combination with p53 KO prevents senescence induction, allowing transformation (PETROULAKIS et al. 2009). F) and G) Kaplan-Meier overall survival probability of breast cancer patients, exhibiting (E) p53 WT or (F) p53 mutation, was analyzed according to high and low *EIF4EBP1* mRNA levels (cutoff: upper quartile) using KM-plotter.

First, stabilization of p53 protein was investigated by measuring total and phosphorylated p53 using immunoblot analysis. Increased levels of phosphorylated p53 indicate activation and are linked to stabilization of the protein. Then, the mRNA expression levels of *TP53* and multiple p53 target genes, *P21*, *FAS*, *PUMA*, *MDM2*, *BAX* for human cell lines and *p21*, *Fas*, *Noxa* and *Puma* for mouse cell lines, were determined by RT-qPCR. Lastly, a firefly luciferase reporter driven by a minimal promoter and multiple p53 binding motifs was used to directly measure p53 activity as reported (VAN MEIR *et al.* 1994). Most of these experiments were performed by the master student Alisa Kahler who was supervised by me. The data are summarized and displayed in Table 3. Taking these data together, it can be concluded that while NT-2197, LN-229 and U-87 MG may contain functional and active p53, U-118 MG and U-251 MG do not exhibit active p53 (Table 3). This supports the hypothesis that the pro-tumorigenic function of 4EBP1 is impacted by p53 activity. However, some of the data for p53 activity are either incomplete or inconclusive and thus more experiments are required.

Table 2: Overview of the reported p53 status and activity in various cell lines.

Cell line	P53 status	P53 genotype	Location of mutation	P53 activity
ACF 1055.1	P53 KO[1)]	Homozygous[1)]	/	/
GL-261	WT[2)] R153P[3)]	Homozygous NA	DBD[5)]	Active p53
LN-229	K164Q[4)]	Heterozygous[4)]	DBD[5)]	Functional p53 activity[4)]
NT-2197	WT	Homozygous	/	Active p53
U-118 MG	R213Q[6)]	Homozygous[6)]	DBD[5)]	NA
U-251 MG	R273H[4)]	NA	DBD[5)]	No active p53[4)]
U-87 MG	WT[4)]	Homozygous[4)]	/	Active p53[4)]

[1)](EICHNER *et al.* 2019) [2)](BLASZCZYK-THURIN *et al.* 2002) [3)](SZATMARI *et al.* 2006) [4)](VAN MEIR *et al.* 1994) [5)](SAHA *et al.* 2015) [6)](RUSSELL *et al.* 1995); DBD: DNA binding domain; NA: not available

Table 3: Overview of the experiments performed to determine p53 activity in glioblastoma cell lines.*

Cell line	P53 stabilization	Induction of p53 target genes	Activity of p53 promoter
GL-261	Stabilized	No	ND
LN-229	Stabilized	Partially	ND
NT-2197	Stabilized	Partially	ND
U-118 MG	Stabilized	No	Decreased
U-251 MG	Stabilized	No	Decreased
U-87 MG	Inconclusive	Yes	No change

*Most experiments were performed by the master student Alisa Kahler under my supervision.

ND: not determined

3.2.3. *TP53* mutation status modulates the prognostic role of *EIF4EBP1* levels on overall survival

Publically available cancer patient datasets were interrogated to search for a potential prognostic relevance of the reliance of 4EBP1 function on p53. The association between *EIF4EBP1* levels and overall survival in a patient cohort with available p53 status data, which was found for breast cancer patients, was analyzed using Kaplan Meier (KM) survival estimates and the prognostic association of *EIF4EBP1* expression levels was determined in patients with p53-WT versus p53-mutant tumors. In patients with p53-WT breast cancers, high *EIF4EBP1* levels significantly correlated with poor prognosis (Figure 11F). On the contrary, in patients with p53-mutant tumors, high *EIF4EBP1* levels were not associated with worse outcome (Figure 11G). These data indicate that the prognostic value of *EIF4EBP1* expression is dependent on the p53 (mutation) status, at least in breast cancer patients. This finding illustrates the interconnection between 4EBP1 and p53 activity in a clinical setting.

3.3. Targeting 4EBP1 - a novel approach

The data from the previous chapters point to a pro-tumorigenic function of 4EBP1 as: i) it protects cancer cells under glucose starvation, ii) promotes oncogenic transformation and glioma tumorigenicity, and iii) its gene expression shows prognostic relevance in glioblastoma patients. Since glioblastoma patients have a median overall survival in the range of only 15 months when treated according standard of care, it is crucial to develop alternative novel treatment options for this lethal disease. The own findings suggest that targeted inhibition of 4EBP1 might represent a potential treatment strategy for glioblastoma. The underlying concept is that blocking 4EBP1 would interfere with tumor adaptation to metabolic stress, while sparing normal surrounding tissues which are not experiencing such a stress and are therefore not dependent on 4EBP1 activity.

3.3.1. Strategy for targeting 4EBP1 activity

A potential targeting strategy to specifically inhibit 4EBP1 activity could be the prevention of the interaction of 4EBP1 with eIF4E. However, such a strategy should not disturb the interaction between eIF4G with eIF4E in order to preserve eIF4E activity and function. This is important as the assembly of the eIF4F complex and active mRNA translation are required to induce cell death upon 4EBP1 deletion under glucose starvation (Manuscript II Figure 1A-C,

Figure 1J and K). To block 4EBP1-eIF4E interaction without affecting eIF4G-eIF4E interaction, a strategy to target specifically the binding of the NC-loop of 4EBP1 to the lateral surface of eIF4E was designed. EIF4E contains a hydrophobic pocked on its lateral site providing an anchoring point for the NC-loop (PETER *et al.* 2015). Since eIF4G does not possess a NC-loop, targeting such a binding interface would not affect the eIF4G-eIF4E interaction, as eIF4G will still be able to bind eIF4E via its canonical α-helix. Although 4EBP1 also possesses a canonical α-helix, it was shown that the NC-loop is crucial for eIF4E binding, as it increases the binding affinity of 4EBP1 thereby providing binding advantages over eIF4G (IGREJA *et al.* 2014).

3.3.2. 4EBP1 protective effect under glucose starvation is mediated by the NC-loop

To determine which structural domain(s) mediate(s) the protective function of 4EBP1 under glucose starvation, the effect of different 4EBP1 mutants and deletants on the survival of HeLa cells under glucose starvation was determined. This particular cell line was chosen as it is highly sensitive to glucose starvation, a phenotype which can be rescued by overexpression of a constitutively active 4EBP1 full length (FL) mutant ($4EBP1^{AA}$) (Figure 12A) (Manuscript II Figure 1L). It could be shown that 4EBP1 binding to eIF4E through the canonical α-helix is required to mediate 4EBP1 protective function in HeLa cells (Figure 12A) (Manuscript II Figure 1L). Indeed, mutation of tyrosine (Y) 54 and leucine (L) 59 ($4EBP1^{AA,\ YL}$) within the canonical α-helix, known to abrogate 4EBP1-eIF4E interaction (MIRON *et al.* 2001, SCHALM *et al.* 2003), disrupted the protective properties of constitutively active 4EBP1-FL in HeLa cells that were glucose-deprived for 72 h (Figure 12A) (Manuscript II Figure 1L).

Next, it was investigated whether the NC-loop and the elbow loop also mediate the protective function of 4EBP1 under glucose starvation. To this aim, deletion mutants of $4EBP1^{AA}$-FL were generated. One generated construct contained all the binding motifs (canonical α-helix, elbow loop and NC-loop) but lacked the C-terminal part of the protein ($4EBP1^{AA}$-Ca+EL+NC) (Figure 12B). Two other constructs were generated with deletions of either the NC-loop ($4EBP1^{AA}$-Ca+EL) or of the NC-loop and the elbow loop ($4EBP1^{AA}$-Ca) to determine the contribution of each domain to the protective function (Figure 12B). Overexpression of $4EBP1^{AA}$-Ca or $4EBP1^{AA}$-Ca+EL did not protect HeLa cells under glucose starvation, as compared to full length $4EBP1^{AA}$ (Figure 12A). The protective effect was only observed when $4EBP1^{AA}$-Ca+EL+NC, containing all binding motifs, was overexpressed in HeLa cells

(Figure 12A). Therefore, one can conclude that the protective function of 4EBP1 under glucose deprived conditions requires 4EBP1 binding to eIF4E through the NC-loop, which will then lead to inhibition of mRNA translation initiation. Based on these data, the interaction surface between 4EBP1 NC-loop and eIF4E represents an appropriate surface to target in order to inhibit 4EBP1 activity and function.

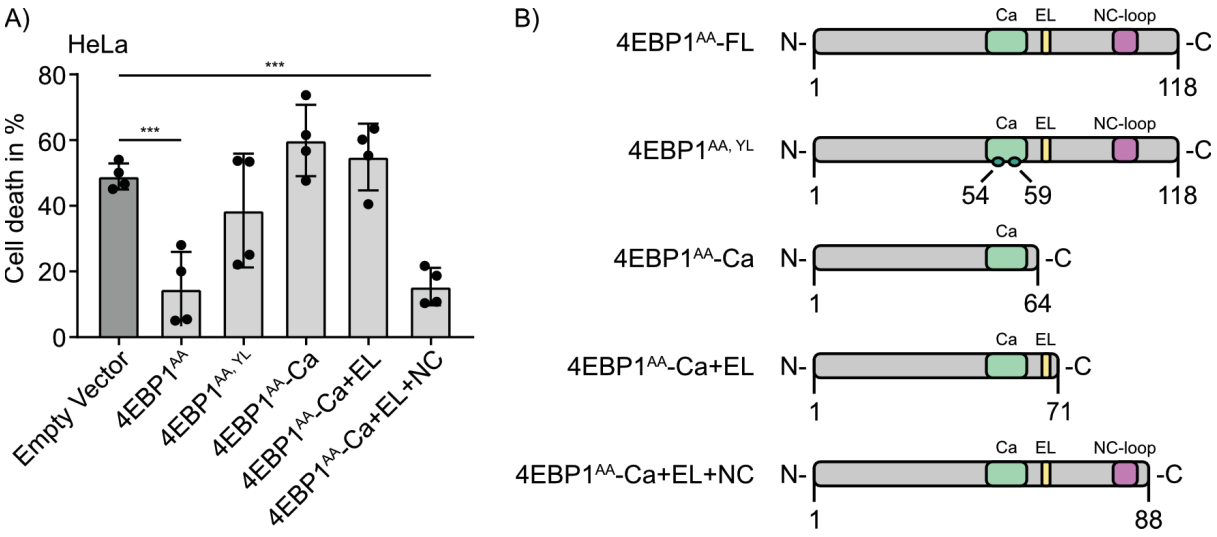

Figure 12: Protective function of 4EBP1 under glucose starvation requires all eIF4E binding motifs. A) Control (empty vector) or stable 4EBP1^{AA}-overexpressing HeLa cells were grown in 1 mM glucose containing medium for 72 h and cell death was measured using propidium iodide staining and analyzed by flow cytometry. Data are represented as mean ± SD of two independent biological replicates. Black data points in the bar graph represent technical replicates. Significance was calculated using a two-tailed parametric t-test (***p<0.001). B) Illustration of the 4EBP1^{AA}-overexpressing constructs with the green binding site representing the canonical α-helix, the yellow site representing the elbow loop and the pink site representing the NC-loop. Mutations in the canonical α-helix are indicated by dark green circles.

3.3.3. Identification of hot spot residues within the 4EBP1 NC loop-eIF4E binding interface and *in silico* screening for potential binding inhibitors

To discover compounds potentially inhibiting the interaction between the NC-loop of 4EBP1 and eIF4E, an *in silico* screen was performed using the crystal structure of 4EBP1 (amino acids 50 to 83) bound to eIF4E (amino acids 36-217) (PDB 4UED) (PETER *et al.* 2015). First, the residues of the NC-loop involved in binding to eIF4E were identified. In collaboration with Prof. Gohlke's laboratory (Institute for Pharmaceutical and Medicinal Chemistry, Heinrich Heine University Düsseldorf), a molecular mechanics generalized Born and surface area (MM-GB/SA) binding free energy calculation was performed, using the crystal structure of the 4EBP1-eIF4E

complex. This calculation revealed isoleucine (I) 78 and valine (V) 81 as two hotspot residues within the 4EBP1 NC-loop involved in the interaction with eIF4E (Figure 13A), confirming reports from the literature (PETER *et al.* 2015). Next, using the same crystal structure, an *in silico* screen was performed by Prof. Gohlke's laboratory to find compounds that might disrupt the interaction of the I78 and V81 residues with eIF4E (NGUYEN *et al.* 2016). A library of few millions of virtual compounds from the MolPort database was used to dock compounds into the binding interface of the 4EBP1 NC-loop with eIF4E, and the impact on the interaction was calculated for each compound (Figure 13B). Based on these results, a list of potential 4EBP1 inhibitory compounds was generated and the top 100 compounds of the list were selected for further experiments.

3.3.4. Tryptophan fluorescent quenching assay

In order to test the ability of the identified compounds to inhibit 4EBP1-eIF4E interaction, an *in vitro* binding assay was performed using a tryptophan fluorescent quenching assay. This assay monitors protein-protein binding affinities by measuring the impact of protein-protein interaction on the intrinsic fluorescence of tryptophan residues. Quenching of intrinsic tryptophan fluorescent signal results either directly from binding of one protein to another or from conformational changes, which might occur upon protein binding. The level of fluorescence quenching indicates the affinity of protein-protein interaction. EIF4E contains eight tryptophan residues within its sequence (SONENBERG 1988, PETER *et al.* 2015). Specifically, tryptophan (W) 73, located within the first α-helix of eIF4E, interacts with L59 in the canonical loop of 4EBP1 and eIF4G (MARCOTRIGIANO *et al.* 1999, PETER *et al.* 2015) (Figure 13C). This binding interaction was demonstrated to quench the intrinsic fluorescence of W73 (NIEDZWIECKA *et al.* 2002). Therefore, it was anticipated that this assay should allow to measure the effect of the 4EBP1 inhibitor candidates on the binding interaction between eIF4E and 4EBP1/eIF4G. Theoretically, in absence of compounds eIF4E and 4EBP1 or eIF4G will interact, leading to a quenched tryptophan fluorescent signal. Thus, addition of a 4EBP1 inhibitory molecule would disrupt the interaction between eIF4E and 4EBP1, while preserving the interaction with eIF4G, as eIF4G does not contain a NC-loop that is targeted by the potential 4EBP1 inhibitor.

3.3.4.1. 4EBP1 or eIF4G interaction with eIF4E results in a quenched tryptophan fluorescent signal

Before screening the identified candidate compounds, the conditions for the tryptophan fluorescent quenching assay using recombinant eIF4E, 4EBP1 and eIF4G peptides were calibrated. Initially, suitable concentrations of the recombinant peptides allowing to detect fluorescence quenching and therefore binding were determined. The following peptides were used for this assay: eIF4E residues 36-217, 4EBP1 residues 50-83, and eIF4G residues 621-637. In addition, a 4EBP1 mutant (mut) peptide, containing mutations of the two hotspot residues I78A and V81A within the NC-loop, was used as a control. Based on the experimental set up reported by Niedzwiecka et al. (2002), 0.2 µM eIF4E peptide was used as an initial starting concentration. Then, either 4EBP1, 4EBP1 mut or eIF4G peptides were titrated to eIF4E and the fluorescent signal of tryptophan was measured.

As expected, all three peptides (eIF4G, 4EBP1 and 4EBP1 mut) led to a quenched fluorescence signal in a concentration dependent manner, indicating their binding to eIF4E. For each of the eIF4G, 4EBP1 and 4EBP1 mut peptides, the signal quenching was saturating at a concentration of 1 nM peptide, reaching a quench of approximately 60% for eIF4G, 40% for 4EBP1 and 30% for 4EBP1 mut (Figure 13D). This was unexpected as this concentration did not result in any fluorescence signal quenching in the published experiments (NIEDZWIECKA *et al.* 2002). This may be due to differences of sensitivity of the spectrometers used for measurements. Despite the mutations within the NC-loop, binding of 4EBP1 mut to eIF4E was observed in the own experiments, indicating that the 4EBP1 mut peptide interacts with eIF4E only via its canonical α-helix, which is expected *in vitro* (IGREJA *et al.* 2014). The quenching effect of the 4EBP1 mut peptide was not as strong as with the 4EBP1 WT peptide, indicating that the additional binding of the NC-loop to eIF4E increases binding affinity between the two proteins (Figure 13D). On the contrary, eIF4G-eIF4E interaction resulted in the strongest quenched signal, although eIF4G does not contain a NC-loop (Figure 13D). The NC-loop becomes important when 4EBP1 has to compete with eIF4G for binding eIF4E *in cellulo* as it serves 4EBP1 with an anchoring point to bind eIF4E (IGREJA *et al.* 2014). Here, *in vitro* assays were performed in which no binding competition was present. Based on this data, it can be concluded that eIF4E interacts with all three eIF4G, 4EBP1 and 4EBP1 mut peptides and that 1 nM peptide is sufficient to

reach a strong quenching, validating the use of tryptophan fluorescent quenching as an assay to monitor protein-protein interaction between these peptides.

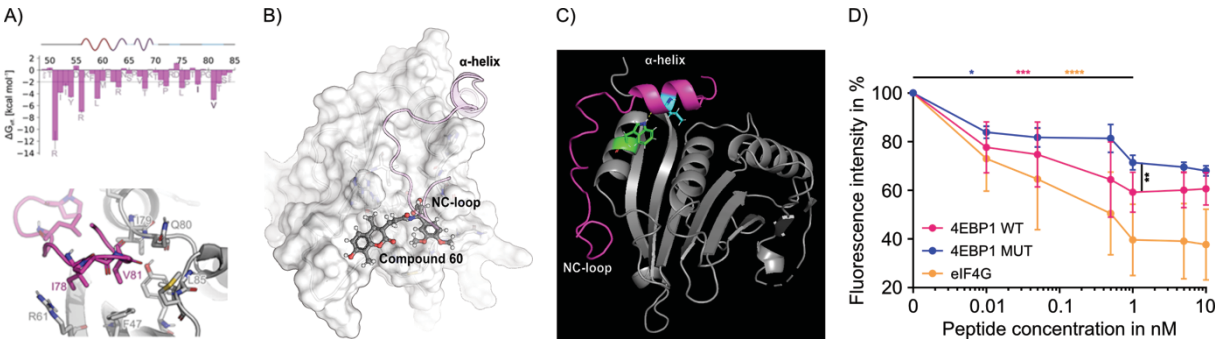

Figure 13: Protein-protein interaction of eIF4E and 4EBP1. A) The crystal structure of the eIF4E-4EBP1 complex (PDB 4UED) was used for molecular mechanics generalized Born and surface area (MM-GB/SA), which was performed by the working group of Prof. H. Gohlke (Heinrich Heine University Düsseldorf). B) Representative picture of compound 60 docking to the eIF4E-4EBP1 binding interface (using PDB 4UED). C) Representation of the interaction of W73 (green) with L59 (light blue) within the eIF4E-4EBP1 binding complex (PDB 4UED). EIF4E is represented in grey and 4EBP1 in pink. Illustration was generated with The PyMOL Molecular Graphics System, Version 2.0 Schrodinger, LLC. C) Fluorescence quenching of W73 located on eIF4E was measured after titrating 4EBP1 WT, 4EBP1 MUT or eIF4G peptides to eIF4E. Fluorescent signal was measured after 30 sec incubation of protein and peptide. Data represented as mean ± SD of three independent replicates. Color code of asterisk indicates which group it is referring to. Black asterisk compares significance between 4EBP1 WT and 4EBP1 MUT at 1 nM. Significance was calculated using a two-way ANOVA (*p<0.05, **p<0.01, ***p<0.001, ****p<0.0001).

3.3.4.2. Tryptophan fluorescent quenching identified binding of compounds to eIF4E

As a next step, the top seventeen compounds from the list generated by *in silico* screening (see section 3.3.3) were selected and their impact on the 4EBP1-eIF4E (and eIF4G-eIF4E) interactions was measured. The goal was to find compounds that would bind to the hydrophobic pocket of eIF4E and disrupt the already existing eIF4E-4EBP1 complex. Using tryptophan fluorescent quenching, the seventeen compounds were individually screened by titrating various drug concentrations to the existing eIF4E-4EBP1 complex formed using the above mentioned 4EBP1 and eIF4E peptides. In addition, the autofluorescence of each compound was measured in absence of the protein and the peptides, only with the buffer, and was subtracted from the fluorescent measurements as one normalization step. The experimental set up is indicated in Figure 14A. None of the screened compounds was able to disrupt the eIF4E-4EBP1 interaction, as titrating different concentrations of each of the

different compounds did not prevent fluorescence quenching (data not shown). As an example, the results for the compound candidates 28 and 60 are displayed in Figure 14B. It turned out that the fluorescence signal increased (i.e. reduction of quenching) in one replicate upon addition of each of the compounds on preexisting eIF4E-4EBP1 complex, indicating a disruption of eIF4E-4EBP1 binding. This effect could not be reproduced in the other two replicates. Therefore, these data indicate that compounds 28 and 60 cannot disrupt the interaction between eIF4E and 4EBP1, similarly to the other fifteen compound candidates. Still, those seventeen compounds should not be excluded from the list as 4EBP1 has a very high binding affinity to eIF4E *in vitro* (MIZUNO *et al.* 2008, PAKU *et al.* 2012), and therefore it may be difficult to disrupt the binding of the preexisting protein-protein complex *in vitro*.

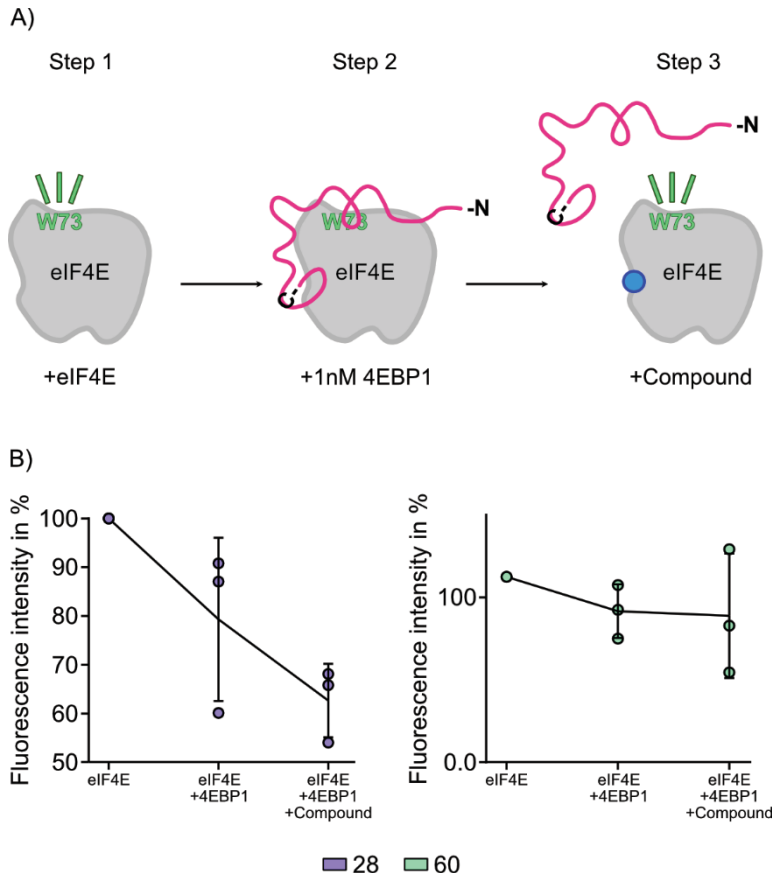

Figure 14: Assessment of compounds ability to disrupt the assembly of the eIF4E-4EBP1 complex *in vitro*. A) Schematic representation of the workflow to achieve disruption of the eIF4E-4EBP1 complex. First, the fluorescence of eIF4E was measured, then 1 nM 4EBP1 peptide was added and incubated for 30 sec to allow formation of the protein-peptide complex - a quenched fluorescent signal was expected. Lastly, the compound was added and incubated for 10 min with the eIF4E-4EBP1 complex. Disruption of the complex and enhanced fluorescent signal is expected. B) The workflow described under (A) was used. 10 µM of compound 28 and 20 µM of compound 60 were added to the complex. Autofluorescence of the buffer or buffer + compound was subtracted and data was normalized to basal fluorescence of eIF4E. Data represented as mean ± SD of three independent replicates.

To overcome this potential issue, another approach was employed where the effect of compounds to block binding of 4EBP1 to eIF4E, before any protein-protein complex was formed, was investigated. This was used to test six of the identified compounds from the *in silico* screen. In this experimental set up, each compound was mixed with eIF4E before adding 4EBP1 or eIF4G. In theory, the compound would bind to the hydrophobic pocket of eIF4E, in turn preventing the binding of 4EBP1 NC-loop to eIF4E. The tryptophan fluorescence of eIF4E alone was first measured, then 50 µM of each compound were added and lastly, 1 nM 4EBP1 or eIF4G peptide was mixed to the solution and incubated for 5 min. EIF4G was used as a control, since it lacks the NC-loop the compound should not interfere with its interaction to eIF4E (Figure 15A). Unexpectedly, addition of each of the compounds to eIF4E, except compound 28, resulted in a quenched fluorescent signal (Figure 15B). This result suggests that these compounds may not bind within the hydrophobic pocket of eIF4E but near W73, thereby influencing the fluorescent signal. Another possibility would be that the compounds quench the fluorescence of other tryptophan residues contained within the accessible surface area of eIF4E. Indeed, we found three tryptophan residues (W46, W56 and W102) to be solvent exposed (Figure 15C). A conformational change of eIF4E upon compound binding is unlikely, as the eIF4E structure is very rigid, especially within its α-helices and beta sheets. Rigidity, flexibility and internal motion within a protein is indicated by the B-Factor, which describes the attenuation of X-ray or neutron scattering caused by thermal motion (SUN *et al.* 2019). Both W46 and W56 lie within a very rigid and structured part (indicated by a thin blue or green structure), whereas W102 lies within a slightly more flexible area (indicated by a yellow-colored structure) (Figure 15D). Compound 28 did not quench but increased the fluorescent signal. Binding of the compound to eIF4E might lead to a fluorescent shift affecting either the excitation or emission of the fluorescent signal. Taken together these data suggest that the tested compounds bind to eIF4E, possibly not in the hydrophobic pocket. This supports that other experimental procedures are needed to determine if any of the compounds can prevent binding of 4EBP1 to eIF4E, as there are too many factors influencing tryptophan fluorescence in this set up.

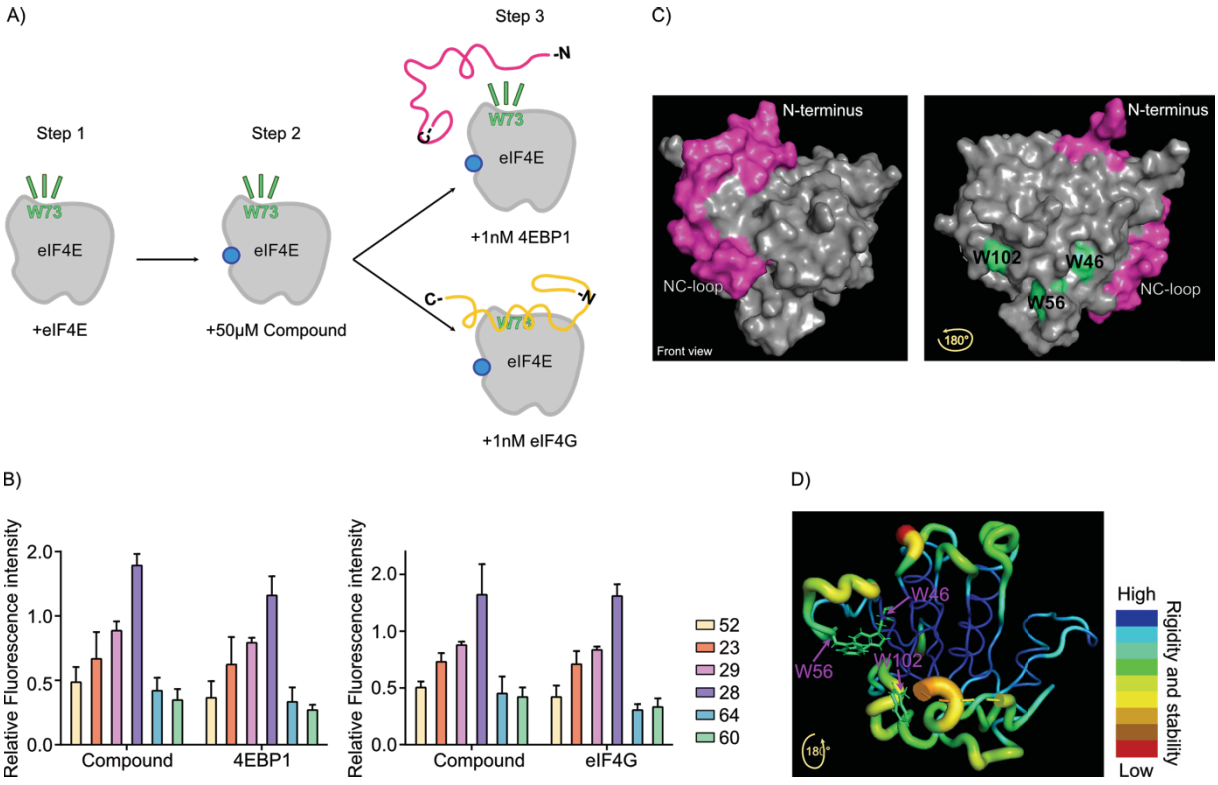

Figure 15: Assessment of compounds ability to prevent the assembly of the eIF4E-4EBP1 complex *in vitro*. A) Illustration of the workflow method to prevent eIF4E-4EBP1 complex formation. After measuring basal fluorescence of eIF4E, 50 µM compound were added and incubated for 30 sec. Then either 1 nM 4EBP1 or eIF4G peptide were added and incubated for 5 min. 4EBP1 was expected not to quench the fluorescent signal, because binding would be abrogated by the compound. EIF4G is expected to quench fluorescence as it only binds eIF4E through the canonical α-helix. B) The workflow described in (A) was followed. Six different compounds were tested individually. Autofluorescence of the buffer or buffer + compound was subtracted and data was normalized to basal fluorescence of eIF4E. Data represented as mean ± SD of three independent replicates. C) Surface representation of the 4EBP1 binding interface on eIF4E. The grey area represents eIF4E, the pink area 4EBP1 and green area represents the solvent accessible surface tryptophans 46, 56 and 102 contained within the eIF4E structure. D) B-factor diagram of eIF4E generated with PyMOL. Blue and thin lines indicate a stable and rigid region whereas the thick yellow and red lines indicate a more flexible area. Pink arrows mark the position of the tryptophans.

4. Discussion

Major questions remain regarding the role and regulation of 4EBP1 in cancer. Is 4EBP1 a tumor suppressive or pro-tumorigenic factor? How is *EIF4EBP1* expression controlled in cancer? In this thesis, the regulation and function of 4EBP1 in glioblastoma was elucidated. Based on the obtained results a model was proposed as detailed below (Figure 16).

The transcription factors ETS1 and MYBL2 are overexpressed in glioblastoma. By binding to *EIF4EBP1* promoter, ETS1 and MYBL2 control *EIF4EBP1* transcription in this tumor entity and drive its overexpression. This has clinical relevance as high levels of *EIF4EBP1* correlate with poor prognosis in patients with glioblastoma or other cancer entities. Because glioblastoma cells are subjected to metabolic stress by the tumor microenvironment, the accumulated 4EBP1 protein is activated and as such contributes to tumorigenesis in several ways. By translationally repressing fatty acid synthesis, to maintain the redox balance and prevent oxidative stress, 4EBP1 promotes oncogenic transformation and glioma tumorigenicity. This occurs by translational inhibition of specific transcripts, such as ACC1, the rate limiting enzyme of fatty acid synthesis. By potentially regulating p53, 4EBP1 may restrict senescence, to drive oncogenic transformation, as an additional mechanism. However, 4EBP1 is not involved in glioblastoma invasive properties, as 4EBP1 had no impact on migration or invasion of glioblastoma cells. Taken together, 4EBP1, whose expression is regulated by oncoproteins, exerts a pro-tumorigenic function in glioblastoma through multiple mechanisms (Figure 16).

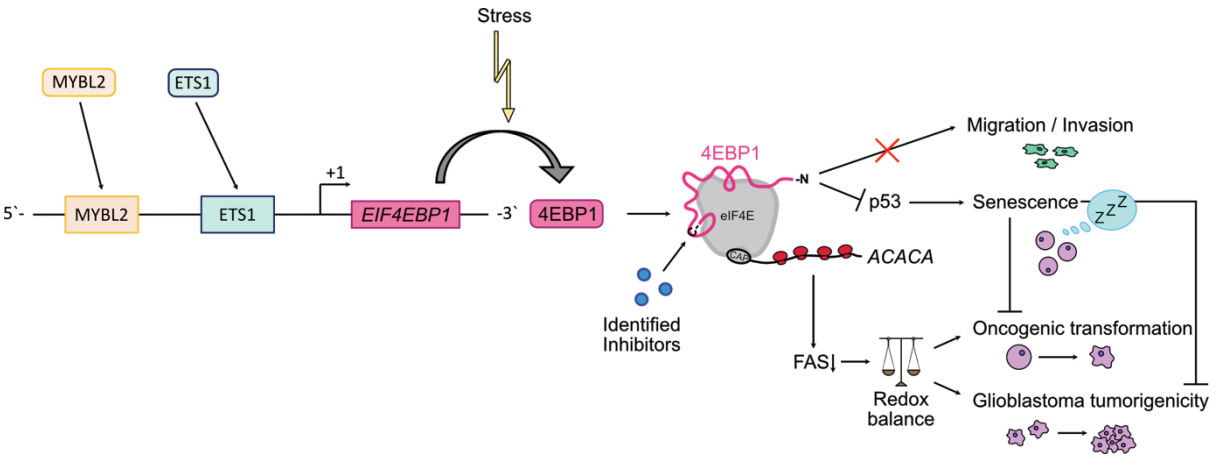

Figure 16: Proposed model for 4EBP1 regulation and function in glioblastoma. MYBL2 and ETS1 induce 4EBP1 overexpression in glioblastoma. When activated by stress, 4EBP1 does not alter migratory and invasive properties of glioblastoma cells but blocks p53, thereby preventing p53-induced senescence. This can promote oncogenic transformation and induce

tumorigenesis. Additionally, 4EBP1 binds eIF4E under stress conditions, which prevents translation of specific transcripts like *ACACA*, resulting in inhibition of fatty acid synthesis (FAS) and maintenance of the redox balance. This in turn stimulates oncogenic transformation and the tumorigenic potential.

4.1. Deregulation of *EIF4EBP1* expression in cancer and role of 4EBP1 in cancer cell migration

Little is known about the transcriptional control of *EIF4EBP1.* So far, very few transcription factors have been identified to regulate *EIF4EBP1* expression. While *EIF4EBP1* has been reported to be overexpressed in various tumor entities (WU & WAGNER 2021), it is currently unknown how this overexpression is driven. Here, the three transcription factors ETS1, MYBL2 and MYC were found to regulate *EIF4EBP1* transcription in glioblastoma, validating previous reports for MYC in other tumor types (BALAKUMARAN *et al.* 2009, TAMEIRE *et al.* 2019). All three transcription factors have been described to be encoded by proto-oncogenes and to be overexpressed in various cancer types (VITA & HENRIKSSON 2006, DITTMER 2015, MUSA *et al.* 2017). In particular, MYC is amplified and/or overexpressed in many different types of cancer, such as for instance in about 20% of NSCLC patients (VITA & HENRIKSSON 2006). The molecular mechanisms underlying *MYBL2* and *ETS1* overexpression in malignant gliomas are to date unknown, however, possible mechanisms can be proposed. In the case of *MYBL2*, this may be due to EGFR signaling that was reported to activate the *MYBL2* promoter in association with E2F1 in various cancer cell lines (HANADA *et al.* 2006). ETS1 activity is directly stimulated by hypoxia (mediated by HIF-1A), ROS (mediated by NRF2) (DITTMER 2015) or induced by the RAS/RAF/MEK/ERK pathway, which is overactivated in glioblastoma (DITTMER 2015). Therefore, such a mechanism may provide a possible explanation for *EIF4EBP1* overexpression reported in many different cancer entities (WU & WAGNER 2021). This may also shed light on our observations that *EIF4EBP1* represents a factor of poor prognosis in certain tumor types, such as glioma, bladder and kidney renal clear cell carcinoma (Manuscript II Figure 7C and D, Supplementary Figure 5C-E). Indeed, the regulators of *EIF4EBP1,* MYC, ETS1 and MYBL2, are known predictors of poor prognosis in some cancers (VITA & HENRIKSSON 2006, DITTMER 2015, REN *et al.* 2015, MUSA *et al.* 2017, MUSA *et al.* 2019). Together, this highlights the clinical relevance of *EIF4EBP1* in cancer and suggests a link to a tumor promoting role for 4EBP1.

To find out more about 4EBP1 functions in cancer, it was reasoned in this thesis that 4EBP1 may mediate the function of its transcriptional regulators and oncoproteins ETS1 and MYBL2.

While multiple functions are reported for these factors, one of them is the promotion of cancer cells migration and invasion (DITTMER 2015, ZHANG *et al.* 2017, XIONG *et al.* 2020). Therefore, it was investigated whether 4EBP1 might play a role in these processes. In the literature, a limited number of studies describe 4EBP1 as a modulator of cancer cell invasion, with different outputs depending on the cell type. Ribosomal profiling identified a fraction of 4EBP1 sensitive transcripts that encode proteins promoting cancer cell invasion (HSIEH *et al.* 2012). By preventing translation of such transcripts, active 4EBP1 was demonstrated to restrain prostate cancer cell invasion (HSIEH *et al.* 2012). In support to that, 4EBP1 was shown to block migration and invasion of colon cancer cell lines by repressing the expression of the driver of epithelial-mesenchymal transition (EMT) Snail (CAI *et al.* 2014). This outcome was validated *in vivo*, as 4EBP1 KD increased colon cancer cell metastasis to the liver in mice (CAI *et al.* 2014). On the contrary, in breast cancer cell lines the overexpression of 4EBP1 prevented the inhibition of EMT, migration and invasion triggered by the natural compound arctigenin (LUO *et al.* 2021). The own findings validated neither of the presented data, since 4EBP1 had no impact on the migratory and invasive properties of glioblastoma cells. It is possible that 4EBP1 exerts different functions on migration and invasion depending on the cancer type, especially considering that glioblastoma is more locally invasive and does not metastasize in contrast to other cancer types such as breast cancer. Clearly, more experiments need to be performed to further delineate the possible roles of 4EBP1 in migration and invasion.

4.2. Tumorigenic potential of 4EBP1 involves control of the redox balance and depends on p53 status

Cancer cells are subjected to different types of extrinsic stress, in part because of the hostile microenvironment they grow in. Metabolic stress, such as glucose starvation, is one of the main stressors cancer cells encounter. When cells undergo oncogenic transformation, they experience intrinsic stress which resembles metabolic stress. Noteworthy, the mechanisms supporting oncogenic transformation or tumorigenic potential are similar to the ones mediating adaptive response to glucose starvation (SCHAFER *et al.* 2009, JEON *et al.* 2012, TRUITT *et al.* 2015). All of these responses being linked to the maintenance of the redox potential (SCHAFER *et al.* 2009, JEON *et al.* 2012, TRUITT *et al.* 2015). One hallmark of oncogenic transformation is the ability of cells to grow under anchorage-independent conditions. It has been shown that under anchorage-independent conditions non-transformed cells exhibit

decreased ATP levels, due to impaired glucose uptake, and are confronted to oxidative stress, together mimicking intracellular conditions induced by glucose deprivation (SCHAFER *et al.* 2009, JEON *et al.* 2012, LABUSCHAGNE *et al.* 2019). Oncogene activation under such conditions restores glucose uptake and ATP levels, and limits oxidative stress (SCHAFER *et al.* 2009). This involves activation of the catabolic process of fatty acid oxidation that contributes to the generation of NADPH, which is eventually used for antioxidant reactions (SCHAFER *et al.* 2009). Another mechanism to reduce intracellular ROS levels in cancer cells is by formation of cell clusters. This induces mitophagy and consequently results in the removal of mitochondrial ROS (LABUSCHAGNE *et al.* 2019). Work in this thesis characterized that 4EBP1 controls an additional mechanism which contributes to the maintenance of the redox balance during transformation and tumorigenicity. The data indicate that 4EBP1 selectively blocks translation of the rate limiting enzyme of the fatty acid synthesis pathway ACC1, which in turn results in reduction of NADPH consumption, maintaining cellular antioxidant capacities. In addition, the own results show that through this mechanism 4EBP1 mediates RAS and HER2 oncogenic transformation and stimulates tumorigenic potential of glioblastoma cell lines. These findings complement already existing reports illustrating the importance of restricting fatty acid synthesis to mitigate oxidative stress and allow oncogenic transformation (SCHAFER *et al.* 2009, JEON *et al.* 2012). In a seemingly apparent contradiction to the own findings, oncogenic transformation by eIF4E was found to rely on eIF4E translational enhancement of mRNAs whose products are involved in ROS detoxification (TRUITT *et al.* 2015). This finding suggests that translation of these transcripts would be blocked when 4EBP1 is active, which would consequently result in increased ROS levels. While no explanation is currently available, this highlights the importance of the ratio between eIF4E and 4EBP1 protein levels and relative activity of each protein in cancer cells, which would depend on extrinsic and intrinsic stress levels.

MYBL2 plays a role in maintaining the redox balance in normal cells as loss of this protein results in elevated ROS levels (ZHOU *et al.* 2017). In addition, MYBL2 was demonstrated to prevent RAS-induced accumulation of ROS (MASSELINK *et al.* 2001), which would otherwise induce cellular senescence (PANIERI *et al.* 2013, MARAZITA *et al.* 2016). As a target gene of MYBL2, *EIF4EBP1* encoded protein may contribute to the ability of MYBL2 to mediate maintenance of the redox balance and support oncogenic RAS transformation. This is in line with existing data showing the supportive role of 4EBP1 in oncogenic RAS transformation

(PETROULAKIS *et al.* 2009), which was demonstrated in this thesis for transformation by another oncogene, HER2. Petroulakis *et al.* (2009) linked the function of 4EBP1 during RAS oncogenic transformation to the inhibition of senescence through 4EBP1 regulation of p53 stabilization. While in p53 WT MEFs 4EBP1 is absolutely required for RAS transformation, in p53 deficient (KO) cells 4EBP1 is dispensable for RAS transformation (PETROULAKIS *et al.* 2009). These data indicate that 4EBP1 pro-oncogenic function requires a functional p53. The own data provide further support to this model as 4EBP1 KD reduced tumorigenic potential in p53 WT cancer cells but not in cancer cells with *TP53* KO or *TP53* mutations, which depending on the mutation results in p53 inactivation.

The connection between 4EBP1 function and p53 mutation status has clinical relevance. Previous data revealed that high levels of *EIF4EBP1* correlates with a worse prognosis in breast cancer patients with WT *TP53*, which was not observed for patients exhibiting a *TP53* mutation (see section 3.2.3, Figure 11F and G). The *TP53* status should therefore be considered when using *EIF4EBP1* expression for prognostic association studies. This is especially critical since *TP53* is one of the most frequently mutated genes in adult tumors. This implicates that in cancers with high somatic *TP53* mutation frequency, such as ovary, colorectal, head and neck and NSCLC (OLIVIER *et al.* 2010, KANDOTH *et al.* 2013), 4EBP1 may not exert a general pro-tumorigenic function and *EIF4EBP1* may not be a factor of poor prognosis in all patients. This would also include glioblastoma, in which *TP53* mutation frequency is around 30% (OLIVIER *et al.* 2010, BRENNAN *et al.* 2013, KANDOTH *et al.* 2013). In support to that, 4EBP1 was reported to display tumor suppressive properties in head and neck carcinoma (WANG *et al.* 2019). In contrast, in cancers with low *TP53* mutation rates, such as in the pediatric cancers neuroblastoma (ACKERMANN *et al.* 2018) and medulloblastoma (LOUIS *et al.* 2016, KRISTENSEN *et al.* 2019), 4EBP1 may have an exclusive pro-tumorigenic function and *EIF4EBP1* expression may predict for poor prognosis. Data from our research group highlight that in neuroblastoma *EIF4EBP1* is overexpressed in the most aggressive and advanced patient subsets and that *EIF4EBP1* is a factor of poor prognosis in this tumor entity (K. Völtzke, personal communication; see Appendix: 6.4. Manuscript III). In addition, we uncovered that in medulloblastoma high *EIF4EBP1* expression is a factor of poor prognosis in all patients, as well as in the most aggressive medulloblastoma subgroups, namely group 3 and 4 (see Appendix: 6.3.). This goes along with the ability of 4EBP1 to contribute to medulloblastoma tumorigenicity *in vitro* (K. Scharov, personal communication). As demonstrated, 4EBP1 exerts

a tumor promoting function in glioblastoma, which makes it a reasonable candidate for drug targeting. This makes it even more important to elucidate the connection between the *TP53* mutation status and 4EBP1 function, as the pro-tumorigenic role of 4EBP1 and prognostic outcome for patients might be altered by *TP53* mutation.

4.3. 4EBP1 represents a potential therapeutic target candidate for glioma

MTORC1 is considered a popular and attractive drug target to treat cancer, as it is hyperactive in many cancers. However, this is only the case in well-vascularized regions of tumors, in opposition to poorly vascularized areas in which mTORC1 is barely active (PALM *et al.* 2015, KUMAR *et al.* 2019). The consequence is that targeting of the mTORC1 results in significantly increased proliferation of cancer cells in hypovascularized regions of tumors, as shown in a mouse model of pancreatic cancer (PALM *et al.* 2015). Therefore, targeting mTORC1 in cancer might result in the exact opposite outcome as initially anticipated. To refine such therapeutic strategy, focus has been put on targeting the oncoprotein eIF4E (LAZARIS-KARATZAS *et al.* 1990), downstream of mTORC1. EIF4E recognizes the 5' m^7G cap structure of mRNAs and associates with translation initiation factors to form the eIF4F complex, allowing mRNA translation to initiate. The aim when targeting eIF4E is to mimic the "tumor suppressive" function of 4EBP1, by blocking assembly of the eIF4F complex and therefore inhibit proliferation and prevent tumor formation. One approach to target eIF4E used a 5' cap analogue to block eIF4E binding to mRNAs, therefore repressing their translation. Since such cap analogues are not so cell permeable (WAGNER *et al.* 2000), this approach has not been promising (PELLETIER *et al.* 2015). Another proposed strategy is to prevent eIF4E binding to eIF4A, by selectively targeting eIF4A with compounds such as rocaglates and in particular silvestrol. The interaction of eIF4A with these compounds either prevents the scanning of the mRNA by ribosomes or the interaction with the eIF4F complex by forcing a non-specific interaction between eIF4A and mRNAs (PELLETIER *et al.* 2015, ZHANG *et al.* 2020). Treatment of engrafted mouse lymphoma models with synthetic rocaglates resulted in anti-neoplastic activity (ZHANG *et al.* 2020). Lastly, the well described MAPK interacting protein kinase 1/2 (MNK1/2) inhibitor eFT508 (REICH *et al.* 2018), was used to block eIF4E phosphorylation. While the inhibitor alone did not impact proliferation of Ras transformed colon carcinoma cell lines *in vivo*, it led to decreased proliferation when combined with rapamycin treatment (KNIGHT *et al.* 2021). Such a drug combination also resulted in decreased MYC levels, which is a translational target of eIF4E (YI *et al.* 2013), and in prolonged survival of mice engrafted with colon carcinoma cells (KNIGHT *et*

al. 2021). Taken together, these data suggest that the combined inhibition of eIF4E phosphorylation and mTORC1, which corresponds to 4EBP1 activation, restrained MYC levels and halted proliferation of colon cancer cells *in vivo* (KNIGHT *et al.* 2021). Based on our data, blocking of mRNA translation will support cancer cells survival under metabolic stress. Therefore, all the above-mentioned targeting strategies might not be effective in cancer types experiencing extensive metabolic stress, such as glioblastoma. Instead, inhibiting 4EBP1, to push mRNA translation activity and interfere with cancer cell adaptation to metabolic stress, might represent a more appropriate approach. In this thesis, first attempts to target 4EBP1 were performed, following identification of potential inhibitors by an *in silico* drug screen. Tryptophan fluorescent quenching assay was established to screen for the ability of some of these compounds to block 4EBP1 binding to eIF4E. This assay came not without technical difficulties. The first approach to disrupt the already formed eIF4E-4EBP1 complex with some of the compounds was unsuccessful. This might be explained by the high binding affinity of 4EBP1 to eIF4E *in vitro* (MIZUNO *et al.* 2008, PAKU *et al.* 2012). In contrast, a lower binding affinity is expected in cells, as eIF4G is present and will compete with 4EBP1 for binding eIF4E (IGREJA *et al.* 2014). As the strong binding affinity between eIF4E and 4EBP1 could not been disrupted, we adjusted our experimental set up and added the compounds before formation of the eIF4E-4EBP1 complex. Unexpectedly, most of the tested compounds already quenched the tryptophan fluorescence signal. This effect may be explained by the presence of three solvent exposed tryptophan additionally to W73 (see Figure 15C). Most likely, the compounds bind either within the W73 region or close to one of the other tryptophan, thereby quenching the fluorescent signal. Based on the results we obtained, tryptophan fluorescence quenching does not appear as a good readout, since the autofluorescence of the compounds and the multiple solvent exposed tryptophan of eIF4E disturb the accuracy of the measurements. Therefore, an alternative method, such as isothermal titration calorimetry, might be a more suitable way to investigate efficacy of the compounds to block 4EBP1 binding to eIF4E.

In conclusion, a novel mechanism of adaption of cancer cells to extrinsic and intrinsic stress factors was revealed in this thesis. The 4EBP1 pathway is hijacked by cancer cells to maintain redox balance through restriction of fatty acid synthesis and thereby supports stress accompanying tumorigenic processes. The clinical relevance of 4EBP1 was highlighted in few cancers, as *EIF4EBP1* represents a factor of poor prognosis in some tumor entities, which could be exploited therapeutically. The function of 4EBP1 in cancer depends on levels of metabolic

stress and likely on *TP53* mutation status, which may open new avenues for patient prognostics and treatment options, especially in glioblastoma (Figure 17).

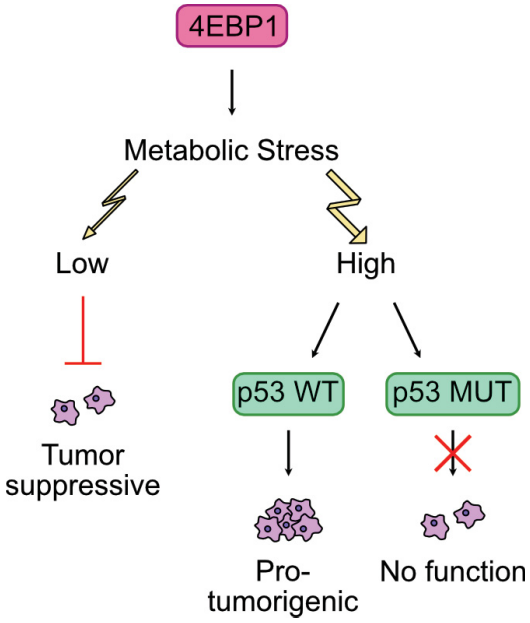

Figure 17: Proposed model for the function of 4EBP1 in cancer. Based on the literature 4EBP1 most likely exerts a tumor suppressive function under low metabolic stress conditions. On the contrary, the role of 4EBP1 under metabolic stress is affected by the p53 status as 4EBP1 has a pro-tumorigenic function in p53 WT cells but no function in cancer cells with p53 mutation.

5. Material and Methods

5.1. Data availability and bioinformatic analysis

Analysis of *MYC* expression in malignant glioma compared to non-neoplastic brain tissues and co-expression analysis of *EIF4EBP1* and *MYC* expression was performed in the same datasets as described in the material and method section of Manuscript I. ChIP-seq data for MYC (UCSC accession: wgEncodeEH000648, wgEncodeEH000545, wgEncodeEH000659, wgEncodeEH000669, wgEncodeEH001867, wgEncodeEH000670, wgEncodeEH002800, wgEncodeEH000536, wgEncodeEH000621, wgEncodeEH001134, wgEncodeEH003436, wgEncodeEH001133, wgEncodeEH002840, wgEncodeEH002816, wgEncodeEH001807, wgEncodeEH002795, wgEncodeEH000542, wgEncodeEH000561, wgEncodeEH001795) were downloaded from ENCODE using the human genome GRCh 38/hg 38. I would like to acknowledge the ENCODE Consortium as well as the Iyer-, Snyder- and Struhl-laboratories for generating the respective datasets. RNA-seq and microarray data were used for overall survival analysis with R^2 AMC (Cavalli Cohort; (CAVALLI *et al.* 2017)) or Kaplan-Meier Plotter (GYORFFY *et al.* 2021).

5.2. Cell culture

The glioblastoma cell lines U-87 MG, U-118 MG and U-251 MG were obtained from American Type Culture Collections (ATCC) and LN-229 were kindly provided by Monika Hegi. The NSCLC cell line ACF 1055.1 was kindly provided by Prof. Dr. Christian Reinhardt from the University Hospital Cologne. Cells were maintained in Dulbecco's modified Eagle Medium (10569010, Thermo Fisher Scientific, Waltham, MA, USA) supplemented with 10% fetal bovine serum (FBS) (10270-106, Thermo Fisher Scientific) and 1% penicillin/streptomycin (10270-106, Sigma Aldrich, St Louis, USA), and cultured in a humidified incubator at 37°C with 5% CO_2. The cell lines were confirmed to be mycoplasma-free by Venor GeM Classic kit (11-1050, Minerva Biolabs, Berlin, Germany). U-251 MG and LN-229 were validated by STR-profiling (Genomics & Transcriptomics Labor [GTL], Heinrich Heine University, Düsseldorf, Germany).

5.3. Transfection of cells with shRNA or siRNA

Cells were transfected with siRNAs as described in Manuscript I. Additional siRNAs used for the thesis were siRNAs targeting *FOXM1* (D-009762-02 & D-009762-03, Dharmacon) and *JUN* (D-003268-09 & D-003268-22, Dharmacon) (see Table 4). Cells were transfected with shRNAs

as described in Manuscript II. Sequences for additional mouse shRNAs targeting *EIF4EBP1* used for the thesis are listed in Table 5.

Table 4: List of siRNA sequences.

Target gene and siRNA name	siRNA sequence
FOXM1 si2	5'- GGACCACUUUCCCUACUUU -3'
FOXM1 si3	5'- GUAGUGGGCCCAACAAAUU -3'
JUN si9	5'- GAGCGGACCUUAUGGCUAC -3'
JUN si22	5'- AAGUCAUGAACCACGUUAA -3'

Table 5: List of shRNA sequences.

Organism	Target gene	shRNA sequence
Mouse	4EBP1 msh2	5'-CCGG**AGGCGGTGAAGAGTCACAATT**CTCGAG**AATTGTGACTC TTCACCGCCT**TTTTTG-3'
Mouse	4EBP1 msh5	5'-CCGG**ATTATCTATGACCGGAAATTT**CTCGAG**AAATTTCCGGTC ATAGATAAT**TTTTTG-3'

Bold letters indicate 4EBP1 targeting sequence

5.4. Migration and invasion assays

5.4.1. Oris™ Cell Migration Assay

For the Oris™ Cell Migration Assay (Platypus Technologies, Madison, WI, USA), U-87 MG and U-118 MG were plated evenly around the provided cell stoppers with a final seeding concentration of 25.000 cells/100 µl/96 well. Cells were allowed to attach for 24 h, before cell stoppers were removed and plates were incubated for 48 h in an incubator at 37°C with 5% CO_2. For workflow see Figure 18.

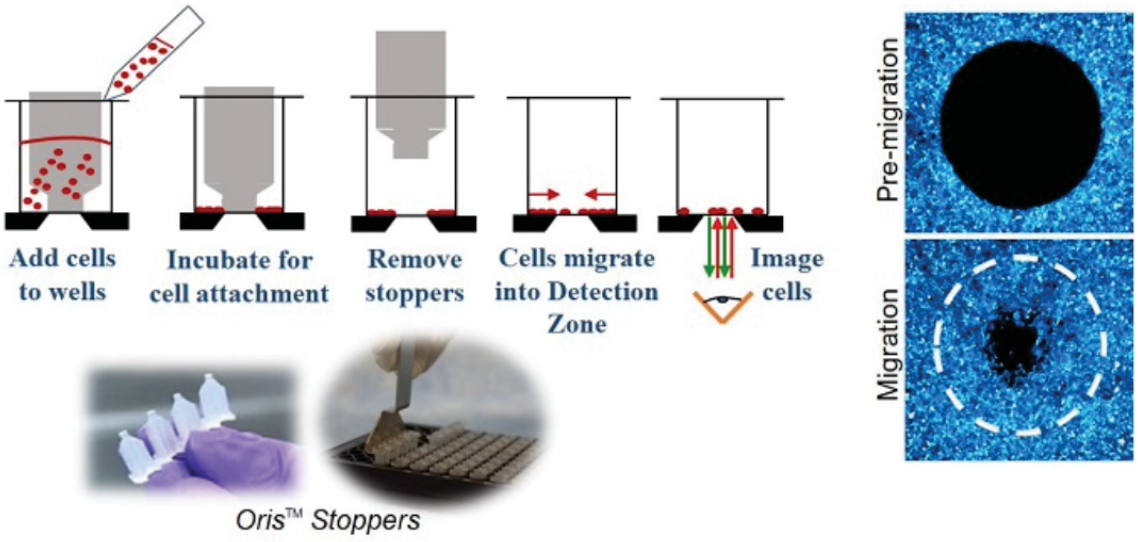

Figure 18: Workflow representing plating and imaging of Oris™ Cell Migration Assay. https://www.platypustech.com/cell-based-assays/oris-cell-migration (13.01.2022)

5.4.2. Oris™ 3D Cell Invasion Assay

For the Oris™ 3D Cell Invasion Assay (Platypus Technologies, Madison, WI, USA), for each 96 well 25.000 U-87 MG or U-118 MG cells embedded in a collagen mix containing 10x PBS, 7.5% sodium bicarbonate, deionized water and rat tail collagen type 1 (#08-115, Sigma Aldrich, St. Louis, MO, USA and #CI48, Platypus Technologies) were plated evenly around the cell stoppers. For collagen polymerization, plates were incubated at 37°C with 5% CO_2 for 1 h. After cell stopper removal, the resulting invasion zone was filled up with the remaining collagen mixture and incubated for another hour in the incubator before 100 µl medium were added. Cells were incubated for 48 h before staining and imaging (see workflow at Figure 19).

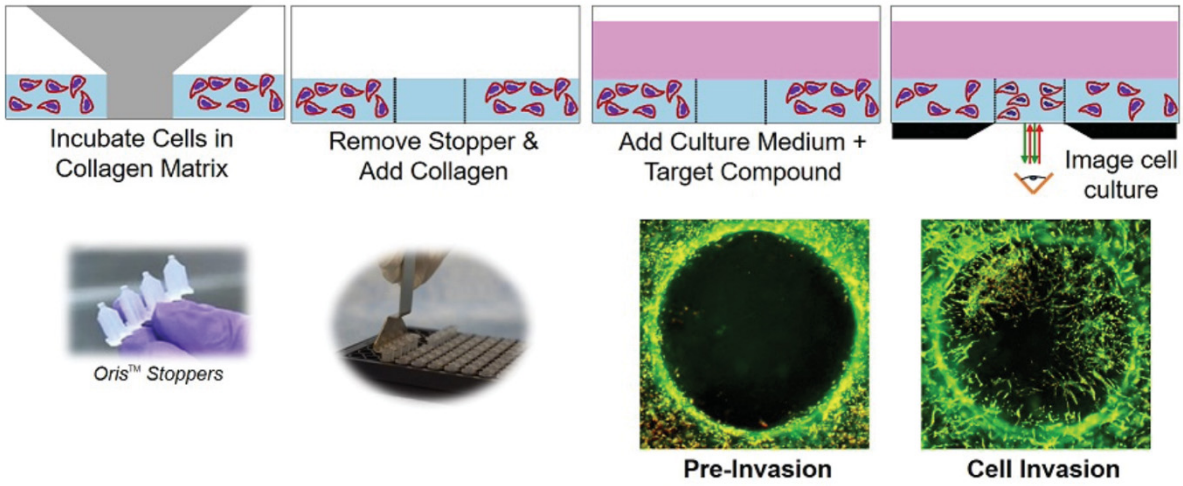

Figure 19: Workflow representing plating and imaging of Oris™ 3D Cell Invasion Assay. https://www.platypustech.com/cell-based-assays/3d-embedded-invasion (13.01.2022).

5.4.3. Staining and imaging of the migration and invasion assays

U-87 MG and U-118 MG were stained with 30 µl of 5 mg/ml Hoechst 33342 (#B2261, Sigma Aldrich, St. Louis, MO, USA) in PBS for 10 min and fluorescence was imaged using the CKX53 microscope (Olympus, Shinjuku, Japan) with DAPI filter. Pictures were taken using an ORCA-spark camera (Hamamatsu, Japan), the OLYMPUS cellSens program (Olympus) and cells were counted with ImageJ.

5.5. Protein binding assays

5.5.1. Peptide synthesis

FLAG-tagged (highlighted in gray) human eIF4E protein residues 36-217 (sequence: MDYKDDDDKATVEPETTPTPNPPTTEEEKTESNQEVANPEHYIKHPLQNRWALWFFKNDKSKTWQANL

RLISKFDTVEDFWALYNHIQLSSNLMPGCDYSLFKDGIEPMWEDEKNKRGGRWLITLNKQQRRSDLDRF WLETLLCLIGESFDDYSDDVCGAVVNVRAKGDKIAIWTTECENREAVTHIGRVYKERLGLPPKIVIGYQSH ADTATKSGSTTKNRFVV) was synthesized by GenScript Biotech (Piscataway Township, NJ, USA) and stored in 10 mM Phosphate buffer (pH 7.5) containing 150 mM NaCl and 2 mM DTT. WT or mutant human 4EBP1 peptides corresponding to residues 50-83 (WT sequence: TRIIYDRKFLMECRNSPVTKTPPRDLPTIPGVTS) (MUT sequence: TRIIYDRKFLMECRNSPVTKTPPRDL PT**A**PG**A**TS) as well as human eIF4G peptide corresponding to residues 569-580 (sequence: KKRYDREFLLGF) was synthesized by GL Biochem (Shanghai, China). All peptides were dissolved in 10 mM Phosphate buffer, 150 mM NaCl and 2 mM DTT (pH 7.5) and 16 % DMSO.

5.5.2. Spectroscopic measurements

Titration experiments were carried out in a standard phosphate buffer 10 mM PB, 150 mM NaCl, 2 mM DTT (pH 7.5). Fluorescence was recorded with the Fluorescence Spectrometer LS-55 (PerkinElmer, Waltham, MA, USA) in a quartz cuvette. For all experiments an excitation wavelength of 290 nm and an emission wavelength of 350 nm were applied (slit 5.0 nm), which ensured observation of tryptophan residues emission only (NIEDZWIECKA *et al.* 2002). Measurements were performed using the FL WinLab software, version 4.00.03 (PerkinElmer). 0.2 µM eIF4E protein was used and 4EBP1 WT, MUT and eIF4G peptides were titrated at various concentrations (0.01-10 nM). Incubation time between titration steps was 30 sec. Magnetic stirring was used to ensure efficient mixing of the protein-peptide mixture. Compounds (Table 6) were dissolved in DMSO only and concentrations between 10-50 µM were added to eIF4E protein or eIF4E protein/peptide mixture.

5.5.3. Candidate 4EBP1 inhibitor compounds, additional PCR primers and antibodies

Table 6 provides an overview of the used 4EBP1 inhibitor compounds and their sources.

Table 6: 4EBP1 inhibitor candidate compounds.

Compound number	ZINC number	Company
23	ZINC000096141174	ChemBridge Corporation (San Diego, CA, USA)
28	ZINC000252568989	ChemBridge Corporation
29	ZINC000011840459	ChemBridge Corporation
52	ZINC000017124164	Vitas-M Laboratory (Hong Kong)
60	ZINC000072401400	Vitas-M Laboratory
64	ZINC000008765202	Vitas-M Laboratory

In addition to the PCR primers and antibodies listed in manucripts I and II, the following Table 7 and Table 8 summarize the additional primers used for RT-qPCR analyses and the additional antibodies used for immunoblot experiments.

Table 7: List of additional RT-qPCR primers used for RT-qPCR analyses.

Primer	Primer sequences
FOXM1	FW: 5'- TGCCCAGCAGTCTCTTACCT -3' RV: 5'- CTACCCACCTTCTGGCAGTC -3'
JUN	FW: 5'- TCGACATGGAGTCCCAGGA -3' RV: 5'- GGCGATTCTCTCCAGCTTCC -3'

Table 8: List of additional antibodies used for immunoblot experiments.

Antibody	Company	Catalog number
FOXM1	Cell signaling (Cambridge, UK)	#20459S
JUN	Cell signaling	# 9165

6. APPENDIX

6.1. Supplementary figures corresponding to manuscript I

Supplementary figure 1

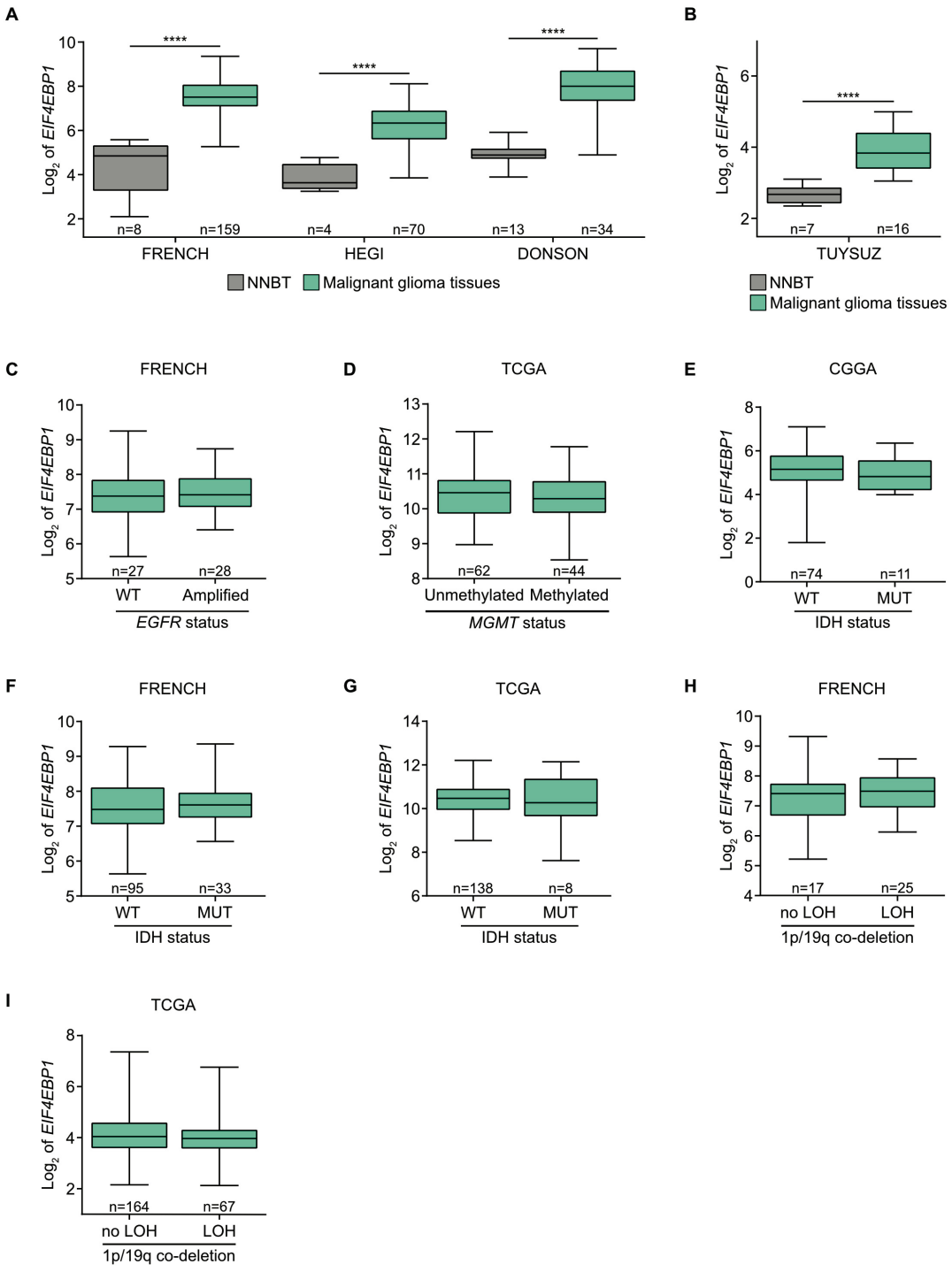

Supplementary Figure 1. EIF4EBP1 expression malignant gliomas in relation to non-neoplastic brain tissue and according to selected genetic and epigenetic alterations. A and B, Expression levels of *EIF4EBP1* in non-neoplastic brain tissue (NNBT) and in glioblastoma/malignant glioma tissue samples from the indicated patient cohorts, i.e. FRENCH

(1), HEGI (2), DONSON (3) (microarray platforms u133p2), and TUYSUZ (4) (microarray platform hugene21t). C, Expression levels of *EIF4EBP1* in *EGFR*-non-amplified (WT) versus *EGFR*-amplified IDH-wildtype glioblastoma tissues of the FRENCH cohort (1). D, Expression levels of *EIF4EBP1* in IDH-wildtype glioblastoma samples of TCGA cohort (5) according to *MGMT* promoter methylation status. E-G, Expression levels of *EIF4EBP1* according to IDH mutation status in CNS WHO grade 4 glioma samples of the (E) CGGA (6), (F) FRENCH (1) and (G) TCGA cohorts (5). H and I, Expression levels of *EIF4EBP1* in CNS WHO grade 2-4 IDH-mutant diffuse glioma samples of the (H) FRENCH (1) and (I) TCGA (5) cohorts stratified according to 1p/19q codeletion status. Significance was calculated using unpaired and two-tailed parametric t-tests (****p<0.0001).

Supplementary figure 2

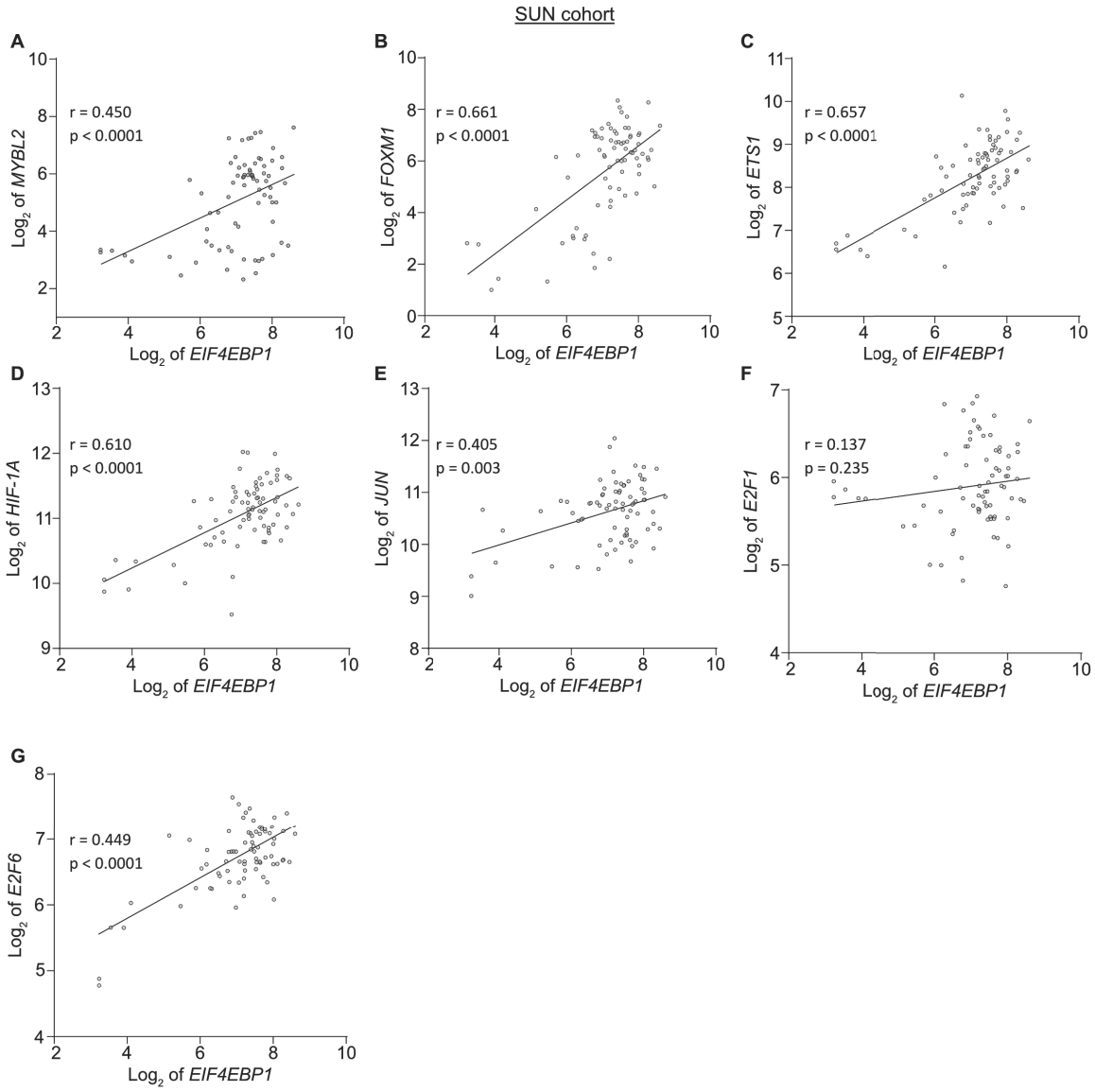

Supplementary Figure 2. Co-expression of *EIF4EBP1* with seven transcription factor genes in glioblastomas. A-G, Expression levels of *EIF4EBP1* in glioblastoma patient samples plotted against the expression levels of (A) *MYBL2*, (B) *FOXM1*, (C) *ETS1*, (D) *HIF-1A*, (E) *JUN*, (F) *E2F1* or (G) *E2F6* in the SUN cohort of 77 glioblastoma samples (7). Co-expression levels were quantified by calculating the Pearson correlation coefficient.

Supplementary figure 3

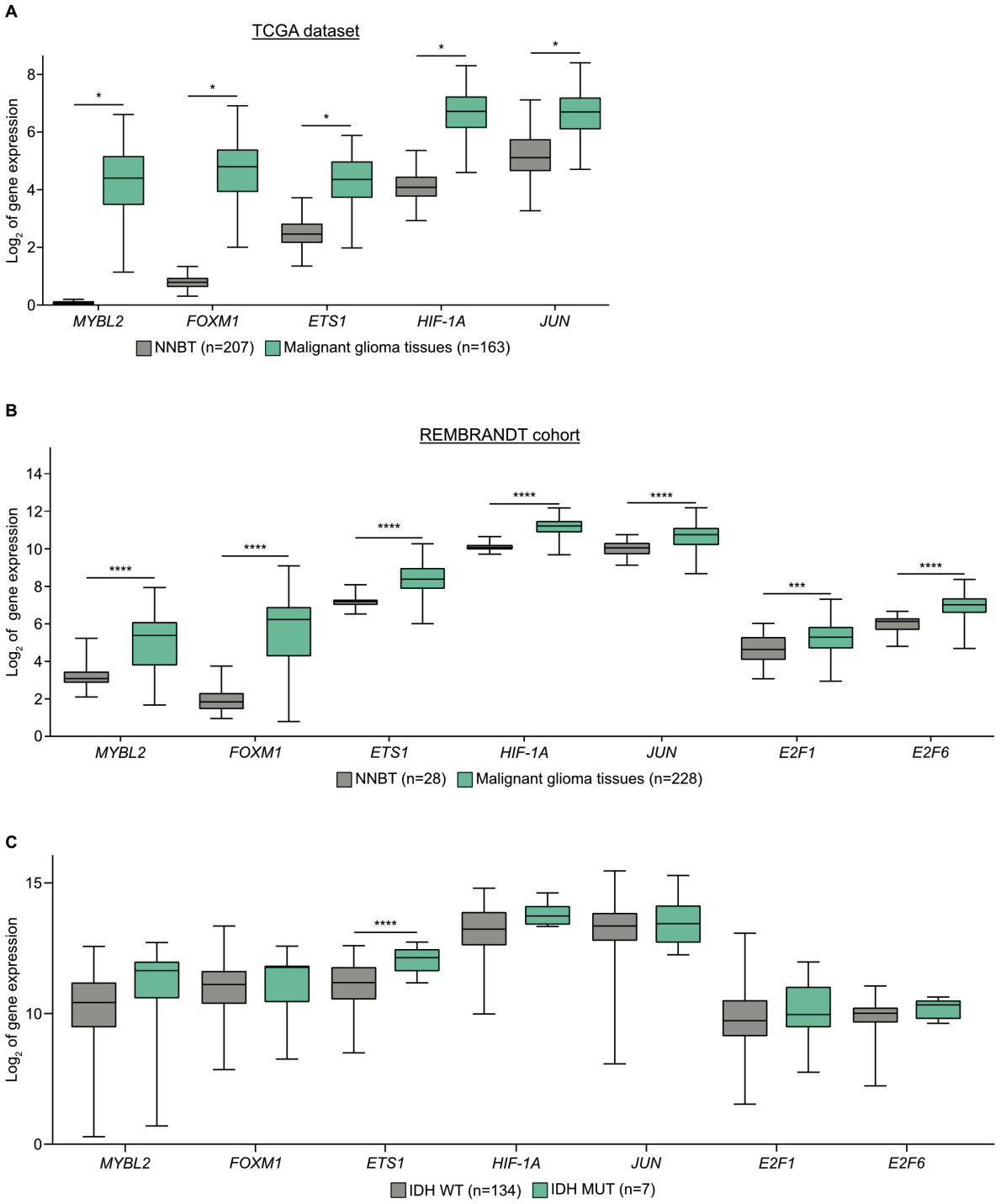

Supplementary Figure 3. Elevated expression of transcription factor candidate genes in malignant gliomas. A and B, Expression levels of the indicated transcription factor genes in non-neoplastic brain tissue (NNBT) of GTEx and in malignant glioma tissues from (A) TCGA (5), which analysed subcohort contains 138 IDH-wildtype, 8 IDH-mutant and 17 malignant glioma samples with unknown IDH status, or (B) REMBRANDT (8) cohorts. Significance for the REMBRANDT data was calculated using unpaired and two-tailed parametric t-tests (***p<0.001, ****p<0.0001). Significance for TCGA data has been calculated by GEPIA website using one-way ANOVA (9). C, Expression levels of the indicated transcription factor genes according to IDH mutation status in malignant glioma tissues were analysed using TCGA

data (5). Significance was calculated using unpaired and two-tailed parametric t-tests (****p<0.0001).

REFERENCES

1. Gravendeel LA, Kouwenhoven MC, Gevaert O, de Rooi JJ, Stubbs AP, Duijm JE, et al. Intrinsic gene expression profiles of gliomas are a better predictor of survival than histology. Cancer research. 2009;69(23):9065-72.

2. Murat A, Migliavacca E, Gorlia T, Lambiv WL, Shay T, Hamou MF, et al. Stem cell-related "self-renewal" signature and high epidermal growth factor receptor expression associated with resistance to concomitant chemoradiotherapy in glioblastoma. J Clin Oncol. 2008;26(18):3015-24.

3. Griesinger AM, Birks DK, Donson AM, Amani V, Hoffman LM, Waziri A, et al. Characterization of distinct immunophenotypes across pediatric brain tumor types. Journal of immunology. 2013;191(9):4880-8.

4. Gulluoglu S, Tuysuz EC, Sahin M, Kuskucu A, Kaan Yaltirik C, Ture U, et al. Simultaneous miRNA and mRNA transcriptome profiling of glioblastoma samples reveals a novel set of OncomiR candidates and their target genes. Brain Res. 2018;1700:199-210.

5. Cancer Genome Atlas Research N, Weinstein JN, Collisson EA, Mills GB, Shaw KR, Ozenberger BA, et al. The Cancer Genome Atlas Pan-Cancer analysis project. Nat Genet. 2013;45(10):1113-20.

6. Zhao Z, Zhang KN, Wang Q, Li G, Zeng F, Zhang Y, et al. Chinese Glioma Genome Atlas (CGGA): A Comprehensive Resource with Functional Genomic Data from Chinese Glioma Patients. Genomics Proteomics Bioinformatics. 2021;19(1):1-12.

7. Sun L, Hui AM, Su Q, Vortmeyer A, Kotliarov Y, Pastorino S, et al. Neuronal and glioma-derived stem cell factor induces angiogenesis within the brain. Cancer Cell. 2006;9(4):287-300.

8. Gusev Y, Bhuvaneshwar K, Song L, Zenklusen JC, Fine H, Madhavan S. The REMBRANDT study, a large collection of genomic data from brain cancer patients. Sci Data. 2018;5:180158.

9. Tang Z, Li C, Kang B, Gao G, Li C, Zhang Z. GEPIA: a web server for cancer and normal gene expression profiling and interactive analyses. Nucleic Acids Res. 2017;45(W1):W98-W102.

6.2. Supplementary tables corresponding to manuscript I

Supplementary table 1: Copy number status of *EIF4EBP1* in malignant gliomas of the TCGA cohort.

Copy number status	Number of cases (% of entire cohort)
Copy number loss (hemizygous deletion)	54 (10,63 %)
Balanced copy number	410 (80,71 %)
Low-level copy number gain	43 (8,46 %)
High level copy number gain (amplification)	0 (0 %)

Supplementary table 2: Overview of the co-expression analysis between *EIF4EBP1* and the different transcription factor gene candidates in the various glioma cohorts analyzed.

Transcription factor	Cohort	r-value	p-value	Total number of cohorts
MYBL2	SUN (1)	0.450	4.13-05	8
	REMBRANDT (2, 3)	0.499	9.2e-16	
	DONSON (4)	0.587	2.6e-04	
	HEGI (5)	0.367	1.8e-03	
	TCGA (6)	0.403	3.2e-07	
	FREIJE (7)	0.393	7.1e-04	
	FRENCH (8)	0.321	3.7e-05	
	KAWAGUCHI (9)	0.465	7.3e-03	
FOXM1	SUN (1)	0.661	6.1e-11	8
	REMBRANDT (2, 3)	0.640	1.1e-27	
	DONSON (4)	0.584	2.9e-04	
	HEGI (5)	0.383	1.1e-03	
	TCGA (6)	0.338	3.5e-11	
	FREIJE (7)	0.597	4.0e-08	
	KAWAGUCHI (9)	0.662	3.7e-05	
	PAUGH (10)	0.445	9.4e-03	
ETS1	SUN (1)	0.657	8.8e-11	6
	REMBRANDT (2, 3)	0.683	1.2e-32	
	DONSON (4)	0.509	2.1e-03	
	HEGI (5)	0.468	4.5e-05	
	FRENCH (8)	0.241	2.3e-03	
	KAWAGUCHI (9)	0.593	0.5e-04	
HIF-1A	SUN (1)	0.610	3.97e-09	4
	REMBRANDT (2, 3)	0.596	4.41e-54	
	FREIJE (7)	0.528	2.22e-06	
	KAWAGUCHI (9)	0.637	8.89e-05	
JUN	SUN (1)	0.405	2.6e-04	7
	TUYSUZ (11)	0.565	0.02	
	REMBRANDT (2, 3)	0.499	9.7e-16	
	HEGI (5)	0.378	1.2e-03	
	FREIJE (7)	0.368	1.6e-03	
	KAWAGUCHI (9)	0.475	6.0e-03	
	PAUGH (10)	0.417	0.04	
E2F1	REMBRANDT (2, 3)	0.245	1.85e-04	1
E2F6	SUN (1)	0.670	2.7e-11	5
	REMBRANDT (2, 3)	0.631	1.0e-26	
	DONSON (4)	0.514	3.2e-09	
	FREIJE (7)	0.642	1.6e-09	
	KAWAGUCHI (9)	0.567	7.2e-04	

EIF4EBP1 is co-expressed with each of the indicated transcription factor in the indicated cohorts. Co-expression levels were calculated with the Pearson correlation coefficient using the R^2 genomic visualization platform (R^2 AMC; http://r2.amc.nl).

Supplementary table 3: Overview of the CNS and non-CNS tumor cohorts used for analyses depicted in figure 5.

Tumor type	Cohort name	GEO ID or PUB med link
Adult glioma	Tumor Glioblastoma - Hegi - 84	GSE7696
	Tumor Glioblastoma - Loeffler - 70	GSE53733
	Tumor Glioma - French - 284	GSE16011
	Tumor Glioma - Kawaguchi - 50	GSE43378
	Tumor Glioma - Sun - 153	GSE4290
	Tumor Glioma - Yan - 21	GSE50774
	Tumor Glioma (CIC mutation status) - Gleize - 30	Unknown
	Tumor Brain (REMBRANDT study) - Madhavan - 550	GSE108474
Breast cancer	Tumor Breast - Black - 107	GSE36771
	Tumor Breast - Bos - 204	GSE12276
	Tumor Breast - Desmedt - 55	GSE16391
	Tumor Breast - EXPO - 351	GSE2109
	Tumor Breast - Iglehart - 123	GSE5460
	Tumor Breast - Yu - 683	GSE102484
	Tumor Breast (Anthracycline) - Sotiriou - 120	GSE16446
	Tumor Breast (Chemotherapy) - Quiles - 61	GSE28844
	Tumor Breast (HER2) - Concha - 66	GSE29431
	Tumor Breast (MDC) - Bertucci - 266	GSE21653
	Tumor Breast (mutation status) - Meijers-Heijboer - 155	GSE27830
	Tumor Breast (TNBC) - Brown - 198	GSE76124
Cancer of the gastrointestinal tract	Tumor Colon - Marra - 32	GSE8671
	Tumor Colon - Olschwang - 130	GSE37892
	Tumor Colon (KRAS mut) - Hase - 59	GSE92921
	Tumor Colon FOLFOX - Yagi - 83	GSE28702
	Tumor Colon Rectum - EXPO - 38	GSE2109
	Tumor Esophageal - Minashi - 40	GSE32701
	Tumor Gastric - Tan - 192	GSE15459
	Tumor Oral Cavity - Holsinger - 103	GSE42743
Gynecologic cancer	Tumor Endometrium - EXPO - 209	GSE2109
	Tumor Ovarian - Anglesio - 90	GSE2109
	Tumor Ovarian - Bowtell - 285	GSE9891
	Tumor Ovarian - McDonald - 31	GSE112798
	Tumor Ovarian (stroma) - McDonald - 45	GSE38666
Leukemia	Tumor ALL (T) - Meijerink - 124	GSE26713
	Tumor ALL (T) - Pieters - 92	GSE10609
	Tumor AML - Delwel - 460	GSE6891
	Tumor AML CEBPA - Verhaak - 525	GSE14468

Supplementary table 3 (Continuation)

Leukemia	Tumor B-cell Lymphoma (High Grade) - Chan - 61	GSE168422
	Tumor B-cell non-Hodgkin Lymphoma (B-NHL) - Green - 290	GSE132929
	Tumor CLL - Kueppers - 46	GSE36907
	Tumor Lymphoma (PCNSL/PMLBCL) - Shipp - 26	GSE61578
	Tumor MALT lymphoma - Du - 14	GSE16024
	Tumor PCNSL Lymphoma - Sano - 34	GSE34771
	Tumor T-cell lymphoma - Iqbala - 147	GSE19069
Lung cancer	Tumor Lung - Bild - 114	GSE3141
	Tumor Lung - EXPO - 121	GSE2109
	Tumor Lung - Peitsch - 150	GSE43580
	Tumor Lung (NSCLC) - Chuang - 120	GSE19804
	Tumor Lung (NSCLC) - Muley - 100	GSE33532
	Tumor Non-small cell lung carcinoma - Plamadeala - 410	GSE63074
Neuroblastoma	Tumor Neuroblastic mixed - Delattre - 64	GSE12460
	Tumor Neuroblastoma - Hiyama - 51	GSE16237
	Tumor Neuroblastoma - Lastowska - 30	GSE13136
	Tumor Neuroblastoma public - Versteeg - 88	GSE16476
Pediatric brain cancer	Tumor ATRT - Kool - 49	GSE70678
	Tumor CNS-PNET - Kool - 182	GSE73038
	Tumor CNS/PNET - Grundy - 24	GSE19404
	Tumor Ependymoma - Donson - 19	GSE16155
	Tumor Ependymoma - Gilbertson - 83	20639864
	Tumor Ependymoma - Hoffman - 65	GSE50385
	Tumor Ependymoma - Pfister - 209	GSE64415
	Tumor Glioma pediatric - Paugh - 53	GSE19578
	Tumor Medulloblastoma - ATRT - Hsieh - 31	GSE67851
	Tumor Medulloblastoma - Gilbertson - 76	GSE37418
	Tumor Medulloblastoma - Pfister - 223	28726821
	Tumor Medulloblastoma Ependymoma - denBoer - 51	GSE74195
	Tumor Medulloblastoma PLoS One - Kool - 62	GSE10327
	Tumor Medulloblastoma public - Delattre - 57	Unknown
	Tumor Pilocytic Astrocytomas - Gutman - 41	GSE5675
Sarcoma	Tumor Ewing Sarcoma - Delattre - 117	GSE34620
	Tumor Ewing Sarcoma - Francesconi - 37	GSE12102
	Tumor Ewing Sarcoma - Surdez - 79	GSE142162
	Tumor Osteosarcoma - Kobayashi - 27	GSE14827
	Tumor Rhabdomyosarcoma - Barr - 58	GSE66533

All cohorts were selected with the microarray mas5.0 - u133p2; GEO ID is indicated by GSE; Pub med link is indicated by a sequence of numbers.

Supplementary table 4: Overview of the IDH status in the various glioma cohorts.

Cohort	Reference	Accession no.	Number of patients	Diagnosis	IDH mutation status
CGGA	(12)		n=85	Primary glioblastoma	wildtype: n=74 mutant: n=11
DONSON	(4)	GSE50161	n=34	Pediatric glioblastoma	Unknown
FREIJE	(7)	GSE4412	n=71	Glioma grade 4	Unknown
FRENCH	(8)	GSE16011	n=159	Glioblastoma grade 4	wildtype: n=59 mutant: n=33 Unknown: n=67
FRENCH	(8)	GSE16011	n= 42	Glioma grade 2-4	mutant: n=42
HEGI	(5)	GSE7696	n=70	Glioblastoma	Unknown: n=70
KAWAGUCHI	(9)	GSE43378	n=32	Glioblastoma	wildtype: n=31 mutant: n=1
PAUGH	(10)	GSE26576	n=25	Pediatric glioblastoma (Diffuse intrinsic pontine gliomas)	Unknown: n=25
REMBRANDT	(2, 3)	GSE108474	n=228	Glioblastoma	not provided
SUN	(1)	GSE4290	n=77	Glioblastoma	not provided
TCGA	(6)		n=507	Glioblastoma	wildtype: n=295 mutant: n=19 Unknown: n=193
TUYSUZ	(11)	GSE90598	n=16	Glioblastoma	wildtype: n=12 mutant: n=4

Supplementary table 5: List of siRNA sequences

Target gene and siRNA name	SiRNA sequence
Dharmacon	
Non-targeting	5’- UAAGGCUAUGAAGAGAUAC -3’
	5’- AUGUAUUGGCCUGUAUUAG -3’
	5’- AUGAACGUGAAUUGCUCAA -3’
	5’- UGGUUUACAUGUCGACUAA -3’
ETS1 si2	5’- GGACCGUGCUGACCUCAAU -3’
ETS1 si3	5’- GGAAUUACUCACUGAUAAA -3’
MYBL2 si4	5’- UAACCGCACUGACCAGCAA -3’
MYBL2 si5	5’- GUAACAGCCUCACGCCCAA -3’
siPool Biotech	
Negative Control si Pool	5’- UAGCGACUAAACACAUCAA -3’
	5’- UAAGGCUAUGAAGAGAUAC -3’
	5’- AUGUAUUGGCCUGUAUUAG -3’
	5’- AUGAACGUGAAUUGCUCAA -3’
E2F6 si Pool	5’- TCACAAGTTAAGGAACTGC -3’
	5’- TATTCTGTCAAACAGTACG -3’
	5’- TCTGCTGGAGCTTTAACTG -3’
	5’- TGATAGAGTCTTCTCTGGG -3’
	5’- ACAAATAGACATCGATAGG -3’

Supplementary table 5 (Continuation)

E2F6 si Pool	5’- TCGATAGGTCCGTTGGTGC -3’
	5’- TTTGGTAAAACCTTTGTTG -3’
	5’- AAGAGGTCCCGACACCTTC -3’
	5’- TCAAACAGCTGCTGAGCAC -3’
	5’- AATCTGGTTTCTGCTGGAG -3’
	5’- TTTGTTACTGGTCTGACCC -3’
	5’- TCTGGGAGCTGGAACATCC -3’
	5’- ATGAATGTCTTGATAGGTC -3’
	5’- TCAGTTGCTTACTTCAAGC -3’
	5’- TCTCCTTAAATATAGATGC -3’
	5’- TGTTAACTCAAACAGCTGC -3’
	5’- TGTTCAGACATTTATTGAG -3’
	5’- TGAGAATCAAATTTGATGC -3’
	5’- TTCTTTAAAAGCAATATTC -3’
	5’- TCTGGATGAGTGCTCTCAG -3’
	5’- TCTCAGATGAAGAGGTCCC -3’
	5’- AATGCCATCAGTTGCTTAC -3’
	5’- TAGGTCACATATGCTAGTC -3’
	5’- AAGCAATTCTTCACTTTGC -3’
	5’- ATCCTTAATTAACTCATCC -3’
	5’- TTTAACTGCAATGACGATC -3’
	5’- TTACTCAGTAATCTAAGTG -3’
	5’- ATGCTAGTCTTTCATTTTC -3’
	5’- TTATTGAGCACTTCTTAAG -3’
	5’- AATGACGATCTGTTCATGG -3’

Supplementary table 6: List of RT-qPCR primers

Primer	**Sequence**
4EBP1	FW: 5’-AGCCCTTCCAGTGATGAGC-3’ RV: 5’-TGTCCATCTCAAACTGTGACTCTT-3’
E2F6	FW: 5’-CGTTTTGATGTATCGCTGGTTTAT-3’ RV: 5’- TGCAACCTTGTTTAAGTCAAGAATACC-3’
ETS1	FW: 5’-AGTGGTGAGGCAAGGACCTA-3’ RV: 5’- ATCCCAAAAGGGGTAGCAAG-3’ (13)
GusB	FW: 5’-GTTTTTGATCCAGACCCAGATG-3’ RV: 5’-GCCCATTATTCAGAGCGAGTA-3’
MYBL2	FW: 5’-ACCTCCCTGAGGAACCATCT-3’ RV: 5’-AGGACTTGCTGCTGATGTGA-3’ (14)
PPIA	FW: 5’-TTATTTGGGTTGCTCCCTTC-3’ RV: 5’-AAGTGTGCCAAATCTGCAAG-3’
β-actin	FW: 5’-TCCCCCAACTTGAGATGTATG-3’ RV: 5’-ACTGGTCTCAAGTCAGTGTACAGG-3’

Supplementary table 7: List of antibodies

Antibody	Company	Catalog number
4EBP1 (53H11)	Cell signaling, Cambridge, UK	# 9644S
E2F1	Cell signaling	# 3742S
E2F6	Abcam, Cambridge, UK	# EPR11201
eEF2	Cell signaling	# 2332S
ETS1 (D808A)	Cell signaling	# 14069S
FOXM1 (D3F2B)	Cell signaling	# 20459S
GAPDH (14C10)	Cell signaling	# 2118S
HIF-1alpha (D2U3T)	Cell signaling	# 14179S
IRDye® 800CW Goat anti-Mouse IgG Secondary Antibody	LI-COR Bioscience, Bad Homburg, Germany	# 925-32210
IRDye® 800CW Goat anti-Rabbit IgG Secondary Antibody	LI-COR Bioscience	# 925-32211
JUN (60A8)	Cell signaling	# 9165L
MYBL2	Abcam	# ab12296
VINCULIN	Cell signaling	# 4650S
β-ACTIN	Sigma Aldrich, St Louis, USA	# A2228

References

1. Sun L, Hui AM, Su Q, Vortmeyer A, Kotliarov Y, Pastorino S, et al. Neuronal and glioma-derived stem cell factor induces angiogenesis within the brain. Cancer Cell. 2006;9(4):287-300.

2. Gusev Y, Bhuvaneshwar K, Song L, Zenklusen JC, Fine H, Madhavan S. The REMBRANDT study, a large collection of genomic data from brain cancer patients. Sci Data. 2018;5:180158.

3. Madhavan S, Zenklusen JC, Kotliarov Y, Sahni H, Fine HA, Buetow K. Rembrandt: helping personalized medicine become a reality through integrative translational research. Mol Cancer Res. 2009;7(2):157-67.

4. Griesinger AM, Birks DK, Donson AM, Amani V, Hoffman LM, Waziri A, et al. Characterization of distinct immunophenotypes across pediatric brain tumor types. Journal of immunology. 2013;191(9):4880-8.

5. Murat A, Migliavacca E, Gorlia T, Lambiv WL, Shay T, Hamou MF, et al. Stem cell-related "self-renewal" signature and high epidermal growth factor receptor expression associated with resistance to concomitant chemoradiotherapy in glioblastoma. J Clin Oncol. 2008;26(18):3015-24.

6. Cancer Genome Atlas Research N, Weinstein JN, Collisson EA, Mills GB, Shaw KR, Ozenberger BA, et al. The Cancer Genome Atlas Pan-Cancer analysis project. Nat Genet. 2013;45(10):1113-20.

7. Freije WA, Castro-Vargas FE, Fang Z, Horvath S, Cloughesy T, Liau LM, et al. Gene expression profiling of gliomas strongly predicts survival. Cancer research. 2004;64(18):6503-10.

8. Gravendeel LA, Kouwenhoven MC, Gevaert O, de Rooi JJ, Stubbs AP, Duijm JE, et al. Intrinsic gene expression profiles of gliomas are a better predictor of survival than histology. Cancer research. 2009;69(23):9065-72.

9. Kawaguchi A, Yajima N, Tsuchiya N, Homma J, Sano M, Natsumeda M, et al. Gene expression signature-based prognostic risk score in patients with glioblastoma. Cancer Sci. 2013;104(9):1205-10.

10. Paugh BS, Broniscer A, Qu C, Miller CP, Zhang J, Tatevossian RG, et al. Genome-wide analyses identify recurrent amplifications of receptor tyrosine kinases and cell-cycle regulatory genes in diffuse intrinsic pontine glioma. J Clin Oncol. 2011;29(30):3999-4006.

11. Gulluoglu S, Tuysuz EC, Sahin M, Kuskucu A, Kaan Yaltirik C, Ture U, et al. Simultaneous miRNA and mRNA transcriptome profiling of glioblastoma samples reveals a novel set of OncomiR candidates and their target genes. Brain Res. 2018;1700:199-210.

12. Zhao Z, Zhang KN, Wang Q, Li G, Zeng F, Zhang Y, et al. Chinese Glioma Genome Atlas (CGGA): A Comprehensive Resource with Functional Genomic Data from Chinese Glioma Patients. Genomics Proteomics Bioinformatics. 2021;19(1):1-12.

13. Khanna A, Mahalingam K, Chakrabarti D, Periyasamy G. Ets-1 expression and gemcitabine chemoresistance in pancreatic cancer cells. Cell Mol Biol Lett. 2011;16(1):101-13.

14. Tripathi V, Shen Z, Chakraborty A, Giri S, Freier SM, Wu X, et al. Long noncoding RNA MALAT1 controls cell cycle progression by regulating the expression of oncogenic transcription factor B-MYB. PLoS Genet. 2013;9(3):e1003368.

6.3. Kaplan-Meier analysis of medulloblastoma patients according to *EIF4EBP1* levels

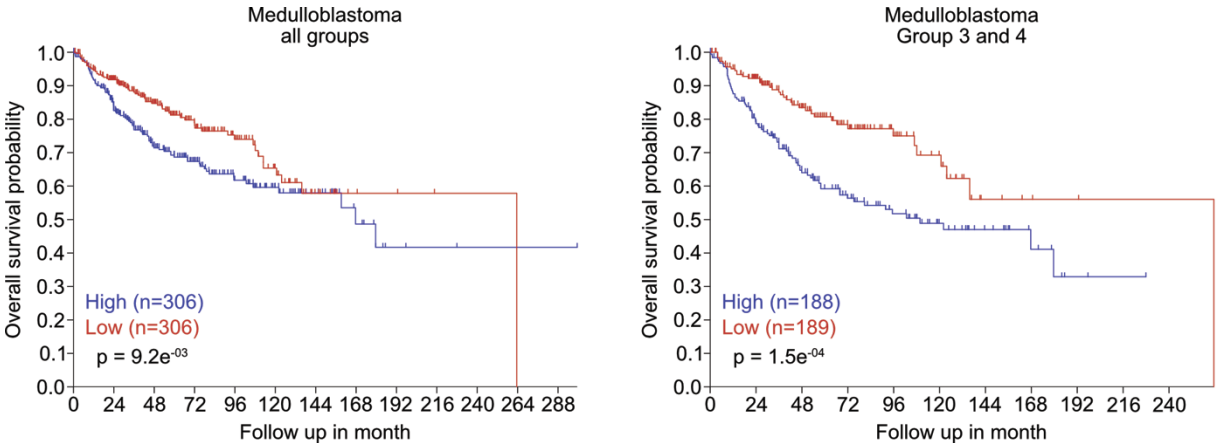

Overall survival analysis of medulloblastoma patients according to *EIF4EBP1* levels. Kaplan-Meier analysis estimates of overall survival of all medulloblastoma (left) or group 3 and 4 (right) patients stratified by their *EIF4EBP1* mRNA (cut-off: median) in the Cavalli cohort (CAVALLI et al. 2017) using R^2 AMC (R^2 AMC; http://r2.amc.nl).

6.4. Manuscript III

EIF4EBP1 is transcriptionally upregulated by MYCN and associates with poor prognosis in neuroblastoma

Kai Voeltzke[1], Katerina Scharov[1,2], Cornelius Funk[3,4,5], Alisa Kahler[1], Daniel Picard[1,2,6], Laura Hauffe[1], Martin F. Orth[3], Marc Remke[1,2,6], Irene Esposito[7], Thomas Kirchner[8,9], Alexander Schramm[10], Barak Rotblat[11], Thomas G. P. Grünewald[3,4,5,12], Guido Reifenberger[1,6], Gabriel Leprivier[1*]

[1]Institute of Neuropathology, Heinrich Heine University, Medical Faculty, and University Hospital Düsseldorf, Düsseldorf, Germany.

[2]Department of Pediatric Oncology, Hematology, and Clinical Immunology, Heinrich Heine University, Medical Faculty, and University Hospital Düsseldorf, Düsseldorf, Germany.

[3]Max-Eder Research Group for Pediatric Sarcoma Biology, Institute of Pathology, Faculty of Medicine, LMU Munich, Munich, Germany.

[4]Division of Translational Pediatric Sarcoma Research, German Cancer Research Center (DKFZ), Heidelberg, Germany.

[5]Hopp Children's Cancer Center (KiTZ), Heidelberg, Germany.

[6]German cancer consortium (DKTK), partner site Essen/Düsseldorf, Düsseldorf, Germany.

[7]Institute of Pathology, Heinrich Heine University, Medical Faculty, and University Hospital Düsseldorf, Düsseldorf, Germany.

[8]Institute of Pathology, Faculty of Medicine, LMU Munich, Munich, Germany.

[9]German cancer consortium (DKTK) partner site Munich, Munich, Germany.

[10]Department of Medical Oncology, West German Cancer Center, University of Duisburg-Essen, Essen, Germany.

[11]Department of Life Sciences, Ben-Gurion University of the Negev, Beer Sheva, Israel; The National Institute for Biotechnology in the Negev, Beer Sheva, Israel.

[12]Institute of Pathology, Heidelberg University Hospital, Heidelberg, Germany.

***Corresponding author:**

Dr. Gabriel Leprivier, Institute of Neuropathology, Heinrich Heine University Düsseldorf, Moorenstrasse 5, D-40225 Düsseldorf, Germany; E-mail: gabriel.leprivier@med.uni-duesseldorf.de.

Running title: *EIF4EBP1* is a prognosis factor in neuroblastoma

ABSTRACT

Neuroblastoma (NB) accounts for 15% of cancer-related deaths in childhood despite considerable therapeutic improvements. While several risk factors, including *MYCN* amplification and alterations in RAS and p53 pathway genes, have been defined in NB, the clinical outcome is very variable and difficult to predict. Since genes of the mechanistic target of rapamycin (mTOR) pathway are up-regulated in *MYCN*-amplified NB, we aimed to define the predictive value of the mTOR substrate-encoding gene eukaryotic translation initiation factor 4E-binding protein 1 (*EIF4EBP1*) expression in NB patients. Using publicly available data sets, we found that *EIF4EBP1* mRNA expression is positively correlated with *MYCN* expression and elevated in stage 4 and high-risk NB patients. In addition, high *EIF4EBP1* mRNA expression is associated with reduced overall and event-free survival in the entire group of NB patients in three cohorts, as well as in stage 4 and high-risk patients. This was confirmed by monitoring the clinical value of 4EBP1 protein expression, which revealed that high levels of 4EBP1 are significantly associated with prognostically unfavorable NB histology. Finally, functional analyses revealed that *EIF4EBP1* expression is transcriptionally controlled by MYCN binding to the *EIF4EBP1* promoter in NB cells. Our data highlight that *EIF4EBP1* is a direct transcriptional target of MYCN whose high expression is associated with poor prognosis in NB patients. Therefore, *EIF4EBP1* may serve to better stratify patients with NB.

Abstract word count: 222 words.

Key words: Neuroblastoma, MYCN, mTOR, 4EBP1

INTRODUCTION

Neuroblastoma (NB) is a pediatric malignant tumor that develops from progenitor cells of the sympathetic nervous system and the adrenal glands [1,2]. NB is the most commonly occurring extracranial solid tumor in childhood and the major cause of cancer-related mortality in infants [2]. NB tumors are classified into five stages (1, 2, 3, 4 and 4S) according to tumor size, the presence of metastasis and the outcome of surgical resection [1]. Noteworthy, stage 4S represents a special form of NB in infants that is associated with a high chance of spontaneous regression despite metastatic spread [1]. Apart from surgical resection, treatment options may include response-adjusted chemotherapy for low to intermediate risk groups or a mix of surgery, high-dose chemotherapy, immunotherapy, and radiation for patients belonging to the high-risk group. The risk level is determined based on the tumor stage combined with age at diagnosis, tumor ploidy, genetic alterations and tumor histology [1,3]. However, NB represents a particularly heterogeneous type of cancer, posing challenges to precisely predict therapeutic response and clinical outcome in the individual patient [4,5]. While some NB tumors may spontaneously regress, high-risk patients have an increased likelihood of relapse and available treatment options for relapsed patients are rarely successful. Indeed, the 5-year overall survival rate for high-risk patients is ranging from 31% to 86%, in contrast to 97-100% for low-risk patients [6]. In addition, success rates of second line treatment in relapsed patients remain poor [5,7]. Therefore, it is critical to define novel stratification factors for NB patients to better predict individual risk and to facilitate administration of the most appropriate therapeutic option.

NB is rarely familial (1-2%) and only few predisposition genes, such as *PHOX2B* and *ALK*, have been reported [4,8–10]. Genetically, several acquired alterations have been detected in NB and linked to patient outcome. These include gain-of-function mutations in *ALK*, gain of chromosome arm 17q, loss of chromosome arm 11q, amplification of *MYCN* [4,11], and, more recently reported, alterations in genes related to the RAS and p53 pathways [12]. *MYCN* amplification is found in about 20% of NB and is associated with aggressive tumors, therapy resistance and poor survival [13]. *MYCN* is a member of the *MYC* oncogene family and encodes a transcription factor that recognizes a specific DNA element referred to as E-box [14,15]. This allows MYCN to regulate the transcription of genes involved in cell cycle progression, proliferation, differentiation and survival [13]. MYCN is a strong driver of NB tumorigenesis, as tissue-specific overexpression of MYCN is sufficient to induce NB tumor development in

mouse models [16]. Mechanistically, MYCN is proposed to rewire metabolism to enable NB tumor cells to proliferate, in turn preserving the intracellular redox balance while producing enough energy by inducing a glycolytic switch [17–19]. In particular, MYCN actively augments the transcription of multiple genes whose products are involved in the protein synthesis machinery [18]. Even though MYCN represents a highly attractive therapeutic target in NB, as a transcription factor that lacks hydrophobic pockets which can be targeted by drug-like small molecules, it is still considered as being "undruggable" [20,21]. Thus, identification of downstream effectors involved in MYCN-driven NB progression is a promising approach to uncover novel targets for molecularly guided therapeutic approaches.

To better delineate the molecular basis of *MYCN*-amplified NB aggressiveness, several approaches have been undertaken. In particular, RNA-sequencing (RNA-seq) has been used to uncover the set of genes induced in *MYCN*-amplified compared to *MYCN*-non-amplified NB [22]. Strikingly, this analysis identified regulators of protein synthesis which are components of the mechanistic target of rapamycin (mTOR) pathway, including the mTOR target eukaryotic initiation factor 4E binding protein 1 (*EIF4EBP1*). The corresponding protein, 4EBP1, is inhibited through mTOR-mediated phosphorylation when nutrients are available, leading to active mRNA translation initiation [23]. Under nutrient-deprived conditions, when mTOR is inhibited, 4EBP1 gets activated and thus binds to the translation initiation factor eIF4E, in turn blocking cap-dependent mRNA translation initiation [23]. At the cellular level, 4EBP1 is negatively regulating proliferation and mitochondrial activity [24,25]. The exact role of 4EBP1 in cancer is still debated. 4EBP1 was found to exert a tumor suppressive function *in vivo*, as 4EBP1 knock-out leads to enhanced tumor formation in mouse models of head and neck squamous cell carcinoma [26], and prostate cancer [27]. In contrast, 4EBP1 was shown to mediate angiogenesis and facilitate tumor growth in a breast cancer model *in vivo*, highlighting a cancer type-specific function of 4EBP1 [28]. In keeping with that, the clinical relevance of *EIF4EBP1* expression depends on the tumor type. *EIF4EBP1* was reported to be overexpressed in a number of tumor entities in adults [29], including breast cancer [30], in which *EIF4EBP1* is amplified as part of the 8p11-12 amplicon, as well as in ovarian and prostate cancer [31,32]. In breast and liver cancer, high *EIF4EBP1* expression has been associated with poor survival [30,33]. In contrast, *EIF4EBP1* expression was found to be reduced in head and neck cancer, in which low expression is correlated with poor prognosis [26]. In NB, the expression of *EIF4EBP1*_is deregulated, even though contradictory findings have been

reported. While *EIF4EBP1* was characterized as a gene upregulated in *MYCN*-amplified versus *MYCN*-non-amplified NB tissues and cells [22], another study reported that *EIF4EBP1* levels were higher in favorable stages of NB as compared to advanced stage 4 tumors [34]. In addition, Meng *et al.* showed that *EIF4EBP1* is part of a gene signature that predicts poor overall survival [35]. However, it was not investigated whether *EIF4EBP1* expression alone can predict NB patient prognosis. Thus, the clinical relevance of *EIF4EBP1* expression in NB needs further evaluation. Overexpression of *EIF4EBP1* in cancer is mediated by certain transcription factors, such as MYC [36,37], androgen receptor [38], and the stress regulators ATF4 [39] and HIF-1 [40], which all bind to and thereby modulate the activity of the *EIF4EBP1* promoter. More specifically, ChIP-sequencing (ChIP-seq) revealed binding of MYCN to the *EIF4EBP1* promoter in NB cells, and MYCN was reported to impact *EIF4EBP1* transcription, pointing to *EIF4EBP1* as a potential MYCN target gene [41,42]. However, how MYCN exactly controls the *EIF4EBP1* promoter is still poorly understood.

In this study, we analyzed publicly available NB patient data sets and revealed that *EIF4EBP1* is overexpressed in NB compared to normal tissues, is significantly co-expressed with *MYCN*, and is elevated in high-risk relatively to low-risk tumor groups. High *EIF4EBP1* levels were found to be significantly linked to poor overall survival in all NB patients, as well as in the more aggressive stage 4 and high-risk groups. In addition, immunohistochemistry staining of NB tissues confirmed the mRNA-based associations and showed that high 4EBP1 protein expression associates with unfavorable histology in NB. Finally, by applying gene reporter assays and by modulating MYCN expression *in vitro*, we found that MYCN upregulates the *EIF4EBP1* promoter activity by binding to three distinct E-boxes.

MATERIALS AND METHODS

Databases

The RNA-seq, microarray and ChIP-seq data were retrieved from 'R2: Genomics Analysis and Visualization Platform' (http://r2.amc.nl). Data were visualized with IGV or Affinity Designer. For the MYCN occupancy profile in BE(2)-C cells, the ChIP-seq data by Durbin *et al.* (GSE94824) were accessed using the human genome GRCh 38/hg 38. For the initial across dataset analysis, "Normal Adrenal gland" dataset from R2 (corresponding to samples taken from multiple data sets [GSE3526, GSE7307, GSE8514] and combined into a single data set) and four publicly

available and independent cohorts, namely the Versteeg *et al.* (GSE16476), Lastowska *et al.* (GSE13136), Hiyama *et al.* (GSE16237), and Delattre *et al.* (GSE14880) datasets were used. The normalization was done automatically by R2 using MAS5.0. The remaining expression, amplification and survival data consisted of the independent SEQC/ MAQC-III Consortium GSE49710), Kocak *et al.* study (GSE45547) and Neuroblastoma Research Consortium [NRC] (GSE49710), Kocak (GSE45547) and NRC (GSE85047) cohorts. For the expression analysis of TH-MYCN transgenic NB model, the dataset from Balamuth *et al.* (GSE17740) was used. For the expression analysis of SH-SY5Y cells treated with all-trans retinoic acid (RA), the dataset from Takeda *et al.* (GSE9169) was used.

Immunohistochemistry

For immunohistochemistry, deparaffinated tissue sections were pretreated with citrate buffer at 98°C for 20 min, cooled down to room temperature, and blocked with 2% horse serum, avidin blocking solution and biotin blocking solution (Avidin/Biotin Blocking Kit, SP-2001, Vector Laboratories, Burlingame, CA, USA) for 10 min each. Staining for 4EBP1 was carried out with monoclonal anti-4EBP1 raised in rabbit (1:200; ab32024, Abcam, Cambridge, UK) for 2 h at 37°C. Detection was carried out using the Dako REAL detection system, alkaline phosphatase/RED, rabbit/mouse following manufacturer´s instructions (Detection Kit #K5005, Agilent Technologies, Santa Clara, CA, USA). Immunostained tissue sections were counterstained with hematoxylin solution according to Mayer (T865.1, Roth, Karlsruhe, Germany).

Evaluation of immunoreactivity of 4EBP1 was carried out in analogy to scoring of hormone receptor Immune Reactive Score (IRS) ranging from 0–12. The percentage of cells with expression of the given antigen was scored and classified in five grades (grade 0 = 0–19%, grade 1 = 20–39%, grade 2 = 40–59%, grade 3 = 60–79% and grade 4 = 80−100%). In addition, the intensity of marker immunoreactivity was determined (grade 0 = none, grade 1 = low, grade 2 = moderate and grade 3 = strong). The product of these two grades defined the final IRS. IRS 0-6 was considered as "low" staining level while IRS 7-12 was categorized as "high" staining level.

Tissue microarrays (TMAs) were constructed by taking three representative cores (each 1 mm in diameter) from respective blocks exhibiting at least 80% viable tumor tissue. Tumor blocks were retrieved from the archives of the Institutes of Pathology of the LMU Munich or the

University Hospital Düsseldorf with IRB approval (study numbers 550-16 UE for LMU Munich and 2018-174 for the University Hospital Düsseldorf). Informed consent was obtained from all patients.

Statistics

All experiments were, if not otherwise stated, independently carried out at least three times. Statistical significance was calculated using Student's t-test or Mann-Whitney U-test in GraphPad Prism 8. For survival analysis, the cohorts were stratified based on relative expression of *EIF4EBP1*. The median was chosen as expression cutoff to determine high and low *EIF4EBP1* level. Statistical significance was determined by the logrank test. Multivariate analysis was performed using the Cox Regression method in SPSS v21 (IBM, Armonk, NY, USA). To calculate significance of the scoring of immunohistochemistry staining, the Chi-square test was used. The data are represented as means +/- standard deviation. A p-value of less than 0.05 was considered significant.

Cell culture

Cells were maintained using standard tissue culture procedures in a humidified incubator at 37°C with 5% CO_2 and atmospheric oxygen. NB cell lines IMR-32 and Kelly, and HEK293-T cells were obtained from American Type Culture Collections (ATCC, Manassas, VA, USA). SHEP-TR-MYCN engineered NB cell lines have been previously described [19]. NB cell lines were cultured in Roswell Park Memorial Institute (RPMI)-1640 medium (Thermo Fisher Scientific, Waltham, MA, USA), while HEK293-T cells were maintained in Dulbecco's modified Eagle medium (DMEM) (Thermo Fisher Scientific). All cell culture media were supplemented with 10% (volume/volume) fetal bovine serum (FBS) (Sigma-Aldrich, St. Louis, MI, USA) and 1% penicillin/streptomycin (Thermo Fisher Scientific). Cells were treated with 3 µg/ml plasmocin (Invivogen, San Diego, CA, USA) to prevent mycoplasma contamination. To induce MYCN expression, SHEP-TR-MYCN cells were treated with 1 µg/ml doxycycline. All cell lines were routinely confirmed to be mycoplasma-free using Venor®GeM Classic kit (Minerva Biolabs, Berlin, Germany). Cell lines were authenticated by STR-profiling (Genomics and Transcriptomics Laboratory, Heinrich Heine University, Dusseldorf, Germany).

RNA extraction, cDNA synthesis and quantitative real time PCR

Total RNA was purified from cells using the RNeasy plus mini kit (QIAgen, Hilden, Germany) according to the manufacturer's handbook. RNA concentration and purity were assessed by

spectrophotometry using the NanoDrop2000 (Thermo Fisher Scientific). Subsequently, each sample was diluted to a concentration of 100 ng/µl in nuclease-free water. For cDNA synthesis, 1 µg RNA was processed in a total reaction volume of 20 µl using the High-Capacity cDNA Reverse Transcription kit (Applied Biosystems, Waltham, MA, USA), following the manufacturer's protocol. Quantitative real time reverse transcription PCR was performed using SYBR green PCR master mix (Applied Biosystems) and the CFX384 Touch Real-Time PCR Detection System (Bio-Rad Laboratories, Hercules, CA, USA). Relative expression levels of *MYCN* and *EIF4EBP1* were normalized to internal housekeeping genes *GUSB* and *PPIA*. The primer list can be found in supplementary table 1.

Immunoblot analysis of protein expression

Cells were washed with phosphate buffered saline (PBS) and lysed in radioimmunoprecipitation assay (RIPA) buffer (150 mM NaCl, 50 mM Tris-HCl, pH 8, 1% Triton X-100, 0.5% sodium deoxycholate, and 0.1% SDS) supplemented with protease inhibitors (Sigma-Aldrich) and phosphatase inhibitors mix (PhosphoSTOP, Roche, Penzberg, Germany). Cell lysates were centrifuged at 21,000 rpm for 15 min at 4°C to separate cell debris and DNA from protein lysates. Protein concentration was measured with the BCA protein assay kit (Thermo Fisher Scientific), according to manufacturer's protocol. Protein lysates were separated by SDS-PAGE and transferred onto a nylon membrane. The membrane was incubated for 1 h in Tris-buffered saline Tween (TBST) (50 *mM* Tris-Cl, 150 *mM* NaCl, pH 7.5, 0.1% Tween-20) containing 5% bovine serum albumin (BSA), to prevent non-specific antibody binding, followed by an overnight incubation at 4°C with the following primary antibodies: 4EBP1 (1:1,000; #9644, Cell Signaling Technology, Cambridge, UK), MYCN (1:1,000; #9405, Cell Signaling Technology), GAPDH (1:1,000; #2118, Cell Signaling Technology), and β-Actin (1:5,000; #A2228, Sigma-Aldrich). The secondary antibodies IRDye 800CW Goat anti-Rabbit (1:10,000; #926-32211, LI-COR Biosciences, Bad Homburg, Germany) or IRDye 800CW Goat anti-Mouse (1:10,000; #926-32210, LI-COR Biosciences) were incubated at room temperature for 1 h, followed by detection of the fluorescent signal with the Odyssey CLx imager (LI-COR Biosciences).

Plasmid construction

The promoter region of the human *EIF4EBP1* gene, spanning from -192 to +1372, was inserted into the SacI and BglII restriction sites of the Firefly Luciferase expressing pGL4.22 plasmid

(Promega, Madison, WI, USA). Each of the three identified MYCN binding site was subsequently mutated alone or in a combination of two sites. Each of the E-box sequence has been mutated to CAAGGC. All cloning was performed by GENEWIZ Germany GmbH (Leipzig, Germany).

Luciferase Reporter Assay

For the promoter reporter assay, HEK293-T cells were seeded into 12-well plates and co-transfected the following day with 500 ng of the *EIF4EBP1* WT or mutant promoter pGL4.22 plasmids, 50 ng of the MYCN overexpressing pcDNA3.1 plasmid or empty pcDNA3.1 plasmid, and 3 ng of the *Renilla* Luciferase expressing pRL-SV40 plasmid (Promega) for normalization. For transfection, plasmids were incubated with 3 µl CalFectin (SignaGen laboratories, Rockville, MD, USA) in Opti-MEM (Thermo Fisher Scientific) for 20 min before adding the mix dropwise onto the cells. 48 h post-transfection, cells were passively lysed and processed according to the protocol of the Dual-Luciferase® Reporter Assay System (Promega), besides using only half the recommended volume of detection buffers. Firefly and *Renilla* luciferase activities were sequentially measured using a Tecan Spark plate reader and the ratio of firefly luciferase to *Renilla* luciferase luminescence was calculated. The experiments were repeated independently for three times.

RESULTS

***EIF4EBP1* expression is increased in NB and correlates with *MYCN* expression**

To assess the clinical significance of *EIF4EBP1* expression, we first examined *EIF4EBP1* mRNA levels in NB tumor tissue samples and normal tissues. We pooled microarray data of four different NB cohorts and retrieved expression data from adrenal tissue used as the corresponding normal tissue (Fig. 1a). This indicated that *EIF4EBP1* expression is significantly elevated in NB compared to adrenal gland ($p<0.0001$, Fig. 1a). We then determined whether *EIF4EBP1* expression is related to the *MYCN* amplification status. By comparing the level of *EIF4EBP1* in *MYCN*-amplified versus *MYCN*-non-amplified NB samples, we found that *EIF4EBP1* is expressed at higher levels in *MYCN*-amplified compared to *MYCN*-non-amplified NB in the SEQC and Kocak cohorts [43,44] ($p<0.0001$, Fig. 1b; $p<0.0001$, Fig. 1c). This further supports and extends previous observations made in a limited number of NB samples (n=20) showing *EIF4EBP1* overexpression in *MYCN*-amplified versus *MYCN*-non-amplified NB tumors [22].

Since *MYCN* amplification may result in different levels of *MYCN*, we next investigated whether expression levels of *MYCN* and *EIF4EBP1* in NB correlate with each other. Our analyses highlight a significant coexpression between *MYCN* and *EIF4EBP1* in the SEQC (correlation coefficient [r]=0.564, p<0.0001, Fig. 1d) and Kocak ([r]=0.532, p<0.0001, Fig. 1e) cohorts. These findings are in line with the reports that *EIF4EBP1* is a potential MYCN target gene in NB [41,42]. We also assessed whether the expression of *EIF4EBP1* is determined by NB stages or risk groups, and found that *EIF4EBP1* levels are increased according to NB tumor aggressiveness in two cohorts (Fig. 1f&g). In particular, *EIF4EBP1* is expressed at higher levels in stage 4 NB tumors as compared to stage 1 and stage 2 tumors (stage 4 versus stage 1, p<0.0001, Fig. 1f; p<0.0001 Fig. 1g). Interestingly, samples from stage 4S NB showed significantly lower *EIF4EBP1* levels compared to stage 4 tumors (stage 4S versus stage 4, p<0.01, Fig. 1f; p<0.001, Fig. 1g). In support of this finding, we observed that in the SEQC cohort *EIF4EBP1* expression is higher in high-risk compared to low-risk NB, as based on the Children's Oncology Group (COG) classification (p<0.0001, Fig. 1h). Such clinical information was not available in any other publicly available cohorts with mRNA expression data. Taken together, we present evidence that *EIF4EBP1* is commonly overexpressed in NB tumors and that *EIF4EBP1* level is increased in *MYCN*-amplified NB and advanced NB stages.

***EIF4EBP1* expression is a factor of poor prognosis in NB**

Since we found *EIF4EBP1* mRNA levels to be elevated in aggressive NB subsets, we examined whether *EIF4EBP1* expression is linked to prognosis in NB patients. Kaplan-Meier estimates univocally showed that high *EIF4EBP1* levels (using median expression level as cut off) were significantly associated with reduced overall and event-free survival in three independent cohorts, namely SEQC, Kocak and NRC cohorts [45] (p=3.1e-08, Fig. 2a; p=4.2e-11, Fig. 2b; p=1.7e-06, Fig. 2c, and supplementary Fig. 1a, b&c). To test dependence of *EIF4EBP1* expression as prognostic factor on established factors of poor prognosis, we performed multivariate analysis to determine the statistical interaction between high *EIF4EBP1* expression and *MYCN* amplification status, tumor stage or age at diagnosis. This indicated that *MYCN* amplification status, tumor stage and age at diagnosis each influenced the prognostic value of high *EIF4EBP1* expression in the SEQC and NRC cohorts (Tables 1&2). Therefore, high *EIF4EBP1* expression is not an independent factor of poor prognosis in NB. However, we uncovered that *EIF4EBP1* expression can predict overall survival in clinically relevant NB subsets, including more advanced and aggressive NB subgroups. Indeed, our analyses

highlighted that high *EIF4EBP1* expression significantly predicted reduced overall survival in *MYCN*-non-amplified patients of the SEQC and NRC cohorts (p=3.8e-03, Fig. 2d; p=0.04, Fig. 2e), while it was significant for event-free survival only in the SEQC cohort (supplementary Fig. 1d&e). On the other hand, Kaplan-Meier survival estimates in high-risk NB patients (SEQC cohort) revealed that high *EIF4EBP1* levels were correlated with poor overall survival (p=7.4e-03, Fig. 2f), as well as with reduced event-free survival (supplementary Fig. 1f), suggesting that *EIF4EBP1* expression can stratify patients within the most aggressive NB subset. We additionally analyzed the prognostic value of *EIF4EBP1* expression in stage 4 NB patients. We found high *EIF4EBP1* expression to significantly predict decreased overall and event-free survival of stage 4 patients in two independent cohorts (SEQC and NRC cohorts) (p=3.2e-04 Fig. 2g; p=3.8e-03, Fig. 2h and supplementary Fig. 1g&h). This highlights that *EIF4EBP1* expression robustly stratifies patients within the advanced NB subgroups. Altogether, our analyses support that *EIF4EBP1* expression is a factor of poor prognosis in all NB, as well as in high-risk and stage 4 NB.

High 4EBP1 protein expression is associated with prognostically unfavorable histology of NB

To independently confirm the prognostic value of *EIF4EBP1*/4EBP1 in NB and to determine the biomarker potential of 4EBP1 protein expression in NB, we immunohistochemically analyzed NB TMAs consisting of 69 patient samples. Staining of the TMAs with a 4EBP1-specific antibody revealed a cytoplasmic staining (Fig. 3a), consistent with the expected cellular localization of 4EBP1 [46]. We semi-quantitatively evaluated 4EBP1 staining intensity and correlated 4EBP1 immunoreactivity with the NB histological subtypes according to the International Neuroblastoma Pathology Classification (INPC), which distinguishes patients with favorable or unfavorable histology based on grade of neuroblastic differentiation and mitosis-karyorrhexis index. We found that tumors with unfavorable histology more frequently exhibited a high 4EBP1 staining score (IRS 7-12) as compared to tumors with favorable histology (Fig. 3b), indicating that high 4EBP1 protein expression is associated with more aggressive NB subsets.

***EIF4EBP1* promoter activity and transcription is controlled by MYCN**

To delineate how elevated *EIF4EBP1* expression is mechanistically connected to *MYCN* amplification and overexpression in NB, we investigated the transcriptional regulation of *EIF4EBP1* by MYCN. A previous report detected the presence of MYCN on *EIF4EBP1* promoter by ChIP in BE(2)-C, a *MYCN*-amplified NB cell line [41,42]. We validated and further extended

this finding by analyzing ChIP-seq data available from an additional *MYCN*-amplified NB cell line, Kelly. This revealed that MYCN binds the endogenous *EIF4EBP1* promoter region (which encompasses exon 1 and a part of intron 1) at three distinct positions, indicating three potential MYCN binding sites (Fig. 4a). *In silico* analysis of the promoter region sequence confirmed the presence of structural E-boxes at the three occupied locations (Fig. 4b). To evaluate the impact of MYCN on the regulation of *EIF4EBP1* promoter activity, we designed a luciferase-based gene reporter assay by cloning the *EIF4EBP1* promoter region (-192 to +1372) in front of a Firefly Luciferase gene (Fig. 4b). The activity of the wildtype *EIF4EBP1* promoter was dose-dependently increased upon forced expression of MYCN in HEK293-T cells (Fig. 4c), which was accompanied by an upregulation of endogenous 4EBP1 protein level (Fig. 4d). To investigate which E-boxes are necessary for the transcriptional activation of the *EIF4EBP1* promoter by MYCN, either a single or a combination of two of the three potential binding sites were mutated. Mutation of either of the three binding sites alone was sufficient to significantly reduce MYCN-induced promoter activity (Fig. 4e). Any combinations of two mutated binding sites further reduced promoter activity driven by MYCN overexpression (Fig. 4e), suggesting that two binding sites, without a specific preference of one over another, are needed for full induction of *EIF4EBP1* promoter activity by MYCN. We next intended to confirm whether MYCN directly regulates *EIF4EBP1* transcription in NB cell lines. To do so, we chose two *MYCN*-amplified NB cell lines, IMR-32 and Kelly, in which we knocked down MYCN expression by siRNA and examined the impact on *EIF4EBP1* mRNA levels by qPCR. The depletion of *MYCN* caused a significant reduction of *EIF4EBP1* transcript levels in both cell lines (Fig. 5a&b). To further support these observations, we assessed the impact of forced MYCN expression on *EIF4EBP1* transcript and protein levels by using SHEP-TR-MYCN cells, which are *MYCN*-non-amplified NB cells engineered to express exogenous MYCN with a tetracycline inducible system [19]. Doxycycline treatment markedly increased *EIF4EBP1* mRNA level over time (Fig. 5c), in parallel with progressive upregulation of MYCN expression (Fig. 5d). This was accompanied by a net increase in the 4EBP1 protein level (Fig. 5d), supporting that MYCN positively controls *EIF4EBP1* mRNA and protein expression in NB cells. To determine whether MYCN regulation of *EIF4EBP1* has relevance during NB differentiation, we analyzed expression data of *MYCN*-non-amplified SH-SY5Y cells treated with RA. This indicated that both *MYCN* and *EIF4EBP1* expression is decreased over time upon treatment, and that levels of both genes are correlated during NB differentiation (Fig. 5e-g). Finally, analyses of

expression data from a transgenic mouse model of MYCN-driven NB (TH-MYCN; [47]) revealed that *EIF4EBP1* expression is upregulated in NB tumors as compared to the corresponding normal tissue, i.e. the ganglia (Fig. 5h). Taken together, our data provide further evidence that *EIF4EBP1* is a transcriptional target of MYCN, potentially providing a mechanistic basis for the observed overexpression of *EIF4EBP1* in *MYCN*-amplified NB patients.

DISCUSSION

MYCN-amplification is accountable for aggressive NB subsets as it has been associated with increased risk of relapse and reduced overall survival of patients [13]. Since MYCN is considered "undruggable", there is a demand for identifying targetable downstream effectors of MYCN [20,21]. In addition, since NB is a clinically heterogenous disease, ranging from spontaneous regression to progression despite aggressive therapies, novel markers that improve patient risk stratification and hence allow for optimal treatment allocation are warranted [4,48,49]. Here, we report that *EIF4EBP1* expression levels are significantly elevated in NB compared to corresponding non-tumor tissues and positively correlate with both *MYCN* expression and *MYCN* amplification status in at least two independent NB patient cohorts. Furthermore, using three independent NB cohorts, we report that high *EIF4EBP1* expression is a strong predictor of poor overall and event-free survival across all NB patients. This was not independent of *MYCN* amplification status, tumor stage or age at diagnosis, which can be explained in part by the regulation of *EIF4EBP1* promoter by MYCN which we characterized. However, *EIF4EBP1* expression can predict prognosis within distinct patient groups like the *MYCN*-non-amplified patient subset, for which little biomarkers have been identified. Moreover, we observed that high *EIF4EBP1* expression was associated with poor prognosis in the group of patients with aggressive stage 4 NB. Of note, less than a third of stage 4 patients carry a *MYCN* amplification. Thus, it may be worth considering that, in addition to *MYCN* amplification status, levels of *EIF4EBP1* expression could help identifying patients carrying clinically more aggressive tumors within the stage 4 NB patient group. *EIF4EBP1* expression was also linked to worse outcome among high-risk NB patients. Given that *MYCN* amplification is not able of predicting outcome within high-risk NB patients [50], it appears that *EIF4EBP1* expression has a prognostic power beyond *MYCN* amplification in this patient subset. Thus, *EIF4EBP1* expression may represent a promising biomarker for prognostic stratification of

high-risk NB patients, in addition to the recently reported genetic alterations in the RAS and p53 pathways [12]. This is further supported by the association we observed between high 4EBP1 protein expression and unfavorable NB histological subtype. Together, our findings highlight a previously underappreciated prognostic factor, i.e., *EIF4EBP1*/4EBP1, which may help refining risk stratification of NB patients, including *MYCN*-non-amplified, stage 4 and high-risk patients, and could potentially assist in tailoring more personalized treatment options. Beyond NB, *EIF4EBP1* expression was reported to be a factor of poor prognosis in breast and liver cancers [30,33], as well as in all TCGA tumor types combined [29]. While our data indicate that *EIF4EBP1* expression has prognostic power in pediatric cancer, together this supports that *EIF4EBP1* expression represents a factor of poor prognosis in a large number of different tumor types.

Our study also extends previous knowledge by providing further experimental evidence to explain the association between *EIF4EBP1* and *MYCN* expression in NB and the overexpression of *EIF4EBP1* in *MYCN*-amplified NB. Our data revealed that MYCN induces transcription of *EIF4EBP1* by regulating its promoter through multiple binding sites, which was originally suggested by detection of MYCN binding to the *EIF4EBP1* promoter by ChIP analysis [41,42]. However, whether MYCN could transcriptionally regulate the *EIF4EBP1* promoter was still elusive. We demonstrate that MYCN activates the *EIF4EBP1* promoter through binding at three distinct E-boxes, which in turn leads to transcriptional increase of *EIF4EBP1* even with low to medium MYCN expression, suggesting a threshold for MYCN level. Together with the previous ChIP analysis, this supports that *EIF4EBP1* is a direct target gene of MYCN in NB cells. These findings are in line with previous studies reporting that MYC controls *EIF4EBP1* by binding its endogenous promoter in colorectal and prostate cancer cells [36,37], as demonstrated by ChIP, highlighting a general regulation of *EIF4EBP1* by MYC family members in cancer cells.

Expression levels of *EIF4EBP1* appear not only elevated in *MYCN*-amplified versus *MYCN*-non-amplified NB but are also upregulated in *MYCN*-non-amplified tumors relative to control tissue. It might be speculated that in *MYCN*-non-amplified NB, *EIF4EBP1* expression may be regulated by transcription factors other than MYCN. In particular, ATF4, which is critical for the metabolic response of NB cells to glutamine starvation [51,52], has been shown to control *EIF4EBP1* promoter and transcription in pancreatic beta cells [39]. This transcription factor is highly expressed in NB, and in particular in advanced stage 4 [52]. In addition, another

transcription factor that is commonly overexpressed in NB is OCT4 [53]. Of note, this transcription factor has been identified by ChIP-seq to bind the promoter region of *EIF4EBP1* in human embryonic stem cells [54,55], thus OCT4 may also activate *EIF4EBP1* transcription in NB cells. Together, these data suggest potential mechanisms underlying the MYCN independent regulation of *EIF4EBP1* expression in *MYCN*-non-amplified NB patients.

Given the prognostic significance of *EIF4EBP1*/4EBP1 in NB, it is possible that 4EBP1 confers advantages to NB tumor growth or tumor cell survival. As evidenced by the presence of necrotic areas flanked by HIF-1 positive staining [56], NB experience metabolic stress, corresponding to nutrient deprivation and hypoxia, as a consequence of abnormal and immature vascularization [57,58]. One important mechanism for cancer cells to adapt to metabolic stress is through reprogramming of mRNA translation [59]. As a major regulator of mRNA translation, 4EBP1 may aid NB cells to cope with hypoxia and nutrient deprivation. This is supported by the report that 4EBP1 promotes survival of breast tumors under hypoxia by stimulating the synthesis of pro-angiogenic factors, like HIF-1 and VEGF, to facilitate tumor angiogenesis *in vivo* [28]. In addition, the control of mRNA translation was shown to be critical to prevent the deleterious effects of MYCN and MYC overexpression, as we and others previously reported [37]. In fact, 4EBP1, by reducing overall protein synthesis, was reported to prevent cell death induced upon MYC overexpression, likely by blunting accumulation of misfolded proteins and proteotoxic ER stress [37]. It is possible that in a similar manner 4EBP1 contributes to inhibit cell death induced by MYCN overexpression in *MYCN*-amplified NB.

In summary, the findings reported here indicate that *EIF4EBP1* is a direct target gene of MYCN in NB, explaining the observed high expression of *EIF4EBP1* in NB, and that *EIF4EBP1* mRNA and protein expression have prognostic values in NB patients, especially for stratifying high-risk NB patients.

AUTHORS CONTRIBUTION

Conception and design: Kai Voeltzke and Gabriel Leprivier.

Provision of study material and patients: Irene Esposito and Thomas Kirchner.

Financial and administrative support: Guido Reifenberger.

Data analysis and interpretation: Kai Voeltzke, Thomas G. P. Grünewald, Alexander Schramm and Gabriel Leprivier.

Critical review and discussion: Barak Rotblat, Marc Remke, Alexander Schramm, Guido Reifenberger and Gabriel Leprivier.

Experimental support: Kai Voeltzke, Katerina Scharov, Cornelius Funk, Alisa Kahler, Daniel Picard, Laura Hauffe and Martin F. Orth.

Manuscript writing: Kai Voeltzke, Guido Reifenberger and Gabriel Leprivier.

Final approval of the manuscript: All authors.

DECLARATION OF INTERESTS

Thomas Kirchner received honoraria for Consulting/Advisory by Amgen, AstraZeneca, BMS, Merck KGaA, MSD, Novartis, Pfizer, Roche, for Research Funding by Merck KGaA and Roche; for talks by Merck KGaA, AstraZeneca.

The other authors declare no conflict of interest.

ACKOWLEDGMENTS

We would like to thank Dr. Bastian Malzkorn (Institute of Neuropathology, Heinrich Heine University Düsseldorf) for helpful discussions.

FUNDING

G.L. was supported by funding from the Elterninitiative Düsseldorf e.V., the Research Commission of the Medical Faculty of Heinrich Heine University, the Deutsche Forschungsgemeinschaft (Grant LE 3751/2-1), and the German Cancer Aid (Grant 70112624). The laboratory of T.G.P.G. is supported by the Barbara und Wilfried Mohr Foundation. BR is supported by the Israel Science Foundation (grant No. 1436/19).

DATA SHARING STATEMENT

The data that support the findings of this study are available from the corresponding author upon reasonable request.

REFERENCES

[1] Maris JM, Hogarty MD, Bagatell R, Cohn SL. Neuroblastoma. The Lancet 2007;369(9579):2106–20. https://doi.org/10.1016/S0140-6736(07)60983-0.

[2] van Arendonk KJ, Chung DH. Neuroblastoma: Tumor Biology and Its Implications for Staging and Treatment. Children (Basel) 2019;6(1). https://doi.org/10.3390/children6010012.

[3] Tolbert VP, Matthay KK. Neuroblastoma: clinical and biological approach to risk stratification and treatment. Cell Tissue Res 2018;372(2):195–209. https://doi.org/10.1007/s00441-018-2821-2.

[4] Maris JM. The biologic basis for neuroblastoma heterogeneity and risk stratification. Current Opinion in Pediatrics 2005;17(1):7–13. https://doi.org/10.1097/01.mop.0000150631.60571.89.

[5] London WB, Castel V, Monclair T, Ambros PF, Pearson ADJ, Cohn SL et al. Clinical and biologic features predictive of survival after relapse of neuroblastoma: a report from the International Neuroblastoma Risk Group project. J Clin Oncol 2011;29(24):3286–92. https://doi.org/10.1200/JCO.2010.34.3392.

[6] Pinto NR, Applebaum MA, Volchenboum SL, Matthay KK, London WB, Ambros PF et al. Advances in Risk Classification and Treatment Strategies for Neuroblastoma. J Clin Oncol 2015;33(27):3008–17. https://doi.org/10.1200/JCO.2014.59.4648.

[7] Simon T, Berthold F, Borkhardt A, Kremens B, Carolis B de, Hero B. Treatment and outcomes of patients with relapsed, high-risk neuroblastoma: results of German trials. Pediatric blood & cancer 2011;56(4):578–83. https://doi.org/10.1002/pbc.22693.

[8] Chen Y, Takita J, Choi YL, Kato M, Ohira M, Sanada M et al. Oncogenic mutations of ALK kinase in neuroblastoma. Nature 2008;455(7215):971–4. https://doi.org/10.1038/nature07399.

[9] Mossé YP, Laudenslager M, Longo L, Cole KA, Wood A, Attiyeh EF et al. Identification of ALK as a major familial neuroblastoma predisposition gene. Nature 2008;455(7215):930–5. https://doi.org/10.1038/nature07261.

[10] Janoueix-Lerosey I, Lequin D, Brugières L, Ribeiro A, Pontual L de, Combaret V et al. Somatic and germline activating mutations of the ALK kinase receptor in neuroblastoma. Nature 2008;455(7215):967–70. https://doi.org/10.1038/nature07398.

[11] Amelio I, Bertolo R, Bove P, Candi E, Chiocchi M, Cipriani C et al. Cancer predictive studies. Biology direct 2020;15(1):18. https://doi.org/10.1186/s13062-020-00274-3.

[12] Ackermann S, Cartolano M, Hero B, Welte A, Kahlert Y, Roderwieser A et al. A mechanistic classification of clinical phenotypes in neuroblastoma. Science (New York, N.Y.) 2018;362(6419):1165–70. https://doi.org/10.1126/science.aat6768.

[13] Huang M, Weiss WA. Neuroblastoma and MYCN. Cold Spring Harb Perspect Med 2013;3(10):a014415. https://doi.org/10.1101/cshperspect.a014415.

[14] Zeid R, Lawlor MA, Poon E, Reyes JM, Fulciniti M, Lopez MA et al. Enhancer invasion shapes MYCN-dependent transcriptional amplification in neuroblastoma. Nat Genet 2018;50(4):515–23. https://doi.org/10.1038/s41588-018-0044-9.

[15] Liu R, Shi P, Wang Z, Yuan C, Cui H. Molecular Mechanisms of MYCN Dysregulation in Cancers. Front. Oncol. 2020;10:625332. https://doi.org/10.3389/fonc.2020.625332.

[16] Weiss WA, Aldape K, Mohapatra G, Feuerstein BG, Bishop JM. Targeted expression of MYCN causes neuroblastoma in transgenic mice. The EMBO journal 1997;16(11):2985–95. https://doi.org/10.1093/emboj/16.11.2985.

[17] Oliynyk G, Ruiz-Pérez MV, Sainero-Alcolado L, Dzieran J, Zirath H, Gallart-Ayala H et al. MYCN-enhanced Oxidative and Glycolytic Metabolism Reveals Vulnerabilities for Targeting Neuroblastoma. iScience 2019;21:188–204. https://doi.org/10.1016/j.isci.2019.10.020.

[18] Boon K, Caron HN, van Asperen R, Valentijn L, Hermus MC, van Sluis P et al. N-myc enhances the expression of a large set of genes functioning in ribosome biogenesis and protein synthesis. The EMBO journal 2001;20(6):1383–93. https://doi.org/10.1093/emboj/20.6.1383.

[19] Tjaden B, Baum K, Marquardt V, Simon M, Trajkovic-Arsic M, Kouril T et al. N-Myc-induced metabolic rewiring creates novel therapeutic vulnerabilities in neuroblastoma. Sci Rep 2020;10(1):7157. https://doi.org/10.1038/s41598-020-64040-1.

[20] Bell E, Chen L, Liu T, Marshall GM, Lunec J, Tweddle DA. MYCN oncoprotein targets and their therapeutic potential. Cancer letters 2010;293(2):144–57. https://doi.org/10.1016/j.canlet.2010.01.015.

[21] Wolpaw AJ, Bayliss R, Büchel G, Dang CV, Eilers M, Gustafson WC et al. Drugging the "Undruggable" MYCN Oncogenic Transcription Factor: Overcoming Previous Obstacles to Impact Childhood Cancers. Cancer Res 2021;81(7):1627–32. https://doi.org/10.1158/0008-5472.CAN-20-3108.

[22] Schramm A, Köster J, Marschall T, Martin M, Schwermer M, Fielitz K et al. Next-generation RNA sequencing reveals differential expression of MYCN target genes and suggests the mTOR pathway as a promising therapy target in MYCN-amplified neuroblastoma. International Journal of Cancer 2013;132(3):E106-15. https://doi.org/10.1002/ijc.27787.

[23] Musa J, Orth MF, Dallmayer M, Baldauf M, Pardo C, Rotblat B et al. Eukaryotic initiation factor 4E-binding protein 1 (4E-BP1): a master regulator of mRNA translation involved in tumorigenesis. Oncogene 2016;35(36):4675–88. https://doi.org/10.1038/onc.2015.515.

[24] Morita M, Gravel S-P, Chénard V, Sikström K, Zheng L, Alain T et al. mTORC1 controls mitochondrial activity and biogenesis through 4E-BP-dependent translational regulation. Cell Metabolism 2013;18(5):698–711. https://doi.org/10.1016/j.cmet.2013.10.001.

[25] Dowling RJO, Topisirovic I, Alain T, Bidinosti M, Fonseca BD, Petroulakis E et al. mTORC1-mediated cell proliferation, but not cell growth, controlled by the 4E-BPs. Science (New York, N.Y.) 2010;328(5982):1172–6. https://doi.org/10.1126/science.1187532.

[26] Wang Z, Feng X, Molinolo AA, Martin D, Vitale-Cross L, Nohata N et al. 4E-BP1 Is a Tumor Suppressor Protein Reactivated by mTOR Inhibition in Head and Neck Cancer. Cancer Res 2019;79(7):1438–50. https://doi.org/10.1158/0008-5472.CAN-18-1220.

[27] Ding M, van der Kwast TH, Vellanki RN, Foltz WD, McKee TD, Sonenberg N et al. The mTOR Targets 4E-BP1/2 Restrain Tumor Growth and Promote Hypoxia Tolerance in PTEN-driven Prostate Cancer. Mol Cancer Res 2018;16(4):682–95. https://doi.org/10.1158/1541-7786.MCR-17-0696.

[28] Braunstein S, Karpisheva K, Pola C, Goldberg J, Hochman T, Yee H et al. A hypoxia-controlled cap-dependent to cap-independent translation switch in breast cancer. Molecular cell 2007;28(3):501–12. https://doi.org/10.1016/j.molcel.2007.10.019.

[29] Wu S, Wagner G. Deep computational analysis of human cancer and non-cancer tissues details dysregulation of eIF4F components and their interactions in human cancers. bioRxiv 2020:2020.10.12.336263. https://doi.org/10.1101/2020.10.12.336263.

[30] Karlsson E, Pérez-Tenorio G, Amin R, Bostner J, Skoog L, Fornander T et al. The mTOR effectors 4EBP1 and S6K2 are frequently coexpressed, and associated with a poor prognosis and endocrine resistance in breast cancer: a retrospective study including patients from the randomised Stockholm tamoxifen trials. Breast cancer research BCR 2013;15(5):R96. https://doi.org/10.1186/bcr3557.

[31] Kremer CL, Klein RR, Mendelson J, Browne W, Samadzedeh LK, Vanpatten K et al. Expression of mTOR signaling pathway markers in prostate cancer progression. The Prostate 2006;66(11):1203–12. https://doi.org/10.1002/pros.20410.

[32] Lee M, Kim EJ, Jeon MJ. MicroRNAs 125a and 125b inhibit ovarian cancer cells through post-transcriptional inactivation of EIF4EBP1. Oncotarget 2016;7(8):8726–42. https://doi.org/10.18632/oncotarget.6474.

[33] Cha Y-L, Li P-D, Yuan L-J, Zhang M-Y, Zhang Y-J, Rao H-L et al. EIF4EBP1 overexpression is associated with poor survival and disease progression in patients with hepatocellular carcinoma. PLOS ONE 2015;10(2):e0117493. https://doi.org/10.1371/journal.pone.0117493.

[34] Fransson S, Abel F, Kogner P, Martinsson T, Ejeskär K. Stage-dependent expression of PI3K/Akt-pathway genes in neuroblastoma. International Journal of Oncology 2013;42(2):609–16. https://doi.org/10.3892/ijo.2012.1732.

[35] Meng X, Li H, Fang E, Feng J, Zhao X. Comparison of Stage 4 and Stage 4s Neuroblastoma Identifies Autophagy-Related Gene and LncRNA Signatures Associated With Prognosis. Front. Oncol. 2020;10:1411. https://doi.org/10.3389/fonc.2020.01411.

[36] Balakumaran BS, Porrello A, Hsu DS, Glover W, Foye A, Leung JY et al. MYC activity mitigates response to rapamycin in prostate cancer through eukaryotic initiation factor 4E-binding protein 1-mediated inhibition of autophagy. Cancer Res 2009;69(19):7803–10. https://doi.org/10.1158/0008-5472.CAN-09-0910.

[37] Tameire F, Verginadis II, Leli NM, Polte C, Conn CS, Ojha R et al. ATF4 couples MYC-dependent translational activity to bioenergetic demands during tumour progression. Nature cell biology 2019;21(7):889–99. https://doi.org/10.1038/s41556-019-0347-9.

[38] Liu Y, Horn JL, Banda K, Goodman AZ, Lim Y, Jana S et al. The androgen receptor regulates a druggable translational regulon in advanced prostate cancer. Science Translational Medicine 2019;11(503). https://doi.org/10.1126/scitranslmed.aaw4993.

[39] Yamaguchi S, Ishihara H, Yamada T, Tamura A, Usui M, Tominaga R et al. ATF4-mediated induction of 4E-BP1 contributes to pancreatic beta cell survival under endoplasmic reticulum stress. Cell Metabolism 2008;7(3):269–76. https://doi.org/10.1016/j.cmet.2008.01.008.

[40] Azar R, Lasfargues C, Bousquet C, Pyronnet S. Contribution of HIF-1α in 4E-BP1 gene expression. Mol Cancer Res 2013;11(1):54–61. https://doi.org/10.1158/1541-7786.MCR-12-0095.

[41] Cheung CHY, Hsu C-L, Tsuei C-Y, Kuo T-T, Huang C-T, Hsu W-M et al. Combinatorial targeting of MTHFD2 and PAICS in purine synthesis as a novel therapeutic strategy. Cell death & disease 2019;10(11):786. https://doi.org/10.1038/s41419-019-2033-z.

[42] Hsu C-L, Chang H-Y, Chang J-Y, Hsu W-M, Huang H-C, Juan H-F. Unveiling MYCN regulatory networks in neuroblastoma via integrative analysis of heterogeneous genomics data. Oncotarget 2016;7(24):36293–310. https://doi.org/10.18632/oncotarget.9202.

[43] SEQC/MAQC consortium. SEQC/MAQC consortium: A comprehensive assessment of RNA-seq accuracy, reproducibility and information. Nature biotechnology 2014;32(9):903–14. https://doi.org/10.1038/nbt.2957.

[44] Kocak H, Ackermann S, Hero B, Kahlert Y, Oberthuer A, Juraeva D et al. Hox-C9 activates the intrinsic pathway of apoptosis and is associated with spontaneous regression in neuroblastoma. Cell death & disease 2013;4(4):e586. https://doi.org/10.1038/cddis.2013.84.

[45] Rajbhandari P, Lopez G, Capdevila C, Salvatori B, Yu J, Rodriguez-Barrueco R et al. Cross-Cohort Analysis Identifies a TEAD4-MYCN Positive Feedback Loop as the Core Regulatory Element of High-Risk Neuroblastoma. Cancer discovery 2018;8(5):582–99. https://doi.org/10.1158/2159-8290.CD-16-0861.

[46] Armengol G, Rojo F, Castellví J, Iglesias C, Cuatrecasas M, Pons B et al. 4E-binding protein 1: a key molecular "funnel factor" in human cancer with clinical implications. Cancer Res 2007;67(16):7551–5. https://doi.org/10.1158/0008-5472.CAN-07-0881.

[47] Balamuth NJ, Wood A, Wang Q, Jagannathan J, Mayes P, Zhang Z et al. Serial transcriptome analysis and cross-species integration identifies centromere-associated protein E as a novel neuroblastoma target. Cancer Res 2010;70(7):2749–58. https://doi.org/10.1158/0008-5472.CAN-09-3844.

[48] Rugolo F, Bazan NG, Calandria J, Jun B, Raschellà G, Melino G et al. The expression of ELOVL4, repressed by MYCN, defines neuroblastoma patients with good outcome. Oncogene 2021;40(38):5741–51. https://doi.org/10.1038/s41388-021-01959-3.

[49] Pieraccioli M, Nicolai S, Pitolli C, Agostini M, Antonov A, Malewicz M et al. ZNF281 inhibits neuronal differentiation and is a prognostic marker for neuroblastoma. PNAS 2018;115(28):7356–61. https://doi.org/10.1073/pnas.1801435115.

[50] Lee JW, Son MH, Cho HW, Ma YE, Yoo KH, Sung KW et al. Clinical significance of MYCN amplification in patients with high-risk neuroblastoma. Pediatric blood & cancer 2018;65(10):e27257. https://doi.org/10.1002/pbc.27257.

[51] Qing G, Li B, Vu A, Skuli N, Walton ZE, Liu X et al. ATF4 regulates MYC-mediated neuroblastoma cell death upon glutamine deprivation. Cancer cell 2012;22(5):631–44. https://doi.org/10.1016/j.ccr.2012.09.021.

[52] Ren P, Yue M, Xiao D, Xiu R, Gan L, Liu H et al. ATF4 and N-Myc coordinate glutamine metabolism in MYCN-amplified neuroblastoma cells through ASCT2 activation. The Journal of pathology 2015;235(1):90–100. https://doi.org/10.1002/path.4429.

[53] Yang S, Zheng J, Ma Y, Zhu H, Xu T, Dong K et al. Oct4 and Sox2 are overexpressed in human neuroblastoma and inhibited by chemotherapy. Oncology reports 2012;28(1):186–92. https://doi.org/10.3892/or.2012.1765.

[54] Gifford CA, Ziller MJ, Gu H, Trapnell C, Donaghey J, Tsankov A et al. Transcriptional and epigenetic dynamics during specification of human embryonic stem cells. Cell 2013;153(5):1149–63. https://doi.org/10.1016/j.cell.2013.04.037.

[55] Čančer M, Hutter S, Holmberg KO, Rosén G, Sundström A, Tailor J et al. Humanized Stem Cell Models of Pediatric Medulloblastoma Reveal an Oct4/mTOR Axis that Promotes Malignancy. Cell Stem Cell 2019;25(6):855-870.e11. https://doi.org/10.1016/j.stem.2019.10.005.

[56] Påhlman S, Mohlin S. Hypoxia and hypoxia-inducible factors in neuroblastoma. Cell Tissue Res 2018;372(2):269–75. https://doi.org/10.1007/s00441-017-2701-1.

[57] Schaaf MB, Garg AD, Agostinis P. Defining the role of the tumor vasculature in antitumor immunity and immunotherapy. Cell death & disease 2018;9(2):115. https://doi.org/10.1038/s41419-017-0061-0.

[58] Lugano R, Ramachandran M, Dimberg A. Tumor angiogenesis: causes, consequences, challenges and opportunities. Cell. Mol. Life Sci. 2020;77(9):1745–70. https://doi.org/10.1007/s00018-019-03351-7.

[59] Leprivier G, Rotblat B, Khan D, Jan E, Sorensen PH. Stress-mediated translational control in cancer cells. Biochimica et biophysica acta 2015;1849(7):845–60. https://doi.org/10.1016/j.bbagrm.2014.11.002.

[60] Nishida Y, Adati N, Ozawa R, Maeda A, Sakaki Y, Takeda T. Identification and classification of genes regulated by phosphatidylinositol 3-kinase- and TRKB-mediated signalling pathways during neuronal differentiation in two subtypes of the human neuroblastoma cell line SH-SY5Y. BMC research notes 2008;1:95. https://doi.org/10.1186/1756-0500-1-95.

FIGURE LEGENDS

Figure 1: *EIF4EBP1* mRNA expression is associated with *MYCN* mRNA expression and is increased in more advanced and aggressive NB subsets. (a) Expression levels of *EIF4EBP1* mRNA in a pool of four different NB cohorts (total n=203), compared to healthy control tissues (adrenal gland, n=13). (b, c) Expression levels of *EIF4EBP1* mRNA n *MYCN*-amplified (n=92, SEQC [b] and n=93, Kocak [c]) compared to *MYCN*-non-amplified (n=401, SEQC [b] and n=550 Kocak [c]) NB patients of the SEQC (b) and Kocak (c) cohorts. (d, e) Expression levels of *EIF4EBP1* mRNA plotted against expression levels of *MYCN* mRNA in SEQC (r=0.5637, d) and Kocak (r=0.5321, e) cohorts. (f, g) Expression levels of *EIF4EBP1* mRNA per NB stage in SEQC (f) and Kocak (g) cohorts. (h) Expression levels of *EIF4EBP1* mRNA in high-risk (n=176) compared to non-high-risk (n=322) NB in the SEQC cohort. Data were retrieved from the R2: Genomics Analysis and Visualization Platform. Statistics were determined using Mann-Whitney U-test. Exact p-values are presented. **P*<0.05, ***P*<0.01, ****P*<0.001, *****P*<0.0001.

Figure 2: *EIF4EBP1* mRNA expression correlates with overall survival in NB patients. (a-c) Kaplan-Meier survival estimates of overall survival of NB patients stratified by their *EIF4EBP1* mRNA expression levels (median cut off) in the SEQC (a), Kocak (b) and NRC (c) cohorts. (d-h) Kaplan-Meier survival estimates of overall survival of patients with *MYCN*-non-amplified NB (d, e), high-risk NB (f) or stage 4 NB (g, h) stratified by their *EIF4EBP1* mRNA expression levels in the indicated NB cohorts. Significance was determined by log rank test. Data were obtained from the R2: Genomics Analysis and Visualization Platform.

Figure 3: 4EBP1 protein expression is associated with histological subtype of NB. (a) Representative images at 40X magnification of low (left panel) and high (right panel) 4EBP1 immunohistochemical staining levels of selected NB samples represented on the NB TMAs. (b) Distribution of NB cases showing low (IRS 0-6) versus high (IRS 7-12) 4EBP1 protein expression in prognostically favorable versus unfavorable histological subtypes according to International Neuroblastoma Pathology Classification (INPC). Fisher's exact test was used to calculate significance. **P*<0.05.

Figure 4: *EIF4EBP1* promoter activity is regulated by MYCN. (a) ChIP peaks of MYCN in the *EIF4EBP1* promoter region in Kelly NB cell line. (b) Scheme of the *EIF4EBP1* promoter reporter highlighting the three E-boxes corresponding to MYCN binding sites. (c) HEK293-T cells were transfected with the wildtype *EIF4EBP1* promoter Firefly Luciferase construct and with the

indicated amounts of MYCN expressing plasmid (pMYCN). A *Renilla* Luciferase vector was used as an internal control. (d) MYCN and 4EBP1 protein expression was monitored in cell lysates from (c) by immunoblot analyses using the indicated antibodies. (e) HEK293-T were transfected with wildtype or different E-box mutants *EIF4EBP1* promoter Firefly Luciferase constructs with or without a MYCN expressing plasmid (pMYCN). A *Renilla* Luciferase vector was used as an internal control. Statistics were determined using Student's t-test or Mann-Whitney U-test. Exact p-values are presented. **P*<0.05, ***P*<0.01, ****P*<0.001, *****P*<0.0001.

Figure 5: *EIF4EBP1* expression is regulated by MYCN in NB. (a, b) Relative *MYCN* and *EIF4EBP1* mRNA levels upon siRNA-mediated knockdown of *MYCN* in the *MYCN*-amplified IMR-32 (a) and Kelly (b) cell lines, as measured by qRT-PCR. (c, d) SHEP-TR-MYCN cells were treated with doxycycline (1 µg/ml) for the indicated times; *EIF4EBP1* mRNA levels were determined by qRT-PCR (c) and levels of MYCN and 4EBP1 proteins were monitored by immunoblot using the indicated antibodies (d). The different 4EBP1 bands correspond to different phosphorylated forms of 4EBP1. (e, f) Expression levels of *MYCN* (e) or *EIF4EBP1* (f) mRNA in SH-SY5Y cells treated with RA for the indicated times (Takeda's dataset, n=2 for each time point; [60]). Statistics were calculated for each time point compared to the control 0 h time point. (g) Expression levels of *EIF4EBP1* mRNA plotted against expression levels of *MYCN* mRNA in SH-SY5Y cells treated with RA (Takeda's dataset, n=2 for each time point; [60]). (h) Relative *EIF4EBP1* mRNA expression in healthy control tissues (ganglia, n=9) and NB tumors (n=26) of a TH-MYCN transgenic mouse model of NB (Balamuth's dataset; [47]). Data were retrieved from the R2: Genomics Analysis and Visualization Platform. Statistics were determined using Student's t-test or Mann-Whitney U-test. Exact p-values are presented. **P*<0.05, ***P*<0.01, ****P*<0.001, *****P*<0.0001.

SUPPLEMENTARY FIGURE LEGENDS

Supplementary Figure 1: *EIF4EBP1* mRNA expression correlates with event-free survival in NB patients. (a-b) Kaplan-Meier survival estimates of event-free survival of NB patients stratified by their *EIF4EBP1* mRNA expression levels (median cut off) in the SEQC (a), Kocak (b) and NRC (c) cohorts. (d-h) Kaplan-Meier estimates of event-free survival of patients with *MYCN*-non-amplified NB (d, e), high-risk NB (f) or stage 4 NB (g, h) stratified by their *EIF4EBP1* mRNA expression levels in the indicated NB cohorts. Significance was determined by log rank test. Data were obtained from the R2: Genomics Analysis and Visualization Platform.

Figure 1

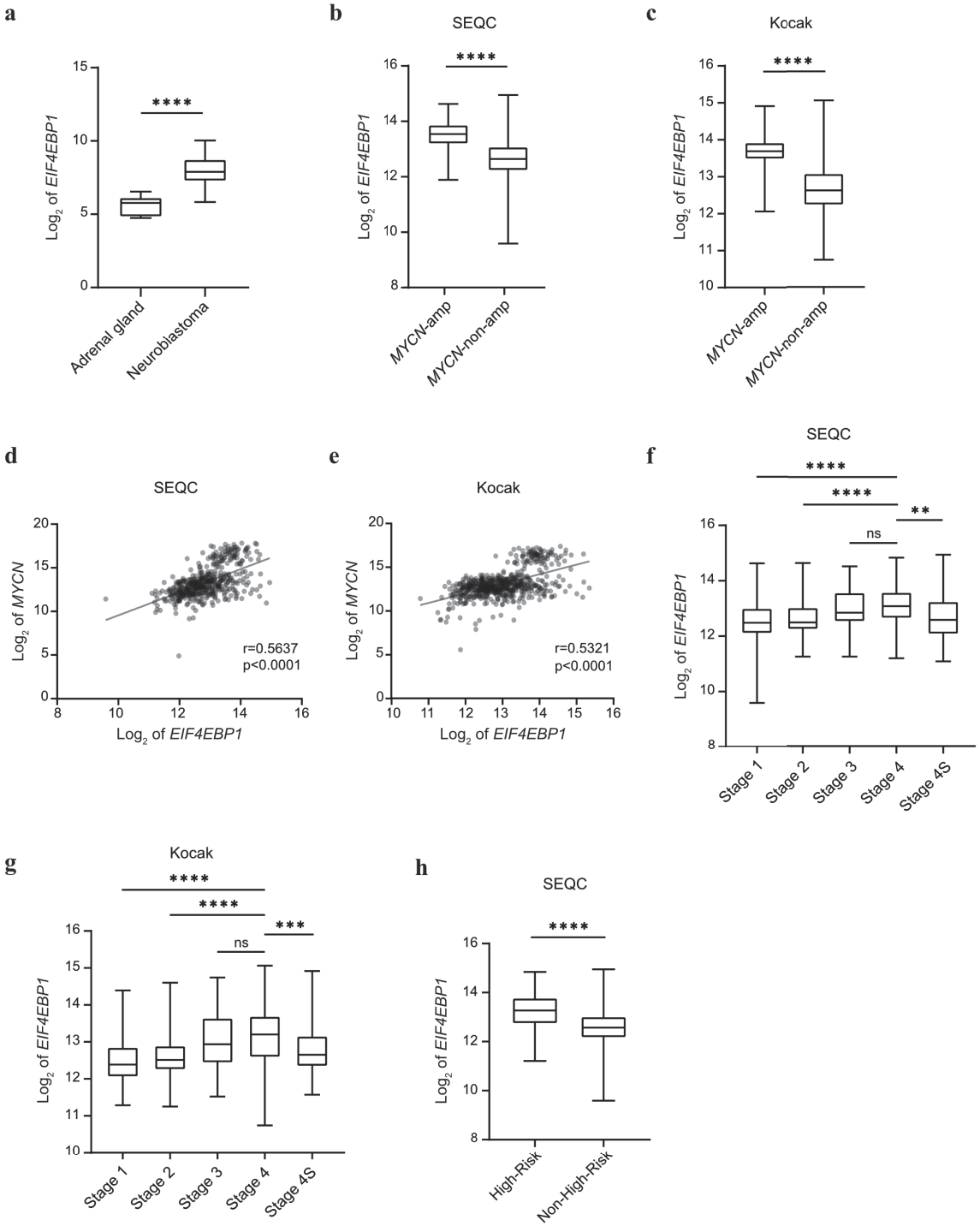
a
Log2 of EIF4EBP1
****
Adrenal gland
Neuroblastoma
b
SEQC
Log2 of EIF4EBP1
****
MYCN-amp
MYCN-non-amp
c
Kocak
Log2 of EIF4EBP1
****
MYCN-amp
MYCN-non-amp
d
SEQC
Log2 of MYCN
r=0.5637
p<0.0001
Log2 of EIF4EBP1
e
Kocak
Log2 of MYCN
r=0.5321
p<0.0001
Log2 of EIF4EBP1
f
SEQC
****
****
**
ns
Log2 of EIF4EBP1
Stage 1
Stage 2
Stage 3
Stage 4
Stage 4S
g
Kocak
****
****
***
ns
Log2 of EIF4EBP1
Stage 1
Stage 2
Stage 3
Stage 4
Stage 4S
h
SEQC
****
Log2 of EIF4EBP1
High-Risk
Non-High-Risk

Figure 2

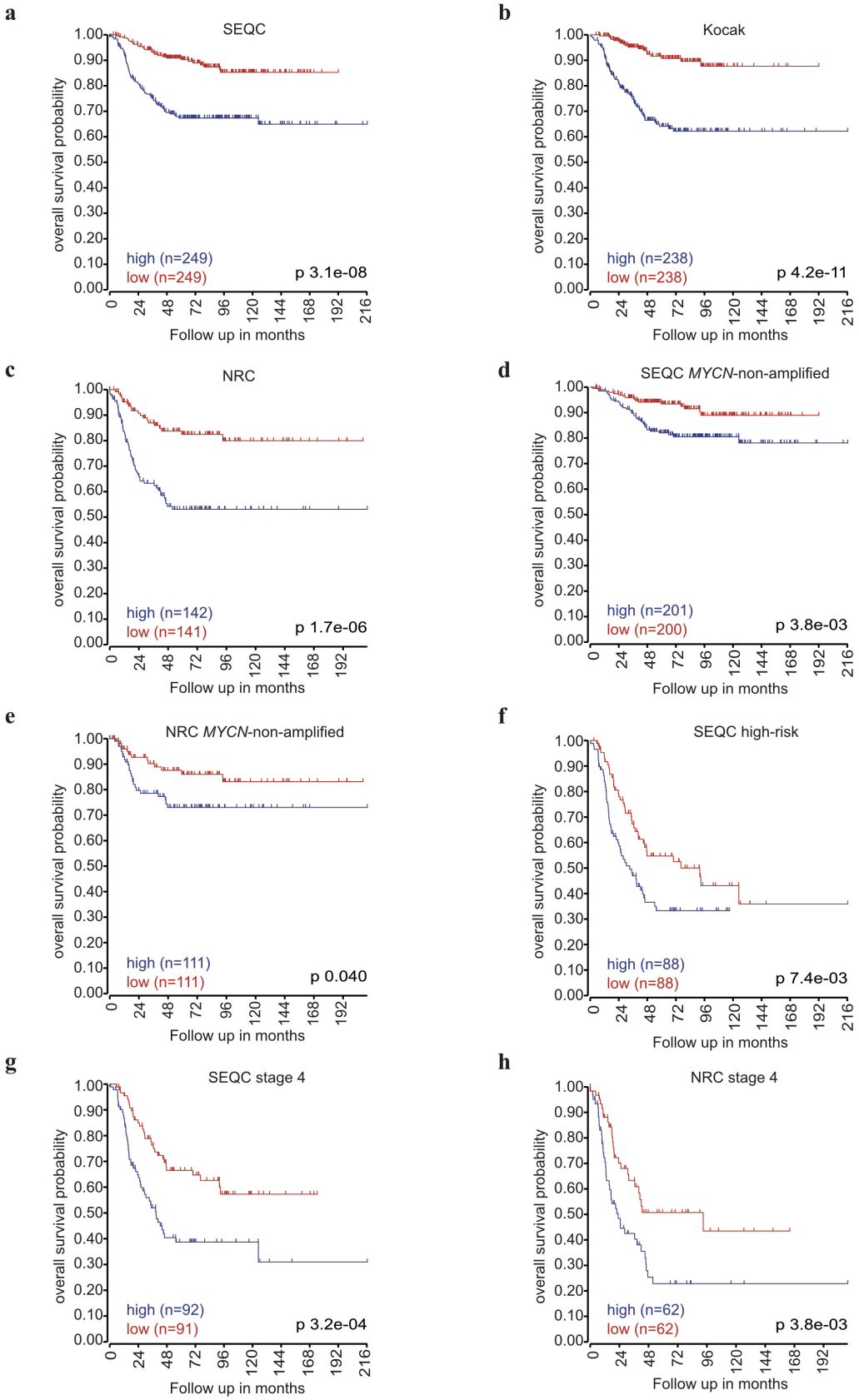
a
SEQC
overall survival probability
high (n=249)
low (n=249)
p 3.1e-08
Follow up in months
b
Kocak
high (n=238)
low (n=238)
p 4.2e-11
c
NRC
high (n=142)
low (n=141)
p 1.7e-06
d
SEQC MYCN-non-amplified
high (n=201)
low (n=200)
p 3.8e-03
e
NRC MYCN-non-amplified
high (n=111)
low (n=111)
p 0.040
f
SEQC high-risk
high (n=88)
low (n=88)
p 7.4e-03
g
SEQC stage 4
high (n=92)
low (n=91)
p 3.2e-04
h
NRC stage 4
high (n=62)
low (n=62)
p 3.8e-03

Figure 3

a

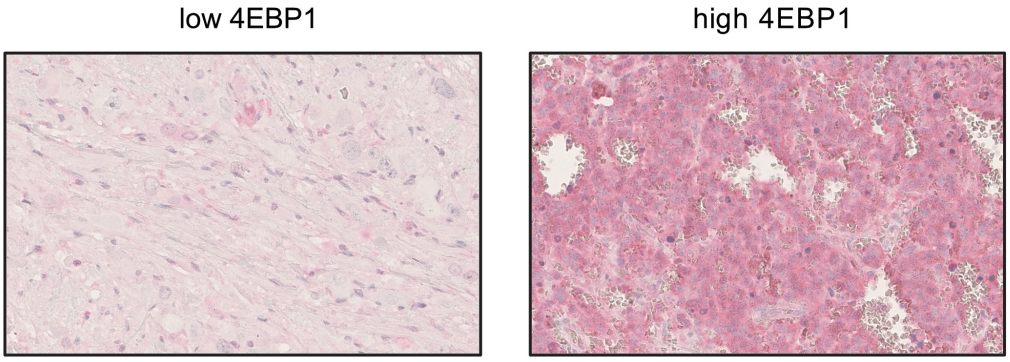
low 4EBP1
high 4EBP1

b

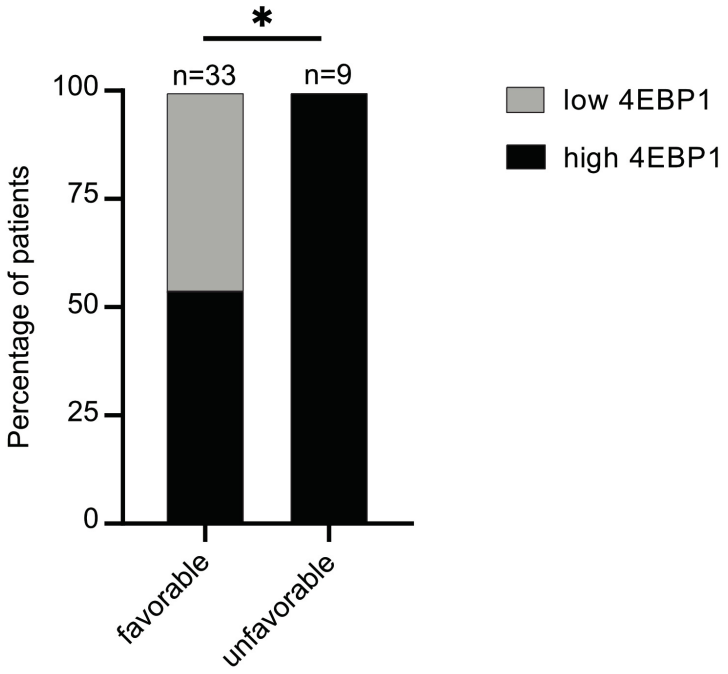
*
n=33
n=9
100
75
50
25
0
Percentage of patients
favorable
unfavorable
low 4EBP1
high 4EBP1

Figure 4

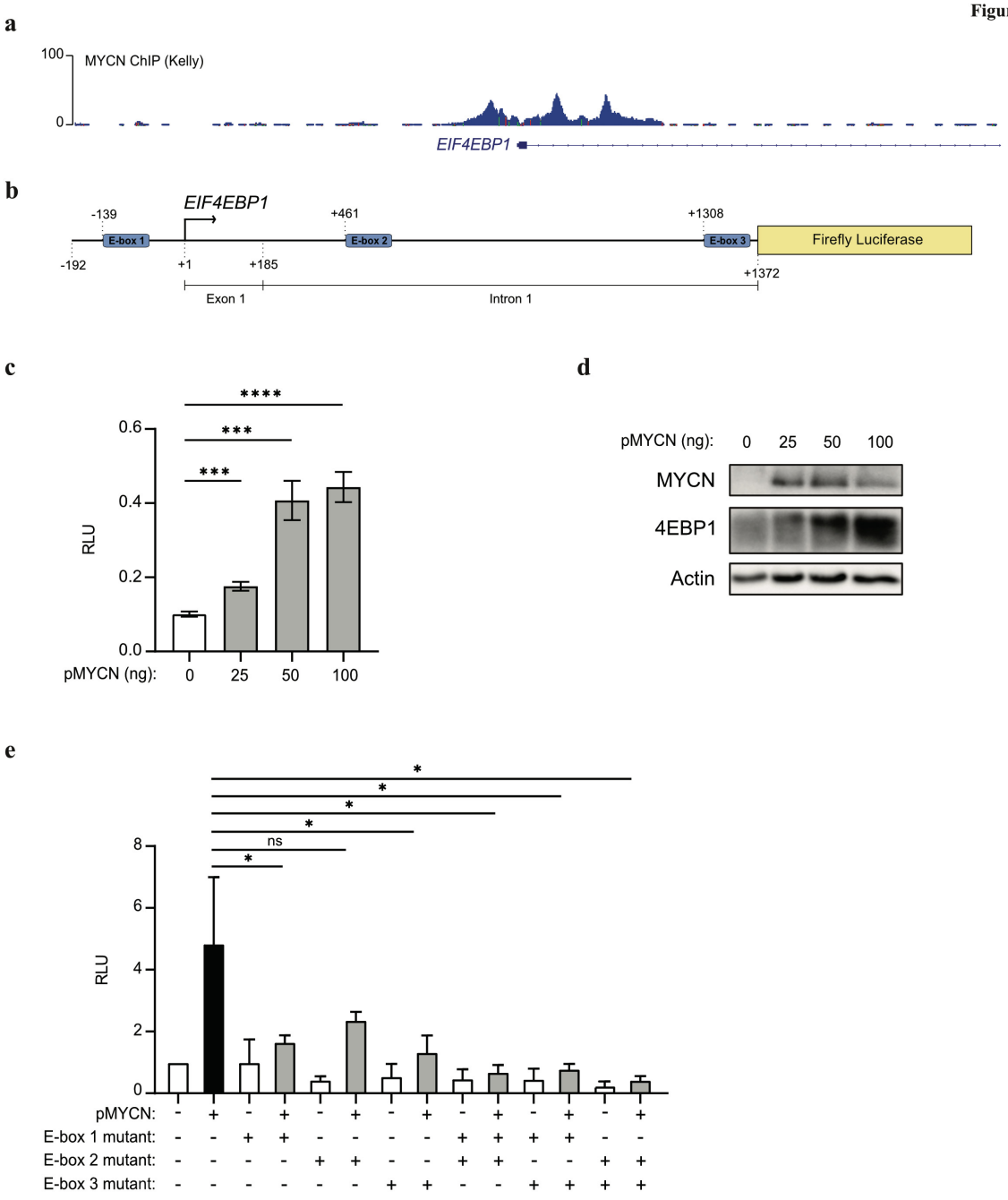
a
100
MYCN ChIP (Kelly)
0
EIF4EBP1
b
EIF4EBP1
-139
+461
+1308
E-box 1
E-box 2
E-box 3
Firefly Luciferase
-192
+1
+185
+1372
Exon 1
Intron 1
c
****
***
***
0.6
0.4
0.2
0.0
RLU
pMYCN (ng): 0 25 50 100
d
pMYCN (ng): 0 25 50 100
MYCN
4EBP1
Actin
e
*
*
*
*
ns
*
8
6
4
2
0
RLU
pMYCN: - + - + - + - + - + - + - + - +
E-box 1 mutant: - - + + - - - - + + + + - -
E-box 2 mutant: - - - - + + - - + + - - + +
E-box 3 mutant: - - - - - - + + - - + + + +

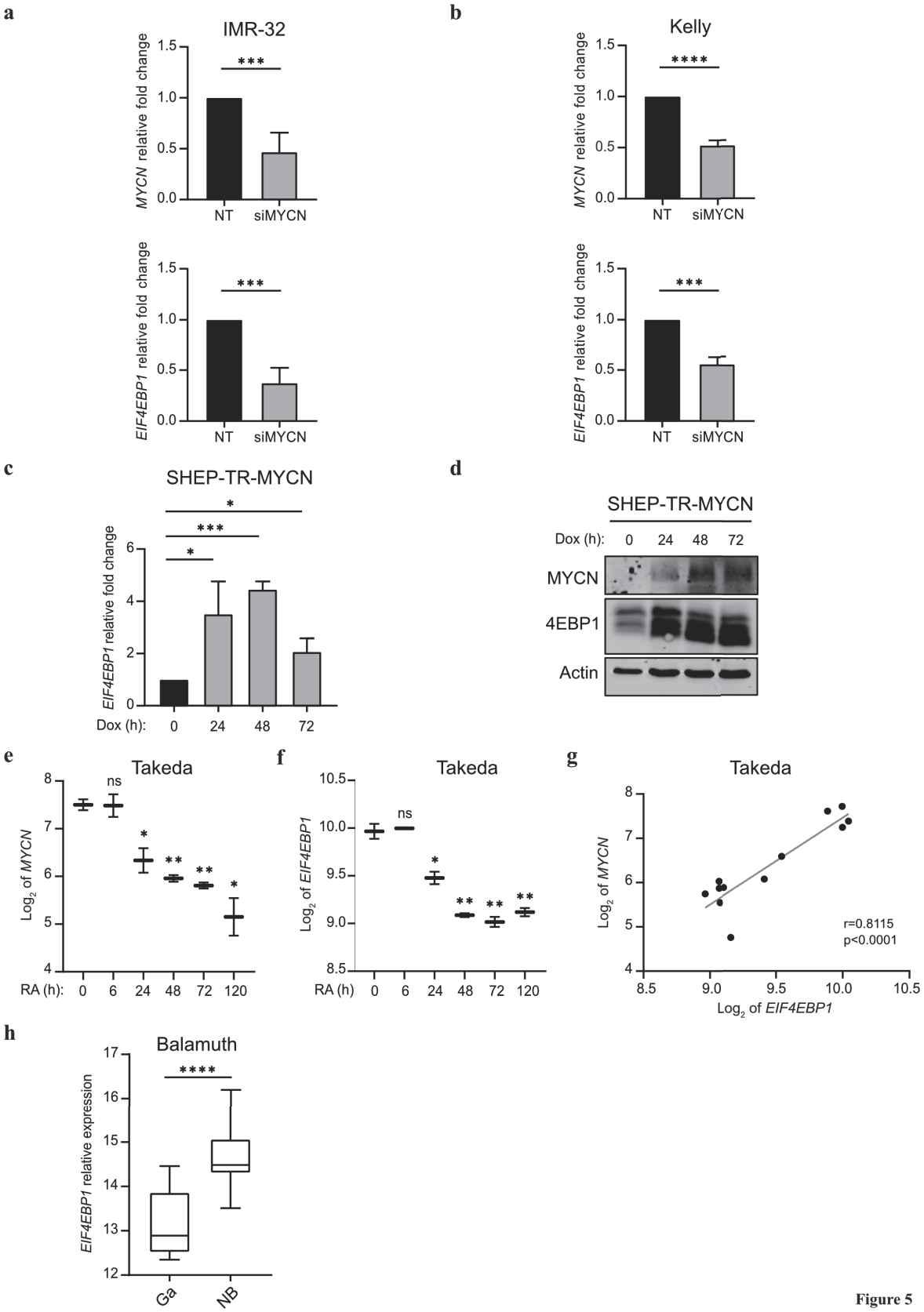
a
IMR-32
MYCN relative fold change
EIF4EBP1 relative fold change
NT
siMYCN
b
Kelly
c
SHEP-TR-MYCN
Dox (h): 0 24 48 72
d
SHEP-TR-MYCN
MYCN
4EBP1
Actin
e
Takeda
Log2 of MYCN
RA (h): 0 6 24 48 72 120
f
Takeda
Log2 of EIF4EBP1
g
Takeda
r=0.8115
p<0.0001
Log2 of EIF4EBP1
h
Balamuth
EIF4EBP1 relative expression
Ga
NB

Figure 5

Supplementary Figure 1

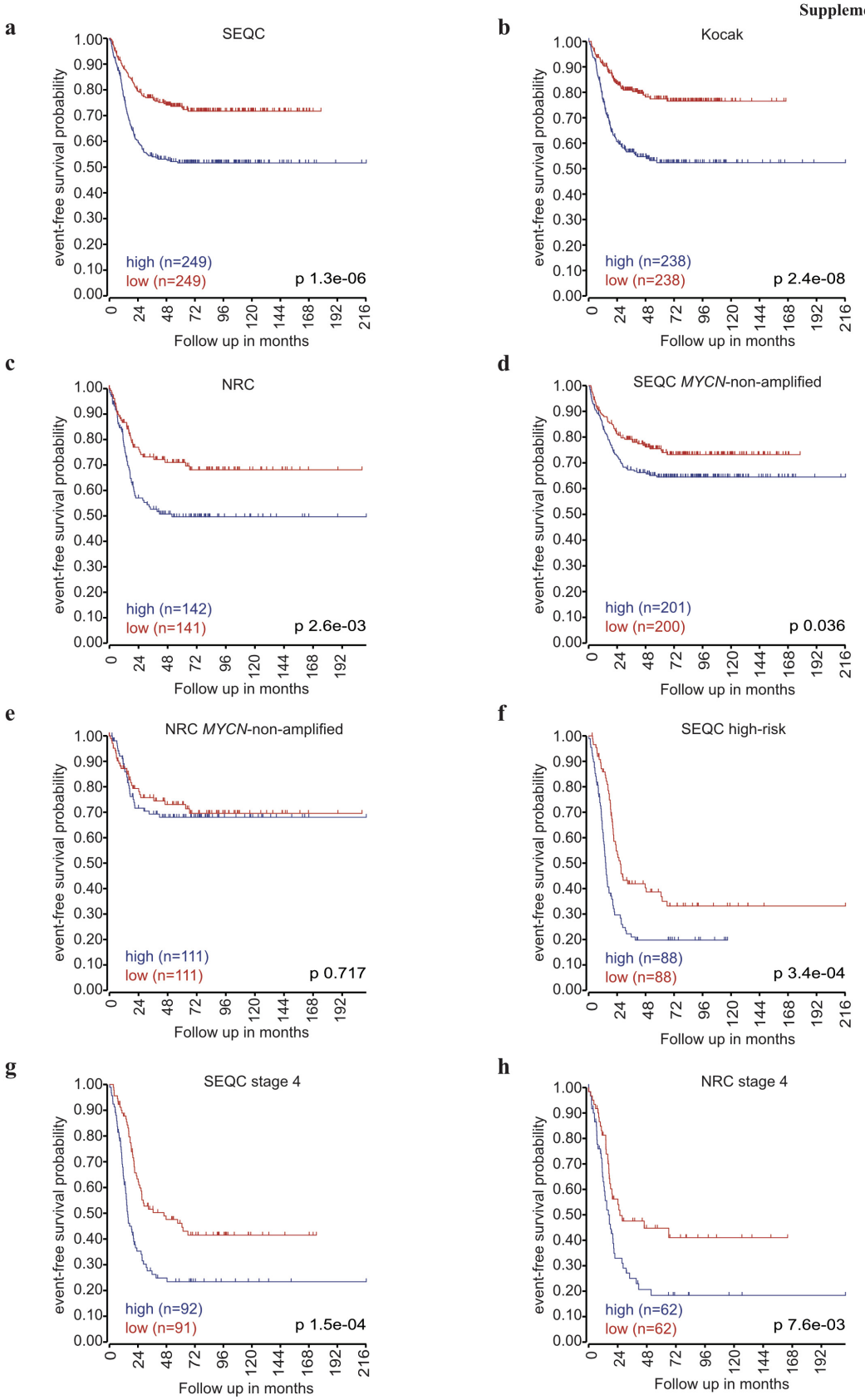

TABLES

Table 1. Multivariate analysis for overall survival of NB patients in the SEQC cohort.

Variables	**HR**	**95.0% CI**	**p value**
MYCN amplification	22.373	8.89-56.306	0
High *EIF4EBP1* mRNA expression	2.16	1.255-3.717	0.005
MYCN amplification*high *EIF4EBP1* mRNA expression	0.222	0.08-0.614	0.004
Variables	**HR**	**95.0% CI**	**p value**
Stage 4	17.618	6.694-46.366	0
High *EIF4EBP1* mRNA expression	5.457	2.026-14.697	0.001
Stage 4*high *EIF4EBP1* mRNA expression	0.292	0.097-0.879	0.029
Variables	**HR**	**95.0% CI**	**p value**
Age at diagnosis	33.018	7.835-139.139	0
High *EIF4EBP1* mRNA expression	12.204	2.832-52.598	0.001
Age at diagnosis*high *EIF4EBP1* mRNA expression	0.16	0.035-0.74	0.019

Table 2. Multivariate analysis for overall survival of NB patients in the NRC cohort.

Variables	**HR**	**95.0% CI**	**p value**
MYCN amplification	4.967	1.118-22.066	0.035
High *EIF4EBP1* mRNA expression	3.031	1.543-5.954	0.001
MYCN amplification*high *EIF4EBP1* mRNA expression	0.656	0.135-3.181	0.601
Variables	**HR**	**95.0% CI**	**p value**
Stage 4	15.050	4.239-53.432	0.018
High *EIF4EBP1* mRNA expression	5.144	1.330-19.895	0
Stage 4*high *EIF4EBP1* mRNA expression	0.36	0.081-1.598	0.179
Variables	**HR**	**95.0% CI**	**p value**
Age at diagnosis	0.27	0.036-2.056	0
High *EIF4EBP1* mRNA expression	0.364	0.048-2.772	0.002
Age at diagnosis*high *EIF4EBP1* mRNA expression	55.427	3.258-942.88	0.005

A. LIST OF FIGURES

Figure 1: Schematic representation of metabolic heterogeneity within the tumor environment. 11

Figure 2: Schematic representation of the 4EBP1 structure including Raptor binding motifs and mTORC1 phosphorylation sites. 14

Figure 3: Regulation of mRNA translation initiation by the mTORC1-4EBP1 axis under normal and stress conditions. 16

Figure 4: Schematic representation of the eIF4E binding motifs of 4EBP1 and eIF4G. 16

Figure 5: Evolutionary timeline of genetic alterations contributing to subclonal heterogeneity in IDH-WT glioblastoma. 25

Figure 6: MYC is a promising transcription factor candidate for regulating *EIF4EBP1* expression in glioblastoma. 43

Figure 7: MYBL2 does not mediate *EIF4EBP1* transcription through its consensus binding site. 46

Figure 8: *EIF4EBP1* mRNA and protein expression is not regulated by E2F6, FOXM1 or JUN 48

Figure 9: 4EBP1 does not impact migration or invasion in glioblastoma cell lines. 50

Figure 10: Illustration of the mechanism underlying the protective role of 4EBP1 under stress conditions. 52

Figure 11: 4EBP1 function in cancer and *EIF4EBP1* prognostic value is dependent on the p53 mutation status. 107

Figure 12: Protective function of 4EBP1 under glucose starvation requires all eIF4E binding motifs. 111

Figure 13: Protein-protein interaction of eIF4E and 4EBP1. 114

Figure 14: Assessment of compounds ability to disrupt the assembly of the eIF4E-4EBP1 complex in vitro. 115

Figure 15: Assessment of compounds ability to prevent the assembly of the eIF4E-4EBP1 complex in vitro. 117

Figure 16: Proposed model for 4EBP1 regulation and function in glioblastoma. 118

Figure 17: Proposed model for the function of 4EBP1 in cancer. 125

Figure 18: Workflow representing plating and imaging of Oris™ Cell Migration Assay.... 127

Figure 19: Workflow representing plating and imaging of Oris™ 3D Cell Invasion Assay. 128

B. LIST OF TABLES

Table 1: Overview of the co-expression analysis between *EIF4EBP1* and *MYC* in various glioma cohorts analyzed. 44

Table 2: Overview of the reported p53 status and activity in various cell lines. 108

Table 3: Overview of the experiments performed to determine p53 activity in glioblastoma cell lines. 108

Table 4: List of siRNA sequences. 127

Table 5: List of shRNA sequences. 127

Table 6: 4EBP1 inhibitor candidate compounds. 130

Table 7: List of additional RT-qPCR primers used for RT-qPCR analyses. 130

Table 8: List of additional antibodies used for immunoblot experiments. 130

C. AUTHOR CONTRIBUTION TO THE MANUSCRIPTS

Manuscript I:

Title: *Eukaryotic translation initiation factor 4E binding protein 1* (*EIF4EBP1*) expression in glioblastoma is driven by ETS1- and MYBL2-dependent transcriptional activation.

Published: 28.02.2022 by Cell Death and Discovery

Contribution: Laura Hauffe substantially conceived and designed the study. She collected bioinformatic data from publically available datasets and performed bioinformatic analysis of these data (except for Figure 1B and C and Figure 2H). In addition, all experimental data as well as the statistical analysis was generated by Laura Hauffe. Finally, she prepared all main and supplementary figures and wrote the manuscript.

Manuscript II:

Title: 4EBP1/2 support cell survival under metabolic stress by translationally regulating fatty acid synthesis

The manuscript is in preparation and will be submitted in the second quarter of 2022 to *Cell*.

Contribution: Laura Hauffe was involved in the conception and design of the study. She collected bioinformatic data from publically available datasets and performed bioinformatic analysis of these data (Figure 7A- D and Supplementary Figure 5A-E). Furthermore, she was involved in planning and performing *in vitro* cell culture experiments such as glucose starvation (Figure 1L) and soft agar assays (Figure A-C and I; Figure 7E-H; Supplementary Figure 4B and Supplementary Figure 6A- D). In addition, Laura Hauffe trained a master student to plan and perform soft agar assays (Supplementary Figure 4A and C). Statistical analysis and preparation of the figures for which she generated data was also prepared by her. Lastly, Laura Hauffe wrote the parts of the manuscript according to her experiments and critically evaluated and commented on the whole manuscript.

Manuscript III:

Title: *EIF4EBP1* is transcriptionally upregulated by MYCN and associates with poor prognosis in neuroblastoma

Accepted: 09.03.2022 by Cell Death and Discovery

Contribution: Laura Hauffe was involved in generating experimental data (Figure 4C and D) as well as training master students analyzing publically available patient data cohorts (Figure 1C) and to perform experiments (Figure 4C-E; Figure 5A and B). Lastly, Laura Hauffe critically evaluated and commented on the whole manuscript.

_____

Laura Hauffe

Düsseldorf, April 2022

D. REFERENCES

1. Abou-El-Ardat, K., Seifert, M., Becker, K., Eisenreich, S., Lehmann, M., Hackmann, K., Rump, A., Meijer, G., Carvalho, B., Temme, A., Schackert, G., Schrock, E., Krex, D. and Klink, B. Comprehensive molecular characterization of multifocal glioblastoma proves its monoclonal origin and reveals novel insights into clonal evolution and heterogeneity of glioblastomas. *Neuro Oncology* **2017**; *19(4)*:546-557.

2. Ackermann, S., Cartolano, M., Hero, B., Welte, A., Kahlert, Y., Roderwieser, A., Bartenhagen, C., Walter, E., Gecht, J., Kerschke, L., Volland, R., Menon, R., Heuckmann, J. M., Gartlgruber, M., Hartlieb, S., Henrich, K. O., Okonechnikov, K., Altmuller, J., Nurnberg, P., Lefever, S., de Wilde, B., Sand, F., Ikram, F., Rosswog, C., Fischer, J., Theissen, J., Hertwig, F., Singhi, A. D., Simon, T., Vogel, W., Perner, S., Krug, B., Schmidt, M., Rahmann, S., Achter, V., Lang, U., Vokuhl, C., Ortmann, M., Buttner, R., Eggert, A., Speleman, F., O'Sullivan, R. J., Thomas, R. K., Berthold, F., Vandesompele, J., Schramm, A., Westermann, F., Schulte, J. H., Peifer, M. and Fischer, M. A mechanistic classification of clinical phenotypes in neuroblastoma. *Science* **2018**; *362(6419)*:1165-1170.

3. Adler, A. J., Scheller, A. and Robins, D. M. The stringency and magnitude of androgen-specific gene activation are combinatorial functions of receptor and nonreceptor binding site sequences. *Mol Cell Biol* **1993**; *13(10)*:6326-6335.

4. Agnihotri, S., Burrell, K. E., Wolf, A., Jalali, S., Hawkins, C., Rutka, J. T. and Zadeh, G. Glioblastoma, a brief review of history, molecular genetics, animal models and novel therapeutic strategies. *Arch Immunol Ther Exp (Warsz)* **2013**; *61(1)*:25-41.

5. Alonso, M. M., Fueyo, J., Shay, J. W., Aldape, K. D., Jiang, H., Lee, O. H., Johnson, D. G., Xu, J., Kondo, Y., Kanzawa, T., Kyo, S., Bekele, B. N., Zhou, X., Nigro, J., McDonald, J. M., Yung, W. K. and Gomez-Manzano, C. Expression of transcription factor E2F1 and telomerase in glioblastomas: mechanistic linkage and prognostic significance. *J Natl Cancer I* **2005**; *97(21)*:1589-1600.

6. Azar, R., Alard, A., Susini, C., Bousquet, C. and Pyronnet, S. 4E-BP1 is a target of Smad4 essential for TGFbeta-mediated inhibition of cell proliferation. *EMBO J* **2009**; *28(22)*:3514-3522.

7. Azar, R., Lasfargues, C., Bousquet, C. and Pyronnet, S. Contribution of HIF-1alpha in 4E-BP1 gene expression. *Mol Cancer Res* **2013**; *11(1)*:54-61.

8. Badie, B. and Schartner, J. Role of microglia in glioma biology. *Microsc Res Tech* **2001**; *54(2)*:106-113.

9. Bai, H., Harmanci, A. S., Erson-Omay, E. Z., Li, J., Coskun, S., Simon, M., Krischek, B., Ozduman, K., Omay, S. B., Sorensen, E. A., Turcan, S., Bakirciglu, M., Carrion-Grant, G., Murray, P. B., Clark, V. E., Ercan-Sencicek, A. G., Knight, J., Sencar, L., Altinok, S., Kaulen, L. D., Gulez, B., Timmer, M., Schramm, J., Mishra-Gorur, K., Henegariu, O., Moliterno, J., Louvi, A., Chan, T. A., Tannheimer, S. L., Pamir, M. N., Vortmeyer, A. O., Bilguvar, K., Yasuno, K. and Gunel, M. Integrated genomic characterization of IDH1-mutant glioma malignant progression. *Nat Genet* **2016**; *48(1)*:59-66.

10. Balakumaran, B. S., Porrello, A., Hsu, D. S., Glover, W., Foye, A., Leung, J. Y., Sullivan, B. A., Hahn, W. C., Loda, M. and Febbo, P. G. MYC activity mitigates response to rapamycin in prostate cancer through eukaryotic initiation factor 4E-binding protein 1-mediated inhibition of autophagy. *Cancer Res* **2009**; *69(19)*:7803-7810.

11. Barthel, A., Okino, S. T., Liao, J., Nakatani, K., Li, J., Whitlock, J. P., Jr. and Roth, R. A. Regulation of GLUT1 gene transcription by the serine/threonine kinase Akt1. *J Biol Chem* **1999**; *274(29)*:20281-20286.

12. Bedard, P. L., Hansen, A. R., Ratain, M. J. and Siu, L. L. Tumour heterogeneity in the clinic. *Nature* **2013**; *501(7467)*:355-364.

13. Bell, R. J., Rube, H. T., Kreig, A., Mancini, A., Fouse, S. D., Nagarajan, R. P., Choi, S., Hong, C., He, D., Pekmezci, M., Wiencke, J. K., Wrensch, M. R., Chang, S. M., Walsh, K. M., Myong, S., Song, J. S. and Costello, J. F. Cancer. The transcription factor GABP selectively binds and activates the mutant TERT promoter in cancer. *Science* **2015**; *348(6238)*:1036-1039.

14. Ben-David, E., Bester, A. C., Shifman, S. and Kerem, B. Transcriptional dynamics in colorectal carcinogenesis: new insights into the role of c-Myc and miR17 in benign to cancer transformation. *Cancer Res* **2014**; *74(19)*:5532-5540.

15. Bi, C., Zhang, X., Lu, T., Zhang, X., Wang, X., Meng, B., Zhang, H., Wang, P., Vose, J. M., Chan, W. C., McKeithan, T. W. and Fu, K. Inhibition of 4EBP phosphorylation mediates the cytotoxic effect of mechanistic target of rapamycin kinase inhibitors in aggressive B-cell lymphomas. *Haematologica* **2017**; *102(4)*:755-764.

16. Blaszczyk-Thurin, M., Ertl, I. O. and Ertl, H. C. An experimental vaccine expressing wild-type p53 induces protective immunity against glioblastoma cells with high levels of endogenous p53. *Scand J Immunol* **2002**; *56(4)*:361-375.

17. Böhm, R., Imseng, S., Jakob, R. P., Hall, M. N., Maier, T. and Hiller, S. The dynamic mechanism of 4E-BP1 recognition and phosphorylation by mTORC1. *Mol Cell* **2021**; *81(11)*:2403-2416 e2405.

18. Bonavia, R., Inda, M. M., Cavenee, W. K. and Furnari, F. B. Heterogeneity maintenance in glioblastoma: a social network. *Cancer Res* **2011**; *71(12)*:4055-4060.

19. Brat, D. J., Aldape, K., Colman, H., Holland, E. C., Louis, D. N., Jenkins, R. B., Kleinschmidt-DeMasters, B. K., Perry, A., Reifenberger, G., Stupp, R., von Deimling, A. and Weller, M. cIMPACT-NOW update 3: recommended diagnostic criteria for "Diffuse astrocytic glioma, IDH-wildtype, with molecular features of glioblastoma, WHO grade IV". *Acta Neuropathol* **2018**; *136(5)*:805-810.

20. Brat, D. J., Castellano-Sanchez, A. A., Hunter, S. B., Pecot, M., Cohen, C., Hammond, E. H., Devi, S. N., Kaur, B. and Van Meir, E. G. Pseudopalisades in glioblastoma are hypoxic, express extracellular matrix proteases, and are formed by an actively migrating cell population. *Cancer Res* **2004**; *64(3)*:920-927.

21. Brat, D. J. and Mapstone, T. B. Malignant glioma physiology: cellular response to hypoxia and its role in tumor progression. *Ann Intern Med* **2003**; *138(8)*:659-668.

22. Braunstein, S., Karpisheva, K., Pola, C., Goldberg, J., Hochman, T., Yee, H., Cangiarella, J., Arju, R., Formenti, S. C. and Schneider, R. J. A hypoxia-controlled cap-dependent to cap-independent translation switch in breast cancer. *Mol Cell* **2007**; *28(3)*:501-512.

23. Brennan, C. W., Verhaak, R. G., McKenna, A., Campos, B., Noushmehr, H., Salama, S. R., Zheng, S., Chakravarty, D., Sanborn, J. Z., Berman, S. H., Beroukhim, R., Bernard, B., Wu, C. J., Genovese, G., Shmulevich, I., Barnholtz-Sloan, J., Zou, L., Vegesna, R., Shukla, S. A., Ciriello, G., Yung, W. K., Zhang, W., Sougnez, C., Mikkelsen, T., Aldape, K., Bigner, D. D., Van Meir, E. G., Prados, M., Sloan, A., Black, K. L., Eschbacher, J., Finocchiaro, G., Friedman, W., Andrews, D. W., Guha, A., Iacocca, M., O'Neill, B. P., Foltz, G., Myers, J., Weisenberger, D. J., Penny, R., Kucherlapati, R., Perou, C. M., Hayes, D. N., Gibbs, R., Marra, M., Mills, G. B., Lander, E., Spellman, P., Wilson, R., Sander, C., Weinstein, J., Meyerson, M., Gabriel, S., Laird, P. W., Haussler, D., Getz, G., Chin, L., TCGA Research Network. The somatic genomic landscape of glioblastoma. *Cell* **2013**; *155(2)*:462-477.

24. Buttgereit, F. and Brand, M. D. A hierarchy of ATP-consuming processes in mammalian cells. *Biochem J* **1995**; *312 (Pt 1)*:163-167.

25. Cai, W., Ye, Q. and She, Q. B. Loss of 4E-BP1 function induces EMT and promotes cancer cell migration and invasion via cap-dependent translational activation of snail. *Oncotarget* **2014**; *5(15)*:6015-6027.

26. The Cancer Genome Atlas Research Network, Weinstein, J. N., Collisson, E. A., Mills, G. B., Shaw, K. R., Ozenberger, B. A., Ellrott, K., Shmulevich, I., Sander, C. and Stuart, J. M. The Cancer Genome Atlas Pan-Cancer analysis project. *Nat Genet* **2013**; *45(10)*:1113-1120.

27. Cavalli, F. M. G., Remke, M., Rampasek, L., Peacock, J., Shih, D. J. H., Luu, B., Garzia, L., Torchia, J., Nor, C., Morrissy, A. S., Agnihotri, S., Thompson, Y. Y., Kuzan-Fischer, C. M., Farooq, H., Isaev, K., Daniels, C., Cho, B. K., Kim, S. K., Wang, K. C., Lee, J. Y., Grajkowska, W. A., Perek-Polnik, M., Vasiljevic, A., Faure-Conter, C., Jouvet, A., Giannini, C., Nageswara Rao, A. A., Li, K. K. W., Ng, H. K., Eberhart, C. G., Pollack, I. F., Hamilton, R. L., Gillespie, G. Y., Olson, J. M., Leary, S., Weiss, W. A., Lach, B., Chambless, L. B., Thompson, R. C., Cooper, M. K., Vibhakar, R., Hauser, P., van Veelen, M. C., Kros, J. M., French, P. J., Ra, Y. S., Kumabe, T., Lopez-Aguilar, E., Zitterbart, K., Sterba, J., Finocchiaro, G., Massimino, M., Van Meir, E. G., Osuka, S., Shofuda, T., Klekner, A., Zollo, M., Leonard, J. R., Rubin, J. B., Jabado, N., Albrecht, S., Mora, J., Van Meter, T. E., Jung, S., Moore, A. S., Hallahan, A. R., Chan, J. A., Tirapelli, D. P. C., Carlotti, C. G., Fouladi, M., Pimentel, J., Faria, C. C., Saad, A. G., Massimi, L., Liau, L. M., Wheeler, H., Nakamura, H., Elbabaa, S. K., Perezpena-Diazconti, M., Chico Ponce de Leon, F., Robinson, S., Zapotocky, M., Lassaletta, A., Huang, A., Hawkins, C. E., Tabori, U., Bouffet, E., Bartels, U., Dirks, P. B., Rutka, J. T., Bader, G. D., Reimand, J., Goldenberg, A., Ramaswamy, V. and Taylor, M. D. Intertumoral Heterogeneity within Medulloblastoma Subgroups. *Cancer Cell* **2017**; *31(6)*:737-754 e736.

28. Ceccarelli, M., Barthel, F. P., Malta, T. M., Sabedot, T. S., Salama, S. R., Murray, B. A., Morozova, O., Newton, Y., Radenbaugh, A., Pagnotta, S. M., Anjum, S., Wang, J., Manyam, G., Zoppoli, P., Ling, S., Rao, A. A., Grifford, M., Cherniack, A. D., Zhang, H., Poisson, L., Carlotti, C. G., Jr., Tirapelli, D. P., Rao, A., Mikkelsen, T., Lau, C. C., Yung, W. K., Rabadan, R., Huse, J., Brat, D. J., Lehman, N. L., Barnholtz-Sloan, J. S., Zheng, S., Hess, K., Rao, G., Meyerson, M., Beroukhim, R., Cooper, L., Akbani, R., Wrensch, M., Haussler, D., Aldape, K. D., Laird, P. W., Gutmann, D. H.,

Network, T. R., Noushmehr, H., Iavarone, A. and Verhaak, R. G. Molecular Profiling Reveals Biologically Discrete Subsets and Pathways of Progression in Diffuse Glioma. *Cell* **2016**; *164(3)*:550-563.

29. Cha, Y. L., Li, P. D., Yuan, L. J., Zhang, M. Y., Zhang, Y. J., Rao, H. L., Zhang, H. Z., Zheng, X. F. and Wang, H. Y. EIF4EBP1 overexpression is associated with poor survival and disease progression in patients with hepatocellular carcinoma. *PLoS One* **2015**; *10(2)*:e0117493.

30. Chao, M. W., Wang, L. T., Lai, C. Y., Yang, X. M., Cheng, Y. W., Lee, K. H., Pan, S. L. and Teng, C. M. eIF4E binding protein 1 expression is associated with clinical survival outcomes in colorectal cancer. *Oncotarget* **2015**; *6(27)*:24092-24104.

31. Choo, A. Y., Kim, S. G., Vander Heiden, M. G., Mahoney, S. J., Vu, H., Yoon, S. O., Cantley, L. C. and Blenis, J. Glucose addiction of TSC null cells is caused by failed mTORC1-dependent balancing of metabolic demand with supply. *Mol Cell* **2010**; *38(4)*:487-499.

32. Encode Project Consortium. An integrated encyclopedia of DNA elements in the human genome. *Nature* **2012**; *489(7414)*:57-74.

33. Davis, C. A., Hitz, B. C., Sloan, C. A., Chan, E. T., Davidson, J. M., Gabdank, I., Hilton, J. A., Jain, K., Baymuradov, U. K., Narayanan, A. K., Onate, K. C., Graham, K., Miyasato, S. R., Dreszer, T. R., Strattan, J. S., Jolanki, O., Tanaka, F. Y. and Cherry, J. M. The Encyclopedia of DNA elements (ENCODE): data portal update. *Nucleic Acids Res* **2018**; *46(D1)*:D794-D801.

34. De Benedetti, A. and Graff, J. R. eIF-4E expression and its role in malignancies and metastases. *Oncogene* **2004**; *23(18)*:3189-3199.

35. DeCordova, S., Shastri, A., Tsolaki, A. G., Yasmin, H., Klein, L., Singh, S. K. and Kishore, U. Molecular Heterogeneity and Immunosuppressive Microenvironment in Glioblastoma. *Front Immunol* **2020**; *11(1402)*:1-18.

36. DeNicola, G. M., Karreth, F. A., Humpton, T. J., Gopinathan, A., Wei, C., Frese, K., Mangal, D., Yu, K. H., Yeo, C. J., Calhoun, E. S., Scrimieri, F., Winter, J. M., Hruban, R. H., Iacobuzio-Donahue, C., Kern, S. E., Blair, I. A. and Tuveson, D. A. Oncogene-induced Nrf2 transcription promotes ROS detoxification and tumorigenesis. *Nature* **2011**; *475(7354)*:106-109.

37. Ding, M., Van der Kwast, T. H., Vellanki, R. N., Foltz, W. D., McKee, T. D., Sonenberg, N., Pandolfi, P. P., Koritzinsky, M. and Wouters, B. G. The mTOR Targets 4E-BP1/2 Restrain Tumor Growth and Promote Hypoxia Tolerance in PTEN-driven Prostate Cancer. *Mol Cancer Res* **2018**; *16(4)*:682-695.

38. Dittmer, J. The role of the transcription factor Ets1 in carcinoma. *Semin Cancer Biol* **2015**; *35:*20-38.

39. Dowling, R. J., Topisirovic, I., Alain, T., Bidinosti, M., Fonseca, B. D., Petroulakis, E., Wang, X., Larsson, O., Selvaraj, A., Liu, Y., Kozma, S. C., Thomas, G. and Sonenberg, N. mTORC1-mediated cell proliferation, but not cell growth, controlled by the 4E-BPs. *Science* **2010**; *328(5982)*:1172-1176.

40. Draaisma, K., Chatzipli, A., Taphoorn, M., Kerkhof, M., Weyerbrock, A., Sanson, M., Hoeben, A., Lukacova, S., Lombardi, G., Leenstra, S., Hanse, M., Fleischeuer, R., Watts, C., McAbee, J., Angelopoulos, N., Gorlia, T., Golfinopoulos, V., Kros, J. M., Verhaak, R. G. W., Bours, V., van den Bent, M. J., McDermott, U., Robe, P. A. and

French, P. J. Molecular Evolution of IDH Wild-Type Glioblastomas Treated With Standard of Care Affects Survival and Design of Precision Medicine Trials: A Report From the EORTC 1542 Study. *J Clin Oncol* **2020**; *38(1)*:81-99.

41. Dubois, L., Magagnin, M. G., Cleven, A. H., Weppler, S. A., Grenacher, B., Landuyt, W., Lieuwes, N., Lambin, P., Gorr, T. A., Koritzinsky, M. and Wouters, B. G. Inhibition of 4E-BP1 sensitizes U87 glioblastoma xenograft tumors to irradiation by decreasing hypoxia tolerance. *Int J Radiat Oncol Biol Phys* **2009**; *73(4)*:1219-1227.

42. Eichner, L. J., Brun, S. N., Herzig, S., Young, N. P., Curtis, S. D., Shackelford, D. B., Shokhirev, M. N., Leblanc, M., Vera, L. I., Hutchins, A., Ross, D. S., Shaw, R. J. and Svensson, R. U. Genetic Analysis Reveals AMPK Is Required to Support Tumor Growth in Murine Kras-Dependent Lung Cancer Models. *Cell Metab* **2019**; *29(2)*:285-302 e287.

43. Fellows, L. K. and Boutelle, M. G. Rapid changes in extracellular glucose levels and blood flow in the striatum of the freely moving rat. *Brain Res* **1993**; *604(1-2)*:225-231.

44. Fingar, D. C. and Blenis, J. Target of rapamycin (TOR): an integrator of nutrient and growth factor signals and coordinator of cell growth and cell cycle progression. *Oncogene* **2004**; *23(18)*:3151-3171.

45. Fingar, D. C., Richardson, C. J., Tee, A. R., Cheatham, L., Tsou, C. and Blenis, J. mTOR controls cell cycle progression through its cell growth effectors S6K1 and 4E-BP1/eukaryotic translation initiation factor 4E. *Mol Cell Biol* **2004**; *24(1)*:200-216.

46. Fingar, D. C., Salama, S., Tsou, C., Harlow, E. and Blenis, J. Mammalian cell size is controlled by mTOR and its downstream targets S6K1 and 4EBP1/eIF4E. *Gene Dev* **2002**; *16(12)*:1472-1487.

47. Flavahan, W. A., Wu, Q., Hitomi, M., Rahim, N., Kim, Y., Sloan, A. E., Weil, R. J., Nakano, I., Sarkaria, J. N., Stringer, B. W., Day, B. W., Li, M., Lathia, J. D., Rich, J. N. and Hjelmeland, A. B. Brain tumor initiating cells adapt to restricted nutrition through preferential glucose uptake. *Nat Neurosci* **2013**; *16(10)*:1373-1382.

48. Flier, J. S., Mueckler, M. M., Usher, P. and Lodish, H. F. Elevated levels of glucose transport and transporter messenger RNA are induced by ras or src oncogenes. *Science* **1987**; *235(4795)*:1492-1495.

49. Freije, W. A., Castro-Vargas, F. E., Fang, Z., Horvath, S., Cloughesy, T., Liau, L. M., Mischel, P. S. and Nelson, S. F. Gene expression profiling of gliomas strongly predicts survival. *Cancer Res* **2004**; *64(18)*:6503-6510.

50. Gao, J., Aksoy, B. A., Dogrusoz, U., Dresdner, G., Gross, B., Sumer, S. O., Sun, Y., Jacobsen, A., Sinha, R., Larsson, E., Cerami, E., Sander, C. and Schultz, N. Integrative analysis of complex cancer genomics and clinical profiles using the cBioPortal. *Sci Signal* **2013**; *6(269)*:pl1.

51. Győrffy, B. Survival analysis across the entire transcriptome identifies biomarkers with the highest prognostic power in breast cancer. Comput Struct Biotechnol J **2021**; 19:4101-4109.

52. Gingras, A. C., Gygi, S. P., Raught, B., Polakiewicz, R. D., Abraham, R. T., Hoekstra, M. F., Aebersold, R. and Sonenberg, N. Regulation of 4E-BP1 phosphorylation: a novel two-step mechanism. *Gene Dev* **1999**; *13(11)*:1422-1437.

53. Gingras, A. C., Raught, B., Gygi, S. P., Niedzwiecka, A., Miron, M., Burley, S. K., Polakiewicz, R. D., Wyslouch-Cieszynska, A., Aebersold, R. and Sonenberg, N. Hierarchical phosphorylation of the translation inhibitor 4E-BP1. *Gene Dev* **2001**; *15(21)*:2852-2864.

54. Gravendeel, L. A., Kouwenhoven, M. C., Gevaert, O., de Rooi, J. J., Stubbs, A. P., Duijm, J. E., Daemen, A., Bleeker, F. E., Bralten, L. B., Kloosterhof, N. K., De Moor, B., Eilers, P. H., van der Spek, P. J., Kros, J. M., Sillevis Smitt, P. A., van den Bent, M. J. and French, P. J. Intrinsic gene expression profiles of gliomas are a better predictor of survival than histology. *Cancer Res* **2009**; *69(23)*:9065-9072.

55. Griesinger, A. M., Birks, D. K., Donson, A. M., Amani, V., Hoffman, L. M., Waziri, A., Wang, M., Handler, M. H. and Foreman, N. K. Characterization of distinct immunophenotypes across pediatric brain tumor types. *J Immunol* **2013**; *191(9)*:4880-4888.

56. Gross, J. D., Moerke, N. J., von der Haar, T., Lugovskoy, A. A., Sachs, A. B., McCarthy, J. E. and Wagner, G. Ribosome loading onto the mRNA cap is driven by conformational coupling between eIF4G and eIF4E. *Cell* **2003**; *115(6)*:739-750.

57. Gruetter, R., Novotny, E. J., Boulware, S. D., Rothman, D. L., Mason, G. F., Shulman, G. I., Shulman, R. G. and Tamborlane, W. V. Direct measurement of brain glucose concentrations in humans by 13C NMR spectroscopy. *P Natl Acad Sci USA* **1992**; *89(3)*:1109-1112.

58. Gulluoglu, S., Tuysuz, E. C., Sahin, M., Kuskucu, A., Kaan Yaltirik, C., Ture, U., Kucukkaraduman, B., Akbar, M. W., Gure, A. O., Bayrak, O. F. and Dalan, A. B. Simultaneous miRNA and mRNA transcriptome profiling of glioblastoma samples reveals a novel set of OncomiR candidates and their target genes. *Brain Res* **2018**; *1700:*199-210.

59. Gusev, Y., Bhuvaneshwar, K., Song, L., Zenklusen, J. C., Fine, H. and Madhavan, S. The REMBRANDT study, a large collection of genomic data from brain cancer patients. *Sci Data* **2018**; *5*:180158.

60. Haghighat, A., Mader, S., Pause, A. and Sonenberg, N. Repression of cap-dependent translation by 4E-binding protein 1: competition with p220 for binding to eukaryotic initiation factor-4E. *EMBO J* **1995**; *14(22)*:5701-5709.

61. Hanada, N., Lo, H. W., Day, C. P., Pan, Y., Nakajima, Y. and Hung, M. C. Co-regulation of B-Myb expression by E2F1 and EGF receptor. *Mol Carcinog* **2006**; *45(1)*:10-17.

62. Hanahan, D. and Weinberg, R. A. Hallmarks of cancer: the next generation. *Cell* **2011**; *144(5)*:646-674.

63. Harding, H. P., Zhang, Y., Bertolotti, A., Zeng, H. and Ron, D. Perk is essential for translational regulation and cell survival during the unfolded protein response. *Mol Cell* **2000**; *5(5)*:897-904.

64. Hay, N. and Sonenberg, N. Upstream and downstream of mTOR. *Gene Dev* **2004**; *18(16)*:1926-1945.

65. Heddleston, J. M., Li, Z., McLendon, R. E., Hjelmeland, A. B. and Rich, J. N. The hypoxic microenvironment maintains glioblastoma stem cells and promotes reprogramming towards a cancer stem cell phenotype. *Cell Cycle* **2009**; *8(20)*:3274-3284.

66. Hegi, M. E., Diserens, A. C., Gorlia, T., Hamou, M. F., de Tribolet, N., Weller, M., Kros, J. M., Hainfellner, J. A., Mason, W., Mariani, L., Bromberg, J. E., Hau, P., Mirimanoff, R. O., Cairncross, J. G., Janzer, R. C. and Stupp, R. MGMT gene silencing and benefit from temozolomide in glioblastoma. *N Engl J Med* **2005**; *352(10)*:997-1003.

67. Hirayama, A., Kami, K., Sugimoto, M., Sugawara, M., Toki, N., Onozuka, H., Kinoshita, T., Saito, N., Ochiai, A., Tomita, M., Esumi, H. and Soga, T. Quantitative metabolome profiling of colon and stomach cancer

microenvironment by capillary electrophoresis time-of-flight mass spectrometry. *Cancer Res* **2009**; *69(11)*:4918-4925.

68. Howe, K. M. and Watson, R. J. Nucleotide preferences in sequence-specific recognition of DNA by c-myb protein. *Nucleic Acids Res* **1991**; *19(14)*:3913-3919.

69. Hsieh, A. C., Liu, Y., Edlind, M. P., Ingolia, N. T., Janes, M. R., Sher, A., Shi, E. Y., Stumpf, C. R., Christensen, C., Bonham, M. J., Wang, S., Ren, P., Martin, M., Jessen, K., Feldman, M. E., Weissman, J. S., Shokat, K. M., Rommel, C. and Ruggero, D. The translational landscape of mTOR signalling steers cancer initiation and metastasis. *Nature* **2012**; *485(7396)*:55-61.

70. Hsieh, A. C., Small, E. J. and Ryan, C. J. Androgen-response elements in hormone-refractory prostate cancer: implications for treatment development. *Lancet Oncol* **2007**; *8(10)*:933-939.

71. Hsu, P. P. and Sabatini, D. M. Cancer cell metabolism: Warburg and beyond. *Cell* **2008**; *134(5)*:703-707.

72. Huang, W. J., Chen, W. W. and Zhang, X. Glioblastoma multiforme: Effect of hypoxia and hypoxia inducible factors on therapeutic approaches. *Oncol Lett* **2016**; *12(4)*:2283-2288.

73. Igreja, C., Peter, D., Weiler, C. and Izaurralde, E. 4E-BPs require non-canonical 4E-binding motifs and a lateral surface of eIF4E to repress translation. *Nat Commun* **2014**; *5*:4790.

74. Jacinto, E. and Hall, M. N. Tor signalling in bugs, brain and brawn. *Nat Rev Mol Cell Biol* **2003**; *4(2)*:117-126.

75. Jeon, S. M., Chandel, N. S. and Hay, N. AMPK regulates NADPH homeostasis to promote tumour cell survival during energy stress. *Nature* **2012**; *485(7400)*:661-665.

76. Juliana, C. A., Yang, J., Rozo, A. V., Good, A., Groff, D. N., Wang, S. Z., Green, M. R. and Stoffers, D. A. ATF5 regulates beta-cell survival during stress. *P Natl Acad Sci USA* **2017**; *114(6)*:1341-1346.

77. Kaminska, B., Czapski, B., Guzik, R., Krol, S. K. and Gielniewski, B. Consequences of IDH1/2 Mutations in Gliomas and an Assessment of Inhibitors Targeting Mutated IDH Proteins. *Molecules* **2019**; *24(5)*:968.

78. Kandoth, C., McLellan, M. D., Vandin, F., Ye, K., Niu, B., Lu, C., Xie, M., Zhang, Q., McMichael, J. F., Wyczalkowski, M. A., Leiserson, M. D. M., Miller, C. A., Welch, J. S., Walter, M. J., Wendl, M. C., Ley, T. J., Wilson, R. K., Raphael, B. J. and Ding, L. Mutational landscape and significance across 12 major cancer types. *Nature* **2013**; *502(7471)*:333-339.

79. Kang, M. J., Vasudevan, D., Kang, K., Kim, K., Park, J. E., Zhang, N., Zeng, X., Neubert, T. A., Marr, M. T., 2nd and Ryoo, H. D. 4E-BP is a target of the GCN2-ATF4 pathway during Drosophila development and aging. *J Cell Biol* **2017**; *216(1)*:115-129.

80. Karlsson, E., Perez-Tenorio, G., Amin, R., Bostner, J., Skoog, L., Fornander, T., Sgroi, D. C., Nordenskjold, B., Hallbeck, A. L. and Stal, O. The mTOR effectors 4EBP1 and S6K2 are frequently coexpressed, and associated with a poor prognosis and endocrine resistance in breast cancer: a retrospective study including patients from the randomised Stockholm tamoxifen trials. *Breast Cancer Res* **2013**; *15(5)*:R96.

81. Karlsson, E., Waltersson, M. A., Bostner, J., Perez-Tenorio, G., Olsson, B., Hallbeck, A. L. and Stal, O. High-resolution genomic analysis of the 11q13 amplicon in breast cancers identifies synergy with 8p12 amplification, involving the mTOR targets S6K2 and 4EBP1. *Genes Chromosomes Cancer* **2011**; *50(10)*:775-787.

82. Kawaguchi, A., Yajima, N., Tsuchiya, N., Homma, J., Sano, M., Natsumeda, M., Takahashi, H., Fujii, Y., Kakuma, T. and Yamanaka, R. Gene expression signature-based prognostic risk score in patients with glioblastoma. *Cancer Sci* **2013**; *104(9)*:1205-1210.

83. Killela, P. J., Reitman, Z. J., Jiao, Y., Bettegowda, C., Agrawal, N., Diaz, L. A., Jr., Friedman, A. H., Friedman, H., Gallia, G. L., Giovanella, B. C., Grollman, A. P., He, T. C., He, Y., Hruban, R. H., Jallo, G. I., Mandahl, N., Meeker, A. K., Mertens, F., Netto, G. J., Rasheed, B. A., Riggins, G. J., Rosenquist, T. A., Schiffman, M., Shih Ie, M., Theodorescu, D., Torbenson, M. S., Velculescu, V. E., Wang, T. L., Wentzensen, N., Wood, L. D., Zhang, M., McLendon, R. E., Bigner, D. D., Kinzler, K. W., Vogelstein, B., Papadopoulos, N. and Yan, H. TERT promoter mutations occur frequently in gliomas and a subset of tumors derived from cells with low rates of self-renewal. *P Natl Acad Sci USA* **2013**; *110(15)*:6021-6026.

84. Knight, J. R. P., Alexandrou, C., Skalka, G. L., Vlahov, N., Pennel, K., Officer, L., Teodosio, A., Kanellos, G., Gay, D. M., May-Wilson, S., Smith, E. M., Najumudeen, A. K., Gilroy, K., Ridgway, R. A., Flanagan, D. J., Smith, R. C. L., McDonald, L., MacKay, C., Cheasty, A., McArthur, K., Stanway, E., Leach, J. D., Jackstadt, R., Waldron, J. A., Campbell, A. D., Vlachogiannis, G., Valeri, N., Haigis, K. M., Sonenberg, N., Proud, C. G., Jones, N. P., Swarbrick, M. E., McKinnon, H. J., Faller, W. J., Le Quesne, J., Edwards, J., Willis, A. E., Bushell, M. and Sansom, O. J. MNK Inhibition Sensitizes KRAS-Mutant Colorectal Cancer to mTORC1 Inhibition by Reducing eIF4E Phosphorylation and c-MYC Expression. *Cancer Discov* **2021**; *11(5)*:1228-1247.

85. Körber, V., Yang, J., Barah, P., Wu, Y., Stichel, D., Gu, Z., Fletcher, M. N. C., Jones, D., Hentschel, B., Lamszus, K., Tonn, J. C., Schackert, G., Sabel, M., Felsberg, J., Zacher, A., Kaulich, K., Hübschmann, D., Herold-Mende, C., von Deimling, A., Weller, M., Radlwimmer, B., Schlesner, M., Reifenberger, G., Höfer, T. and Lichter, P. Evolutionary Trajectories of IDH(WT) Glioblastomas Reveal a Common Path of Early Tumorigenesis Instigated Years ahead of Initial Diagnosis. *Cancer Cell* **2019**; *35(4)*:692-704 e612.

86. Koritzinsky, M., Rouschop, K. M., van den Beucken, T., Magagnin, M. G., Savelkouls, K., Lambin, P. and Wouters, B. G. Phosphorylation of eIF2alpha is required for mRNA translation inhibition and survival during moderate hypoxia. *Radiother Oncol* **2007**; *83(3)*:353-361.

87. Kristensen, B. W., Priesterbach-Ackley, L. P., Petersen, J. K. and Wesseling, P. Molecular pathology of tumors of the central nervous system. *Ann Oncol* **2019**; *30(8)*:1265-1278.

88. Kumar, S., Sharife, H., Kreisel, T., Mogilevsky, M., Bar-Lev, L., Grunewald, M., Aizenshtein, E., Karni, R., Paldor, I., Shlomi, T. and Keshet, E. Intra-Tumoral Metabolic Zonation and Resultant Phenotypic Diversification Are Dictated by Blood Vessel Proximity. *Cell Metab* **2019**; *30(1)*:201-211 e206.

89. Labuschagne, C. F., Cheung, E. C., Blagih, J., Domart, M. C. and Vousden, K. H. Cell Clustering Promotes a Metabolic Switch that Supports Metastatic Colonization. *Cell Metab* **2019**; *30(4)*:720-734 e725.

90. Laplante, M. and Sabatini, D. M. mTOR signaling in growth control and disease. *Cell* **2012**; *149(2)*:274-293.

91. Lazaris-Karatzas, A., Montine, K. S. and Sonenberg, N. Malignant transformation by a eukaryotic initiation factor subunit that binds to mRNA 5' cap. *Nature* **1990**; *345(6275)*:544-547.

92. Lee, M., Kim, E. J. and Jeon, M. J. MicroRNAs 125a and 125b inhibit ovarian cancer cells through post-transcriptional inactivation of EIF4EBP1. *Oncotarget* **2016**; *7(8)*:8726-8742.

93. Leprivier, G., Remke, M., Rotblat, B., Dubuc, A., Mateo, A. R., Kool, M., Agnihotri, S., El-Naggar, A., Yu, B., Somasekharan, S. P., Faubert, B., Bridon, G., Tognon, C. E., Mathers, J., Thomas, R., Li, A., Barokas, A., Kwok, B., Bowden, M., Smith, S., Wu, X., Korshunov, A., Hielscher, T., Northcott, P. A., Galpin, J. D., Ahern, C. A., Wang, Y., McCabe, M. G., Collins, V. P., Jones, R. G., Pollak, M., Delattre, O., Gleave, M. E., Jan, E., Pfister, S. M., Proud, C. G., Derry, W. B., Taylor, M. D. and Sorensen, P. H. The eEF2 kinase confers resistance to nutrient deprivation by blocking translation elongation. *Cell* **2013**; *153(5)*:1064-1079.

94. Leprivier, G., Rotblat, B., Khan, D., Jan, E. and Sorensen, P. H. Stress-mediated translational control in cancer cells. *Biochim Biophys Acta* **2015**; *1849(7)*:845-860.

95. Leprivier, G. and Sorensen, P. H. How does oncogene transformation render tumor cells hypersensitive to nutrient deprivation? *Bioessays* **2014**; *36(11)*:1082-1090.

96. Li, M., Ge, Q., Wang, W., Wang, J. and Lu, Z. c-Jun binding site identification in K562 cells. *J Genet Genomics* **2011**; *38(6)*:235-242.

97. Li, S., Sonenberg, N., Gingras, A. C., Peterson, M., Avdulov, S., Polunovsky, V. A. and Bitterman, P. B. Translational control of cell fate: availability of phosphorylation sites on translational repressor 4E-BP1 governs its proapoptotic potency. *Mol Cell Biol* **2002**; *22(8)*:2853-2861.

98. Li, Z., Bao, S., Wu, Q., Wang, H., Eyler, C., Sathornsumetee, S., Shi, Q., Cao, Y., Lathia, J., McLendon, R. E., Hjelmeland, A. B. and Rich, J. N. Hypoxia-inducible factors regulate tumorigenic capacity of glioma stem cells. *Cancer Cell* **2009**; *15(6)*:501-513.

99. Lim, J. K. M., Delaidelli, A., Minaker, S. W., Zhang, H. F., Colovic, M., Yang, H., Negri, G. L., von Karstedt, S., Lockwood, W. W., Schaffer, P., Leprivier, G. and Sorensen, P. H. Cystine/glutamate antiporter xCT (SLC7A11) facilitates oncogenic RAS transformation by preserving intracellular redox balance. *Proc Natl Acad Sci U S A* **2019**; *116(19)*:9433-9442.

100. Liu, B. and Qian, S. B. Translational reprogramming in cellular stress response. *Wiley Interdiscip Rev RNA* **2014**; *5(3)*:301-315.

101. Liu, G. Y. and Sabatini, D. M. mTOR at the nexus of nutrition, growth, ageing and disease. *Nat Rev Mol Cell Biol* **2020**; *21(4)*:183-203.

102. Liu, L., Markowitz, S. and Gerson, S. L. Mismatch repair mutations override alkyltransferase in conferring resistance to temozolomide but not to 1,3-bis(2-chloroethyl)nitrosourea. *Cancer Res* **1996**; *56(23)*:5375-5379.

103. Liu, Y., Horn, J. L., Banda, K., Goodman, A. Z., Lim, Y., Jana, S., Arora, S., Germanos, A. A., Wen, L., Hardin, W. R., Yang, Y. C., Coleman, I. M., Tharakan, R. G., Cai, E. Y., Uo, T., Pillai, S. P. S., Corey, E., Morrissey, C., Chen, Y.,

Carver, B. S., Plymate, S. R., Beronja, S., Nelson, P. S. and Hsieh, A. C. The androgen receptor regulates a druggable translational regulon in advanced prostate cancer. *Sci Transl Med* **2019**; *11(503)*

104. Louis, D. N., Ohgaki, H., Wiestler, O. D., Cavenee, W. K., Burger, P. C., Jouvet, A., Scheithauer, B. W. and Kleihues, P. The 2007 WHO classification of tumours of the central nervous system. *Acta Neuropathol* **2007**; *114(2)*:97-109.

105. Louis, D. N., Perry, A., Reifenberger, G., von Deimling, A., Figarella-Branger, D., Cavenee, W. K., Ohgaki, H., Wiestler, O. D., Kleihues, P. and Ellison, D. W. The 2016 World Health Organization Classification of Tumors of the Central Nervous System: a summary. *Acta Neuropathol* **2016**; *131(6)*:803-820.

106. Louis, D. N., Perry, A., Wesseling, P., Brat, D. J., Cree, I. A., Figarella-Branger, D., Hawkins, C., Ng, H. K., Pfister, S. M., Reifenberger, G., Soffietti, R., von Deimling, A. and Ellison, D. W. The 2021 WHO Classification of Tumors of the Central Nervous System: a summary. *Neuro Oncol* **2021**; *23(8)*:1231-1251.

107. Luo, W., Wang, F., Luo, H. and Liu, H. Arctigenin inhibits human breast cancer cell proliferation, migratory and invasive abilities and epithelial to mesenchymal transition by targeting 4EBP1. *Exp Ther Med* **2021**; *21(6)*:547.

108. Mader, S., Lee, H., Pause, A. and Sonenberg, N. The translation initiation factor eIF-4E binds to a common motif shared by the translation factor eIF-4 gamma and the translational repressors 4E-binding proteins. *Mol Cell Biol* **1995**; *15(9)*:4990-4997.

109. Madhavan, S., Zenklusen, J. C., Kotliarov, Y., Sahni, H., Fine, H. A. and Buetow, K. Rembrandt: helping personalized medicine become a reality through integrative translational research. *Mol Cancer Res* **2009**; *7(2)*:157-167.

110. Malmstrom, A., Gronberg, B. H., Marosi, C., Stupp, R., Frappaz, D., Schultz, H., Abacioglu, U., Tavelin, B., Lhermitte, B., Hegi, M. E., Rosell, J., Henriksson, R. and Nordic Clinical Brain Tumour Study, G. Temozolomide versus standard 6-week radiotherapy versus hypofractionated radiotherapy in patients older than 60 years with glioblastoma: the Nordic randomised, phase 3 trial. *Lancet Oncol* **2012**; *13(9)*:916-926.

111. Marazita, M. C., Dugour, A., Marquioni-Ramella, M. D., Figueroa, J. M. and Suburo, A. M. Oxidative stress-induced premature senescence dysregulates VEGF and CFH expression in retinal pigment epithelial cells: Implications for Age-related Macular Degeneration. *Redox Biol* **2016**; *7*:78-87.

112. Marcotrigiano, J., Gingras, A. C., Sonenberg, N. and Burley, S. K. Cap-dependent translation initiation in eukaryotes is regulated by a molecular mimic of eIF4G. *Mol Cell* **1999**; *3(6)*:707-716.

113. Masselink, H., Vastenhouw, N. and Bernards, R. B-myb rescues ras-induced premature senescence, which requires its transactivation domain. *Cancer Lett* **2001**; *171(1)*:87-101.

114. Miron, M., Verdu, J., Lachance, P. E., Birnbaum, M. J., Lasko, P. F. and Sonenberg, N. The translational inhibitor 4E-BP is an effector of PI(3)K/Akt signalling and cell growth in Drosophila. *Nat Cell Biol* **2001**; *3(6)*:596-601.

115. Mizuno, A., In, Y., Fujita, Y., Abiko, F., Miyagawa, H., Kitamura, K., Tomoo, K. and Ishida, T. Importance of C-terminal flexible region of 4E-binding protein in binding with eukaryotic initiation factor 4E. *FEBS Lett* **2008**; *582(23-24)*:3439-3444.

116. Morita, M., Gravel, S. P., Chenard, V., Sikstrom, K., Zheng, L., Alain, T., Gandin, V., Avizonis, D., Arguello, M., Zakaria, C., McLaughlan, S., Nouet, Y., Pause, A., Pollak, M., Gottlieb, E., Larsson, O., St-Pierre, J., Topisirovic, I. and Sonenberg, N. mTORC1 controls mitochondrial activity and biogenesis through 4E-BP-dependent translational regulation. *Cell Metab* **2013**; *18(5)*:698-711.

117. Murakami, T., Nishiyama, T., Shirotani, T., Shinohara, Y., Kan, M., Ishii, K., Kanai, F., Nakazuru, S. and Ebina, Y. Identification of two enhancer elements in the gene encoding the type 1 glucose transporter from the mouse which are responsive to serum, growth factor, and oncogenes. *J Biol Chem* **1992**; *267(13)*:9300-9306.

118. Murat, A., Migliavacca, E., Gorlia, T., Lambiv, W. L., Shay, T., Hamou, M. F., de Tribolet, N., Regli, L., Wick, W., Kouwenhoven, M. C., Hainfellner, J. A., Heppner, F. L., Dietrich, P. Y., Zimmer, Y., Cairncross, J. G., Janzer, R. C., Domany, E., Delorenzi, M., Stupp, R. and Hegi, M. E. Stem cell-related "self-renewal" signature and high epidermal growth factor receptor expression associated with resistance to concomitant chemoradiotherapy in glioblastoma. *J Clin Oncol* **2008**; *26(18)*:3015-3024.

119. Musa, J., Aynaud, M. M., Mirabeau, O., Delattre, O. and Grunewald, T. G. MYBL2 (B-Myb): a central regulator of cell proliferation, cell survival and differentiation involved in tumorigenesis. *Cell Death Dis* **2017**; *8(6)*:e2895.

120. Musa, J., Cidre-Aranaz, F., Aynaud, M. M., Orth, M. F., Knott, M. M. L., Mirabeau, O., Mazor, G., Varon, M., Holting, T. L. B., Grossetete, S., Gartlgruber, M., Surdez, D., Gerke, J. S., Ohmura, S., Marchetto, A., Dallmayer, M., Baldauf, M. C., Stein, S., Sannino, G., Li, J., Romero-Perez, L., Westermann, F., Hartmann, W., Dirksen, U., Gymrek, M., Anderson, N. D., Shlien, A., Rotblat, B., Kirchner, T., Delattre, O. and Grunewald, T. G. P. Cooperation of cancer drivers with regulatory germline variants shapes clinical outcomes. *Nat Commun* **2019**; *10(1)*:4128.

121. Musa, J., Orth, M. F., Dallmayer, M., Baldauf, M., Pardo, C., Rotblat, B., Kirchner, T., Leprivier, G. and Grunewald, T. G. Eukaryotic initiation factor 4E-binding protein 1 (4E-BP1): a master regulator of mRNA translation involved in tumorigenesis. *Oncogene* **2016**; *35(36)*:4675-4688.

122. Nagy, J. A., Chang, S. H., Dvorak, A. M. and Dvorak, H. F. Why are tumour blood vessels abnormal and why is it important to know? *Br J Cancer* **2009**; *100(6)*:865-869.

123. Nagy, J. A., Chang, S. H., Shih, S. C., Dvorak, A. M. and Dvorak, H. F. Heterogeneity of the tumor vasculature. *Semin Thromb Hemost* **2010**; *36(3)*:321-331.

124. Nguyen, G. T., Erlenkamp, G., Jack, O., Kuberl, A., Bott, M., Fiorani, F., Gohlke, H. and Groth, G. Chalcone-based Selective Inhibitors of a C4 Plant Key Enzyme as Novel Potential Herbicides. *Sci Rep* **2016**; *6*:27333.

125. Niedzwiecka, A., Marcotrigiano, J., Stepinski, J., Jankowska-Anyszka, M., Wyslouch-Cieszynska, A., Dadlez, M., Gingras, A. C., Mak, P., Darzynkiewicz, E., Sonenberg, N., Burley, S. K. and Stolarski, R. Biophysical studies of eIF4E cap-binding protein: recognition of mRNA 5' cap structure and synthetic fragments of eIF4G and 4E-BP1 proteins. *J Mol Biol* **2002**; *319(3)*:615-635.

126. Nojima, H., Tokunaga, C., Eguchi, S., Oshiro, N., Hidayat, S., Yoshino, K., Hara, K., Tanaka, N., Avruch, J. and Yonezawa, K. The mammalian target of rapamycin (mTOR) partner, raptor, binds the mTOR substrates p70 S6 kinase and 4E-BP1 through their TOR signaling (TOS) motif. *J Biol Chem* **2003**; *278(18)*:15461-15464.

127. Ochs, K. and Kaina, B. Apoptosis induced by DNA damage O6-methylguanine is Bcl-2 and caspase-9/3 regulated and Fas/caspase-8 independent. *Cancer Res* **2000**; *60(20)*:5815-5824.

128. Okunieff, P., Hoeckel, M., Dunphy, E. P., Schlenger, K., Knoop, C. and Vaupel, P. Oxygen tension distributions are sufficient to explain the local response of human breast tumors treated with radiation alone. *Int J Radiat Oncol Biol Phys* **1993**; *26(4)*:631-636.

129. Oldham, S. and Hafen, E. Insulin/IGF and target of rapamycin signaling: a TOR de force in growth control. *Trends Cell Biol* **2003**; *13(2)*:79-85.

130. Olivier, M., Hollstein, M. and Hainaut, P. TP53 mutations in human cancers: origins, consequences, and clinical use. *Cold Spring Harb Perspect Biol* **2010**; *2(1)*:a001008.

131. Osthus, R. C., Shim, H., Kim, S., Li, Q., Reddy, R., Mukherjee, M., Xu, Y., Wonsey, D., Lee, L. A. and Dang, C. V. Deregulation of glucose transporter 1 and glycolytic gene expression by c-Myc. *J Biol Chem* **2000**; *275(29)*:21797-21800.

132. Ostrom, Q. T., Gittleman, H., Liao, P., Vecchione-Koval, T., Wolinsky, Y., Kruchko, C. and Barnholtz-Sloan, J. S. CBTRUS Statistical Report: Primary brain and other central nervous system tumors diagnosed in the United States in 2010-2014. *Neuro Oncol* **2017**; *19(suppl_5)*:v1-v88.

133. Paku, K. S., Umenaga, Y., Usui, T., Fukuyo, A., Mizuno, A., In, Y., Ishida, T. and Tomoo, K. A conserved motif within the flexible C-terminus of the translational regulator 4E-BP is required for tight binding to the mRNA cap-binding protein eIF4E. *Biochem J* **2012**; *441(1)*:237-245.

134. Palm, W., Park, Y., Wright, K., Pavlova, N. N., Tuveson, D. A. and Thompson, C. B. The Utilization of Extracellular Proteins as Nutrients Is Suppressed by mTORC1. *Cell* **2015**; *162(2)*:259-270.

135. Panieri, E., Gogvadze, V., Norberg, E., Venkatesh, R., Orrenius, S. and Zhivotovsky, B. Reactive oxygen species generated in different compartments induce cell death, survival, or senescence. *Free Radic Biol Med* **2013**; *57*:176-187.

136. Patel, A. P., Tirosh, I., Trombetta, J. J., Shalek, A. K., Gillespie, S. M., Wakimoto, H., Cahill, D. P., Nahed, B. V., Curry, W. T., Martuza, R. L., Louis, D. N., Rozenblatt-Rosen, O., Suva, M. L., Regev, A. and Bernstein, B. E. Single-cell RNA-seq highlights intratumoral heterogeneity in primary glioblastoma. *Science* **2014**; *344(6190)*:1396-1401.

137. Pelletier, J., Graff, J., Ruggero, D. and Sonenberg, N. Targeting the eIF4F translation initiation complex: a critical nexus for cancer development. *Cancer Res* **2015**; *75(2)*:250-263.

138. Perry, J. R., Laperriere, N., O'Callaghan, C. J., Brandes, A. A., Menten, J., Phillips, C., Fay, M., Nishikawa, R., Cairncross, J. G., Roa, W., Osoba, D., Rossiter, J. P., Sahgal, A., Hirte, H., Laigle-Donadey, F., Franceschi, E., Chinot, O., Golfinopoulos, V., Fariselli, L., Wick, A., Feuvret, L., Back, M., Tills, M., Winch, C., Baumert, B. G., Wick, W.,

Ding, K., Mason, W. P. and Trial, I. Short-Course Radiation plus Temozolomide in Elderly Patients with Glioblastoma. *N Engl J Med* **2017**; *376(11)*:1027-1037.

139. Peter, D., Igreja, C., Weber, R., Wohlbold, L., Weiler, C., Ebertsch, L., Weichenrieder, O. and Izaurralde, E. Molecular architecture of 4E-BP translational inhibitors bound to eIF4E. *Mol Cell* **2015**; *57(6)*:1074-1087.

140. Petroulakis, E., Parsyan, A., Dowling, R. J., LeBacquer, O., Martineau, Y., Bidinosti, M., Larsson, O., Alain, T., Rong, L., Mamane, Y., Paquet, M., Furic, L., Topisirovic, I., Shahbazian, D., Livingstone, M., Costa-Mattioli, M., Teodoro, J. G. and Sonenberg, N. p53-dependent translational control of senescence and transformation via 4E-BPs. *Cancer Cell* **2009**; *16(5)*:439-446.

141. Reich, S. H., Sprengeler, P. A., Chiang, G. G., Appleman, J. R., Chen, J., Clarine, J., Eam, B., Ernst, J. T., Han, Q., Goel, V. K., Han, E. Z. R., Huang, V., Hung, I. N. J., Jemison, A., Jessen, K. A., Molter, J., Murphy, D., Neal, M., Parker, G. S., Shaghafi, M., Sperry, S., Staunton, J., Stumpf, C. R., Thompson, P. A., Tran, C., Webber, S. E., Wegerski, C. J., Zheng, H. and Webster, K. R. Structure-based Design of Pyridone-Aminal eFT508 Targeting Dysregulated Translation by Selective Mitogen-activated Protein Kinase Interacting Kinases 1 and 2 (MNK1/2) Inhibition. *J Med Chem* **2018**; *61(8)*:3516-3540.

142. Ren, F., Wang, L., Shen, X., Xiao, X., Liu, Z., Wei, P., Wang, Y., Qi, P., Shen, C., Sheng, W. and Du, X. MYBL2 is an independent prognostic marker that has tumor-promoting functions in colorectal cancer. *Am J Cancer Res* **2015**; *5(4)*:1542-1552.

143. Rolli-Derkinderen, M., Machavoine, F., Baraban, J. M., Grolleau, A., Beretta, L. and Dy, M. ERK and p38 inhibit the expression of 4E-BP1 repressor of translation through induction of Egr-1. *J Biol Chem* **2003**; *278(21)*:18859-18867.

144. Ruggero, D. Translational control in cancer etiology. *Cold Spring Harb Perspect Biol* **2013**; *5(2)*

145. Russell, S. J., Ye, Y. W., Waber, P. G., Shuford, M., Schold, S. C., Jr. and Nisen, P. D. p53 mutations, O6-alkylguanine DNA alkyltransferase activity, and sensitivity to procarbazine in human brain tumors. *Cancer* **1995**; *75(6)*:1339-1342.

146. Rutkovsky, A. C., Yeh, E. S., Guest, S. T., Findlay, V. J., Muise-Helmericks, R. C., Armeson, K. and Ethier, S. P. Eukaryotic initiation factor 4E-binding protein as an oncogene in breast cancer. *BMC Cancer* **2019**; *19(1)*:491.

147. Saha, T., Kar, R. K. and Sa, G. Structural and sequential context of p53: A review of experimental and theoretical evidence. *Prog Biophys Mol Biol* **2015**; *117(2-3)*:250-263.

148. Sandelin, A., Alkema, W., Engstrom, P., Wasserman, W. W. and Lenhard, B. JASPAR: an open-access database for eukaryotic transcription factor binding profiles. *Nucleic Acids Res* **2004**; *32*:D91-94.

149. Saxton, R. A. and Sabatini, D. M. mTOR Signaling in Growth, Metabolism, and Disease. *Cell* **2017**; *168(6)*:960-976.

150. Schafer, Z. T., Grassian, A. R., Song, L., Jiang, Z., Gerhart-Hines, Z., Irie, H. Y., Gao, S., Puigserver, P. and Brugge, J. S. Antioxidant and oncogene rescue of metabolic defects caused by loss of matrix attachment. *Nature* **2009**; *461(7260)*:109-113.

151. Schalm, S. S., Fingar, D. C., Sabatini, D. M. and Blenis, J. TOS motif-mediated raptor binding regulates 4E-BP1 multisite phosphorylation and function. *Curr Biol* **2003**; *13(10)*:797-806.

152. Schmelzle, T. and Hall, M. N. TOR, a central controller of cell growth. *Cell* **2000**; *103(2)*:253-262.

153. Schroeder, T., Yuan, H., Viglianti, B. L., Peltz, C., Asopa, S., Vujaskovic, Z. and Dewhirst, M. W. Spatial heterogeneity and oxygen dependence of glucose consumption in R3230Ac and fibrosarcomas of the Fischer 344 rat. *Cancer Res* **2005**; *65(12)*:5163-5171.

154. Sengupta, S., Peterson, T. R. and Sabatini, D. M. Regulation of the mTOR complex 1 pathway by nutrients, growth factors, and stress. *Mol Cell* **2010**; *40(2)*:310-322.

155. Seystahl, K., Wick, W. and Weller, M. Therapeutic options in recurrent glioblastoma--An update. *Crit Rev Oncol Hematol* **2016**; *99*:389-408.

156. Soeda, A., Hara, A., Kunisada, T., Yoshimura, S., Iwama, T. and Park, D. M. The evidence of glioblastoma heterogeneity. *Sci Rep* **2015**; *5*:7979.

157. Sonenberg, N. Cap-binding proteins of eukaryotic messenger RNA: functions in initiation and control of translation. *Prog Nucleic Acid Res Mol Biol* **1988**; *35*:173-207.

158. Sottoriva, A., Spiteri, I., Piccirillo, S. G., Touloumis, A., Collins, V. P., Marioni, J. C., Curtis, C., Watts, C. and Tavare, S. Intratumor heterogeneity in human glioblastoma reflects cancer evolutionary dynamics. *Proc Natl Acad Sci U S A* **2013**; *110(10)*:4009-4014.

159. Streitberger, K. J., Lilaj, L., Schrank, F., Braun, J., Hoffmann, K. T., Reiss-Zimmermann, M., Kas, J. A. and Sack, I. How tissue fluidity influences brain tumor progression. *Proc Natl Acad Sci U S A* **2020**; *117(1)*:128-134.

160. Stupp, R., Mason, W. P., van den Bent, M. J., Weller, M., Fisher, B., Taphoorn, M. J., Belanger, K., Brandes, A. A., Marosi, C., Bogdahn, U., Curschmann, J., Janzer, R. C., Ludwin, S. K., Gorlia, T., Allgeier, A., Lacombe, D., Cairncross, J. G., Eisenhauer, E., Mirimanoff, R. O., European Organisation for, R., Treatment of Cancer Brain, T., Radiotherapy, G. and National Cancer Institute of Canada Clinical Trials, G. Radiotherapy plus concomitant and adjuvant temozolomide for glioblastoma. *N Engl J Med* **2005**; *352(10)*:987-996.

161. Sun, L., Hui, A. M., Su, Q., Vortmeyer, A., Kotliarov, Y., Pastorino, S., Passaniti, A., Menon, J., Walling, J., Bailey, R., Rosenblum, M., Mikkelsen, T. and Fine, H. A. Neuronal and glioma-derived stem cell factor induces angiogenesis within the brain. *Cancer Cell* **2006**; *9(4)*:287-300.

162. Sun, Z., Liu, Q., Qu, G., Feng, Y. and Reetz, M. T. Utility of B-Factors in Protein Science: Interpreting Rigidity, Flexibility, and Internal Motion and Engineering Thermostability. *Chem Rev* **2019**; *119(3)*:1626-1665.

163. Szatmari, T., Lumniczky, K., Desaknai, S., Trajcevski, S., Hidvegi, E. J., Hamada, H. and Safrany, G. Detailed characterization of the mouse glioma 261 tumor model for experimental glioblastoma therapy. *Cancer Sci* **2006**; *97(6)*:546-553.

164. Tameire, F., Verginadis, II, Leli, N. M., Polte, C., Conn, C. S., Ojha, R., Salas Salinas, C., Chinga, F., Monroy, A. M., Fu, W., Wang, P., Kossenkov, A., Ye, J., Amaravadi, R. K., Ignatova, Z., Fuchs, S. Y., Diehl, J. A., Ruggero, D. and

Koumenis, C. ATF4 couples MYC-dependent translational activity to bioenergetic demands during tumour progression. *Nat Cell Biol* **2019**; *21(7)*:889-899.

165. Tanaka, K., Sasayama, T., Nagashima, H., Irino, Y., Takahashi, M., Izumi, Y., Uno, T., Satoh, N., Kitta, A., Kyotani, K., Fujita, Y., Hashiguchi, M., Nakai, T., Kohta, M., Uozumi, Y., Shinohara, M., Hosoda, K., Bamba, T. and Kohmura, E. Glioma cells require one-carbon metabolism to survive glutamine starvation. *Acta Neuropathol Commun* **2021**; *9(1)*:16.

166. Tang, D., Huang, T., Tian, Q. and Wang, J. MYC/NBS1-Mediated DNA Damage Response is Involved in the Inhibitory Effect of Hydroxysafflor Yellow A on Glioma Cells. *Drug Des Devel Ther* **2021**; *15*:1749-1763.

167. Tee, A. R. and Proud, C. G. Caspase cleavage of initiation factor 4E-binding protein 1 yields a dominant inhibitor of cap-dependent translation and reveals a novel regulatory motif. *Mol Cell Biol* **2002**; *22(6)*:1674-1683.

168. Teicher, B. A. Hypoxia and drug resistance. *Cancer Metastasis Rev* **1994**; *13(2)*:139-168.

169. Teicher, B. A., Lazo, J. S. and Sartorelli, A. C. Classification of antineoplastic agents by their selective toxicities toward oxygenated and hypoxic tumor cells. *Cancer Res* **1981**; *41(1)*:73-81.

170. Thoreen, C. C., Chantranupong, L., Keys, H. R., Wang, T., Gray, N. S. and Sabatini, D. M. A unifying model for mTORC1-mediated regulation of mRNA translation. *Nature* **2012**; *485(7396)*:109-113.

171. Truitt, M. L., Conn, C. S., Shi, Z., Pang, X., Tokuyasu, T., Coady, A. M., Seo, Y., Barna, M. and Ruggero, D. Differential Requirements for eIF4E Dose in Normal Development and Cancer. *Cell* **2015**; *162(1)*:59-71.

172. Tsukiyama-Kohara, K., Poulin, F., Kohara, M., DeMaria, C. T., Cheng, A., Wu, Z., Gingras, A. C., Katsume, A., Elchebly, M., Spiegelman, B. M., Harper, M. E., Tremblay, M. L. and Sonenberg, N. Adipose tissue reduction in mice lacking the translational inhibitor 4E-BP1. *Nat Med* **2001**; *7(10)*:1128-1132.

173. Ulgen, E., Karacan, S., Gerlevik, U., Can, O., Bilguvar, K., Oktay, Y., C, B. A., S, K. Y., A, E. D., Tihan, T., Sezerman, O. U., Yakicier, M. C., Pamir, M. N. and Ozduman, K. Mutations and Copy Number Alterations in IDH Wild-Type Glioblastomas Are Shaped by Different Oncogenic Mechanisms. *Biomedicines* **2020**; *8(12)*

174. Van Meir, E. G., Kikuchi, T., Tada, M., Li, H., Diserens, A. C., Wojcik, B. E., Huang, H. J., Friedmann, T., de Tribolet, N. and Cavenee, W. K. Analysis of the p53 gene and its expression in human glioblastoma cells. *Cancer Res* **1994**; *54(3)*:649-652.

175. Verhaak, R. G., Hoadley, K. A., Purdom, E., Wang, V., Qi, Y., Wilkerson, M. D., Miller, C. R., Ding, L., Golub, T., Mesirov, J. P., Alexe, G., Lawrence, M., O'Kelly, M., Tamayo, P., Weir, B. A., Gabriel, S., Winckler, W., Gupta, S., Jakkula, L., Feiler, H. S., Hodgson, J. G., James, C. D., Sarkaria, J. N., Brennan, C., Kahn, A., Spellman, P. T., Wilson, R. K., Speed, T. P., Gray, J. W., Meyerson, M., Getz, G., Perou, C. M., Hayes, D. N. and Cancer Genome Atlas Research, N. Integrated genomic analysis identifies clinically relevant subtypes of glioblastoma characterized by abnormalities in PDGFRA, IDH1, EGFR, and NF1. *Cancer Cell* **2010**; *17(1)*:98-110.

176. Vita, M. and Henriksson, M. The Myc oncoprotein as a therapeutic target for human cancer. *Semin Cancer Biol* **2006**; *16(4)*:318-330.

177. Vuorinen, V., Hinkka, S., Farkkila, M. and Jaaskelainen, J. Debulking or biopsy of malignant glioma in elderly people - a randomised study. *Acta Neurochir (Wien)* **2003**; *145(1)*:5-10.

178. Wagner, C. R., Iyer, V. V. and McIntee, E. J. Pronucleotides: toward the in vivo delivery of antiviral and anticancer nucleotides. *Med Res Rev* **2000**; *20(6)*:417-451.

179. Wang, Z., Feng, X., Molinolo, A. A., Martin, D., Vitale-Cross, L., Nohata, N., Ando, M., Wahba, A., Amornphimoltham, P., Wu, X., Gilardi, M., Allevato, M., Wu, V., Steffen, D. J., Tofilon, P., Sonenberg, N., Califano, J., Chen, Q., Lippman, S. M. and Gutkind, J. S. 4E-BP1 Is a Tumor Suppressor Protein Reactivated by mTOR Inhibition in Head and Neck Cancer. *Cancer Res* **2019**; *79(7)*:1438-1450.

180. Warburg, O. On respiratory impairment in cancer cells. *Science* **1956**; *124(3215)*:269-270.

181. Weller, M., van den Bent, M., Preusser, M., Le Rhun, E., Tonn, J. C., Minniti, G., Bendszus, M., Balana, C., Chinot, O., Dirven, L., French, P., Hegi, M. E., Jakola, A. S., Platten, M., Roth, P., Ruda, R., Short, S., Smits, M., Taphoorn, M. J. B., von Deimling, A., Westphal, M., Soffietti, R., Reifenberger, G. and Wick, W. EANO guidelines on the diagnosis and treatment of diffuse gliomas of adulthood. *Nat Rev Clin Oncol* **2021**; *18(3)*:170-186.

182. Wieman, H. L., Wofford, J. A. and Rathmell, J. C. Cytokine stimulation promotes glucose uptake via phosphatidylinositol-3 kinase/Akt regulation of Glut1 activity and trafficking. *Mol Biol Cell* **2007**; *18(4)*:1437-1446.

183. Wippold, F. J., 2nd, Lammle, M., Anatelli, F., Lennerz, J. and Perry, A. Neuropathology for the neuroradiologist: palisades and pseudopalisades. *AJNR Am J Neuroradiol* **2006**; *27(10)*:2037-2041.

184. Wu, S. and Wagner, G. Deep computational analysis details dysregulation of eukaryotic translation initiation complex eIF4F in human cancers. *Cell Syst* **2021**; *12(9)*:907-923 e906.

185. Xiong, Y. C., Wang, J., Cheng, Y., Zhang, X. Y. and Ye, X. Q. Overexpression of MYBL2 promotes proliferation and migration of non-small-cell lung cancer via upregulating NCAPH. *Mol Cell Biochem* **2020**; *468(1-2)*:185-193.

186. Yaes, R. J. Tumor heterogeneity, tumor size, and radioresistance. *Int J Radiat Oncol Biol Phys* **1989**; *17(5)*:993-1005.

187. Yamaguchi, S., Ishihara, H., Yamada, T., Tamura, A., Usui, M., Tominaga, R., Munakata, Y., Satake, C., Katagiri, H., Tashiro, F., Aburatani, H., Tsukiyama-Kohara, K., Miyazaki, J., Sonenberg, N. and Oka, Y. ATF4-mediated induction of 4E-BP1 contributes to pancreatic beta cell survival under endoplasmic reticulum stress. *Cell Metab* **2008**; *7(3)*:269-276.

188. Yellen, P., Saqcena, M., Salloum, D., Feng, J., Preda, A., Xu, L., Rodrik-Outmezguine, V. and Foster, D. A. High-dose rapamycin induces apoptosis in human cancer cells by dissociating mTOR complex 1 and suppressing phosphorylation of 4E-BP1. *Cell Cycle* **2011**; *10(22)*:3948-3956.

189. Yi, T., Papadopoulos, E., Hagner, P. R. and Wagner, G. Hypoxia-inducible factor-1alpha (HIF-1alpha) promotes cap-dependent translation of selective mRNAs through up-regulating initiation factor eIF4E1 in breast cancer cells under hypoxia conditions. *J Biol Chem* **2013**; *288(26)*:18732-18742.

190. Yu, H., Li, Z. and Wang, M. Expression and prognostic role of E2F transcription factors in high-grade glioma. *CNS Neurosci Ther* **2020**; *26(7)*:741-753.

191. Zhang, X., Bi, C., Lu, T., Zhang, W., Yue, T., Wang, C., Tian, T., Zhang, X., Huang, Y., Lunning, M., Hao, X., Brown, L. E., Devine, W. G., Vose, J., Porco, J. A., Jr. and Fu, K. Targeting translation initiation by synthetic rocaglates for treating MYC-driven lymphomas. *Leukemia* **2020**; *34(1)*:138-150.

192. Zhang, X., Lv, Q. L., Huang, Y. T., Zhang, L. H. and Zhou, H. H. Akt/FoxM1 signaling pathway-mediated upregulation of MYBL2 promotes progression of human glioma. *J Exp Clin Cancer Res* **2017**; *36(1)*:105.

193. Zhao, Z., Zhang, K. N., Wang, Q., Li, G., Zeng, F., Zhang, Y., Wu, F., Chai, R., Wang, Z., Zhang, C., Zhang, W., Bao, Z. and Jiang, T. Chinese Glioma Genome Atlas (CGGA): A Comprehensive Resource with Functional Genomic Data from Chinese Glioma Patients. *Genomics Proteomics Bioinformatics* **2021**; *19(1)*:1-12.

194. Zhou, Z., Yin, Y., Chang, Q., Sun, G., Lin, J. and Dai, Y. Downregulation of B-myb promotes senescence via the ROS-mediated p53/p21 pathway, in vascular endothelial cells. *Cell Prolif* **2017**; *50(2)*

195. Zid, B. M., Rogers, A. N., Katewa, S. D., Vargas, M. A., Kolipinski, M. C., Lu, T. A., Benzer, S. and Kapahi, P. 4E-BP extends lifespan upon dietary restriction by enhancing mitochondrial activity in Drosophila. *Cell* **2009**; *139(1)*:149-160.

E. ACKNOWLEDGEMENT

First of all, a big thank you goes to Prof. Dr. Guido Reifenberger for being my first supervisor, for kindly welcoming our research group at the institute of neuropathology, for the good advice and input regarding experimental approaches and for correcting my thesis.

Secondly, I would like to thank Prof. Dr. Sebastian Wesselborg for accompanying me and discussing experimental approaches with me throughout the PhD and for evaluating my thesis.

A giant thank goes out to Dr. Gabriel Leprivier, who managed to boost my self-confidence and helped me through his guidance and supervision to evolve into the scientist I am today. Gabriel, I really enjoyed working with you and furthermore I also appreciated our talks and that you inspired me to give red wine and chevre de fromage another chance. Please keep up being this kind and great supervisor that you are.

Next, I want to thank my fellow PhD student Kai, who I could always talk to about experiments and results but who also joked around with me a lot. Thank you for your support.

Moreover, I really want to thank both of master students Alisa and Kati. Both of you were great students and helped me to move my project along. Kati, without you the time in the lab was always fun and I am so glad I found a good friend in you.

Next, a big thank you belongs to Prof. Dr. Georg Groth, who supported one of my side projects and welcomed me to his lab to perform some experiments. A special thanks also goes to Dr. Alexander Minges, I could not have performed those experiments that well without you, especially in this short amount of time. Also, thank you for having a look at my thesis.

My gratitude goes also to Prof. Dr. Holger Gohlke, his post doc Dr. Mohan Gopalaswamy and his student David Bickel for the nice collaboration and support in the targeting project.

A huge shoutout goes to Prof. Dr. Barak Rotblat and his lab, specifically Tal and Khawla. I enjoyed the great collaboration and most of all I am grateful for the very warm welcome and all the support I experienced when I came to Israel.

A big thank you is also deserved by Andreas, Else, Svenja and Ingrid, who were not just great office mates, but also helped me scientifically with good input and discussions.

In addition to that, I would like to thank the whole department of Neuropathology and Neurosurgery for a warm welcome, inspiring talks and advice.

A big thanks also to all members of the KMT-Lab, who made my first two PhD years very enjoyable.

I want to thank my sporty girls Kati and Vera, without our training sessions my frustration levels might not have been as stable as they were. Also, a big thanks to my mom, dad and the rest of the family for always having faith in me and my abilities, for pushing me during though times and for just being there. I love you.

Last but not least I want to thank my boyfriend Mathi for his incredible support, listening patiently to me when I went on and on about scientific problems and my project, although biology is like voodoo to him. I respect you for that and I could not wish for a better stable rock in my life. I love you, Kocham cię.